On the climatic synergies at the local, regional, and global scales. The impact on the built environment.

Author:
Khan, Hassan

Publication Date:
2022

DOI:
https://doi.org/10.26190/unsworks/24459

On the climatic synergies at the local, regional, and global scales. The impact on the built environment.

By

Hassan Saeed Khan

A thesis submitted in fulfillment of the requirements for the degree of

Doctor of Philosophy

School of Built Environment (SBE)

Faculty of Arts, Design, and Architecture.

The University of New South Wales (UNSW), Sydney.

Primary Supervisor:

Scientia Prof. Mat Santamouris

Co-supervisors:

Dr. Riccardo Paolini

Dr. Laurance Kimmel

Data-61 supervisor:

Dr. Peter Caccetta

JUNE 2022

ORIGINALITY, COPYRIGHT AND AUTHENTICITY STATEMENTS

Thesis submission for the degree of Doctor of Philosophy

Thesis Title and Abstract | Declarations | Inclusion of Publications Statement | Corrected Thesis and Responses

ORIGINALITY STATEMENT

☑ I hereby declare that this submission is my own work and to the best of my knowledge it contains no materials previously published or written by another person, or substantial proportions of material which have been accepted for the award of any other degree or diploma at UNSW or any other educational institution, except where due acknowledgement is made in the thesis. Any contribution made to the research by others, with whom I have worked at UNSW or elsewhere, is explicitly acknowledged in the thesis. I also declare that the intellectual content of this thesis is the product of my own work, except to the extent that assistance from others in the project's design and conception or in style, presentation and linguistic expression is acknowledged.

COPYRIGHT STATEMENT

☑ I hereby grant the University of New South Wales or its agents a non-exclusive licence to archive and to make available (including to members of the public) my thesis or dissertation in whole or part in the University libraries in all forms of media, now or here after known. I acknowledge that I retain all intellectual property rights which subsist in my thesis or dissertation, such as copyright and patent rights, subject to applicable law. I also retain the right to use all or part of my thesis or dissertation in future works (such as articles or books).

For any substantial portions of copyright material used in this thesis, written permission for use has been obtained, or the copyright material is removed from the final public version of the thesis.

AUTHENTICITY STATEMENT

☑ I certify that the Library deposit digital copy is a direct equivalent of the final officially approved version of my thesis.

INCLUSION OF PUBLICATIONS STATEMENT

Thesis submission for the degree of Doctor of Philosophy

Thesis Title and Abstract | Declarations | Inclusion of Publications Statement | Corrected Thesis and Responses

UNSW is supportive of candidates publishing their research results during their candidature as detailed in the UNSW Thesis Examination Procedure.

Publications can be used in the candidate's thesis in lieu of a Chapter provided:

- The candidate contributed **greater than 50%** of the content in the publication and are the "primary author", i.e. they were responsible primarily for the planning, execution and preparation of the work for publication.
- The candidate has obtained approval to include the publication in their thesis in lieu of a Chapter from their Supervisor and Postgraduate Coordinator.
- The publication is not subject to any obligations or contractual agreements with a third party that would constrain its inclusion in the thesis.

☑ The candidate has declared that **some of the work described in their thesis has been published and has been documented in the relevant Chapters with acknowledgement**.

A short statement on where this work appears in the thesis and how this work is acknowledged within chapter/s:

My thesis contains the following published papers in chapters 2,3,5,6,7, and 8.
• Journal articles from the Ph.D. thesis:

1. Khan, H. S., Paolini, R., Caccetta, P., & Santamouris, M. (2022). On the combined impact of local, regional, and global climatic changes on the urban energy performance and indoor thermal comfort—The energy potential of adaptation measures. Energy and Buildings, 112152. https://doi.org/10.1016/j.enbuild.2022.112152
Chapter 8 presents the main findings.
2. Khan, H. S., Santamouris, M., Kassomenos, P., Paolini, R., Caccetta, P., & Petrou, I. (2021). Spatiotemporal variation in urban overheating magnitude and its association with synoptic air-masses in a coastal city. Scientific Reports, 11(1), 6762. https://doi.org/10.1038/s41598-021-86089-2
Chapter 5 presents the main findings.
3. Khan, H. S., Santamouris, M., Paolini, R., Caccetta, P., & Kassomenos, P. (2021). Analyzing the local and climatic conditions affecting the urban overheating magnitude during the Heatwaves (HWs) in a coastal city: A case study of the greater Sydney region. Science of The Total Environment, 755, 142515. https://doi.org/10.1016/j.scitotenv.2020.142515
Chapter 7 presents the main findings.
4. Khan, H. S., Paolini, R., Santamouris, M., & Caccetta, P. (2020). Exploring the Synergies between Urban Overheating and Heatwaves (HWs) in Western Sydney. Energies 2020, Vol. 13, Page 470, 13(2), 470. https://doi.org/10.3390/EN13020470
Chapter 6 presents the main findings.
5. Khan, H. S., Santamouris, M., Paolini, R., & Caccetta, P., (under progress). A review on the local, regional, and global climatic interactions and their impact on the built environment.

Book chapters:
1. Khan, H. S., Santamouris, M., Paolini, (submitted). Synergies and exacerbation: Effects of warmer weather and climate change, Elsevier.
Chapters 2 and 3 present the main content.

Peer-reviewed conference papers:
1. Khan, H. S., Santamouris, M., Kassomenos, P., Paolini, R., Caccetta, P. (submitted). Investigating the synergistic interactions between urban overheating (UO), and multivariate weather types (WTs) during heatwaves in a coastal city, 2022 PLEA Conference in Santiago, Chile.
Chapter 5 presents the main findings.

Candidate's Declaration

I declare that I have complied with the Thesis Examination Procedure.

ABSTRACT

Most cities across the globe are affected by urban overheating (UO), which is one of the most well-documented local-scale climate change phenomena. Extreme heat events have become more intense and severe in the twenty-first century, posing a substantial hazard to human health. Over the years, significant variations in global weather patterns have also been documented. The UO alters the land-atmospheric interactions and affects the regional and global climatic conditions. The synergies between such local, regional, and global climate changes, which may adversely affect health, economy, energy, and environmental quality, have never been examined and are a major concern in the context of global warming and rapid urbanization. Further, the combined impact of such climatic changes on the built environment has never been investigated and is also a pressing issue in the context of overheating and GHG emissions.

The dissertation's primary goal is to examine the interactions between local-scale UO, regional-scale heatwaves, and large-scale synoptic climatology and to assess how these affect the built environment. The association between UO, heatwaves, and large-scale weather patterns was investigated using the surface energy budget and innovative techniques, including the gridded weather typing classification (GWTC). The newly developed urban building energy models (UBEMs) were employed to investigate the combined impact of such climatic changes on the built environment. There had been reports of positive synergy between UO and heatwaves when the magnitude of UO increased dramatically. The key synergistic interactions between UO and heatwaves were the advective heat flux and land-coast distance, where the lack of coastal winds penetration during heatwaves kept the inland regions warmer by altering the available energy. The tropical maritime Tasman airmass (coming from north of the Tasman sea) and temperate maritime weather patterns were primarily responsible for humid-warm (HW) and humid conditions in the region during heatwaves. In addition to these moist unstable conditions, a significant impact of tropical continental airmass, arising over central Australia, was also documented during heatwaves, another thermal regulator between inland and coastal zones. A drastic increase in urban cooling energy needs and serious overheating issues in the built environment was also concluded under the combined impact of such climate changes, which was associated with the same dualistic large-scale weather systems. This research is the first of its kind, identifying the impact of microscale and mesoscale climate on the built environment and presenting the solutions to counteracting the global climatic change. The guidelines provided in the dissertation will aid in designing thermally resilient and heat-responsive cities.

Keywords: Urban overheating, heatwaves, large-scale weather patterns, climatic synergies, climate change, urban cooling energy, indoor comfort, passive survivability, adaptive measure

ACKNOWLEDGEMENT

Without the grace of Almighty Allah, who led me through thick and thin and to whom I owe all my achievements, none of this would have been possible.

My deepest gratitude and appreciation go to Prof Mattheos Santamouris, my primary supervisor, for his invaluable guidance and encouragement throughout my doctoral studies. His extensive expertise and experience were crucial in determining the appropriate direction for my Ph.D. research. He motivated me to conquer my limitations and inspired me with his enthusiasm. I am immensely thankful to my co-supervisor, Dr. Riccardo Paolini, for providing me with all necessary technical support, arranging the essential meteorological data for this project, and allowing me to assist in his courses. My thanks also go to Dr. Peter Caccetta, my Data-61 CSIRO supervisor, who helped me obtain the Data-61 top-up scholarship and has always assisted me in acquiring other data needed for my study. I also would like to thank Dr. Kassomenos Pavlos, University of Ioannina, Greece, for guiding me in identifying the interactions between urban overheating and large-scale weather systems.

I am also grateful to the Australian Bureau of Meteorology (BOM) for providing the meteorological data. The data post-processing was funded by Sydney Water and the CRC for Low Carbon Living through the SP0012 research contract and by the City of Parramatta under the 'Parramatta Urban Overheating' study contract. I would also like to thank Prof Cameron C. Lee, Kent University, USA, for providing the appropriate GWTC data for Sydney utilized in this dissertation (https://www.personal.kent.edu/~cclee//gwtc2global.html). I would also like to thank KAEMCO for giving access to CitySim Pro for urban energy analyses and Dr. Jerome Henri Kampf for providing technical support on the program.

I am also grateful to the University of New South Wales (UNSW) and Data-61 CSIRO for supporting my doctoral studies through various scholarships. My heartfelt appreciation to the School of Built Environment (BE), BE HDR team, and postgraduate research coordinator (Dr. Paola Favaro) for fostering an environment conducive to my study. I also appreciate the support of my review panel, Dr. Sisi Zlatanova, Dr. Elisa Palazzo, and Dr. Gloria Pignatta, who tracked my progress during annual reviews and helped me improve the quality of my work. I am thankful to the anonymous reviewers of several research articles related to this dissertation for their insightful suggestions and remarks.

I also want to thank my entire family, especially my parents, whose prayers enabled me to realize a long-cherished goal. I would like to thank my wife, who endured much owing to my hectic schedule but always encouraged me to accomplish my goals. My daughter, who was always there to cheer me up through my dismal moments, deserves much gratitude. I am also grateful to my six-day-old son, who pushed me (during pregnancy) to earn my Ph.D. before his birth. I also would like to express my gratitude to my siblings for their support whenever I needed them. Big thanks to my nephews and nieces for their love and prayers.

TABLE OF CONTENTS

LIST OF FIGURES

LIST OF TABLES

LIST OF ABBREVIATIONS

UO	Urban overheating
UC	Urban cooling
ΔT	T_{suburb}- T_{CBD}
ΔUO	Heatwave - background UO magnitude difference
AH	Absolute humidity
ΔAH	Suburban- Urban moisture contrast (AH_{suburb}-AH_{CBD})
LCLU	Land-cover, and Land-use classification
ATT	Absolute temperature threshold
RTT	Relative temperature threshold
T_{max}	Daily maximum temperature
T_{min}	Daily minimum temperature
T_a	Ambient temperature
T_s	Surface temperature
T_{dew}	Dewpoint temperature
T_{risk}	Minimal Indoor risk temperature for heat-related health effects by WHO
T_{accep}	Maximum acceptable indoor temperature by WHO
AT	Apparent temperature
HI	Humidity index
UTCI	Universal thermal Climatic Index
EHF	Excessive heat factor
EHI (sig)	Excess Heat
EHI (accl)	Heat Stress
HP	High pressure
LP	Low pressure
MSLP	Mean sea level pressure
CPC	Circulation-pattern-based classification
WTC	Weather typing classification
SSC	Spatial synoptic classification
GWTC	Gridded weather typing classification
WT	Weather type
cP	Continental Polar
mP	Maritime Polar
cT	Continental tropical

mT	Maritime tropical
DP	Dry polar
DM	Dry moderate
DT	Dry tropical
MP	Moist polar
MM	Moist moderate
MT	Moist tropical
TR	Transitional
HC	Humid cold
HW	Humid warm
DC	Dry cool
DW	Dry warm
H	Humid
D	Dry
C	Cool
W	Warm
CFP	Cold frontal passage
WFP	Warm frontal passage
S	Seasonal
CBD	Central business district
PD	Population density
IEQ	Indoor environmental
RSD	Remaining summer days (without heatwaves)
BEM	Building energy model
UBEM	Urban Building energy model
TMY	Typical Meteorological Year
NSW	New South Wales
NCC	National Construction Code
NatHERS	Nationwide House Energy Rating Scheme
HVAC	Heating, ventilation, and airconditioning
HD	High-density settlement (Apartments)
LD	Low-density settlement (Houses)
O	Outdoor
I	Indoor

WHO	World Health organization
PL	Penrith Lakes
CT	Campbelltown
LP	Liverpool
HK	Horsley Park
OP	Olympic Park
CY	Canterbury
SA	Sydney Airport
TH	Terrey Hills
OH	Observatory Hills
Humidex-HD	Heat humidity index
D-winds	Desert/ continental winds
C-winds	Coastal winds
IW	Inland winds from the west
IE	Inland winds from the east
SD	Standard deviation
TI	Thermal Inertia
WD	Wind direction

LIST OF PUBLICATIONS, AWARDS, AND ACHIEVEMENTS

Journal Articles:

- ### Journal articles from the Ph.D. thesis:

1. Khan, H. S., Paolini, R., Caccetta, P., & Santamouris, M. (2022). On the combined impact of local, regional, and global climatic changes on the urban energy performance and indoor thermal comfort—The energy potential of adaptation measures. *Energy and Buildings*, 112152. https://doi.org/10.1016/j.enbuild.2022.112152

Chapter 8 presents the main findings.

2. Khan, H. S., Santamouris, M., Kassomenos, P., Paolini, R., Caccetta, P., & Petrou, I. (2021). Spatiotemporal variation in urban overheating magnitude and its association with synoptic air-masses in a coastal city. *Scientific Reports*, *11*(1), 6762. https://doi.org/10.1038/s41598-021-86089-2

Chapter 5 presents the main findings.

3. Khan, H. S., Santamouris, M., Paolini, R., Caccetta, P., & Kassomenos, P. (2021). Analyzing the local and climatic conditions affecting the urban overheating magnitude during the Heatwaves (HWs) in a coastal city: A case study of the greater Sydney region. *Science of The Total Environment*, *755*, 142515. https://doi.org/10.1016/j.scitotenv.2020.142515

Chapter 7 presents the main findings.

4. Khan, H. S., Paolini, R., Santamouris, M., & Caccetta, P. (2020). Exploring the Synergies between Urban Overheating and Heatwaves (HWs) in Western Sydney. *Energies 2020, Vol. 13, Page 470*, *13*(2), 470. https://doi.org/10.3390/EN13020470

Chapter 6 presents the main findings.

5. Khan, H. S., Santamouris, M., Paolini, R., & Caccetta, P., (under progress). A review on the local, regional, and global climatic interactions and their impact on the built environment.

- ### Journal articles related to the Ph.D. thesis:

1. Kassomenos, P., Kissas, G., Petrou, I., Begou, P., Khan, H. S., & Santamouris, M. (2022). The influence of daily weather types on the development and intensity of the urban heat island in two Mediterranean coastal metropolises. *Science of The Total Environment*, *819*, 153071.

https://doi.org/10.1016/j.scitotenv.2022.153071

Book chapters:

1. Khan, H. S., Santamouris, M., Paolini, (submitted). Synergies and exacerbation: Effects of warmer weather and climate change, Elsevier.

   Chapters 2 and 3 present the main content.

Peer-reviewed conference papers:

1. Khan, H. S., Santamouris, M., Kassomenos, P., Paolini, R., Caccetta, P. (submitted). Investigating the synergistic interactions between urban overheating (UO), and multivariate weather types (WTs) during heatwaves in a coastal city, 2022 PLEA Conference in Santiago, Chile.

   Chapter 5 presents the main findings.

Awards and Scholarships:

- ### Scholarships:

1. University international postgraduate award (UIPA), by UNSW, Australia, for 3.5 years.
2. Wightman Bequest Top-up scholarship awarded by School of Built environment, UNSW, for 3 years.
3. Data 61-CSIRO Ph.D. Top-up scholarship awarded by CSIRO for 3 years.
4. HDR completion scholarship, awarded by UNSW, Australia.
5. Supervisor top-up scholarship, awarded by UNSW, Australia
6. Data-61 Ph.D. completion scholarship, awarded by CSIRO.

- ### Awards and achievements:

1. ADA HDR research output award 2021 for the research article published in Science of the Total Environment.
2. ADA HDR research output award 2022 for the research article published in Nature Scientific Reports.
3. Interview published in NewScientist based on publication in Nature Scientific Reports, “Sydney’s inland suburbs are 10°C warmer than the coast in heat waves”, https://www.newscientist.com/article/2273355-sydneys-inland-suburbs-are-10c-warmer-than-the-coast-in-heat-waves/

CHAPTER 1: INTRODUCTION

This chapter introduces the subject, summarizes the research background, highlights the topic's significance, identifies research gaps, and discusses the dissertation's research questions and primary objectives. Further, it presents the thesis structure and the chapter's outline.

1.1 Research background:

Urban overheating (UO) is a local-scale phenomenon wherein temperatures in urban regions are exceptionally higher than their rural counterparts [1]. UO is primarily utilized to assess the degree of urbanization that modifies land-atmosphere interactions [2]. The sensible, latent, radiative, and aerodynamic responses of surfaces are altered by urbanization, resulting in varying heating and cooling rates in urban and rural settlements. The urban-rural thermal gradient is primarily caused by changes in the urban fabric (e.g., less vegetated surfaces, surfaces that retain more heat, have lower albedo and reduced permeability), changes in the city's layout (e.g., geometry, size, topography, population density, industrial development), enlarged anthropogenic effect and higher pollutant levels in the urbanized areas, and synoptic-scale weather and meteorological conditions [3,4]. Cities are made up of a variety of Land covers and Land use classifications (LCLU), each with its own set of thermal characteristics based on the surface properties [5].

A heatwave is a regional-scale phenomenon in which the temperatures in the entire region are elevated for an extended period. Large-scale meteorological conditions, soil moisture, and land-atmosphere interactions are all thought to impact the phenomenon [6]. Further, clear skies, intense solar radiation, and low wind speed are associated with heatwaves [7,8]. Extreme heat events are rising worldwide, while extreme cold occurrences are declining [9]. Many studies have found that extreme heat events would become more common, last longer, be more severe in the twenty-first century, and pose a severe threat to the global community [7,10,11].

Weather patterns observed at a horizontal scale of 1000 km to 4000 km are known as synoptic, large, or cyclonic-scale conditions. Due to the planet's rotation around the sun, some parts of the earth receive more solar radiation than others. Global circulation patterns are formed by the uneven distribution of these solar radiations. The global circulation patterns generate the air masses that make up the exceptionally large body of air, extending across the troposphere [12]. These air masses have uniform thermal and humid characteristics in any horizontal direction and at a given altitude. The atmospheric variables, including temperature, humidity, wind speed, atmospheric pressure, and cloud cover, are affected by urbanization due to alterations in land-atmospheric thermal and moisture exchange and may affect these global weather circulations. In recent decades, there has also been a significant variation reported in the frequency and magnitude of these atmospheric variables. For instance, over the last century, global average temperatures have risen by 0.85°C and are adversely affecting thermal comfort [13]. Similarly, wind speed has generally decreased [14], whereas land-based precipitation has increased for the mid-latitudes due to higher evaporation rates (in response to higher temperatures), increasing the absolute humidity [15].

The adverse effects of UO or heatwaves on mortality [16,17], morbidity [18], social susceptibility [19], cooling energy [20], peak power demand [21], environmental stability [22–25], capital losses [26,27], and infrastructure failure [28] are well-known worldwide. UO, extreme heat events, and large-scale weather patterns may interact synergistically and magnify these detrimental effects further, particularly in urban settlements [29,30]. According to several studies, a projected increase in heatwaves' frequency, duration, and severity will be even more detrimental for urbanites, with significant suffering and penalties in medical spending, electricity bills, and catastrophe compensation [10,11]. The combined impact of these local, regional, and global climatic changes has recently gained increasing interest, and multiple studies have documented their influence, either individually or holistically.

Extreme heat occurrences put urbanites at higher thermal risk. The impact of heatwaves on human health is devastating and is one of the leading causes of climate-related mortality and morbidity worldwide [16,18]. Summer heatwaves have been identified as Australia's deadliest natural hazard [17]. During heatwaves in the United States, a 7.9 percent increase in daytime mortality and a 2.2 percent increase in nighttime mortality were documented for every one °C increase in temperature [31,32]. During the 2003 extreme heat events in Europe, over 70,000 people died, with France, Italy, and Spain accounting for more than a third of all deaths [33]**.** Further, during such intense heat events, the elderly, women, children, those with chronic conditions, and low socioeconomic status have been at higher thermal risk [34]. In Sydney, elderly and female mortality rates increased dramatically during heatwaves [34,35], and an additional 13 percent of deaths were reported in the summer of 2011 [36]. Heatwaves have also been identified as one of the leading causes of climate-related hospitalization worldwide [16]. Aside from hyperthermia (heat stroke, heat cramps, and exhaustion) and respiratory illness, life-threatening conditions such as heat-related cardiovascular disease (CVD), including myocardial infarction, were reported to occur more often during such intense heat events [37,38].

The combined impact of climate change also adversely affects cooling energy consumption and peak power demand. Between 1970 and 2010, the average increase in buildings' cooling demand under the combined impact of UO and global climate change was around 23 percent, while the average decrease in heating demand was 19 percent [29]. Sydney's extreme temperatures resulted in a 29 to 86 percent increase in cooling energy demand for typical residential, school, and office buildings [39]. By 2050, the cooling energy consumption of residential and commercial buildings is expected to increase by 275 percent and 750 percent globally, respectively [21]. Similarly, In various cities worldwide, an extra increase of 0.45 to 12.3 percent in peak electricity consumption was also documented with every one °C rise in temperature under the combined effects of UO and global climate change [29]. The elevated temperatures during extreme heat events may also reduce the power plant efficiency. The combined impact of UO and global climate change was reported to reduce power plant efficiency by 0.6 to 2.0 percent for every one °C increase in temperature [40]. During extreme heat events, the power plant's lower efficiency will raise the electricity cost, which will also be remunerated by the urbanites in addition to extra air conditioner usage expenses. Further, running power plants for an extended period during extreme heat events will also worsen atmospheric pollution, consequently raising regional temperatures and promoting the airconditioning (AC) usage. A projected rise in heatwave frequency and severity, as well as an increase in cooling energy, and peak electricity demand along with a decline in power plant efficiency, would place additional strain on electric systems during heatwaves, resulting in more blackout periods [41]. During these blackouts, the low-income population and individuals with health-related difficulties will be especially susceptible.

The NO_X and volatile organic compounds (VOC) from industrial and vehicular exhaust react chemically with heat and sunlight to form ozone- a hazardous pollutant to human and environmental health. High temperatures promote ozone formation during heatwaves and adversely affect the environmental quality [42]. During heatwaves, the ozone concentration was reported to rise by 9.6 to 20 percent [22,23]. Similarly, it was also reported that due to a one °C increase in outdoor temperature, the frequency of days above the Ozone concentration threshold increased by 10 percent [24]. The combined impact of enhanced ozone formation during heatwaves and post-heatwave pollutant transportation (owing to coastal wind activation) was documented in western Sydney, resulting in a considerable rise in ozone levels [43]. Further, higher ozone levels were also linked to more hospitalizations (760 hospital admissions in Sydney in 2007 owing to respiratory infections) and premature deaths (160 premature deaths in Sydney in 2007) [44,45]. Several studies have also studied the influence of heatwaves on financial losses. The cost of crop failure in Europe during the summer of 2003 heatwaves was estimated to be over US$ 12.3 billion [26]. In Australia, about A$ 40 billion in the financial loss was anticipated during the 2019-20 bushfire season, which destroyed around 20 million acres, caused over 0.5 billion animal deaths, and killed roughly 33 people [27].

1.2 Research gaps:

The synergistic interactions between local, regional, and global-scale weather conditions have never been studied. How local conditions affect the regional and global atmospheric conditions and vice versa is an open question. A few studies have examined the impact of heatwaves, meteorological conditions, or weather conditions on UO; however, how the multiple levels of climatic conditions synergistically interact and affect the built environment has never been investigated.

Further, there is no consensus on the variation of UO magnitude during heatwaves, and the synergies between both phenomena are also investigable [31,46–52]. Heatwaves have the potential to amplify UO magnitude [31,41]. Independent studies conducted at various locations have reported conflicting estimations of the shift in the extent of UO during heatwaves. An exacerbation of UO magnitude during heatwaves was documented in the studies conducted in the United States [53] and 70 European cities [54,55]. Other studies, on the other hand, reported a decline in UO magnitude during extreme heat events in 54 US cities [56], 89 Indian cities [57], Perth, Australia [58], and Prague, Czech Republic [47]. No UO magnitude variations were also reported during heatwaves in Philadelphia, USA [59]. Varying responses to diurnal variations in UO magnitude during heatwaves were also reported. For instance, an exacerbated daytime UO magnitude during heatwaves was recorded in New York [59], Karachi [46], Shanghai [51], Nicosia [60], and Athens [50], while amplified nighttime UO magnitude during heatwaves was also documented in Oklahoma [61], Bucharest [49], Berlin [62], Melbourne [63], Adelaide [58], Washington, DC; Baltimore [41], Beijing [48], and Athens [64]. The inconsistent responses might be attributed to variations in meteorological conditions (wind patterns, radiative input), different boundary conditions, and varying methods of UO estimation and heatwaves identification.

The key contributors affecting the UO magnitude during heatwaves are also investigable. Contrasting responses were reported while identifying the major synergistic interactions between UO and heatwaves. Some studies reported variation in convective heat fluxes as a critical interaction, altering the available energy balance at urban and rural settlements in the form of sensible and latent heat fluxes [60,65]. Other studies reported advection from the coastal winds as a primary contributor affecting UO during heatwaves [66,67]. Enhanced anthropogenic fluxes [31,51] and variation in heat storage fluxes [48,63] during heatwaves were also concluded as major synergistic interactions between UO and heatwaves. The sensible heat and storage heat fluxes might be more pronounced in urban settings during heatwaves due to the surfaces with higher thermal inertia, which allows them to store more energy during the day and release it at night [59]. Further, a significant amount of available energy in urban settings is partitioned into the sensible heat flux due to a lack of surface moisture [68,69]. Rural surfaces, in contrast to urban surfaces, have a higher capacity to retain moisture, which might result in a higher evaporative/ latent cooling during heatwaves [70]. During heatwaves, the varying evaporation rates in urban and rural settings might disrupt the available energy balance and intensify UO [31]. Precipitation is particularly crucial in maintaining the surface latent cooling capacity in rural settings; otherwise, in the absence of soil moisture, the synergies between UO and heatwaves may diminish [71]. In Nicosia, the evaporation of dew formed on urban and rural surfaces during heatwaves exacerbated the UO magnitude [60].

Heatwaves are generally associated with low wind speed, linked to high-pressure anticyclonic systems. Low wind speeds might result in less advective cooling from the adjacent non-urban region in urban settings, enhancing the UO magnitude during heatwaves [41]. Amplification in the thermal storage heat flux was also documented during heatwaves, attributed to low-wind speed [70]. In proximity to water bodies such as the ocean, the advective heat flux might also become a crucial component that may affect UO [72]. The coastal regions are swiftly cooled due to the activation of coastal winds caused by secondary air circulation (higher surface temperatures during heatwaves relative to stable sea surface temperatures) [51]. Distance from the coast in a coastal city might also play an important role in UO intensification during heatwaves. Some studies imply that distance from the coast may interfere with UO during heatwaves [72], while others find that coastal breezes do not influence UO [58]. During heatwaves, increased anthropogenic heat flux in the form of excessive heat emitted by air conditioning units or from fuel-intensive power production plays an essential role in amplifying UO [51,73]. The UO magnitude may also be affected by population density (PD). PD was shown to have a favorable connection with UO during heatwaves in Madison, USA [53], but the PD was concluded to not affect UO during heatwaves in Europe [54].

In the context of interactions between UO and large-scale weather patterns, the associations between meteorological variables and UO has been widely researched. Regional wind speed and cloud cover, for example, have been identified as the most important meteorological variables influencing UO by modifying the region's ventilation and insolation conditions [74]. Regional wind speed and cloud cover are thought to have an inverse association with UO as a rule of thumb, and the magnitude of the association between UO and meteorological factors varies by location [75]. Depending on the urban layout, increased regional wind speed (wind flow from high-pressure rural to low-pressure urban zones) lessens the UO magnitude [41,75,76]. Similarly, longwave radiative losses at urban and rural surfaces are minimized under cloudy conditions at night, lowering the urban-rural thermal gradient. In contrast, under cloudless conditions, rapid radiative cooling in rural regions and longwave emission in urban fabric from daytime heat storage aggravate the urban-rural temperature imbalance at night [63,77,78].

The association between large-scale weather patterns and UO, which may seriously influence the local climatic conditions, has never been investigated during heatwaves. While exploring the relationship between UO and large-scale weather patterns during normal summer conditions, various classifications, including circulation-pattern-based classification (CPC) [75,79,80] and multivariate weather-typing classification (WTC) [81–83], have been utilized. In circulation-pattern-based classification, anticyclonic conditions were often linked with clear skies and intense solar radiations, whereas cyclonic conditions were mainly associated with cloudy conditions [84]. More into it, anticyclonic conditions, low wind speed, and a lower cloud cover fraction were connected with aggravated UO in Melbourne [75], Buenos Aires [79], Birmingham [80], Poznan [74], Debrecen [85], Szeged [84], and Athens [86]. Contrarily, in Poznan [74] and Szeged [84], cyclonic conditions were significantly associated with reduced UO magnitude or with urban cooling (UC). In multivariate WTC, mostly, dry weather types (WTs) in general [82], and dry tropical WTs in particular, were found to be responsible for aggravated nighttime UO as reported in Atlanta [81] and northeastern states in the USA (Baltimore, Philadelphia, New York) [87], and Phoenix [83]. However, under wet WTs, greater ambient temperatures were found in both urban and rural areas in the northeast United States [87]. The lower mean UO in multivariate WTC was associated with moist-polar WT, as concluded in Atlanta [81]. More into it, a link was found between dry WTs and clear and calm meteorological conditions [83,87], whereas a link between wet WTs and cloudy meteorological conditions was also reported [84].

Multiple studies have examined the independent impacts of UO, heatwaves, or future climatic conditions on the built environment. However, the combined impact of local, regional, and global climatic changes on the built environment has never been studied. Further, most studies ignored the microclimatic context while investigating the buildings' thermal performance, which may seriously affect the buildings' thermal response to climatic changes. Under the impact of UO on the built environment, some studies reported an increase in cooling needs [20,88,89], whereas others reported a decline in cooling and total energy [90]. Further, the impact of UO on indoor thermal comfort is also largely unexplored. Similarly, while assessing the impact of heatwaves on buildings' thermal performance, a few studies concluded an increase in cooling needs [91], whereas others reported lower energy needs during heatwaves than on typical summer days [92]. Contrasting results have also been reported when comparing the thermal performance of insulated buildings with uninsulated buildings during heatwaves. A few studies reported that insulated buildings might cause overheating during heatwaves and negatively affect the cooling energy consumption [93], whereas others concluded insulated buildings perform better than existing building stock during extreme heat conditions [94].

1.3 Research aims and questions:

The dissertation aims to examine the interactions between local, regional, and global climatic changes and investigate their combined impact on the built environment. The dissertation was stratified into three main sections, and research objectives were defined accordingly. The main scientific problems addressed in the dissertation are as follows:

Problem statement-1: How does the local-scale UO interact with large-scale weather patterns and affect the communities? The main objectives while addressing the problem were:

1. To investigate the variations in large-scale weather patterns over the year and comprehend which weather types (WTs) have occurred more frequently.
2. To evaluate the spatiotemporal variations in UO magnitude (variations in UO magnitude over the year, seasonal variations, and variations at multiple locations within the city).
3. To comprehend the impact of various air masses according to their geographical characteristics.
4. To investigate the association between UO and large-scale weather patterns:
    - **4.1.** To investigate the WTs causing the maximum 5 percent of UO magnitude over the years (for more than 15 years).
    - **4.2.** To investigate the WTs causing the minimum 5 percent of UO magnitude over the years.
    - **4.3.** To investigate the association between seasonal variations in UO magnitude and large-scale weather patterns.
    - **4.4.** To investigate the association between diurnal variations in UO magnitude and large-scale weather patterns.
    - **4.5.** To investigate the association between UO magnitude during heatwaves and large-scale weather patterns.

Problem statement-2: How does local-scale UO interact with regional-scale heatwaves and affect the communities? The main objectives while addressing the problem were:

1. To investigate the variation in UO magnitude during heatwaves, compared to the background conditions, and examine if synergies exist between both phenomena (positive, negative, or no change).
2. To investigate the key contributor affecting UO magnitude during heatwaves by utilizing the surface energy budget.
    - **2.1.** To analyze the impact of convective phenomena (sensible, latent heat fluxes) on UO during heatwaves compared to background conditions.
    - **2.2.** To analyze the impact of advection on UO during heatwaves compared to background conditions.

- **2.3.** To analyze the impact of land-coastal distance on UO during heatwaves, compared to background conditions.
- **2.4.** To analyze the impact of site characteristics (potentially plantable surfaces, tree canopy cover, etc.) on UO during heatwaves, compared to background conditions.
- **2.5.** To analyze the impact of Population density on UO during heatwaves, compared to background conditions.

Problem statement-3: How does the built environment respond to the combined impact of local, regional, and global climatic changes? The main objectives while addressing the problem were:

1. To investigate the impact of local-scale UO on urban cooling energy, indoor temperatures, and passive survivability.
2. To investigate the impact of regional-scale heatwaves on urban cooling energy, indoor temperatures, and passive survivability.
3. To investigate the synergistic impact of UO, heatwaves, and large-scale weather patterns on urban cooling energy, indoor temperatures, and passive survivability.
4. To investigate the impact of urban density on urban cooling energy, indoor temperatures, and passive survivability under the influence of climate changes.
5. To investigate the spatiotemporal variations in urban cooling energy, indoor temperatures, and passive survivability under the influence of climate changes.
6. To investigate the impact of various adaptation and mitigation measures under the influence of climate change.
7. To investigate the appropriateness of national construction codes (NCC) and examine how NCC thermally regulated buildings perform under the combined impact of climate change.

1.4 Thesis Structure:

The dissertation has been arranged into three main sections, based on problem statements, comprising nine chapters, as illustrated in Figure 1-1.

Chapter 1 briefly introduces UO, heatwaves, large-scale weather patterns, and their adverse impacts on human health, energy, environment, and economy. Further, it discusses the synergistic interactions between UO and large-scale weather patterns and presents the research gaps in the literature. Afterward, the chapter provides an overview of the interactions between UO and heatwaves and highlights the inconsistencies in the literature. Later, it presents the irregularities in the literature on the impact of climate change on the built environment. Subsequently, it presents the research gap, problem statements, and dissertation's main objectives.

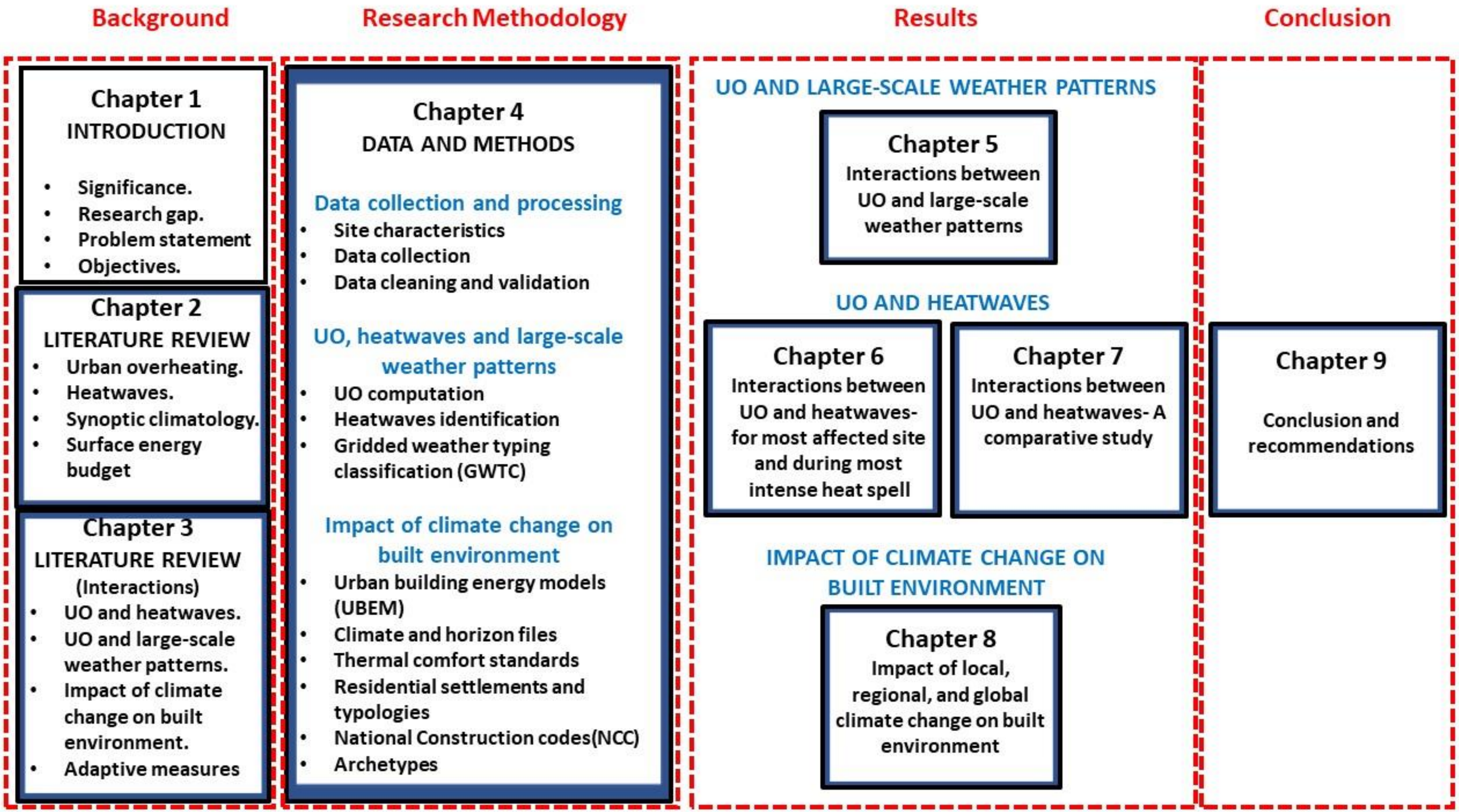

Figure 1-1 Thesis structure

Chapter 2 comprehensively reviews the fundamentals of UO, heatwaves, and large-scale weather patterns. Further, it discusses the causes and quantification/ identification methods of these multiscale climatic change phenomena. Finally, the surface energy budget equation and the primary components of the equation were discussed.

Chapter 3 has been arranged in three main sections. The first section reviews the synergies between UO and heatwaves and discusses the key contributors affecting UO magnitude during extreme heat conditions. In the second section, synergies between UO and large-scale weather patterns have been discussed. The last section covers the impact of these multiscale climate changes on the built environment.

Chapter 4 delineates the data and method section of the dissertation. Firstly, a brief was presented about the sites studied in the project- locations, site characteristics (tree canopy cover, potentially plantable surfaces, population densities, etc.). Afterward, data acquisition, data cleaning, and validation procedures were discussed. Subsequently, the methods used in the dissertation were described, including i) heatwaves identification, ii) UO computation, iii) multivariate weather typing classification, and utilization of Gridded weather typing classification, and iv) urban building energy models and tools selected for building's thermal performance evaluation. Further, the procedures to develop the climate and horizon files for energy simulation were discussed. Later, the thermal comfort standards and selected residential settlements were discussed. National construction codes (NCC) related to building thermal performance and compliance criteria were explained afterward. Details about the thermophysical characteristics of the existing building stock and the characteristics proposed in current regulations were discussed.

Chapter 5 elucidates the variation in UO magnitude over the years. Further, it investigates the variation in the frequency of large-scale weather patterns over time. Afterward, the association between UO and large-scale weather patterns during heatwaves, normal summer conditions, and other seasons was discussed.

Chapter 6 examines the synergies between UO and heatwaves during the most intense heatwave spell for the most affected location in the city. Further, it investigates the energy budget response to extreme heat conditions to identify the key contributor exacerbating UO during heatwaves.

Chapter 7 comparatively analyzed the UO response to heatwaves at multiple locations in the city to comprehend the spatiotemporal variations in UO magnitude during heatwaves. In addition to energy budget response evaluation, the impact of land-coast distance, site characteristics, and population density were also evaluated on UO magnitude during heatwaves.

Chapter 8 assesses the combined impact of local, regional, and global climatic conditions on urban cooling energy and indoor comfort. Further, sensitivity analyses were performed to evaluate the impact of various adaptive measures, and subsequently, the combined impact of the most suitable adaptive measures was gauged during extreme heat conditions. Further, the building's thermal performance according to current national thermal regulation was also examined under the impact of climate change, and the remediation in the policies was proposed.

Chapter 9 summarizes the dissertation's key findings and elucidates the contributions to knowledge, thesis limitations, and future directions. The chapter gives concise responses to the research questions stated in Chapter 1 and in other chapters in which the research issues are addressed in greater detail. The research implies how the combined impact of the local, regional and global conditions is essential to address global warming issues and design thermally resilient cities.

CHAPTER 2: URBAN OVERHEATING, HEATWAVES, AND SYNOPTIC CLIMATOLOGY

This chapter discusses UO, its primary causes, and the commonly used quantification methodologies in the literature. Similarly, heatwaves, their types, and approaches for identifying them have been reviewed. Later, the principles of synoptic climatology and synoptic classification systems, often used in urban-climatological or bioclimatological investigations, were presented. Lastly, the surface energy budget components were discussed, which can potentially influence the local, regional, and global climatic conditions.

2.1 Urban overheating (UO):

Generally, cities are hotter than their rural counterparts, attributed to UO [95]. UO is one of the most-reported climate change phenomena, with over 400 cities worldwide affected by it [4]. According to United Nations (UN) 2018 population estimates, cities are home to 55 percent of the global population, with that number anticipated to rise to 68 percent by 2050 [96]. Further changes in land surface features will significantly impact the local and global temperatures and affect the communities.

2.1.1 UO causes:

UO is generally caused by i) variations in land cover and land use (LCLU) type, including altered surface characteristics, greenery ratio, tree canopy cover, etc. ii) variation in the city's configuration, including size, geometry, topography, geographical location, distance from the water bodies, continentality, orography, population density, etc. iii) variations in anthropogenic emissions, mainly from buildings, industries, and transportation sector and iv) variations in meteorological conditions, including precipitation, wind patterns, cloud cover, etc.

The principal contributor to the thermal imbalance between urban and peripheral areas is modified urban surfaces (Figure 2-1). Specifically, thermal emissivity, solar reflectance, and heat storage capacity are the prominent surface characteristics determining urbanization's impact. Due to greater thermal inertia, construction materials, including concrete, asphalt, etc., often have a greater thermal storage capacity. Consequently, urban surfaces absorb more heat during the day and release it at night [97]. Likewise, thermal emissivity is the metric used to quantify the emission of longwave radiation from the surfaces. Surfaces with a higher thermal emissivity radiate heat more rapidly, remaining cooler. Solar reflectance, also called albedo, determines the proportion of solar radiation that the surface reflects. Darker urban surfaces reflect fewer radiations and have lower solar reflectance.

The urban fabric's fewer vegetation and permeable surfaces hinder evaporation and evapotranspiration rates, contribute to the rapid run-off of precipitation, and raise the ambient temperature. The moisture released in the air by plants or porous surfaces through evaporation and evapotranspiration (in the form of latent heat flux) contributes to the dissipation of ambient heat [69,97]. Furthermore, attributable to the photosynthesis process, plants convert fewer incident radiations into heat energy, reducing the sensible heat flux. According to a study, every 10 percent growth in vegetated surfaces can reduce surface temperatures by 1.3°C [98]. In addition to limited vegetated and porous surfaces, reduced tree canopy cover in the urban fabric is another prominent factor. Higher tree canopy cover typically improves evapotranspiration rates and provides shading, further reducing ambient temperatures [99]. Additionally, trees were found to offer higher evapotranspiration rates than grassland.

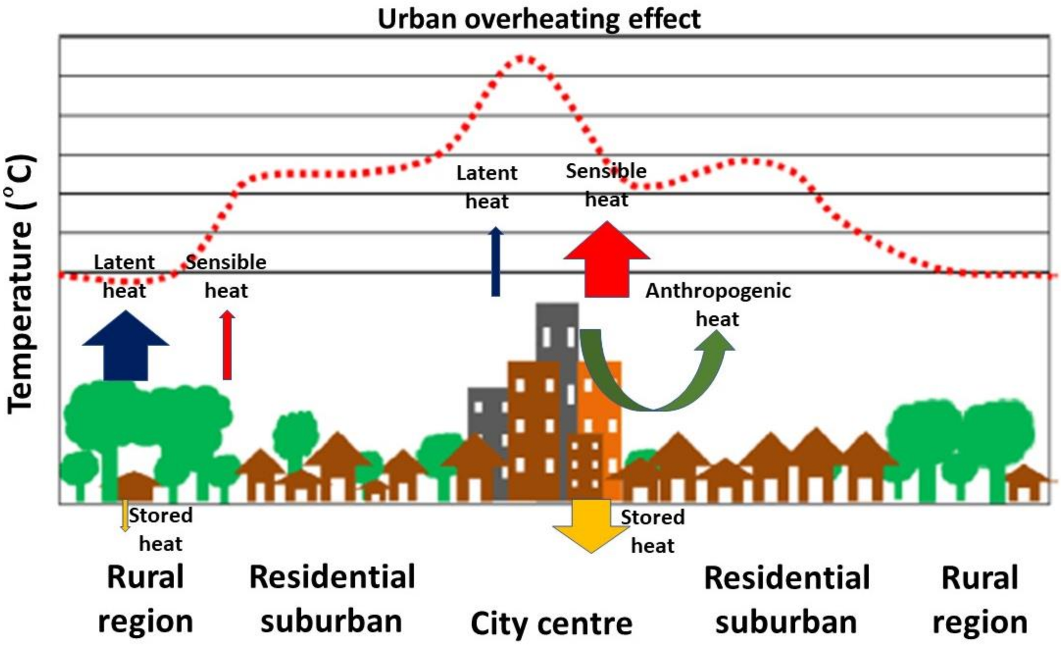

Figure 2-1 Temperature/ energy balance variations in urban and rural counterparts. Image reproduced from [100]

Urban geometry also critically influences UO intensity. The wind patterns and nocturnal longwave emission are affected by building height, aspect ratio (building height to street width), street orientation, and urban roughness [101]. Multiple reflections increase shortwave radiation's absorption and longwave radiation reabsorption in complex urban geometry [97]. Anthropogenic heat released in the urban areas as a result of human activities, such as heating and cooling of buildings, transportation, and manufacturing (exhaust from vehicles and industrial plants), not only exacerbates the UO [73,102] but also contributes to the pollutant formation [103]. Air pollutants influence incoming shortwaves and enhance the absorption of reflected longwave, intensifying ambient temperatures [104]. The UO intensity is also influenced by the city's topography (e.g., mountainous or plain region), elevation [72], location (e.g., coastal or non-coastal), size (e.g., compacted or sprawl city) [105], and population density [54].

The impact of meteorological conditions on UO is also quite evident. Precipitation, cloud cover, and relative humidity are all believed to reduce the UO magnitude, whereas clear (cloudless) and calm (low-winds) conditions exacerbate the UO magnitude. Further, while investigating the impact of wind patterns on UO, it was concluded that moderate winds increase the cooling rates in urban areas by improving the secondary air circulations, consequently reducing UO [106]. However, the effect of increasing wind speed on UO is conflicting, as some studies concluded a decrease in cooling rate in urban areas with an increase in wind speed over 3 m/sec [102], whereas others reported homogenization and reduction in urban temperature with wind speed greater than 6m/s [107].

2.1.2 UO quantification methods:

Typically, urban-rural/suburban thermal contrast (UO = T_{urb} - T_{rural}) estimates UO. The UO is computed using near-surface or land surface temperatures (LST). The near-surface temperatures (ambient temperature) are primarily obtained from meteorological/ground stations [51,58,62,108], whereas the LST dataset is either derived from satellite data (remote sensing) [52,54,57], or processed by the weather research and forecasting (WRF) models coupled with land-use data [41,63,109]. Surface UO is generally greater than the UO computed at 2m height [110]; nonetheless, UO at 2m height is regarded as more significant since it directly impacts thermal comfort. Several temperature expressions are used to determine the UO. For instance, UO magnitude has been estimated using hourly temperatures [50,60], daily maximum or minimum temperature [56,57], daily average temperature [62,109], daytime and nighttime average temperatures [41], and monthly average temperature [54].

The urban increment approach is also used to estimate the UO [111]. The urban increment method considers the city's spatial extension and computes the temperature differential between the controlled and experimental scenarios. All urban surfaces are substituted with rural surfaces in the experimental case, whereas the original city case serves as the controlled case [112]. Similarly, in another method, the composite urban temperatures (all urban stations' average temperature) and the composite rural temperatures (all rural stations' average temperature) are also utilized to compute the UO to account for the spatial extension of the city [61,75].

The heat-humidity index (Humidex-HD) also quantifies the urbanization effect in terms of heat stress [61,64]. The Humidex-HD delivers a degree of comfort while considering the combined impact of temperature and humidity. The universal thermal climate index (UTCI) is another energy balance stress metric that considers the human body's heat exchange and thermo-physiological characteristics; while using ambient temperatures, humidity, wind speed, and mean radiant temperature [64]. In coastal cities, the humidity index is a better metric for estimating the UO effect [55].

2.2 Heatwaves:

Heatwave is a regional phenomenon often ascribed to large-scale stagnant high-pressure systems that draw warm air from the troposphere and cause elevated regional temperatures [41]. Heatwaves have grown in frequency and intensity over several decades [113], and trends are anticipated to escalate in the twenty-first century [114,115]. Based on intensity, heatwaves are categorized into three main types, i) low-intensity heatwaves, ii) severe heatwaves, and iii) extreme heatwaves [116]. Low-intensity heatwaves are more common during summer and can easily be coped with by a large population. Severe heatwaves are comparatively less frequent but may adversely affect the vulnerable population. Extreme heatwaves are rare but may involve a large population segment if precautions are not taken, irrespective of their health condition. Figure 2-2 depicts the temperature fluctuations during one of the extreme heatwaves in Australia in February 2017.

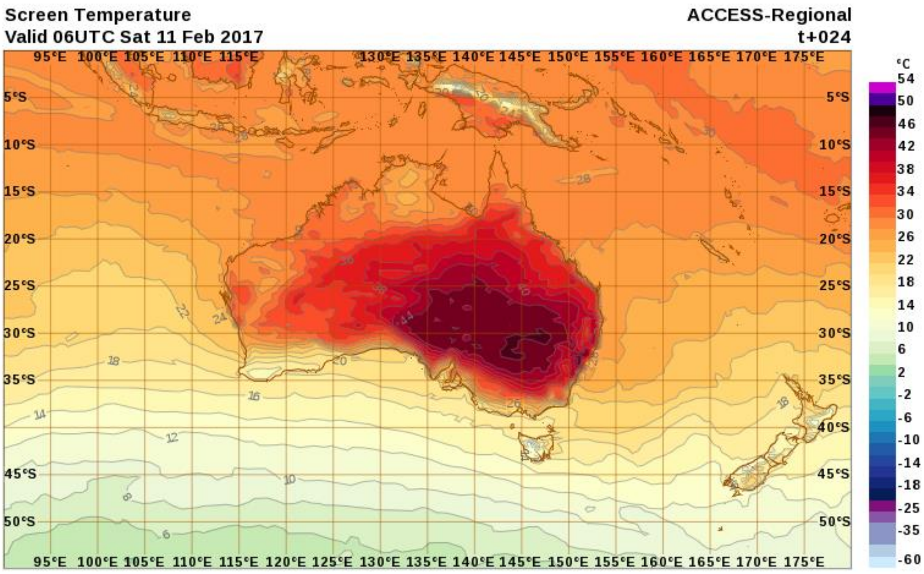

Figure 2-2 Australia's temperature (°C) variations during one of the most intense heatwave days (11th February 2017) in recent decades. Image source: Australian Bureau of Meteorology (BOM) [117].

2.2.1 Heatwaves identification methods:

People respond differently to intense heat events, and their responses differ depending on their geographical locations. There is no unified definition of heatwaves because of differential thermal adaptation in various regions and differing heatwave impacts in several sectors, including health, energy, and bushfire control [7]. Furthermore, there is no consensus on whether heatwaves are exclusively a summer phenomenon or can happen in other seasons, and as a result, several indexes exist [113]. However, three criteria are deemed critical for understanding the phenomenon: i) threshold temperature, ii) duration of the extreme heat events, and iii) the geographical extension of the city where the regional-scale phenomenon occurs [113,118,119]

In literature, various metrics, including absolute temperature threshold (ATT) [51,53] and relative temperature threshold (RTT) [58,60], were used to establish the threshold temperature. A fixed temperature was used in the ATT metric, whereas percentile-based temperatures were calculated in the RTT metric to determine the threshold temperature. Unlike the ATT metric, the RTT metric may account for spatiotemporal variation since the calculations are based on a specific time and location [113]. Further, temperature expressions such as daily maximum temperature (T_{max}) [50,60] and/or daily minimum temperature (T_{min}) have been used to define the threshold temperature [56,57]. For instance, T_{max} greater than or equal to 32.2 °C [59], 35 °C [51], or 37 °C was defined as threshold temperature using the ATT metric, which primarily represents thermal stress during the daytime. Additionally, a daily minimum temperature greater than or equal to 20 °C was considered as the threshold temperature when using the T_{min} in ATT metric, primarily representing thermal discomfort at night [120].

Using the RTT metric, threshold temperature was defined as T_{max} higher than or equal to the 90th percentile [62], 95th percentile [60], or 97.5th percentile [48,70] of the daily maximum temperature. Similarly, when using T_{min} in the RTT metric, the threshold temperature was determined to be larger than or equal to the 90th percentile [121] or 95th percentile [56] of the daily lowest temperature. Some studies have employed dual criteria to determine the temperature threshold [70,111,122]. For example, in a study, heatwave days were counted as the average number of days with T_{max} greater than 35 °C and T_{min} greater than 20 °C [123]. Similarly, a multiple threshold index was also employed to define the threshold temperature. For example, in a study, only days that met the following criteria were regarded as heatwaves: i) T_{max} exceeding 97.5th percentile for at least three days in a row, ii) average T_{max} exceeding 97.5th percentile for the entire period, and iii) T_{max} exceeding 81st percentile for each day of the heatwave [7].

Upon analyzing various temperature expressions, it was determined that T_{min}-based heatwaves might be appropriate for agricultural research, where the daily minimum temperature may significantly impact the plant's growth [113]. In contrast, T_{max}-based heatwave might be advantageous for engineering studies, such as UO, electricity, and transportation systems, whereas the combined effect of T_{min} and T_{max} might be more beneficial in health-related studies. Similar to the temperature thresholds, there is also a lack of agreement on heatwave duration. The minimum duration for heatwaves in the United States was two consecutive days and two to five consecutive days in Europe and Australia [113,124]. Several studies, however, have counted three days in a row as the minimum duration for a heatwave spell [7,113,123]. Because heatwave is a regional-scale phenomenon, the city's geographical extension must also be considered. Increased anthropogenic heat may raise local temperature; hence, evaluating those spells coinciding in multiple zones of the region is critical. Excessive heat factor (EHF), which is the combined effect of excess heat (EHI_{sig}), and heat stress (EHI_{accl}), is also used to define heatwaves [124]. This index considers the intensity, duration, and spatial distribution of heatwaves. Furthermore, this index is characterized by both expressions-daily maximum and daily minimum temperatures.

$$\mathrm{EHF} = \max[1, \mathrm{EHI(accl.)}] \times \mathrm{EHI(sig.)} \tag{1}$$

Excessive heat (EHI_{sig}) symbolizes the excessive heat from the amplified daytime temperatures, which is not emitted at night due to higher nighttime temperatures. EHI_{sig} is defined as three-days temperature anomalies compared to the extreme temperature threshold (T_{95}- 95th percentile temperature for the study period). The average daily temperature, T_i, for a given day "I" is calculated as the mean of T_{min} and T_{max} over the 24 hours cycle, as shown in the equation.

$$\mathrm{EHI(sig.)} = [(T_i + T_{i-1} + T_{i-2})/3] - T_{95} \tag{2}$$

Heat stress (EHI_{accl}) calculates the temperature deviation relative to the recent past. Typically, three-days temperature deviations are compared to the preceding 30 days' temperature [124]. In addition to the i-day, the effect of two previous days (i-1 and i-2) are accounted for in both equations. Furthermore, the EHF must be positive for (i, i+1, and i+2) to be considered a heatwave.

$$\mathrm{EHI(accl.)} = [(T_i + T_{i-1} + T_{i-2})/3] - [(T_{i-3} + \ldots + T_{i-32})/30] \tag{3}$$

Heatwaves are also identified by Humidity Index (HI)/ Apparent temperature (AT). This index considers a few consecutive days with a daily maximum HI greater than 65 °C as heatwaves [46,60]. Because the index considers temperature and humidity parameters, it is more useful in cities where moist large-scale weather patterns are more prevalent [111,125]. The following equation can be used to calculate HI.

$$\mathrm{AT} = c_1 + c_2\mathrm{T} + c_3\mathrm{RH} + c_4\mathrm{TRH} + c_5\,\mathrm{T}^2 + c_6\,\mathrm{RH}^2 + c_7\mathrm{T}^2\mathrm{RH} + c_8\,\mathrm{TRH}^2 + c_9\,\mathrm{T}^2\mathrm{RH}^2 \tag{4}$$

$$c_1 = -42.379; c_2 = 2.04901523;\ c_3 = 10.14333127;\ c_4 = -0.22475541;\ c_5 = -6.83783\text{x}10^{-3};\ c_6 = -5.481717\text{x}10^{-2};\ c_7 = 1.22874\text{x}10^{-3};\ c_8 = 8.5282\text{x}10^{-4};\ c_9 = -0.199\text{x}10^{-6}, and\ temperature\ is\ in\ \text{Fahrenheit}$$

2.3 Synoptic climatology:

The local and regional scale climate study that fundamentally examines the properties and behavior of the atmosphere over a specific region is known as synoptic climatology. The weather patterns are observed at a horizontal length scale of 1000 km or above (approximately 4000 km) in the synoptic scale, also known as the large-scale or cyclonic scale. Global circulation patterns are created by the uneven distribution of solar radiations around the sphere, which drive large bodies of air known as air masses [12]. These airmass extends throughout the troposphere and has uniform thermal and humidity properties in any horizontal direction and at a given altitude. Its formation place dictates the features of an airmass. However, the airmass's characteristics may alter as it travels between locations. Fronts are formed when two air masses with contrasting characteristics collide [126]. When the lightweight warm airmass hits the static heavyweight cold airmass, warm fronts form. In the warm fronts, warm airmass moves upward after colliding with cold airmass, forming horizontal clouds. Contrarily, when cold airmass collides with lightweight static warm airmass, the warm airmass' vertical movement becomes steeper, and vertical clouds form. The phenomenon is referred to as a cold front [126].

In the absence of earth rotation, for example, if the earth were stationary, air would have circulated from the high-pressure (HP) poles to the low-pressure (LP) equator. However, due to the earth's rotation, the circulating air deflects to the right in the northern hemisphere and to the left in the southern hemisphere [126]. This phenomenon is referred to as the Coriolis effect. In terms of cyclonic and anticyclonic circulations, vertical upward or downward airflow is defined. A cyclonic circulation is an LP system where winds from the outer HP side rotate to the inner LP side due to the Coriolis effect, i.e., convergence at the surface and divergence at the upper level [126]. The rotation of cyclones is clockwise in the southern hemisphere and anticlockwise in the northern hemisphere due to Coriolis forces. In cyclonic movement, warm ground air rises due to convergence, cools upon reaching a higher altitude, and releases moisture, forming clouds. The anticyclonic phenomenon is the reverse of cyclonic. In anticyclonic conditions, winds diverge outside the LP zone from the central HP zone at the surface [127]. As a substitute, the converging winds in the upper atmosphere descend to the surface, become warmer as they descend, absorb moisture, and produce clear sky conditions. Due to the Coriolis effect, anticyclonic circulations are clockwise in the northern and anticlockwise in the southern hemispheres.

2.3.1 Classification:

In bioclimatological or urban-climatological research, both, circulation-pattern-based classification (CPC) and weather typing classification (WTC) have been used [9,128,129]. CPCs are based on pressure patterns and have been investigated and used more in Europe [130,131]. On the other hand, WTCs are based on atmospheric conditions and have been more developed and used in the United States [132–134]. In addition, various approaches have been used in urban climatology to explore the relationship between surface temperature and large-scale weather patterns, such as circulation-to-environment [80,87] and environment-to-circulation [75]. The UO dataset is arranged according to large-scale weather patterns in the circulation-to-environment approach, whereas large-scale patterns are organized according to UO groups in the environment-to-circulation approach.

In CPC, large-scale weather circulations were categorized based on directional (wind flow) and non-directional (cyclonic and anticyclonic circulation) characteristics. Thirteen large-scale circulations were established in Szeged-Hungary based on cyclonic and anticyclonic movements [84], and both environment-to-circulation and circulation-to-environment approaches were applied. Similarly, the Niedzwiedz calendar, which includes twenty-one cyclonic and anticyclonic circulation types, was used in Poznan, Poland [74]. In Athens-Greece, atmospheric circulations were distinguished into eight a priori categories at 850-hPa, using the five parameters: equivalent potential temperature, temperature, wind speed, wind direction, and geopotential height [86]. Eleven Lamb weather types were utilized to characterize the large-scale circulations in Birmingham, including two non-directional (anticyclonic and cyclonic), eight directional types (wind flows), and one unclassified type [80]. In Melbourne, using the environment-to-circulation approach, mean sea level pressure (MSLP) charts for each UO group were compared with average monthly conditions to determine large-scale daily circulations [75].

Large-scale weather patterns are mostly classified into daily airmasses in WTC. The most significant WTC classifications are spatial synoptic classification (SSC) [133], and Gridded weather typing classification (GWTC) [134,135]. In both WTCs, temperature and humidity are partitioned to generate daily weather patterns using meteorological variables such as ambient temperature, dew point temperature, mean sea level pressure, wind direction, wind speed, and cloud cover. The SSC was initially classified into six [132] and then into seven weather types (WTs) [133]: dry polar (DP), dry moderate (DM), dry tropical (DT), moist polar (MP), moist moderate (MM), moist tropical (MT), and transitional (TR), as shown in Table 2-1, based on the traditional WTC- continental polar (cP), maritime polar (mP), continental tropical (cT), and maritime tropical (mT).

Table 2-1 Definition of airmasses in Spatial synoptic classification (SSC) available at [136].

Sr No.	Airmass	Definition
1	Dry Polar (DP)	is synonymous with the traditional cP air mass classification. This air mass is generally advected from polar regions around a cold-core anticyclone and is usually associated with the lowest temperatures observed in a region for a particular time of year, as well as clear, dry conditions.
2	Dry Moderate (DM)	air is mild and dry. It has no traditional analog but is often found with the zonal flow in the middle latitudes, especially in the lee of mountain ranges. It also arises when a traditional air mass such as cP or mT has been advected far from its source region and has thus modified considerably.
3	Dry Tropical (DT)	weather type is similar to the cT air mass; it represents the hottest and driest conditions found at any location. There are two primary sources of DT: either it is advected from the desert regions, such as the Sonoran or the Sahara Desert, or it is produced by rapidly descending air, whether via orography (such as the chinook) or strong subsidence.
4	Moist Polar (MP)	air is a large subset of the mP air mass; weather conditions are typically cloudy, humid, and cool. MP air appears either by inland transport from a cool ocean or due to frontal overrunning well to the south of the region. It can also arise in situ as a modified cP air mass, especially downwind of the Great Lakes.
5	Moist Moderate (MM)	is considerably warmer and more humid than MP. The MM air mass typically appears in a zone south of MP air, still in an area of overrunning but with the responsible front much nearer. It can also arise within an mT air mass on days when high cloud cover suppresses the temperature.
6	Moist Tropical (MT)	analogous to the traditional mT air mass, is warm and very humid. It is typically found in warm sectors of mid-latitude cyclones or in a return flow on the western side of an anticyclone; as one approaches the tropics, this weather type dominates.
7	Transition (TR)	days are defined as days in which one weather type yields to another based on large shifts in pressure, dew point, and wind over the course of the day.

Humid characteristics of weather patterns are denoted by the first letter in the nomenclature, whereas the second letter represents the thermal characteristics. The dry or continental weather patterns originate from the land, while moist weather patterns emerge from the ocean/ sea. Similarly, tropical weather patterns develop from the tropical side of the region and are hot, whereas polar weather patterns come from the polar side and are cold. More information on SSC can be found at (http://sheridan.geog.kent.edu/ssc.html), and the definitions of SSC airmasses are also provided in Table 2-1.

The GWTC is a newly developed WTC system that is categorized into eleven weather patterns: four with extreme characteristics- humid cold (HC), humid warm (HW), dry warm (DW), and dry cool (DC), four with moderate/average characteristics- humid (H), dry (D), warm (W), and cool (C), and two transitional- cold frontal passage (CFP) and warm frontal passage (WFP), and seasonal (S), as depicted in Table 2-2.

Table 2-2: Definition of airmasses in Gridded weather typing classification (GWTC) available at [137].

Sr No.	Airmass	Symbol	Definition
1	Humid Cool	HC	Cooler and more humid than normal for the location and time of year
2	Humid	H	More humid than normal for the location and time of year
3	Humid Warm	HW	Warmer and more humid than normal for the location and time of year
4	Cool	C	Cooler than normal for the location and time of year
5	Seasonal	S	Near-normal conditions for the location and time of year
6	Warm	W	Warmer than normal for the location and time of year
7	Dry Cool	DC	Cooler and drier than normal for the location and time of year
8	Dry	D	Drier than normal for the location and time of year
9	Dry Warm	DW	Warmer and drier than normal for the location and time of year
10	Cold Front Passage	CFP	Transitional weather days often with a drop in temperatures and dew points and rising sea-level pressure
11	Warm Front Passage	WFP	Transitional weather days often with increasing temperatures and dew points and lowering sea-level pressure

The GWTC also incorporates regional and seasonal relevance, which reduces the patterns' seasonal fluctuation and makes the classification portable to different locations. As a result, the same airmass might occur in different seasons and locations with varying features [135]. Further information on GWTC may be found at (https://www.personal.kent.edu/~cclee/gwtc2global.html), and the definitions of GWTC weather patterns are also provided in Table 2-2. In addition to SSC and GWTC, the K-means clustering approach was used to create six weather patterns in Buenos Aires: very cold (C++), southern (S), warm (W+), southwestern (SW), very warm (W++), and southeastern (SE). Airmasses were also connected to circulation patterns to explore the relationship between airmasses and the circulation field [79]. The fluctuation in large-scale weather patterns during an extreme heat event in North America in July 2021 is illustrated in Figure 2-3 using GWTC.

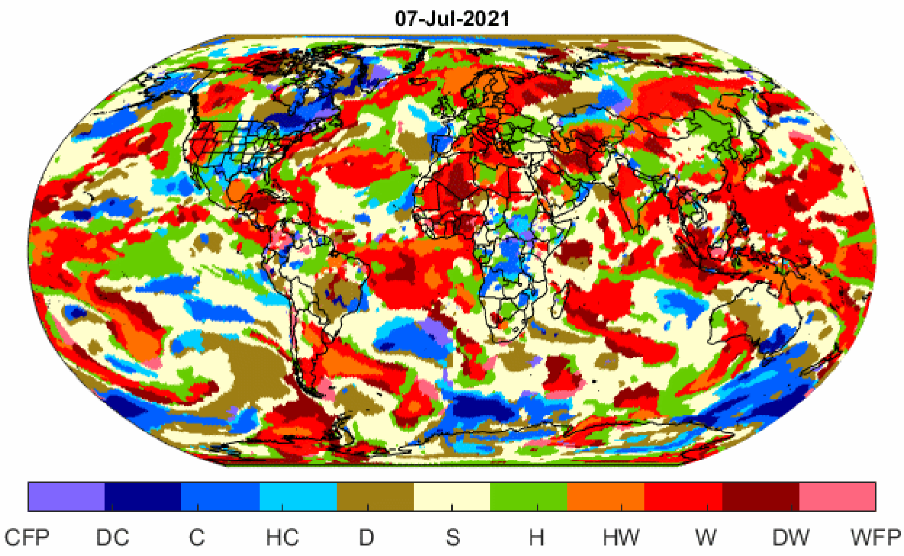

Figure 2-3 Large-scale weather patterns (GWTC) around the globe during the heatwave in North America on July 7th, 2021. Image source: Global GWTC (GWTC-2) [138].

2.4 Surface energy budget:

The natural balance of water, carbon, and energy in the urban environment may be disrupted as a result of changes in local and microclimatic conditions, which may eventually contribute to global warming. With the increased demand for infrastructures such as housing and transportation, anthropogenic emissions are growing, causing the system's mass balance to be disturbed [139]. Generally, the energy budget equation quantifies the changes in UO magnitude. The urban-rural temperature contrast is evaluated in terms of sensible, latent, anthropogenic, advective, storage, and net all-wave radiative heat fluxes [50]. The net all-wave radiative heat flux consists of incoming and outgoing shortwave and longwave radiations, while the available energy is estimated as the sum of sensible and latent heat fluxes. The energy budget equation is quantified as

$$Q^* + Q_F = Q_H + Q_E + \Delta Q_S + \Delta Q_A \ (\mathrm{W/m^2}) \tag{5}$$

Where

Q^* = Net all wave radiative heat flux at the earth's surface.

Q_F = Anthropogenic heat flux

Q_H & Q_E = Turbulent sensible and latent heat fluxes (Total available energy).

ΔQ_s = Storage heat flux

ΔQ_A= Advective heat flux.

Net wave radiation ($Q^* = K^* + L^* = K\downarrow - K\uparrow + L\downarrow - L\uparrow$): Solar radiations that reach the earth's surface are classified as shortwave (K*) and longwave (L*). Incoming shortwave radiations (K↓-ultraviolet-visible light) are in the spectral range of 290-4000nm, while incoming longwave radiations (L↓-infrared) are in the range of 4000-100,000nm. Incoming shortwave radiations are denoted by K↓, whereas reflected shortwave radiations are denoted by K↑ [140]. Solar height, atmospheric transmissivity, shadowing and reflection from structures, and air pollution influence incoming shortwave radiations. Net shortwave radiations (($K^* = K\downarrow - K\uparrow = (1-\alpha)K\downarrow$) can be quantified by estimating the incoming shortwave radiations and the surface albedo (α). K* is the proportion of radiations that are not reflected by the surface. Contrarily, surface albedo provides the fraction of the radiations reflected by the surface and assists in computing the net shortwave radiations. The albedo of vegetated surfaces is typically between 0.2 to 0.25, whereas the surfaces like asphalt may have albedo lower than 0.05.

Net longwave radiations ($\mathbf{L}^* = \mathbf{L}\downarrow - \mathbf{L}\uparrow$), are influenced by apparent sky temperature, GHG emission, and sky emissivity. L↓ is the incoming longwave radiations, and L↑ is the reflected longwave radiations. Surface temperature and surface emissivity affect the outgoing longwave radiations. The outgoing longwave radiations can be computed as ($L\uparrow = \varepsilon\sigma T^4$), where σ is the Stefan-Boltzman constant (5.7 x 10^{-8} W/m^2K^4), ε is surface emissivity, and T is surface temperature in K.

Anthropogenic Heat Flux (Q_F): It is the heat produced from human activities, including waste heat from industries, buildings, etc. Geographic, climate, population density, transportation, energy consumption, and industrial activities affect this phenomenon [141]. For instance, the energy provided to satisfy the buildings' heating and cooling needs elevate the anthropogenic heat flux [142] and intensifies the UO. The impact of anthropogenic heat flux on the energy balance equation is hard to estimate; thus, some indirect assessment methods have been devised [106]. For instance, some studies suggest that it can be roughly 10^{-4} of the energy our planet receives from the sun [143], while others think it is approximately 100-200 W/m^2/Yr. [144]

Sensible Heat flux ($Q_H = -\rho \cdot C_p \cdot \frac{\Delta T}{r_H}$): It is a convective phenomenon induced due to the thermal gradient between surface and atmosphere. It depends upon air density (ρ), air heat capacity (Cp), surface-air thermal difference, and transfer resistance (rH). Sensible heat fluxes are typically higher in urban areas, owing to urban surfaces/ materials having higher thermal inertia.

Latent Heat Flux (Q_E): Moisture exchange between the surface and atmosphere is governed by latent heat flux, owing to the surface-atmosphere vapor pressure gradient. Due to the higher vegetated/ porous surfaces, latent heat flux is generally higher in rural areas [106].

Storage Heat Flux (ΔQ_S): it determines the energy stored in urban and rural fabric, including air, surfaces, buildings, trees, etc. [145]. Urban fabric usually has higher storage heat flux due to higher thermal inertia. Due to difficulty in measuring the storage flux, some studies have suggested estimating it as a residual of the energy balance equation [106]; however, inconsistencies in anthropogenic heat flux estimation may yield contrasting results.

Advective heat flux (ΔQ_A): A fluid transporting mechanism from one place to another that depends on fluid motion. The pressure gradient at various locations (land-land/ land-ocean) may promote the advective heat fluxes in the form of secondary air circulations.

CHAPTER 3: SYNERGIES BETWEEN URBAN OVERHEATING, HEATWAVES, AND SYNOPTIC CLIMATOLOGY, AND THEIR IMPACT ON THE BUILT ENVIRONMENT

This chapter discusses the synergies between local, regional, and global-scale weather patterns and their impact on the built environment. The first section covers the synergy between UO and heatwaves and the variability in the responsiveness of the surface energy budget to extreme heat conditions. Next, variables that contribute to inconsistent UO responses during extreme heat conditions are explored. The second section reviews the research on the synergies between UO, meteorological conditions, and large-scale weather patterns. The third part focuses on UO, microclimatic conditions, and heatwaves' impacts on energy performance and indoor comfort. Additionally, adaptation methods and their effectiveness in the face of climate change were also discussed.

3.1 Synergies between UO and heatwaves:

The increased urbanization influences regional and continental-scale circulations by regulating the earth-atmosphere heat and moisture exchange [71,72]. The UO and heatwaves may interact synergistically and aggravate the UO intensity. Moreover, rapid urban growth may exacerbate regional warming and amplify the frequency and intensity of heatwaves [146,147]. To adequately realize the synergy between UO and heatwaves, it is crucial to comprehend the surface energy budget's response during heatwaves.

3.1.1 Variations in surface energy budget during heatwaves:

Climatic synergies between local, regional, and global climatic conditions can be examined by investigating the surface energy budget response in urban and rural settings. The key factors affecting UO intensity are net radiative heat flux, latent heat flux, sensible heat flux, storage heat flux, anthropogenic heat flux, and advective heat flux [50].

3.1.1.1 Alteration in radiative input during heatwaves:

During heatwaves, the high temperatures experienced in regions are caused by the large-scale stagnant high-pressure system that brings warm air from the troposphere [41]. Further, the clear sky conditions bring exceptionally intense solar radiation to the region during heatwaves than during background conditions [148]. These intense solar radiations may adversely impact the surface energy balance in urban and rural locations. Intense solar radiations throughout the spring and early summer in Europe prior to the 2003 heatwave were also responsible for the early depletion of soil moisture

[71]. It was also stated that these dry soil anomalies strengthened the anticyclonic circulation, which was the primary cause of 2003's intense heatwaves in Europe.

3.1.1.2 Alteration in sensible and latent heat flux during heatwaves:

The restricted vegetated areas and higher impervious surfaces in the urban fabric modify the available energy partitioning, surging the sensible heat flux and lowering the latent heat flux [65]. In contrast, the latent heat flux is more significant in rural regions due to the higher proportion of plantable surfaces (retaining higher moisture) and tree canopy cover [60]. During heatwaves, high solar radiation promotes evaporation in both urban and rural areas, aggravating the urban-rural moisture differential and, subsequently, the thermal gradient [31,52,149]. Convection and evaporation are relatively modest at night due to the absence of solar radiation; thus, the urban-rural moisture contrast is not a critical synergistic interaction at night. Figure 3-1 depicts the temperature fluctuations at several urban and suburban sites during a heatwave in Sydney.

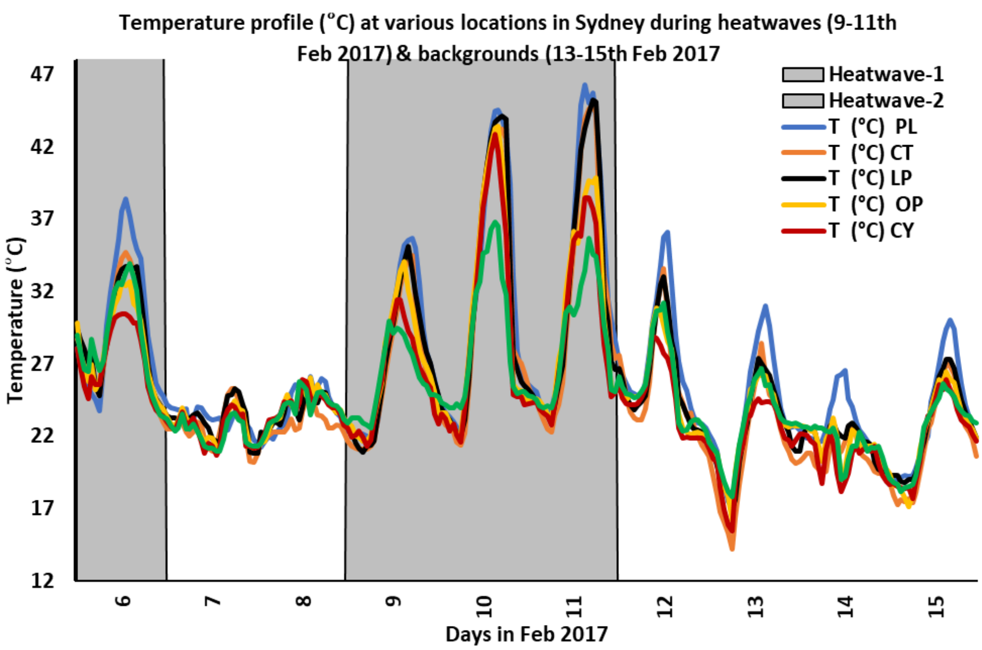

Figure 3-1 Ambient temperature (°C) variations at various locations (PL, CT, LP, OP, and CY) in Sydney during heatwaves in February 2017.

The surface latent cooling potential in rural areas is influenced by the precipitation in the region during that year, especially before or during the summer, when heatwaves are predominantly documented [71]. Without sufficient topsoil moisture in rural areas, heatwave and UO interactions may decline as, like urban surfaces, rural surfaces begin to partition more energy into sensible heat flux [31,71]. Due to urban greens losing their evapotranspiration potential due to prolonged intense heatwaves, the UO intensity during heatwaves in Europe was exacerbated [54].

Urban shading was also observed to limit the daytime thermal gains (sensible heat) in urban environments, lowering the daytime UO. Possibly owing to urban/solar shade, southern Europe responded better to intense heatwaves than their northern European counterparts [54].

3.1.1.3 Alteration in advective heat flux during heatwaves:

Wind flows from the high-pressure zone to the low-pressure zone. The urban-rural thermal gradient promotes secondary air circulation, reducing UO [41]. Generally, the regional wind speed is inversely related to UO intensity. The lower the regional wind speed, the less urban mixing there is, which means less advective cooling from adjacent rural areas, and the greater the magnitude of the UO [75]. During heatwaves, there was a further decrease in regional wind speed, which was attributed to high-pressure anticyclones [41,149].

In coastal cities, localities next to the coastline are cooled by the constant coastal winds owing to secondary air circulation. During heatwaves, secondary circulation becomes more influential due to a greater thermal difference between urban and steady sea surfaces [50,51,72]. However, when the distance from the coast grows, the UO may intensify due to inland areas' lack of coastal wind penetration. Consequently, distance from the coast is crucial in amplifying UO intensity during heatwaves [150].

3.1.1.4 Alteration in anthropogenic heat flux during heatwaves:

Dense urban regions with a high concentration of commercial buildings and heavy vehicular activity tend to have higher anthropogenic heat flux. During typical summer days, amplified anthropogenic heat flux was reported to amplify the daytime and nighttime UO [151]. Increased airconditioning use in buildings and automobiles during intense heat events, and higher fossil-fuel energy production to meet end-user energy needs during heatwaves, may worsen UO intensity even more [51]. In addition to latent heat, amplified anthropogenic heat flux was reported as the primary source of daytime aggravated UO during heatwaves [31].

3.1.1.5 Alteration in heat storage flux during heatwaves:

During the day, urban fabric (such as concrete) absorbs and stores more heat than non-urban areas. This heat is emitted at night as sensible heat flux, causing nighttime UO in many cities [152]. Due to increasing daytime radiative input during heatwaves, more heat can be stored in the urban fabric, exacerbating nocturnal UO [48,63]. The heat absorbed by the urban fabric may be released during the post-heatwave period, allowing the hot conditions in the city to last longer [41,70].

3.1.2 UO response to heatwaves in various cities:

Various studies have revealed the inconsistent response of surface energy budget to the extra incoming solar radiations while investigating the UO-heatwaves synergies. For example, there were reports of no change in UO magnitude during heatwaves [111], a decrease in UO magnitude during heatwaves [57], amplified UO during daytime [60], intensified UO during nighttime [63], and amplified UO at both daytime and nighttime [41].

3.1.2.1 Exacerbated daytime UO during heatwaves:

Coastal cities, such as Athens [50], Shanghai [51], Nicosia [60], New York [59], and Karachi [46], reported the intensified daytime UO during heatwaves. Moreover, in these investigations, advective heat flux and urban-rural moisture difference were the key interactions that intensified the daytime UO during heatwaves. The coastal regions were kept cooler by advective heat flux in the form of coastal winds, while inland locations were warmer due to the lack of coastal wind penetration. In addition, advection from the coastal winds increased the coastal sites' moisture content, thereby increasing the urban-rural moisture contrast and influencing the UO intensity. During heatwaves in Los Angeles, the highest daytime surface temperatures were reported at inland locations or in densely populated areas [72]. Analyses referencing a coastal station in Shanghai, China, revealed an increase in daytime UO concentrations [51]. In addition, the peak heatwave-background UO intensity difference (ΔUO) in Shanghai was 1.3 °C. Additionally, the large-scale weather patterns associated with heatwaves in Shanghai (lower regional wind speed and higher sea breeze) were concluded to be the primary synergistic interaction between UO and heatwaves.

Similarly, in Athens, both daytime and nighttime UO were amplified during heatwaves, but the daytime UO impact was more apparent (peak average ΔUO = 3.5 °C) [50]. In addition, it was discovered that advection from coastal breezes intensified the UO magnitude in Athens during heatwaves. The highest ΔUO was recorded in New York during the day (ΔUO = 2.0 °C), with the main contributor to amplified UO being a change in wind pattern from coastal southerlies to westerlies during heatwaves [59]. Another research in New York found comparable outcomes during heatwaves and indicated that the future UO magnitude will be 4 °C greater than it is now [109].

During heatwaves, the urban-rural moisture difference (△AH) was also cited as one of the leading causes of the daytime intensification of UO [31,60]. For example, amplified daytime UO response to heatwaves was reported in a temperate US city, where ΔUO with ambient temperature was 0.4 °C, and ΔUO with surface temperature was 2.8 °C [31]. Furthermore, major synergistic interactions between UO and heatwaves were identified as the urban-rural moisture contrast and enhanced anthropogenic heat flux. Similarly, in Nicosia, Cyprus, an increase in the UO during the daytime during heatwaves was seen (△UO = 0.9 - 1.3 °C) during the 2007-2014 hourly investigation. In addition, the key synergistic interaction during heatwaves in Nicosia was the evaporation of dew from urban and rural surfaces. The process was explained by the fact that dew formed on urban surfaces dissipated fast, but dew formed on rural areas was absorbed by non-urban surfaces, hence amplifying the daytime UO [60].

3.1.2.2 Exacerbated nighttime UO during heatwaves:

The amplified nocturnal UO during heatwaves was reported in Berlin [62], Szeged-Hungary [153], Seoul [149], Athens [64], Adelaide [58], Bucharest [49], and Melbourne [63], which were concluded either as non-coastal cities or inland locations. In addition, these studies inferred that an increase in heat storage flux, an increase in anthropogenic heat, and a decrease in regional wind speed were significant synergistic interactions between UO and heatwaves.

At night, the response of UO to heatwaves was observed to be enhanced in Berlin (peak ΔUO = 1.0 ^{o}C) [62]. During heatwaves in Seoul, Korea, ΔUO was most intense in the afternoon to late-night (peak ΔUO = 4.5 °C), while it was lowest in the early morning [149]. In addition, intense UO-heatwaves synergies were reported in Seoul under low-velocity regional winds and in densely urbanized areas. Even though Melbourne and Adelaide are coastal cities, increased UO was reported at night during heatwaves [58]. The ΔUO was 1.4 ^{o}C in Melbourne, whereas ΔUO was 1.2 ^{o}C in Adelaide. In another study conducted in Melbourne using the WRF model, storage heat flux was identified as the primary synergy intensifying urban temperatures during heatwaves [63]. In Szeged-Hungary, nocturnal UO amplification was also reported during heatwaves [153]. Using the WRF model, the nocturnal UO impact was more prominent during heatwaves in Washington and Baltimore (peak ΔUO = 1.5 to 2.0 ^{o}C). Moreover, contrary to previous studies, urban-rural soil moisture deficit was the primary cause of the observed difference [59]. During the heatwaves in Baltimore and Washington, the urban-rural moisture differential rose twofold relative to background conditions [59].

3.1.2.3 Exacerbated UO at both daytime and nighttime:

Several studies have also found that UO is sensitive to both daytime and nocturnal heatwaves [41,48,53,108,154]. For example, in Beijing, China, UO showed a positive response to heatwaves during both day (peak average ΔUO = 0.4 ^{o}C) and night (peak average ΔUO = 1.0 ^{o}C); nevertheless, the nocturnal UO impact was more prominent [108]. The intensified UO at daytime and nighttime was caused by increased urban wind speed during the day and reduced urban wind speed at night. The same conclusions were reached in another study conducted in Beijing; however, instead of advective heat flux, available energy difference and the heat storage flux were mainly accountable for exacerbated UO during heatwaves [48]. Another study conducted in Beijing using the WRF model [154] revealed similar results: an intensified UO during both daytime and nighttime, with the nighttime impact being more pronounced (peak average ΔUO = 0.78 ^{o}C). In the study, the daytime UO amplification was attributed to urban-rural moisture contrast, while the nocturnal UO amplification was ascribed to increased anthropogenic heat flux and higher warm advection. Baltimore also reported amplified daytime and nighttime UO during heatwaves, with the more pronounced nighttime effect [108]. In Baltimore, the principal UO-heatwaves synergistic interactions were the urban-rural moisture difference and low wind speed. During heatwaves in Madison, USA, both daytime and nighttime UO were more intense than on ordinary summer days, and the effect was especially pronounced in densely populated areas [108].

3.1.2.4 No change in UO magnitude during heatwaves:

In several investigations, there was either no change or a negligible response of UO to heatwaves. Using the WRF simulation model for one urban-rural station in Singapore, the UO response to heatwaves was studied over a single heatwave spell. The UO intensity was the same under both heatwaves and normal summer conditions, and there were no significant variations in soil moisture, heat storage, or wind speed [108]. An aggravated UO response was reported in Dijon, France, either before or within the first few days of heatwaves [108]. Later, a reduction in UO response during subsequent heatwave days was seen, and a statistically insignificant association was inferred between heatwaves and UO. Furthermore, nocturnal rural temperatures were significantly higher during heatwaves than nocturnal urban temperatures, which was linked to reduced soil moisture in Dijon, France. In Philadelphia, insignificant UO-heatwave feedback was linked to the city’s geometry [108]. The post-heatwave phase in Phoenix, USA, was reported to have a higher UO intensity (in current and future climatic scenarios), and the synergistic interactions between both phenomena were unclear [108].

3.1.2.5 A decline in UO magnitude during heatwaves:

A decreased response of UO to heatwaves has been reported in several studies [47,56–58]. In a research done in 54 U.S. cities, with a primary focus on nocturnal UO response to heatwaves, it was demonstrated that owing to wet weather conditions; rural nighttime temperatures were largely magnified [56]. In another study, 63 percent of the daytime and 74 percent of the nighttime UO responses were negative in 89 of India's most populous metropolitan regions based on land-surface temperatures [57]. In addition, it was shown that depleted soil moisture in rural areas was the key contributor behind declined UO intensity, which was related to harvesting before summer. Moreover, most of the non-urban regions evaluated in this study were in agriculturally dominated zones. In Perth, Australia, cooler urban areas during heatwaves can be ascribed to advection by coastal breezes due to the proximity of metropolitan zones to the coast [58].

3.1.3 Inconsistent response of UO to heatwaves- critical factors:

Numerous factors, including different boundary conditions (e.g., coastal or non-coastal cities), the city's physical size, population density, land-coast distance, and varying meteorological conditions (e.g., wind patterns, cloud cover, radiative input, etc.), may account for the inconsistent response of UO to heatwaves. Additionally, varying techniques of UO estimation, inconsistent methods of heatwave identification, neglecting the city's geographical expansion, UO estimation for a few heatwave incidents, and inconsistent site selection methods (inland sites/coastal sites) may also contribute to varied findings.

3.1.3.1 Different boundary conditions:

Different city boundary conditions may produce variable results. For example, the UO response to heatwaves may differ if the analyses were conducted for a coastal or non-coastal city. Coastal cities exhibited an intensified UO response to heatwaves during the day [50,51,60], whereas non-coastal cities reported UO being more pronounced at night [61,62]. Similarly, the choice of urban and rural stations is an essential factor that can lead to discrepancies in results. While investigating the UO-heatwaves interactions in Shanghai, China, higher daytime UO was reported for coastal stations, whereas nighttime UO was amplified when UO was computed using the inland station [51]. Moreover, UO estimated using the coastal station was much greater than UO calculated using the inland location [51]. In contrast, despite being coastal cities, Melbourne and Adelaide experienced a heightened nighttime UO response during heat waves [58]. It was primarily due to the selection of an inland location to mitigate the effects of the coastal wind. To conclude, advection from the coastal breeze may greatly impact a coastal city's UO response to heatwaves [108]. Similarly, another variable might be computing UO as a thermal gradient between urban and rural locations or a gradient between several locations inside the city. For example, studies performed in cities that extensively included non-urban LCLUs (e.g., Berlin) and studies conducted in cities that solely evaluated the city core (e.g., Barcelona) were identified as potential causes of error in [54].

3.1.3.2 Inconsistent UO quantification methods:

UO quantification using surface or ambient temperatures may also result in inconsistencies. For example, higher convection may cause the surface temperature to drop at night (reduced surface UO), amplifying ambient temperatures (exacerbated ambient UO) [31]. When assessed using surface temperatures, enlarged daytime UO was often recorded [31], while ambient temperatures primarily produced the prominent nocturnal UO owing to the release of stored heat in urban fabric [31].

Similarly, different temperature expressions for UO computation (hourly temperatures, daily maximum or minimum temperatures, daily average temperatures, daytime and nighttime average temperatures, monthly average temperatures) may produce inconsistencies. Three-day averages of all meteorological variables were calculated in Singapore to compare the UO during heatwaves with background conditions [111]. Using averages of temperature, relative humidity, and wind pattern throughout the heatwaves/backgrounds in Singapore may have led to conflicting findings. Wind patterns, for example, change rapidly, especially during extreme heatwave events [31], and hence daily, monthly, or annual averages may not capture the diurnal variations. As a result, it may produce varying results, especially in cities where large-scale weather patterns heavily influence the interactions between UO and heatwaves.

3.1.3.3 Inconsistent heatwaves identification methods:

Inaccessibility to a universal definition of heatwaves may also be a factor, yielding contrasting results. Some studies identified heatwaves using daily maximum temperatures [50], whereas others used daily lowest temperatures [56,57]. Generally, contradictory findings were recorded using the daily lowest temperature to identify heatwaves, as determined in [62]. When determining heatwaves, the geographical extent of the city is an essential factor to take into account. Numerous studies have employed a single urban or rural meteorological station to detect heatwave occurrences [48,51,60], potentially contributing to contradictory results. Limiting the investigation to a single urban and rural location and ignoring the city's geographical extension may also be a limitation of the study in Nicosia. Unlike other coastal research, the influence of advective heat was negligible in Nicosia [60].

Similarly, some research defined the threshold temperature using absolute temperatures [31,50], whereas others used relative temperatures [48]. More into it, the heatwave duration might be another variable since different studies have used two consecutive days, three consecutive days [31,50], or four consecutive days [60] to determine the heatwave duration. In Dijon, France, chosen threshold temperatures (daily maximum = 32 °C and daily minimum = 16 °C) were lower than regional health alerts (daily maximum = 34 °C and daily minimum 19 °C), which were measured for only two consecutive days [122]. Since no statistically significant association was shown between temperature anomalies and UO in Dijon-France, the less extreme heatwave spell might have produced conflicting results.

Another variant could look at UO-heatwaves interactions for a single heatwave spell or a limited period. A sudden change in climatic conditions before the selected heatwave spell, for example, could lead to inaccurate results. Temperature anomalies in Europe during extreme heat events in the summer of 2003 were attributed to a 25 percent reduction in soil moisture during the spring due to low precipitation [71]. Several studies have investigated the synergies between UO and heatwaves using a single heatwave spell, which was also considered a limitation of those studies [41,46,53,61].

3.2 Synergies between large-scale weather patterns and UO:

Globally, an increase of 0.85 ^{o}C in average temperature has been reported over the past century [13]. The outdoor thermal comfort is not only affected by the temperature, but other meteorological variants, including wind pattern, ambient moisture, atmospheric pressure, and cloud cover, holistically interact and adversely affect human thermal comfort. A significant change in sea-level pressure [155] and generally a reduction in wind speed was also reported in recent decades [156]. Further, higher evaporation rates were also associated with the higher temperature, consequently increasing the land-based precipitation in mid-latitude and humidity levels [15,157]. In North America, warm airmasses were reported to occur more frequently every year (e.g., humid-warm: +6.1%, dry-warm: +2.9%), particularly in recent years, whereas a drop in the frequency of cool airmasses was also reported (e.g., dry-cold:-4.5%, Cold: -5.7%)[158].

The synergies between local-scale UO and large-scale weather patterns are a continuous seesaw, and both conditions may affect each other at different times and locations. Large-scale weather conditions may alter UO intensity by modifying the wind pattern, cloud cover, humidity, and outgoing longwave radiation. Typically, clear sky conditions, low wind speed, and low atmospheric pressure were associated with exacerbated UO at nighttime [159,160]. The exacerbated UO magnitude during heatwaves in European cities was presumed to be associated with large-scale weather patterns [54]. Further, in several studies, the urban-rural moisture contrast was reported as the major contributor to exacerbating the daytime UO magnitude [159], and it is predominantly governed by large-scale weather conditions [161] and the surface cover [162]. A positive response between soil moisture and large-scale weather conditions was reported in France during the 2003 heatwaves, where drought conditions were associated with tropospheric circulations [71]. Contrarily, rapid urbanization and the surface roughness in the urban fabric were reported to affect the wind patterns, cloud cover, and atmospheric pressure [163–165]. A study reported 30-40 percent lower mean annual wind speed in cities than their rural counterparts due to UO [166].

Primarily, meteorological parameters have been utilized to evaluate an association between UO and large-scale weather patterns. The wind pattern and cloud cover are considered the most important meteorological parameters, causing differential heating and cooling rates between urban and rural areas due to the change in ventilation and insolation conditions [74,79]. Low pressures induced by UO in highly urbanized areas foster airflow from high-pressure rural areas, resulting in reduced UO magnitude [81]. However, lower regional wind speed results in higher UO intensity [75]. The wind speed and cloud cover were concluded to be inversely proportional to the fourth root of UO in Melbourne, though the relational magnitude may vary from city to city [76]. Radiative cooling at nighttime in rural areas is enhanced under clear (cloudless) and calm (low wind speed) weather conditions [167]. These clear and calm conditions were mainly associated with anticyclonic circulation patterns or the dry conditions in the region [83,85,87]. Under clear sky conditions at nighttime, not only radiative cooling is enhanced at rural sites, but the longwave emission in the urban fabric from daytime thermal storage also amplifies the urban ambient temperatures, which strengthens the nocturnal UO [63,77]. In contrast to dry conditions, moist conditions during the daytime reduce the latent heat flux potential, particularly in rural areas, and more available energy is partitioned into sensible heat flux, which may lead to UC in the daytime [87]. Further, an association between moist/ cloudy conditions and cyclonic circulation patterns was also reported [84].

The synergies between local and large-scale weather patterns also depend on other factors, including geographical location, topography, urban geometry, etc. Urban shading/ geometry plays a pivotal role in keeping the cities warmer at nighttime by decelerating the radiative losses due to decreased sky view [168]. Contrarily, lower urban temperatures early in the day were also reported around the buildings due to urban shading, which may result in UC during daytime [80,169]. Urban shading was one of the critical reasons behind amplified nighttime UO and daytime UC in New York [87]. Further, the area's topography also affects the interactions between UO and large-scale weather patterns. Leeward flow in the valley was reported to elevate the temperatures drastically through adiabatic warming [170].

Synoptic-scale classifications, including circulation-pattern-based classification (CPC) and the weather typing classification (WTC), have been employed to identify the interactions between local and large-scale phenomena. Further, the association between local and large-scale phenomena has been mostly examined during normal summer conditions. While using the CPC, in Szeged-Hungary, anticyclonic circulation, cloudless sky, and calm wind speed exacerbated UO, whereas lower UO was reported under cyclonic conditions [84]. Similarly, in Debrecen-Hungary, while employing the mobile measurement, magnified UO (mean max UO: 2.3 ^{o}C) was reported under anticyclonic conditions, whereas UO diminished under cyclonic conditions [85]. In Poznan-Poland, exacerbated UO (average UO: 1.2 ^{o}C) was reported mostly at nighttime under anticyclonic circulations, while urban cooling (UC) was mainly reported during daytime in the colder part of the year, under cyclonic circulations [74]. In Athens-Greece, high-pressure ridges (anticyclonic categories) favored the UO formation, whereas cold air advection from northerly component winds terminated the UO [86]. In Birmingham, while associating the surface and ambient UO with large-scale circulation, maximum ambient UO (Max/

mean UO: 7.0/2.5 °C) was reported at nighttime under anticyclonic conditions [80]. Similarly, Birmingham's higher surface UO (UO: 4.16 °C) was reported in the city center at nighttime under cloudless anticyclonic conditions. In Melbourne-Australia, anticyclonic conditions were responsible for the warmest 17 percent UO events (mean group UO: 3.56 °C) [75]. Further, these anticyclonic circulations in Melbourne were associated with weak warm and dry N to NE airflow, which resulted in clear and calm conditions. The weakest UO in Melbourne was observed under northwesterly airflow instead of cyclonic conditions.

While utilizing the WTC (SSC) in northeastern cities of the USA (Baltimore, Philadelphia, Boston, and New York), the most intense UO was reported at nighttime (peak average UO: 3.5 °C in New York) under dry-tropical (hot and dry) weather pattern. The absolute maximum temperatures at both urban and rural sites were recorded under moist weather conditions [87]. Similar results in the same northeastern US cities were reported in another study, where dry airmasses (dry-moderate, dry-polar, dry-tropical) were responsible for higher UO magnitude (2 to 5 °C) compared to all moist airmasses [82]. In Atlanta, while utilizing the SSC, dry-tropical (hot and dry) weather patterns at nighttime and moist-tropical (hot and moist) patterns at daytime were reported as influential large-scale weather conditions exacerbating the UO intensity [161]. Further, the UO intensity in Atlanta under dry-tropical patterns at nighttime was comparatively higher (peak average UO: 3.84 °C) than in moist-tropical patterns in the daytime. In the same study, moist airmasses were also linked to UO-associated precipitation. In Buenos Aires-Argentina, exacerbated UO at nighttime during winter (Max mean UO: 2.8 °C) was attributed to cold airmasses, which were associated with cold-core anticyclones, low wind speed, and low cloud cover [79]. In Phoenix-USA, using the monthly mean minimum temperature for June from 1990-2014, a 2 to 4 °C spatial UO effect was reported under dry-tropical (dry and hot) weather patterns along with clear and calm conditions [83].

In addition to urban-climatology, bioclimatological response to large-scale weather patterns is also well-documented. While investigating the association between large-scale weather patterns and mortality rate during summer, dry-tropical and moist-tropical weather patterns in New York [171] and Rome and moist-tropical patterns in Shanghai were the most oppressive [133]. In Canada, moist-tropical and dry-tropical patterns were also associated with higher air pollution and, consequently, higher mortality rates [172]. In the 19 USA cities, dry-polar conditions during winter and dry-tropical conditions during summer were associated with increased cardiovascular mortality [173]. Further, it was also reported that moist airmasses affect human thermal comfort more in the humid climate [52,53], while dry-tropical patterns in the arid region. Therefore, moist-tropical patterns in coastal cities were associated with higher mortality rates, whereas dry-tropical patterns in dry regions.

3.3 The impact of multilevel climatic changes on the built environment:

The United Nations (UN) sustainable development goals (SDGs) emphasized resilience and decarbonization- SDGs related to climate actions and sustainable cities and communities [174–177]. Globally, buildings consume more than a third of the primary energy and emit 40 percent CO_2 [178,179]. Additionally, global reports indicate a considerable increase in building cooling requirements and a decrease in heating requirements [20,180,181]. Building cooling requirements have tripled globally since 1990, growing at an average rate of 4 percent per year, and now account for approximately 16 percent of total power consumption in buildings [182]. Building cooling requirements are expected to grow, reaching 34 percent of global net energy consumption in 2050 and 61 percent in 2100 [21]. Along with lowering GHG emissions from fuel-intensive mechanical cooling, addressing overheating concerns in the built environment would be one of the most challenging jobs in the following decades. As a result, climate-resilient and low-carbon buildings are critical for addressing the issues associated with overheating and decarbonization.

Globally, as a result of climate change, airconditioning (AC) penetration increased by around 130 percent between 2000 and 2020 and is expected to climb another 40 percent by 2030 [182]. Air conditioner usage during extreme heat conditions may improve interior thermal comfort; however, it increases energy consumption and peak power demand, increases anthropogenic heat, raises the ambient temperature, and increases the likelihood of extreme heat events. More into it, extreme heat conditions reduce the efficiency of power plants and contribute to the stress on electric grids. As a result, electricity costs rise, energy poverty worsens, and more blackouts occur [29]. This chain of events exacerbates socioeconomic disparity and susceptibility, and the low-income population, which lives in poorly planned/located communities and in uninsulated dwellings, is particularly vulnerable to extreme heat conditions [183].

Numerous studies have been conducted to determine the impact of UO and heatwaves on the thermal performance of buildings [89,91]. However, no study has ever been conducted on how buildings adapt to the cumulative influence of local, regional, and global climate changes. Additionally, the microclimatic context was often overlooked when measuring the influence of such local, regional, and global climatic changes. The set of local atmospheric conditions, including ambient temperature, surface temperature, humidity, and wind pattern, differs from one zone to another and is defined as the microclimate [184]. Microclimatic conditions and building operations are inter-relatable. The anthropogenic heat released from the buildings harms the urban environment by exacerbating the ambient temperatures, whereas the altered urban environment significantly affects the building's thermal performance [185].

3.3.1 The impact of microclimatic context on building thermal performance:

Cities exhibit greater heterogeneity than surrounding landscapes, and the microclimatic environment can significantly impact a building's thermal efficiency. In San Francisco, USA [186], Lausanne, Switzerland [185], Qianjiang Newtown, China [187], Toronto, Canada [188], Sydney, Australia [189], and Antwerp, Belgium [190], a significant impact of urban microclimate on building thermal performance was reported. This effect was attributed to changes in the local urban context, including modified surfaces, greenery, water bodies, urban configuration, anthropogenic emissions, and local meteorological conditions. In San Francisco, USA, annual heating requirements varied by over 100 percent, cooling requirements varied by over 65 percent, peak electricity demand varied by up to 30 percent, and indoor temperatures varied by up to 5°C; when assessing building thermal performance with and without microclimatic context [186]. Similarly, In Antwerp, Belgium, the residential buildings adjacent to the parks exhibited 13.9 percent lower cooling needs than the buildings surrounded by other structures [190]. Typically, building energy simulations were conducted using building energy models (BEMs), with the local microclimatic setting being largely disregarded.

3.3.2 The impact of urban overheating (UO) on building thermal performance:

Apart from the microclimatic environment, various investigations have demonstrated a significant effect of UO on building thermal performance [191]. The influence of UO on energy consumption was evaluated empirically in Beijing, China [88], and Seoul, Korea [192], as well as utilizing BEMs in Rome, Italy [20], Barcelona, Spain [193], Duran, Ecuador [89], south American pacific coastal cities [194], Nanjing, China [195], and Tehran, Iran [196], and by utilizing the urban building energy model (UBEM) in Padua, Italy [197]. The UO-induced cooling energy penalties reported in various cities were as follows: a 6-8 percent penalty in Padua, Italy [197], a 12-24 percent penalty in Nanjing, China [195], around 18-28 percent penalty in Barcelona, Spain [193], a 29 percent penalty in Beijing, China [88], a 30-70 percent penalty in residential buildings in Duran, Ecuador [89], an around 53-74 percent penalty in Rome, Italy [20], and a 15-200 percent penalty in south American pacific coastal cities [194]. Additionally, while most of these studies found a positive trend in cooling requirements owing to UO, they also reported a negative trend in heating requirements. In contrast, Tokyo, Japan [90] found a decrease in cooling energy requirements for residential structures and a decrease in overall net energy consumption as a result of UO. Heating and cooling energy requirements were calculated in the study using a mathematical equation developed based on energy consumption patterns and ambient temperatures. In addition to varying local and climatic conditions, the variation/contradiction in previous studies could be a result of differences in i) the application of various computational methods/tools, ii) disragarding microclimatic context, iii) the use of inconsistent meteorological data, i.e., either typical meteorological year (TMY) or realtime climatic data, iv) disregarding spatiotemporal variations, and v) variations in input settings, such as cooling setpoints, etc.

3.3.3 The impact of heatwaves on building thermal performance:

Similarly, inconsistent findings were obtained when examining the influence of heatwaves on building thermal performance. The impact of heatwaves on building thermal performance has primarily been investigated in the following categories: i) improving buildings heating performance and monitoring overheating concerns during summer (particularly in colder climates or in highly insulated passive houses/zero energy buildings) [198–201]. ii) exploring the trade-off between building cooling needs and thermal resilience [201,202], and iii) investigating the survivability of low-income/poorly constructed existing structures in substantially warmer regions [203]. The research were conducted in Houston and Phoenix, USA [204], Zielona Gora, Poland [205], Paris, France [206], Badajoz, Spain, Evora, Portugal, and Porto, Portugal [205], Perugia, Italy [92], and Toronto, Canada [188]. During heatwaves, the indoor temperatures were calculated using TMY data and the BEM In Houston and Phoenix, USA [204], and the discomfort index exceeded the critical level within six hours of a power disruption. Similarly, the empirical technique was used to assess the influence of heatwaves on indoor thermal comfort in Athens, and it was discovered that almost 85 percent of the time, the indoor temperature of existing dwellings exceeded the WHO indoor temperature recommendation [203]. In contrast, using BEM and meteorological data from four heatwave events in Perugia, Italy, the daily average cooling requirements during heatwaves were lower than typical summer days [92].

In two Australian cities, Adeliade [202]and Melbourne [93,94,207], the influence of heatwaves on building energy consumption and thermal comfort was explored by comparing star-rated insulated buildings to existing non-insulated buildings. In Adelaide, a tool recommended by the Nationwide house energy rating scheme (NatHERS) was used to evaluate energy efficiency, that uses TMY data. The NatHERS, it was determined, does not promote heat-resistant buildings, and the risk of overheating grows with the star rating [202]. While conducting experimental research in 107 residences in Melbourne during heatwaves, it was established that higher star-rated buildings perform worse in terms of energy usage and indoor thermal comfort [93]. The study assessed AC usage based on fluctuation in indoor temperatures, and the study's limitation was a simplified technique for estimating cooling energy consumption.

Conversely, in another study conducted in Melbourne and assessing the mitigating impact of improved energy-efficient buildings on indoor heat stress during heatwaves, it was discovered that residents of existing uninsulated houses were 50 percent more susceptible than residents of 5.4 star-rated homes. The study used the BEM to determine the building's thermal performance during a heatwave event

[94]. The study's limitation was the approximation of heatwave identification. Another research conducted in Melbourne employed the numerical model to assess the thermal performance of eight different wall systems during heatwaves [207]. Similar to the prior study, an insulated wall system with higher thermal inertia was determined to be the most suitable alternative over an uninsulated wall system. However, in that study, daytime and nighttime variations were evaluated using separate models, and the effect of daytime heat accumulation on overnight thermal performance was neglected. The varying responses during heatwaves in the previous studies could be the result of i) examining the thermal performance of buildings during a single heatwave episode/summer, ii) utilizing data TMY data and ignoring temperature extremes, and iii) inconsistent methodologies for identifying heatwaves.

3.3.4 The combined impact of UO and heatwaves on building thermal performance:

The combined effect of UO and heatwaves on the buildings' energy performance has been studied in Milan and Rome, Italy [91,208]. In Milan, UO-induced cooling penalties were 39-41 percent, whereas heating savings were 12-16 percent when the thermal performance of a single standalone ten-story residential building was examined in urban and rural climatic contexts, using meteorological data from 2002 to 2008 [208]. Further, during heatwaves, an increase of 1.5-2.2°C in indoor temperature was noted in urban settings compared to rural settings [208]. In Rome, Italy, an evaluation of the thermal performance of standalone uninsulated and insulated buildings in three urban and one rural setting revealed an increase in cooling demand of 87 percent due to heatwaves, a 72–87 percent increase in cooling demand due to UO, and a 176–196 percent increase in cooling demand under the combined effect of UO and heatwaves [91]. Additionally, as a result of the synergistic effect of UO and heatwaves, the average operating temperature increased by more than 5°C. Both studies investigated the thermal performance of buildings at the building scale using BEMs, which had the disadvantage of ignoring the urban context.

3.4 Adaptive measures:

Adapting to extreme heat through suitable adaptation and mitigation measures is critical for mitigating local, regional, and global climate changes [205,209–211]. Adaptation measures fall into three broad categories: i) heat prevention, ii) heat modulation, and iii) heat dissipation. Heat prevention and modulation approaches concentrate on reducing/modifying heat gain from external and internal loads, whereas heat dissipation techniques remove heat from the heat sink to the climate via heat transfer. The strategies, including thermal insulation, solar control, internal gain control, behavioral changes, etc., are considered heat-preventive measures.

Insulated envelope -opaque (wall, roof, floor) or transparent (glazing) surfaces- reduces the heat transfer by radiation from the building envelope [69,73]. While evaluating the thermal performance of insulated envelopes under heatwaves or global climate change, contradictory findings have been published in the literature. Several studies concluded that insulation has a favorable impact on cooling energy and indoor environment quality (IEQ) [204,206,212], a favorable impact on cooling energy only [91,201], and adverse impacts on both cooling energy and IEQ [92,93] during extreme heat events. Insulation reduces the thermal gain during summer and heat losses during winter, reducing energy consumption during the year. Hyper-insulated envelopes may trap daytime radiations and increase the nighttime discomfort in non-airconditioned buildings. Certain studies also indicated a risk of overheating in highly insulated buildings under future climatic conditions, even though the same insulated envelopes functioned effectively under current climatic conditions [198]. In the temperate climate of Zielona Gora- Poland, while conducting an empirical study to evaluate the buildings' thermal performance during heatwaves, moderately insulated envelopes with higher thermal inertia performed better in energy consumption and IEQ than the lightweight double-insulated envelope [213]. Similarly, while examining the influence of glazing on building thermal performance, it was claimed that efficient glazing might result in a more than 40 percent savings in building energy consumption under future climatic conditions in Darwin [212] and Sydney [39]. However, the performance of highly improved glazing during heatwaves is critical to investigate.

The building envelope resistance to inward or outward air leakages is defined as envelope airtightness. When the envelope's airtightness was examined in the context of climate change, conflicting findings were obtained. In Darwin, Australia, airtightness of the envelope had a favorable impact on cooling energy and passive survivability under future climatic conditions [212], whereas in Houston, and Phoenix, USA, a delayed nighttime cooling response due to airtight envelope was determined during heatwaves under a free-floating condition [204]. Thermal inertia (TI) as a heat modulation measure absorbs/ stores/ releases the heat on a cyclic basis- absorbs heat during daytime and emits it at night time. Further, the energy demand shift to low-tariff intervals makes it a cost-effective measure [214]. Several studies have demonstrated a promising effect of TI on the buildings' thermal performance when combined with heat dissipation strategies during heatwaves [210,213]. Additionally, TI efficiency was concluded to be independent of the length of heatwaves and stays constant during periods of severe heat [213]. In contrast, increased TI at night proved detrimental in Sydney [202] and Melbourne [207] during protracted periods of intense heat.

A framework encompassing vulnerability, resistance, robustness, and recovery is utilized to examine buildings' thermal resilience under excessive heat conditions [174]. Thus, structures must function effectively during all four stages to mitigate the effects of severe heat, particularly during protracted periods of heatwaves. The key to reducing daytime susceptibility is nocturnal recovery through natural ventilation. The nighttime ventilation as a heat-dissipative measure may cool the interior areas and the fabric of the structure, delaying the day's peaks. The pressure gradient (wind flow from high-pressure to low-pressure side) and the buoyancy/ stack effect (rising warm air) are the main driving forces that activate natural ventilation. During heatwaves, natural ventilation using cross-ventilation, windcatchers, and solar chimneys has been demonstrated to be effective [215,216]. In Rome, Italy, when the night ventilation rate was altered from 1.5ACH to 3ACH, the operating temperature reduced below 30°C for 70-90 percent of the time under the combined impact of UO and heatwaves [91].

Behavioral adjustments and maintaining the cooling setpoint at a higher acceptable level, notably during heatwaves, were effective adaptation approaches in Paris, France [206] and Zielona Gora, Poland [213]. In Paris, increasing the cooling setpoint from 23 to 28°C reduced AC demand by around 43 percent and substantially improved outdoor thermal comfort [206]. Heatwaves are often linked with low wind speeds, and mitigating techniques such as vegetated surfaces (with enhanced evapotranspiration) and high-albedo surfaces may help reduce outdoor temperatures while also improving regional ventilation. Reflective ground surfaces have been demonstrated to have a promising effect on building thermal performance in Toronto [217], Sydney [206], and Duran, Ecuador [89]. In Sydney, the combined impact of modifying the streets and pavement albedo resulted in a 4 percent decrease in cooling energy consumption [189]. Similarly, the influence of cool roofs (with roof albedo varying between 0.5 and 0.7) on building thermal performance has been thoroughly investigated in Evora and Porto in Spain [205], Adeliade [218], Sydney [1,39], Houston and Phoenix-USA [204], and Toronto [217]. However, given recent developments in passive daytime radiative cooling (PDRC) [219], it is necessary to evaluate the influence of highly reflective/super cool roofs on building thermal performance during heatwaves. Supercool roofs may not only attenuate urban heat and minimize building cooling demands, but they can also passively cool buildings owing to their surface temperature being lower than the ambient temperature [220].

3.5 Conclusion:

The local, regional, and large-scale weather conditions are affected by urbanization due to the change in the surface's sensible, latent, radiative, and dynamic responses. UO, heatwaves, and synoptic-scale weather conditions may synergistically interact and severely affects the communities. A contradictory response of UO to heatwaves was reported in the literature, where daytime UO exacerbation, nighttime UO exacerbation, UO exacerbation at both daytime and nighttime, the inconclusive response of UO to heatwaves, and a declined UO response during heatwaves were concluded. Further, urban-rural moisture contrast at daytime, whereas storage heat fluxes at nighttime mainly were reported as the primary synergistic interaction between UO and heatwaves. Advective heat flux in coastal cities was also quite evident during heatwaves.

Interactions between UO magnitude and large-scale weather conditions were investigated by utilizing both CPC and WTC. Exacerbated UO magnitude was reported under anticyclonic conditions while utilizing the CPC, whereas warm and dry conditions were responsible for magnified UO magnitude while employing the WTC. Contrarily, cyclonic conditions in CPC and moist conditions in WTC were associated with lower UO or UC. In some studies, UC was associated with northerly cold air advection instead of cyclonic conditions and northwesterly airflows, respectively. Generally, anticyclonic conditions in CPC and dry weather conditions in WTC were linked to clear (cloudless sky) and calm (low wind speed) meteorological conditions that bring the undisturbed radiations and magnify the UO intensity. Contrarily, cyclonic conditions in CPC and moist conditions in WTC were mostly associated with cloudy conditions and lower UO magnitude.

The impact of multilevel climatic conditions on the built environment is also investigable. While measuring the individual impacts of UO and heatwaves on building thermal performance, inconsistent responses were reported. Some studies reported an increase in cooling energy, and deterioration in IEQ under the impact of UO, whereas others reported a decline in cooling energy consumption. A similar type of response was also reported under the impact of heatwaves.

CHAPTER 4: DATA AND METHODS:

The fourth chapter of this dissertation discusses the data and methods employed. This chapter was primarily organized into three sections, i) assessing the interactions between UO and heatwaves, ii) evaluating the interactions between UO and large-scale weather patterns, and iii) evaluating the impact of multi-level climatic changes on the built environment. First, a brief introduction to the case study was presented (section 4.1). Subsequently, the studied locations were discussed, focusing on site characteristics and demographic factors (section 4.2). Meteorological data acquisition, data cleaning, and validation procedures were detailed in section 4.3. Later, the heatwaves identification procedure and selected heatwave events were explained (section 4.4). This section was organized according to the main chapter classification, where heatwaves were identified for i) UO-heatwaves interactions, ii) UO-large scale weather patterns interactions, and iii) impact on the built environment. Next, large-scale weather pattern classification was described, which is used to evaluate the association between local and global-scale climatic conditions (section 4.5). The following section, 4.6, explained the archetypes, national codes, and software used to evaluate the impact of climate change on the built environment. Further, the section also demonstrated the methods used to create the climate and horizon files and evaluate the IEQ. The last section, 4.7, presented the principal methods used in this dissertation for all three areas separately.

4.1 Case study:

Climate change has significantly affected Australian cities. The severity of heatwaves [221,222] and UO intensity [223,224] have risen in Australian cities. The probability of fire season in Australian cities has increased by at least 30 percent, attributed to human-induced climate change [225]. Sydney is one of Australia's most impacted cities due to its distinctive geographical features, including the ocean and mountains on opposing ends. In this dissertation, Sydney has been taken as a case study.

Sydney is the geographically largest (12,367.7 km^2 land area) and the most populous (over 5.3 million population) city in Oceania [226]. The city has a Cfa classification under the Koppen-Geiger classification (humid-subtropical) [227]. The city's Central Business District (CBD) is situated in the proximity of the Tasman Sea in the east, whereas the metropolitan area is extended by 70 km in the west to the Blue Mountains and is exposed to one of the largest arid biome [228–230]. Further, being surrounded by the national parks in the north and south, the city's urban growth is largely taking place in the west. In parallel with the city's expansion in the west, a 34 percent increase in the city's population is projected by 2053, as the population would increase from 5.3 million to 8 million [226,231]. It is also estimated that by 2036, the greater western Sydney would accommodate more than 50 percent of greater Sydney's population as two more city centers are being developed in western Sydney along with the new airport [232].

4.2 Sites studied:

It is crucial to examine the geographical extension of the city to minimize the impact of site selection on multilevel climatic interactions. Six locations, including Penrith Lakes (PL), Campbelltown (CT), Liverpool (LP), Olympic Park (OP), Canterbury (CY), and Observatory Hill (OH), were selected in three distinct zones of Sydney, as shown in Figure 4-1. The split was done based on the station distance from the coast: PL, CT, and LP in western Sydney, OP, and CY in inner Sydney, whereas OH in eastern Sydney were considered.

OH (urban station), located in the proximity of the coast and Sydney Business District (CBD), was selected as the reference station, as recommended in [1,230,233]. Inner Sydney sites (OP and CY) were approximately 8-12 km away from the nearest coast. The minimum distance of any western Sydney site from the nearest coast was around 25 km, whereas the PL was 50 km away from the coast. The tree canopy cover was least in Sydney CBD and increased from eastern to western Sydney: Sydney CBD: 15 percent, inner Sydney: 15-17 percent, and western Sydney: 25-35 percent [234]. Similarly, potentially plantable surfaces were also lower in Sydney CBD and higher in inner and western Sydney: Sydney CBD: 13 percent, inner Sydney: 22-32 percent, and western Sydney: 40-50 percent [234]. The population density (PD) was highest in Sydney CBD (over 6000 pop/ km²) and lowered from inner to western Sydney: inner Sydney: 2500-4000 pop/ km², and western Sydney: 500-650 pop/ km².

Figure 4-1 Location of weather stations and site characteristics. (Image source: Google map).

4.2.1 Penrith Lakes (PL):

Penrith Lakes is a suburb located in western Sydney, 55 km northwest of the Sydney CBD (Table 4-1). The nearest coast is at 49 km in the southeast of the station. The station is located in the Penrith Lakes regional park (150°40'42"E, 33°43'10"S, 24.7 m asl), surrounded by green areas, bare soil, and lakes [235]. The Aquapark and aqua golf facilities are also available nearby, and the Nepean River flows to the west of the station. The tree canopy cover of the suburb is almost 25 percent, while 15.3 percent of the suburb is non-plantable, and around 54 percent of the suburb area is potentially plantable, showing the high proportion of available non-urban surfaces [234]. Primarily residential and commercial buildings are available in the suburb. The area's population density is 484 persons/km^2, which is low compared to the other locations. On-site, the NE/SE winds represent the Inland winds from the suburb's eastern side (IE), whereas NW/SW denotes the desert/ continental Wind (D).

4.2.2 Campbelltown (CT):

Campbelltown is located in western Sydney, in the southwest of Sydney CBD at 44.2 km distance, and the nearest coast is at 27 km in the southeast of the station (Table 4-1). There are two weather stations in Campbelltown, one installed by the Bureau of Meteorology (BOM) in the Australian botanic garden (150°46'25"E, 34°3'41"S, 112m asl), while the other is provided by the New South Wales (NSW) government in TAFE NSW Campbelltown park (150°47'43"E, 34°03' 00"S, 112 m asl)[235]. The distance between both stations is about 2 km. The missing meteorological parameters in the BOM data were acquired from the NSW station. Around the weather stations, greenery, trees, and bare soil are available.

The city of Campbelltown is mainly a residential or semi-rural area. The Nepean river runs southwest of the station. The area's tree canopy cover is 34.2 percent, much higher than the Sydney CBD and Penrith Lakes. Around 38.5 percent of the land is potentially plantable, while 12 percent of the land is unplantable [234]. The population density of the area is 509.4 persons/ km^2. On-site, the NE/SE winds represent inland (IE) winds from the suburb's eastern side, whereas the NW/SW are desert/ continental winds (D).

4.2.3 Liverpool (LP):

Liverpool is a suburb located in the greater western Sydney region at a 28.9 km distance from Sydney CBD, and the nearest coast is at a 23 km distance in the southeast of the station (Table 4-1). Liverpool weather station is situated in Raine park (150° 54' 21"E, 33° 55' 58"S, 22m asl), having greenery and asphalt roads in the surrounding [235]. The city of Liverpool has mixed land use, mostly residential and commercial buildings in the surrounding. The suburb's tree canopy cover is around 23.3 percent, while 51.1 percent of the land is potentially plantable [234]. The population density of the suburb is

668.8 persons/km². Like PL and CT, the NE/SE winds represent inland winds from the suburb's eastern side (IE), whereas NW/ SW means the desert/ continental winds (D).

4.2.4 Olympic Park (OP):

Olympic Park is located in the city of Auburn, northwest of the Sydney CBD, at a 12.7 km distance. The nearest coast is 13.5 km southeast of the station (Table 4-1). The Olympic Park weather station is located in the Olympic park Archery center (151°4'18"E, 33°50'2"S, 4m asl)[235]. The weather station is surrounded by greenery, creeks, and the Paramatta River (north of the station). The Auburn area has mixed land used and has residential, commercial, and industrial regions and parklands in the surrounding. The tree canopy cover of the suburb is 15.4 percent, while 31.1 percent of the land is potentially plantable, and 50.4 percent of the surface is non-plantable [234]. The population density of the area is 2527.88 persons/ km². Winds from the NE/ SE of the suburb represent coastal winds (C), while the NW/SW denote the inland winds from the west (IW).

4.2.5 Canterbury (CY):

Canterbury is situated in the southwest of Sydney CBD at a 17 km distance, and the nearest coast is in the southeast of the station at a 7.5 km distance (Table 4-1). The Canterbury weather station is situated in Canterbury racecourse park (151°6'48"E, 33°54'21"S, 3m asl), having greenery and a pond in the surrounding [235]. Cooks river runs in the south of the station and bifurcates the city of Canterbury into two dense residential areas. Further, the suburb also consists of light industrial and commercial zones. The tree canopy cover of the suburb is around 17.5 percent, while 54.4 percent of the total area is unplantable, and 22.8 percent of the total area is potentially plantable [234]. The population density of the suburb is 4303 persons /km². On-site, the NE/SE winds represent the coastal winds (C), while the NW/SW shows the inland winds from the west (IW).

4.2.6 Observatory Hill (OH):

OBS Hill is taken as a reference station. The weather station is situated in the heart of the Sydney Central Business District (CBD) (151°12'18"E, 33°51'39"S, 39m asl)[235]. Roads, greenery, and high-rise buildings are available in the surrounding of the weather station (Table 4-1). The nearest coast is 0.6 km away from the weather station. The tree canopy cover of the area is 15.2 percent of the total, while 69.1 percent of the land is non-plantable, and only 13.2 percent of the land is potentially plantable, showing the magnitude of the urbanization [234]. Mostly, commercial buildings and parks are available in the neighborhood. The area's population density is 6160 persons/ km², much higher than the other locations. On-site, the NE/SE winds represent the coastal Winds (C), while NW/SW means the inland winds coming from the western side (IW).

4.3 Meteorological data collection and processing:

The Bureau of Meteorology (BOM), Australia, was the primary source of meteorological data [235]. BOM data was provided for PL, OP, CY, and OH from 1999 to 2017. BOM data was available for CT from December 2006 to the present. For Liverpool, meteorological data was collected from the NSW government [236] and was accessible from 2013-onward. Some other weather stations, including Sydney Airport (SA), Horsley Park (HK), and Terrey Hills (TH), were also utilized for heatwaves identification, and Australian BOM provided the temperature data from 1999 to 2017.

Initially, semi-hourly data provided by BOM were cleansed. Estevez's [237] validation techniques were employed to eliminate outliers and null values from the meteorological data. The range, step, persistent, and relational tests were primarily performed. Gaps were filled using linear interpolation and genetic algorithms. Linear interpolation was used to fill the gaps of up to three hours, whereas the triangulation technique was employed to build genetic algorithms (data from the three nearest stations) for longer intervals. From the half-hourly data, hourly averages were determined for all weather stations. The meteorological variables provided by BOM included ambient temperatures (T_a- temperatures at 2m height- ^{o}C), relative humidity (RH- %), and wind pattern (wind speed-m/s and wind direction-degree). Further, the following equations were used to determine the dew point temperature and absolute humidity (AH).

Absolute humidity (n) in g/m³ was calculated using the following equation.

$$PV = nRT. \tag{1}$$

Where P is the vapor pressure, R is the gas constant for water = 462 Pa.m³/(K.kg), and T is the absolute temperature in kelvins.

The vapor pressure was obtained using the following equations. First, saturated pressure was computed using the following equation to calculate the vapor pressure.

$$p_{\text{sat}} = 610{,}5\, \mathrm{e}^{\frac{17{,}269\ \theta}{237{,}3+\theta}} \quad \text{for } \theta \geq 0\ °\text{C} \tag{2}$$

Where P_{sat} is the saturated pressure, and θ is the temperature in °C.

Vapor pressure was calculated by using the following equation.

$$\varphi = \frac{p}{p_{\text{sat}}} \tag{3}$$

Where p is vapor pressure, P_{sat} is saturated pressure, and φ is the Relative humidity/ 100.

Table 4-1: Site data and land characteristics of the sites

Station Location [235]	**Zone**	**Station surrounding**	**Surface Cover (%)** [234]	**Water source presence**	**Area classification**	**Distance from CBD (km)**	**Distance from the nearest coast (km)**	**Population density (persons/km²)** [226]
(A) PL, BOM-067113								
Penrith Lakes regional park (150°40'42"E , 33°43'10"S, 24.7 m asl)	- Western Sydney	- Greenery - bare soil - lakes	- 25% tree canopy cover - 15.3% non-plantable - 54% potentially plantable	- Aquapark and aqua golf facility nearby - The Nepean River in the west of the site.	Primarily residential and commercial buildings	55km northwest of CBD	49 km southeast of the station	484
(B) CT, BOM-068257								
The Australian Botanic garden (150°46'25"E , 34°3'41"S, 112m asl)	- Western Sydney	- Greenery - Trees - bare soil	- 34.2% tree canopy cover - 12% non-plantable - 38.5% potentially plantable	. Lake Nadungamba near the station, - Annan lake in northwest of the station (1.43 km)	Residential /semi-rural area	46 km southwest of CBD.	28 km southeast of the station	509.4
(C) LP (NSW government)								
Raine park (150° 54' 21"E, 33° 55' 58"S, 22m asl)	- Western Sydney	- Greenery - roads	- 23.3% tree canopy cover - 16.3% non-plantable - 51.1% potentially plantable.	None	Mixed residential and commercial area.	28.9 km southwest of CBD	23 km southeast of the station	668.82
(D) OP, BOM- 066212 (city of Auburn)								
Olympic park archery center	- Inner Sydney	- Greenery - creeks	- 15.4% tree canopy cover	-Paramatta river - Many creeks in the surrounding	Mixed used (residential, commercial,	12.7 km northwest of CBD	13.5 km southeast of the station.	2527.88

(151°4'18"E, 33°50'2"S, 4m asl)		- Parramatta river	- 50.4% non-plantable - 31.1% potentially plantable.	- Duck river	industrial, recreational areas, and parkland uses)			
(E) CY, BOM - 066194								
Canterbury racecourse park (151°6'48"E, 33°54'21"S, 3m asl)	- Inner Sydney	- Greenery - Ponds - Cooks River	- 17.5% tree canopy cover - 54.5% non-plantable - 22.8% potentially plantable.	- Cooks River - Pond	Primarily residential and light industrial.	17 km southwest of CBD.	7.5 km southeast of the station.	4303
(F) OH, BOM -066062								
Observatory Hill (151°12'18"E, 33°51'39"S, 39m asl)	- Eastern Sydney	- Roads - Greenery - High rise buildings	- 15.2% tree canopy cover - 69.1% non-plantable - 13.2% potentially plantable	- Site near coast	Commercial buildings, parks, etc.	N/A	0.6 km northeast of the station	6160

4.4 Heatwave identification and selected heatwave events:

As discussed in section 2.2.1, "heatwaves identification methods," threshold temperature, heatwave duration, and city's spatial extension are required to define heatwaves. This dissertation uses the RTT metric to establish the threshold temperature to account for spatiotemporal variation. Further, three consecutive days were considered the minimum duration of heatwaves, as utilized in several other global studies [50,113]. More into it, only those episodes were considered, which co-occurred at all locations in eastern, inner, and western Sydney, to assume the spatial extension of the phenomenon. Table 4-2 demonstrates the total number of heatwaves (days and periods) identified from 1999 to 2017, using the 97th, 95th, and 90th percentiles.

Western Sydney suburbs demonstrated higher threshold temperatures (particularly at PL) than inner and eastern Sydney sites (Table 4-2). The threshold temperatures were around 3.5°C lower in the inner Sydney suburbs and 4.5°C lower in eastern Sydney suburbs than PL. In addition to the temperature threshold, the frequency of heatwaves reported in western Sydney was extremely high than inner and eastern Sydney between 1999 and 2017 (Table 4-2).

The number of heatwaves computed for western Sydney suburbs using the 97th percentile of the daily maximum temperature was greater than ten but reduced to almost half in the inner Sydney suburbs over the same period. Eastern Sydney even substantially reduced the number of heatwaves than inner Sydney. At the 97th percentile temperature threshold, only a few heatwaves were identified across all Sydney locations, and those that were seen did not occur concurrently, indicating local overheating. Numerous heatwaves were seen at all Sydney locations at the 95th percentile; hence, the 95th percentile of daily maximum temperature was used as a temperature threshold for investigation.

Figure 4-2 depicts all Sydney locations' heatwaves between 1999 and 2017. It is worth noting that the highest number of heatwaves occurred in 2009, while the lowest number occurred in 2012. Additionally, it is clear that the heatwave phenomenon was inconsistent from 1999 to 2008 but has increased in frequency and severity after 2013. Further, the intensity of the heatwave events increased from 2015 to 2017, as a larger frequency of heatwaves exceeding the 97th percentile was observed. Additionally, the analysis shows that the number of heatwave days was high in previous years, particularly in 2004, 2006, and 2013. However, the number of heatwave periods was low, particularly at the 95th and 97th percentiles, indicating that higher temperatures did not persist for an extended period, and the city cooled down after a day or two.

Table 4-2: Identified heatwaves at various stations from 1999-to 2017 using the RTT metric

Sr No	Weather Stations	RTT criteria	Threshold Temperature (^{o}C)	Heatwave days	Heatwave periods
1	OH- Reference Station- (Eastern)	97th Percentile	31.2	209	4
2		95th Percentile	29.4	345	14
3		90th Percentile	27.6	703	60
4	SA (Eastern)	97th Percentile	32.4	206	3
5		95th Percentile	30.7	346	15
6		90th Percentile	28.6	696	57
7	CY (Inner)	97th Percentile	32.5	212	5
8		95th Percentile	31	350	16
9		90th Percentile	28.7	689	56
10	OP (Inner)	97th Percentile	33.7	211	6
11		95th Percentile	32.1	346	13
12		90th Percentile	29.7	684	63
13	HK (Western)	97th Percentile	34.9	205	11
14		95th Percentile	33.1	343	26
15		90th Percentile	30.5	693	77
16	PL (Western)	97th Percentile	36.4	208	12
17		95th Percentile	34.7	342	31
18		90th Percentile	32	691	84
Identified heatwaves at various stations from 2006 to 2017 using the RTT metric.					
1	TH (Eastern)	97th Percentile	31.6	118	3
2		95th Percentile	29.9	202	9
3		90th Percentile	27.4	402	37
4	CT (Western)	97th Percentile	35	119	7
5		95th Percentile	33.2	205	16
6		90th Percentile	30.8	393	44

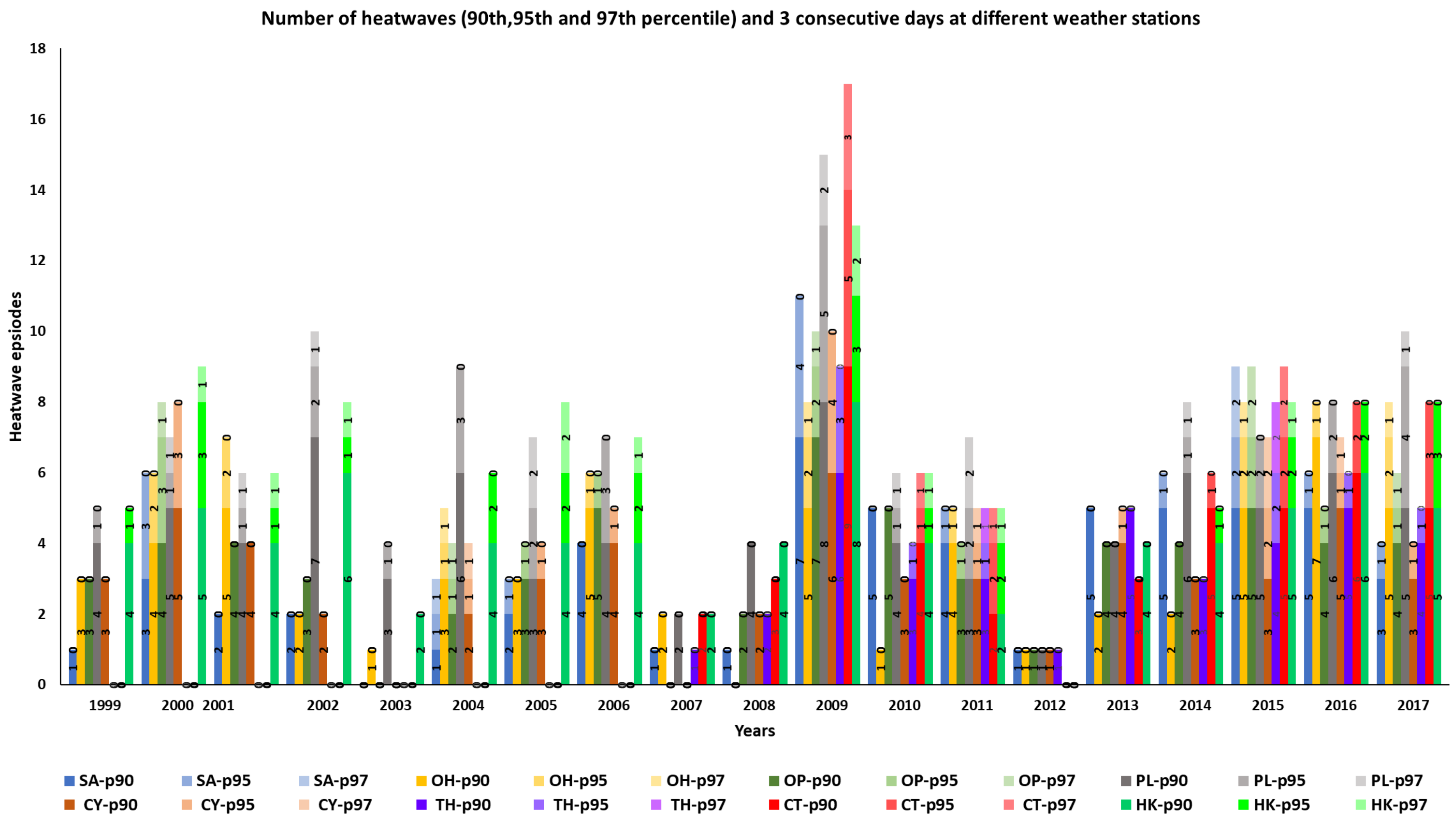

Figure 4-2 Heatwaves frequency from 1999 to 2017.

4.4.1 Heatwaves selected to determine synergies between UO and heatwaves:

A time-series investigation of the ambient temperature over Sydney from 1960 to 2016 revealed a rise in mean and maximum temperatures in recent years [224]. In 2017, record-breaking heatwaves affected northern Victoria, New South Wales (NSW), and southern Queensland, with Sydney and Brisbane recording the highest mean monthly temperatures [238]. Thus, heatwaves in recent years, 2015, 2016, and 2017 were chosen to investigate the relationships between UO and heatwaves. Because heatwaves were evaluated for three consecutive days, the background conditions were also examined for an equal number of consecutive days. Background conditions are defined as the consecutive equal number of days before or after heatwaves. In 2017, PL reported four heatwave incidents; CT and LP recorded three, while the inner Sydney locations recorded two (Table 4-3). The most intense heatwave event occurred in 2017 between 9-11th February, whereas the comparable background conditions occurred between 13-15th February. On February 11th, 2017, about 93 percent of NSW was 10 degrees warmer than normal [43]. Rather than severe temperatures, the prolonged period of persistently high temperatures distinguished summer 2017 as an extraordinary occurrence [238].

Additionally, it was planned to examine pair of background conditions, one preceding and one following each heatwave, to better understand the nexus between UO and heatwaves, as previously described [41,50]. However, the gap of only two days between the two heatwaves (4-6th Feb and 9-11th Feb) disqualified the preceding background event. Along with the intense heatwave event in 2017, two more concurrently occurred extreme heatwaves and background conditions were evaluated in 2016 and 2015. The common heatwave in 2016 was January 19-21st, whereas the comparable background condition was January 22-24th. Similarly, in 2015, a concurrent heatwave occurred between 18-20th November, whereas the equivalent background condition occurred between 15-17th November.

4.4.2 Heatwaves selected to determine synergies between UO and large-scale weather patterns:

To comprehend the changes in large-scale weather patterns through time, increasingly severe and concurrently occurring heatwaves from 1999 to 2017 were investigated, using the exact definition (threshold temperature> 95th percentile of daily maximum temperature for a minimum of three consecutive days at multiple locations). As indicated in Table 4-4, ten heatwaves and background incidents were evaluated. More heatwaves were chosen for this section because, in contrast to synergies between UO and heatwaves where qualitatively hourly analyses were performed, daily analyses were carried out to compare the daily large-scale weather patterns with UO.

Table 4-3: Heatwaves in 2015, 2016, and 2017 at various locations in Sydney using RTT (95th percentile) and three consecutive days.

Sr No	Weather stations	Threshold Temperature (°C) 95th Percentile	Number of Heatwaves in 2015	Number of Heatwaves in 2016	Number of Heatwaves in 2017	Heatwave events in 2017	Background conditions in 2017
1	OH- Reference Station (Eastern)	29.4	2	1	3	29-31 Jan 4-6 Feb 9-12 Feb	26-28 Jan 1-3 Feb 13-16 Feb
2	TH (Eastern)	29.9	2	1	2	4-6 Feb 9-11 Feb	1-3 Feb 13-15 Feb
3	SA (Eastern)	30.7	2	1	2	9-11 Feb 4-6 Feb	13-15 Feb 1-3 Feb
4	CY (Inner)	31.0	2	1	2	9-11 Feb 4-6 Feb	13-15 Feb 1-3 Feb
5	OP (Inner)	32.1	2	1	2	9-11 Feb 4-6 Feb	13-15 Feb 1-3 Feb
6	HK (Western)	33.1	2	2	3	8-11 Jan 4-6 Feb 9-12 Feb	4-7 Jan 1-3 Feb 13-16 Feb
7	CT (Western)	33.2	2	2	3	9-11 Jan 4-6 Feb 9-12 Feb	6-8 Jan 1-3 Feb 13-16 Feb
8	PL (Western)	34.7	2	2	4	8-11 Jan 16-18 Jan 4-6 Feb 9-12 Feb	4-7 Jan 19-21 Jan 1-3 Feb 13-16 Feb

Table 4-4: Heatwaves and background events from 1999-2017 at all studied sites.

#	**Year**	**heatwaves**	**Background events**
1	2000	24-26 Dec	28-30 Dec
2	2001	23-26 Jan	28-31 Jan
3	2004	12-14 Oct	16-18 Oct
4	2005	30 Dec- 01 Jan	4-6 Jan 2006
5	2009	20-22 Nov	23-25 Nov
6	2011	01- 05 Feb	7-10 Feb
7	2015	18-20 Nov	15-17 Nov
8	2016	19-21 Jan	22-24 Jan
9	2017	4-6 Feb	1-3 Feb
10	2017	9-11 Feb	13-15 Feb
Total days		**33**	**32**

4.4.3 Heatwaves selected to determine the combined impact of UO, heatwaves, and large-scale weather patterns on the built environment:

While evaluating the impact of multi-level climatic conditions on the built environment, heatwaves were defined as the interval when the daily ambient temperature was more than the 90^{th} percentile of the daily maximum temperature for a minimum of three consecutive days in various zones of Sydney, as used in [66,223,233] (Table 4-5). As discussed in section 2.2.1., the 90^{th} [58,62], 95^{th}[57,64], and 97^{th}[48,70] percentiles of daily maximum temperature have been used to establish threshold temperature; however, not many heatwaves were recorded with the 97^{th} and 95^{th} percentiles, required for energy analyses.

Table 4-5: Selected heatwaves to evaluate the multi-climatic implications on the built environment.

#	Year	Heatwaves	Heatwave days	Max temp at any station (°C)	Min temp at any station (°C)
Summer 2015-2016 (RSD: 81)					
1	2015	4-6 Oct	3	38	27.6
2	2015	18-20 Nov	3	42.4	30.8
3	2015	18-20 Dec	3	39.6	27.6
4	2016	19-21 Jan	3	39.1	29.6
5	2016	23-25 Feb	3	41.8	28.3
Heatwave days/ mean temperature			**15**	**40.18**	**28.78**
Summer 2016-2017 (RSD: 69)					
1	2016	28-30 Dec	3	39.5	27.7
2	2017	8-11 Jan	4	41.4	27.6
3	2017	16-18 Jan	3	43.4	27.6
4	2017	28-31 Jan	4	42.8	28.6
5	2017	4-6 Feb	3	40.6	29.3
6	2017	9-12 Feb	4	46.3	29.2
Heatwave days/ mean temperature			**21**	**42.3**	**28.3**

Further, as discussed earlier, hourly analyses were performed to examine the association between UO and heatwaves, and three selected (most intense) heatwaves during three successive years (2015, 2016, and 2017) were sufficient for qualitatively examining the interactions during heatwaves compared to backgrounds. Nonetheless, when assessing the influence of multilevel climatic changes on the built environment during heatwaves, the thermal performance of buildings was compared to that of the remaining summer days (RSD). Therefore, more heatwaves were considered using the 90^{th} percentile RTT metric. RSD is defined as the entire summer without heatwaves. The summer months are December, January, and February. Inconsistent findings may emerge from analyzing the energy performance of a building during a single heatwave [186,204,217]; hence, the summers of 2015-2016 and 2016-2017 were assessed. Table 4-5 stated that five extreme heat events were recorded in 2015-2016, whereas six were identified in 2016-2017. During 2015-16 and 2016-17, the average maximum temperature was roughly 40.2 °C and 42.3 °C, respectively (Table 4-5).

4.5 The classification used to define the large-scale weather patterns:

Both the circulation-pattern-based classifications (CPC) and the multivariate weather typing classification (WTC) have been utilized to examine the association between large-scale weather patterns and surface dynamics [9,129,170]. In bioclimatological [173] and urban-climatological [239] research, the WTC has been shown to be more practical [128], as discussed in section 2.3.1. The SSC has been extensively employed in the multivariate WTC to determine the relationship between large-scale weather patterns and UO [82,83,87]. However, geographic and seasonal relative measurements of the meteorological conditions are vital aspects to include in the daily weather patterns due to human adaption to local climates. The SSC may not sufficiently contemplate the seasonal and spatial variability [134]; nevertheless, such variations are incorporated in GWTC [135]. The automatic deseasonalized z-score initial typing technique used at the GWTC causes the character of airmass to appear in the various region throughout the year. As a result, any weather pattern can happen at any time of year/month, reducing seasonal variations. Furthermore, the characteristics of the same airmass might differ depending on the season and geography. The degree to which the two variables -temperature and humidity- are partitioned among the weather patterns also varies by location and season.

In this dissertation, the GWTC has been utilized to associate the UO with large-scale weather patterns for the first time. (https://www.personal.kent.edu/cclee/gwtc2global.html) was used to retrieve the appropriate GWTC data for Sydney. As stated in section 2.3.1, in GWTC, six near-surface meteorological variables, including temperature, dew point temperature, wind speed, wind direction, mean sea level pressure, and cloudiness, are used to classify days into eleven weather patterns (nine core and two transitional) [135]. Further details about GWTC airmass characteristics are provided in Table 2-2, and Figure 4-3.

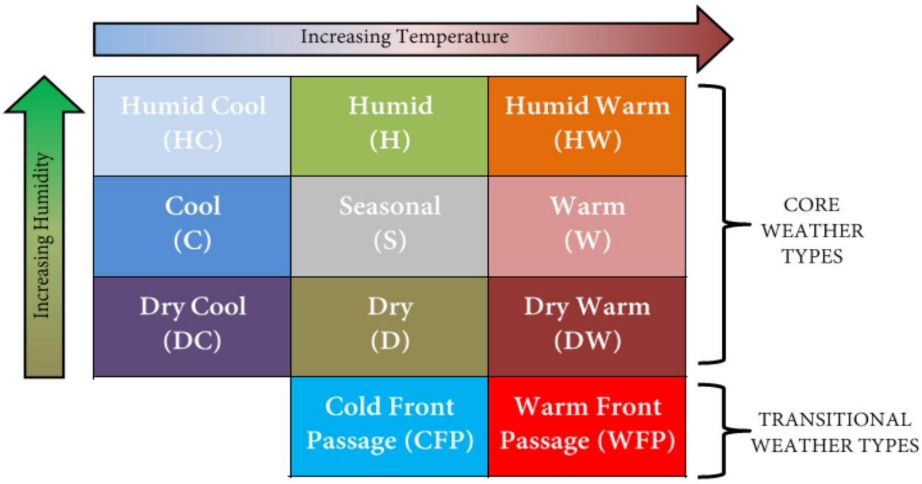

Figure 4-3: Weather patterns according to GWTC. (Image source [135])

4.6 The urban settlements utilized to measure the impact of climate changes on the built environment:

According to a report published by the office of environment and heritage in New South Wales (NSW), 70 percent of the state's housing stock (2.8 million dwellings) is comprised of detached houses, followed by units (19 percent) and semi-detached housing (11 percent) [240]. Based on urban density, two residential settlements were chosen for the thermal performance assessment, i) open single dwelling (OT1) and compact medium-rise housing (CT4) [241]. The NSW Department of Planning and Environment has defined these typologies as part of fourteen major archetypes [241]. Typically, geometrical and non-geometrical parameters are retrieved from archetypes, which are essential for energy modeling, particularly at a broader scale (neighborhood/ district/ city), and are otherwise impossible to estimate for each individual structure [242]. For instance, envelope detailing, schedules (occupancy, lighting, etc.), internal loads, etc., can be acquired from archetypes based on the building age and function. Figure 4-4 depicts the OT1 as a typical low-density (LD) detached residential settlement (houses), whereas the CT4 outlines a typical high-density (HD) settlement (apartments).

Each model consisted of two hundred buildings and their respective microclimatic contexts. The Sketchup pro-2017 was used to create urban building models of both typologies. Table 4-6 provides more information about the two archetypes. From the archetypes, geometrical characteristics such as road breadth, the distance between buildings, microclimatic context, building height and area, number of stories, etc., and other unique attributes such as window-wall ratio (WWR), window spacing, etc. were obtained.

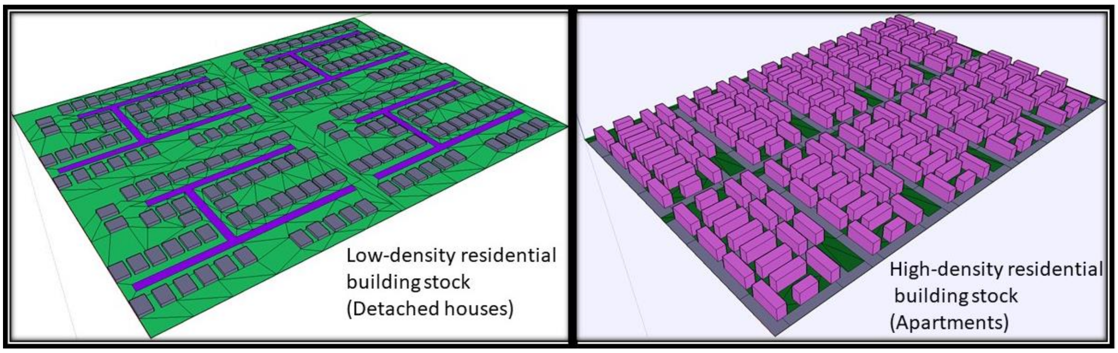

Figure 4-4 LD and HD residential settlement models

Table 4-6: Building Modelling features in LD and HD settlements.

Building Type	Building Size	Building height	Stories	Story height	WWR	Occupant density	Internal gains		Mechanical ventilation
	(m²)	(m)	*	(m)	(%)	(m²/P)	Sensible Loads (W/P)	Latent Loads (W/P)	*
House	15*20 (300)	4	1	4	25	50	91	45	The ideal system is considered without considering efficiency to maintain setpoints.
Apartment	65*20 (1300)	30	8	3.75	35	25	91	45	
Note: Sensible/ latent loads are calculated using NatHERS internal sensible (including people, lighting, and appliances) and latent heat loads daily schedule (daily average)-calculated for four households-Appendix B.1									

Both typologies' thermophysical attributes, including thermal properties of construction assemblies, internal loads, HVAC details, etc., have been defined using National Construction codes (NCC). NatHERS' daily internal load schedules were used to determine the internal loads [243]. The total sensible heat load was determined by adding the daily averages of illumination, people, and appliance loads. Likewise computed were daily averages per person for latent heat loads, which are also in accordance with ASHRAE guidelines as stated in ASHRAE Fundamentals [244]. According to Australian National Construction codes [245], detached dwellings are designated as class-1A structures, while apartments are categorized as class-2. The criteria for apartments and other commercial facilities are included in NCC Volume 1, whereas detached residences are covered in NCC Volume 2 [245].

4.6.1 NCC and NatHERS climatic zones for energy analyses:

The NCC divides Australia into eight climatic zones: zones one through eight, with zone one representing a warmer climate and zone eight representing a colder climate [246]. Eastern and inner Sydney have been designated climatic zone 5 (warm temperate), while Western Sydney has been assigned climate zone 6 (mild temperate) [247]. In addition to the NCC climate categorization, NatHERS—designed for the energy efficiency evaluation of residential buildings—has split the country into 69 climatic zones, with maximum yearly energy demands established against a star band (0.5-10 star bands- with 0.5-star band increment) for each climatic zone [243]. The selected sites in eastern, inner, and western Sydney have been placed in NatHERs zones 17, 56, and 28, respectively, and accordingly, simulation inputs (for instance, setpoint temperature) have been provided.

4.6.2 The software utilized to evaluate the urban thermal performance:

The building's thermal performance has been extensively evaluated using building energy models (BEMs) [92,198,212], where the microclimatic context was mainly ignored. With the progression in computing resources, the multi-extent and multi-disciplinary complex urban energy simulations have been capacitated at a larger scale by developing the urban building energy models (UBEMs) [248–250]. The UBEM is an essential instrument for comprehending the impact of the urban energy budget (net radiative heat flux- shortwave absorption and longwave emission, available energy- sensible and latent heat fluxes, anthropogenic, storage, and advective heat fluxes) on building thermal performance.

Based on the simulation approaches employed, UBEM tools may be divided into top-down and bottom-up models [242]. In the bottom-up method, rather than linearly scaling up from one building to several structures, building physics and engineering models are utilized to simulate the dynamic and complex associations between buildings and the urban environment [250]. Modern UBEM tools include Urban modeling interface (UMI) [251], CitySim [252], and City energy Analyst (CEA) [253]. In this dissertation, while evaluating the impact of multilevel climatic changes on the built environment, the most recent version of CitySim pro was used to conduct neighborhood-scale detailed energy simulations.

CitySim is a C++-based graphical user interface (GUI) that performs comprehensive dynamic simulations using a physics-based model based on electrical circuit analogies (resistor-capacitor network) [185,250]. Further, the simulation utilizes the hourly urban radiation model (based on the simplified radiosity algorithm-SRA), building thermal, HVAC equipment, energy conversion, and occupant behavior models [248]. Previously, the software's findings were validated using the Building Energy simulation test (BESTEST) validation technique [254], where the software's results were compared to those of a group of other programs, i.e., the IEA BESTEST suite [255]. Also, the results from CitySim were similar to the monitored data on energy use, with only minor differences, as was concluded in [254]. The software can simulate/ generate hourly buildings' energy and electricity demand, indoor temperature, surface shortwave irradiance and convective heat transfer, outdoor surface temperature, and surface evapotranspiration, using the hourly meteorological data. Further, CitySim employs an ideal HVAC system for simulation.

4.6.2.1 Climate and horizon files for building thermal performance evaluation:

The accuracy of meteorological data is crucial for effectively anticipating buildings' energy and thermal performance in urban and rural settings. In cities where the UO impact is more vigorous, the influence of adequate climatic data on the thermal response of buildings is critical. Historically, typical meteorological year (TMY) data were predominantly used to evaluate the effect of heatwaves on building energy performance [202,204]. However, since it is collected based on the average year (from past years), it ignores historical extremes and regional variability, and cannot assess the true impact of extreme heat events on energy use**.** Moreover, in the majority of research, meteorological data have been gathered from airports, which, as they are located outside metropolitan areas, do not accurately represent urban characteristics.

As mentioned in section 4.3, "Meteorological data collection and processing," the Australian BOM half-hourly meteorological data was used for climate file compilation for the selected sites [235]. The meteorological data included ambient temperature, relative humidity, wind speed, and wind direction. Further, instead of six locations, three sites in three zones of Sydney were chosen for energy analyses, and accordingly, climate files were created. Consideration was given to PL (the most affected site in western Sydney), OP (a dense area in inner Sydney), and OH (reference station in eastern Sydney). After data validation and meteorological data hourly-averages calculation, climate files were created for 2015-16 and 2016-17. The radiation data for the specified sites were not accessible, and even if it was, it had several gaps and was unsuitable for constructing the climate files. The Parramatta station (-33.78, 151.02) in the western Sydney region provided global horizontal radiation (W/m²), diffuse horizontal irradiance (W/m²), and solar normal irradiance (W/m²). Figure 4-5 depicts ambient temperature and radiation variations at several Sydney locations.

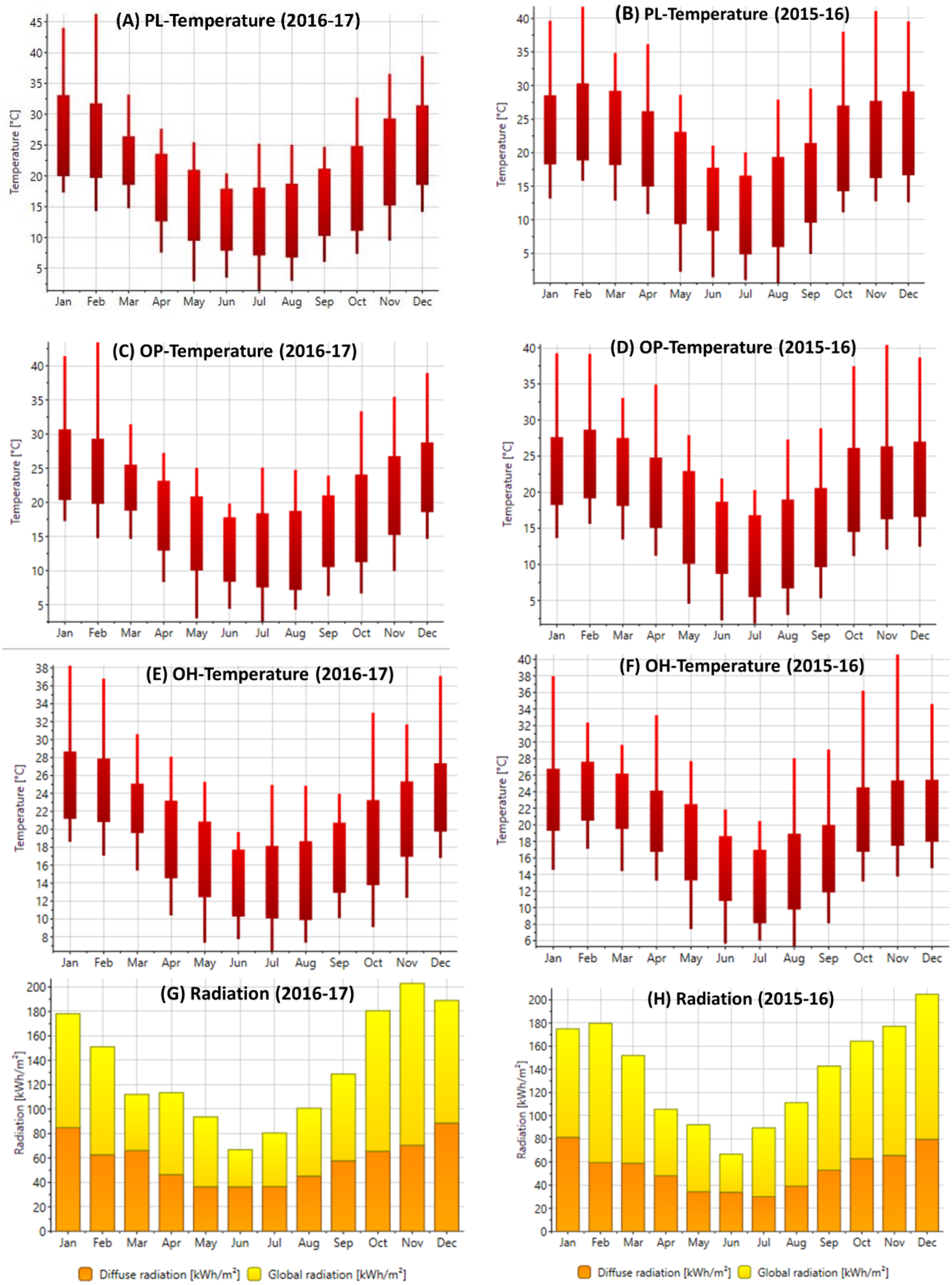

Figure 4-5 Variations in temperature and radiation data at various Sydney sites in 2016-17, and 2015-16. Temperature variations: A) PL-2016-17, B) PL-2015-16, C) OP-2016-17, D) OP-2015-16, E) OH-2016-17, F) OH-2015-16. Radiation: A) 2016-17, B) 2015-16.

The climate (.cli) and horizon (.hor) files were created using Meteonorm 8.0 [256]. Further, the climate file was created hourly for an entire year (8760 hours). The cloud-cover fraction (Octas), precipitation (mm), and surface temperature (°C) were the additional factors necessary for energy simulation on CitySim. Using Meteonorm, the missing parameters were computed, where Meteonorm employs radiation time series to create cloud-cover and precipitation data, and radiations were supplied as inputs. Figure 4-6 shows the horizon files compiled for each examined location. The horizon file comprises i) obstruction angle and ii) spatial position. The obstruction angle is the hindrance from external natural components (e.g., mountains)- specified from 0 to 90 degrees in elevation. In contrast, the spatial position angle is measured as 0 degrees for the south, 90 degrees for the west, 180 degrees for the north, and -90 degrees for the east.

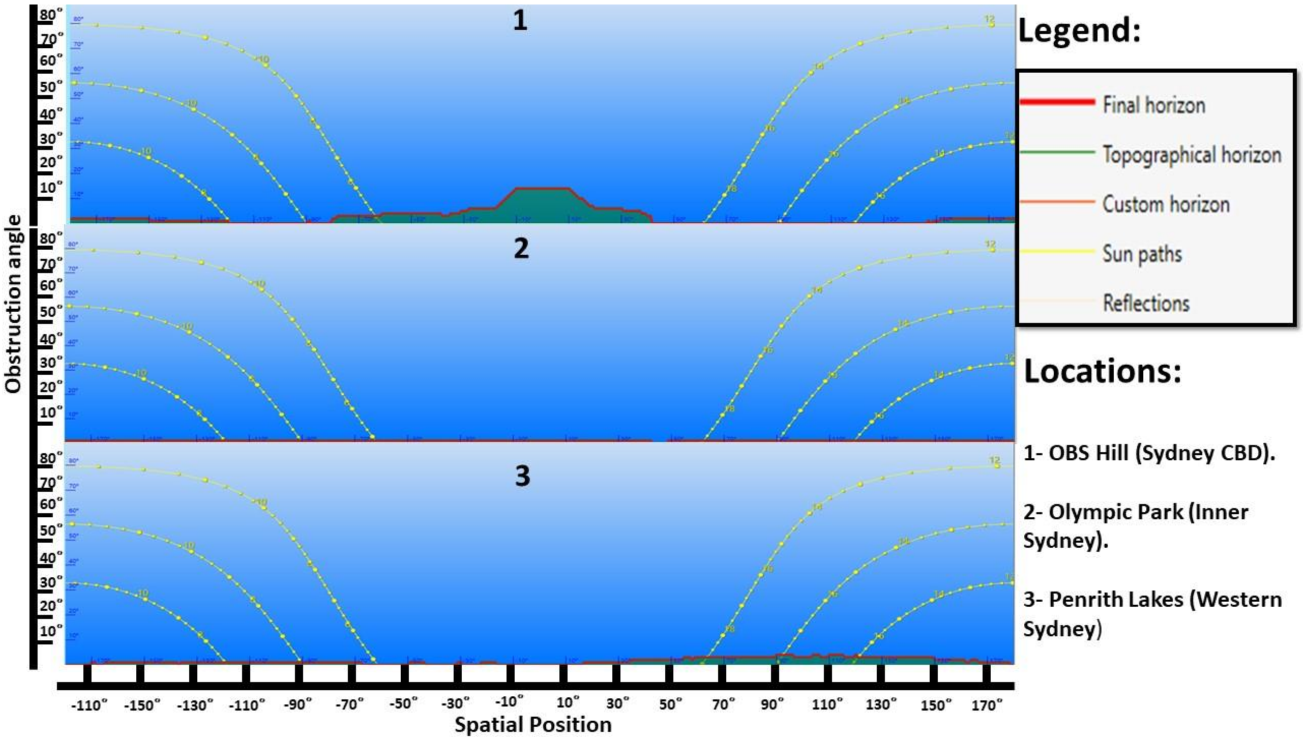

Figure 4-6: Horizon files 1) OH, 2) OP, and 3) PL, created using Meteonorm 8.0.

4.6.3 The passive survivability standards employed to measure the impact of climate changes on the built environment:

The indoor temperature above which heat-related illnesses arise varies by region. Subsequently, the World Health Organization (WHO) has established the minimal indoor risk temperature (above which health issues/ morbidity risk arises-T_{risk}) and the maximum acceptable indoor temperature (critical indoor temperature for human health- T_{accep}) for various regions [207,257]. Given the recent fast rise in heatwave severity and frequency in Australia (particularly in Sydney), WHO-recommended indoor temperature thresholds for Thailand's subtropical (hot and humid) climate [257] were used.

Thailand's suggested T_{risk} is 30°C, while the T_{accep} is 32°C, at which health concerns may emerge. Similarly, the chartered institute of building services engineers (CIBSE) recommends a thermal discomfort threshold of 28°C for the living room and 26°C for the bedroom as part of their overheating criterion for free-floating dwellings [207,258,259]. While evaluating the combined impact of climatic changes on IEQ, this dissertation estimated passive survivability as the fraction of hours over threshold temperature to the total hours, either during heatwaves or RSD, as described in [207]. Using the WHO and CIBSE standards, the threshold temperature was set at 26, 28, 30, and 32°C.

4.7 Methodology:

The approaches used to explore the relationship between multi-level climatic conditions and their effect on the built environment are presented below.

4.7.1 Methods used to examine the association between UO and heatwaves.

Typically, the urban heat island (UHI) is used to measure the effects of urbanization. Generally, UHI is calculated as a thermal gradient between urban and rural locations. Inner-urban thermal contrast was estimated (UO) in this research as an alternative to UHI for measuring the impact of urbanization in various parts of the city. Further, UO was estimated as the temperature gradient between Sydney's suburbs and the central business district ($UO = T_{suburbs} - T_{CBD}$) since Sydney's suburbs (inland) are far more susceptible to extreme weather occurrences and are losing their habitability compared to Sydney CBD (coastal locations), as stated by several studies [224,260]. Further, the suburban-urban thermal gradient was expressed as UO, UC (urban cooling), and ΔT (thermal difference). UO represents the positive value of thermal gradient when suburban temperatures are greater than the CBD. UC reflects the negative value of thermal gradient when suburban temperatures are lower. ΔT is a generic terminology employed, regardless of whether the temperature gradient is positive or negative.

Different responses to UO during heatwaves might emerge from implementing different UO calculation methodologies. Calculating UO utilizing either the ambient temperature (T_a) [1,230] or the surface temperature (T_s) [52,54,57] may yield contrasting results. Generally, nighttime UO was magnified when UO was computed with T_a (owing to the stored heat in urban fabric releasing at night and raising the near-surface temperature) [159], whereas daytime UO was considerably amplified with T_s [261,262]. Because T_a at 2 m height has a direct impact on human thermal comfort, thus, UO was determined using T_a.

Formerly, UO was computed using hourly temperature [49], median temperature [58], daily average temperature [62], daytime and nighttime average temperature [41], and monthly average temperature [54], with varying findings. Qualitative hourly studies were undertaken in this segment for each heatwave/background event, instead of daily analyses, to comprehend the diurnal fluctuations in meteorological patterns, mainly winds, which abruptly change.

The synergies between UO and heatwaves were examined in two sections. In the first section, hourly qualitative investigations were carried out for the most affected suburb in Sydney (PL); during the most severe heatwave in recent decades (heatwaves: 9-11th Feb 2017, corresponding background condition: 13-15th Feb 2017) to comprehend the critical factors caused this extreme heat event. In the second section, the analyses were extended to all selected sites in three zones of Sydney during three consecutive summers (2015, 2016, 2017) for all selected heatwaves, as discussed in section 4.4.1. Further, in the second phase, in addition to hourly qualitative analyses, statistical models were employed to find the association between UO and heatwaves. More into it, while performing these spatiotemporal analyses, the impacts of population density, land-coast distance, and site characteristics (tree canopy cove, plantable/ non-plantable surfaces) were also examined on UO during heatwaves.

In both sections, initially, variations in UO magnitude during heatwaves were examined compared to background conditions. The heatwave-background hourly average UO contrast was termed $\triangle$UO. Later, the associations between UO and absolute humidity (AH) were analyzed during heatwaves and background conditions to comprehend the available energy variations. Similar to UO, the absolute humidity difference ($\triangle$AH) between the urban and suburban sites was computed as ($\triangle AH = AH_{suburb} – AH_{CBD}$). After analyzing the variations in available energy, the hourly qualitative analyses were performed to associate UO with wind patterns during both heatwaves and background conditions. Later, the connection between advective heat flux and available energy was also examined during heatwaves and background conditions. During the summer, due to daylight saving time, daytime was regarded to be from 8 a.m. to 8 p.m., and nighttime was from 10 p.m. to 6 a.m.

4.7.2 Methods used to examine the association between UO and large-scale weather patterns.

As mentioned in the previous section, UO was computed as ($UO = T_{suburbs} - T_{CBD}$), using the T_a. Formerly, numerous UO expressions were employed to determine the relationship between UO and large-scale weather patterns. Daily large-scale weather patterns, for example, were compared to average daily UO [74,79,87], maximum daily UO [86], or minimum daily UO [83,84,263]. This dissertation compares daily maximum and minimum temperature differences (UO and UC) to the daily large-scale weather pattern to determine both extremes rather than averages, as accomplished in numerous previous studies [80,82]. A link between UO and large-scale weather patterns has been evaluated using circulation-to-environment [80,82,87] and environment-to-circulation [75] approaches, as discussed in section 2.3.1. This thesis grouped ΔT according to daily large-scale weather patterns, making circulation-to-environment the principal application approach. Previously, a comparison between UO and large-scale weather patterns was also conducted for a shorter length of time (one to two years) [85,86], which may have produced conflicting findings. This thesis compares ΔT to large-scale weather patterns from 1999 to 2017.

First, large-scale weather patterns' overall and seasonal frequency from 1999 to 2017 was examined to discover which weather patterns happened more often. Following this, the daytime and nocturnal ΔT frequency were analyzed to determine when UO and UC occurred most frequently. Changes in ΔT magnitude from 1999 to 2017 were analyzed to comprehend the variations in UO magnitude over time. The top five percent of maximum daily ΔT (UO) and the bottom five percent of minimum daily ΔT (UC) were compared to daily large-scale weather patterns to determine which weather patterns predominantly caused exacerbated UO and UC. The diurnal ΔT changes (maximum daily daytime ΔT and minimum daily nighttime ΔT) were correlated with daily large-scale weather patterns to corroborate the UO and UC results.

According to dawn and sunset, daytime and nighttime lengths were determined. The seasonal fluctuations in maximum daily ΔT were similarly associated with the large-scale weather patterns. The relationship between large-scale weather patterns and UO was also investigated during heatwaves and background conditions to comprehend the prevailing conditions affecting UO during heatwaves. The selected heatwaves and backgrounds are discussed in section 4.4.2 and in Table 4-4. The large-scale weather patterns are discussed in section 4.5.

4.7.3 Methods used for estimating the impact of climate changes on the built environment:

Firstly, the thermal responsiveness of both settlements (LD and HD) to spatial and temporal fluctuations, urban overheating, heatwaves, and the cumulative influence of UO-heatwaves were examined, taking into account the existing building features, using CitySim as discussed in section 4.6. As discussed previously, Sydney suburbs are experiencing scorching temperatures during both heatwaves and RSD; therefore, UO was estimated as the thermal gradient between suburbs and Sydney CBD ($UO= T_{suburb}- T_{CBD}$). Comparing the thermal performance of both settlements in the suburbs with the thermal performance in the Sydney CBD ($TP_{UO}= TP_{suburbs} – TP_{CBD}$) independently during heatwaves and RSD allowed quantifying the UO influence on urban thermal performance. The cumulative influence of urban overheating and heatwaves on the thermal performance of both settlements was assessed by comparing thermal performance in the suburbs during heatwaves to thermal performance in Sydney CBD during RSD. The influence of heatwaves on urban thermal performance was evaluated by comparing the settlement's thermal performance during each summer's heatwaves to the RSD for that year.

The cooling energy, indoor temperature, and passive survivability were all taken into account while calculating the thermal performance of both settlements. Indoor comfort was tested using free-floating conditions, whereas variations in energy patterns of both settlements were assessed with thermostat settings- suggested by NatHERS. The influence of the adaption scenarios on buildings' thermal performance was assessed for one summer (2016-17), and sensitivity assessments were conducted in all zones, for both settlements, during heatwaves and RSD. In a larger perspective, sensitivity assessments were conducted under three primary categories: i) Uninsulated, ii) Intermediately Insulated, and iii) Hyper Insulated.

The majority of NSW residential building stock (70 percent) was built before 1990 with an uninsulated envelope. Therefore, the uninsulated scenario in this dissertation was chosen according to existing building characteristics, as listed in Table 4-7. The NCC-2019 energy efficiency standards were used to define hyper-insulated scenarios to check how star-rated buildings perform during extreme heat conditions (Table 4-9). Further, there are two approaches to ensure NCC compliance. The first is "Simulation compliance," which employs NatHERS-authorized tools such as AccuRate to certify the energy rating of a building depending on its design, materials, usage, and climate [202,218,243]. The second option is to employ the "elemental approach," which involves deemed-to-satisfy (DTS) solutions listed in the NCC- based on the building category [264,265]. Compliance with DTS standards ensures that performance criteria are met automatically. Since AccuRate employs TMY climate data for simulation and disregards climatic extremes, the NCC requirements for hyper-insulated scenarios were met using DTS criteria. Lesosai was employed to tailor the building envelope details to NCC specifications [266]. The optimal degree of insulation was added in the intermediately insulated option, as described in [39]. Further details about intermediately insulated envelopes are presented in Table 4-8.

Table 4-7: Uninsulated building envelope details for LD settlement and HD settlement in Zone 5 and 6 of Sydney (Layer's arrangement in all composites are from the external side to the internal side).

Envelope type (CitySim ID)	Layer (CitySim ID)	Thickness (m)	Total thickness (m)	Thermal conductivity (W/m*K)	Heat capacity Cp (J/kg*K)	Density (kg/m^3)	Composite U-value (W/m^2*K)
Uninsulated roof for Class-1 (house) building in both climates 5 and 6							
Roof-RH-O (76)	Clay tile (81)	0.015	0.38	1	800	2000	1.221
	Air layer (1)	0.0254		*	*	*	
	Timber planks (349)	0.03		0.15	2700	470	
	Air layer (1)	0.3		*	*	*	
	Gypsum plasterboard (358)	0.0125		0.21	799.2	850	
Uninsulated roof for Class-2 (Apartment) building in both climates 5 and 6							
Roof-RA-O (77)	Clay tile (81)	0.015	0.24	1	800	2000	2.1
	Air layer (1)	0.0254		*	*	*	
	Reinforced cement concrete (31)	0.2		1.6	1000	2200	
Uninsulated external wall for Class-1 (house) and Class-2 (apartment) buildings in both climates 5 and 6							
Wall-RHRA-O (54)	Solid fired clay brick (328)	0.11	0.16	1	1000	1600	2.079
	Air layer (1)	0.04		*	*	*	
	Plaster board (172)	0.01		0.4	799.2	1000	
Uninsulated floor for Class-1 (House) and Class 2 (Apartment) buildings in climates 5 and 6							
Floor-RHA-O (92)	Cast concrete (31)	0.16	0.176	1.6	1000	2200	3.206
	Lightweight mortar (332)	0.004		0.85	1000	1200	
	Ceramic tiles (199)	0.012		1	1000	1900	
GROUND_Asphalt							
Ground-AS (21)	Cast Asphalt (201)	0.025	4.00	0.7	1100	2150	-
	Soil, sand, and gravel (281)	0.02		2	1051	2000	
	Gravel (376)	0.1		2	1051	2000	
	Soil, clay, and slime (280)	3.855		1.5	2098	1500	

GROUND_Green							
Ground-GR (100)	Clay (160)	1	1	0.93	900	1700	-

Table 4-8: Intermediately insulated building envelope details for LD settlement and HD settlement in Zone 5 and 6 of Sydney (Layer's arrangement in all composites are from external side to internal side).

Envelope type (CitySim ID)	**Layer (CitySim ID)**	**Thickness (m)**	**Total thickness (m)**	**Thermal conductivity (W/m*K)**	**Heat capacity Cp (J/kg*K)**	**Density (kg/m^3)**	**Composite U-value (W/m^2*K)**
Intermediately insulated roof for Class-1 (house) building in both climates 5 and 6							
Roof-RH-M (78)	Clay tile (81)	0.015	0.45	1	800	2000	0.362
	Air layer (1)	0.0254		0.025	1000.8	1.23	
	Vapor Barrier (350)	0.001		0.2	1400.4	920	
	Rockwool (224)	0.07		0.036	600	90	
	Timber planks (349)	0.03		0.15	2700	470	
	Air layer (1)	0.3		*	*	*	
	Gypsum plasterboard (358)	0.0125		0.21	799.2	850	
Intermediately insulated roof for Class-2 (apartment) building in both climates 5 and 6							
Roof-RA-M (79)	Clay tile (81)	0.015	0.31	1	800	2000	0.41
	Air layer (1)	0.0254		0.025	1000.8	1.23	
	Vapor Barrier (350)	0.001		0.2	1400.4	920	
	Rockwool (224)	0.07		0.036	600	90	
	Reinforced cement concrete (31)	0.2		1.6	1000	2200	
Intermediately insulated external wall for Class-1 (house) and Class-2 (apartment) buildings in both climates 5 and 6							
Wall-RHRA-M (55)	Hollow brick (150)	0.11	**0.31**	0.7	1100	1200	0.49
	Air layer (1)	0.04		0.025	1000.8	1.23	
	Rockwool (224)	0.05		0.036	600	90	

	Hollow brick (150)	0.11		0.7	1100	1200	
External wall with thermal inertia (intermediate level) for Class-1 (house) and Class-2 (apartment) buildings in both climate 5 and 6							
Wall-MTM-RHRA-M (56)	Hollow brick (150)	0.11	**0.26**	0.7	1100	1200	1.54
	Air layer (1)	0.04		*	*	*	
	Hollow brick (150)	0.11		0.7	1100	1200	
Intermediately insulated floor for Class-1 (house) and class 2 (apartment) buildings in both climate 5 and climate 6							
Floor-RHA-M (93)	Cast concrete (31)	0.16	0.206	1.6	1000	2200	0.873
	Rockwool (224)	0.03		0.036	600	90	
	Lightweight mortar (332)	0.004		0.85	1000	1200	
	Ceramic tiles (199)	0.012		1	1000	1900	

Table 4-9: Highly insulated building envelope details for LD settlement and HD settlement in compliance with NCC 2019 DTS in Zone 5 and 6 of Sydney (Layer's arrangement in all composites are from the external side to the internal side).

Envelope type (CitySim ID)	Layer (CitySim ID)	Thickness (m)	Total thickness (m)	Thermal conductivity (W/m*K)	Heat capacity Cp (J/kg*K)	Density (kg/m3)	Composite U-value (W/m^2*K)-DTS criteria
Highly insulated roof for Class-1 (house) building in both climates 5 and 6							
Roof-RH-H (80)	Clay tile (81)	0.015	0.55	1	800	2000	0.180 < 0.19
	Air layer (1)	0.0254		*	*	*	
	Vapor Barrier (350)	0.001		0.2	1400.4	920	
	Rockwool (224)	0.17		0.036	600	90	
	Timber planks (349)	0.03		0.15	2700	470	
	Air layer (1)	0.3		*	*	*	
	Gypsum plasterboard (358)	0.0125		0.21	799.2	850	
Highly insulated roof for Class-2 (apartment) building in both climates 5 and 6							
Roof-RA-H (81)	Clay tile (81)	0.015	0.38	0.44	900	1100	0.228 < 0.27/0.31
	Air layer (1)	0.0254		0.025	1000.8	1.23	

	Vapor Barrier (350)	0.001		0.2	1400.4	920	
	Rockwool (224)	0.14		0.036	600	90	
	Reinforced cement concrete (31)	0.2		1.6	1000	2200	
Highly insulated external wall for Class-1 (houses) and Class-2 (apartment) buildings in both climate 5 and 6							
Wall-RHRA-H (57)	Hollow brick (150)	0.11	**0.36**	0.7	1100	1200	0.292 < 0.35
	Air layer (1)	0.04		*	*	*	
	Rockwool (224)	0.1		0.036	600	90	
	Hollow brick (150)	0.11		0.7	1100	1200	
External wall with thermal inertia (high level) for Class-1 (house) and Class-2 (apartment) buildings in both climate 5 and 6							
Wall-MTM-RHRA-H (58)	Hollow concrete block (150)	0.19	**0.42**	0.7	1100	1200	1.116
	Air layer (1)	0.04		*	*	*	
	Hollow concrete block (150)	0.19		0.7	1100	1200	
Highly insulated floor for Class-1 (house) building in climate 6, and Class-2 (apartment) building in both climate 5 and 6							
Floor-RHA-H (95)	Cast concrete (31)	0.16	0.25	1.6	1000	2200	0.443 <0.44/0.5/1.0
	Rockwool (224)	0.07		0.036	600	90	
	Lightweight mortar (332)	0.004		0.85	1000	1200	
	Ceramic tiles (199)	0.012		1	1000	1900	

Table 4-10: Base-case and adaptive scenarios for LD and HD settlements.

Purpose	Adaptation strategy	Strategy level	Type/ standard/ method	Details	Reference
Heat gain reduction	Insulation	**Base-Case:** Non-insulated	Typical residential building.	**Roof (house):** U-Value= 1.2 W/m². K	Table 4-7, Roof-RH-O (76)
				Roof (apartment): U-Value= 2.1 W/m².K	Table 4-7, Roof-RA-O (77)
				Wall (house/ apartment): brick veneer, U-Value= 2.08 W/m². K	Table 4-7, Wall-RHRA-O (54)
				Floor (house/ apartment): U-Value= 3.206 W/m². K	Table 4-7, Floor-RHA-O (92)
		M1- Intermediately insulated	Optimized level of insulation	**Roof (house):** U-Value= 0.362 W/m². K	Table 4-8, Roof-RH-M (78)
				Roof (apartment): U-Value= 0.41 W/m². K	Table 4-8, Roof-RA-M (79)
				Wall (house/ apartment): Double hollow brick wall with cavity and insulation, U-Value= 0.49 W/m². K	Table 4-8, Wall-RHRA-M (55)
				Floor (house/ apartment): U-Value= 0.873 W/m². K	Table 4-8, Floor-RHA-M (93)
		M2-Highly insulated	In accordance with NCC-2019 DTS.	**Roof (house):** U-Value= 0.18 < 0.19 W/m². K	Table 4-9, Roof-RH-H (80)
				Roof (apartment): U-Value= 0.228 < 0.27/0.31 W/m². K	Table 4-9, Roof-RA-H (81)
				Wall (house/ apartment): Double hollow brick wall with cavity and insulation, U-Value= 0.292<0.35 W/m².K	Table 4-9, Wall-RHRA-H (57)
				Floor (house/ apartment): U-Value= 0.43<0.44/0.5/1.0 W/m². K	Table 4-9, Floor-RHA-H (95)
Heat gain reduction	Thermal inertia (Walls)	**Base-Case:** Typical condition	Non-insulated brick veneer (solid brick, cavity, and plasterboard)	**Wall (house/ apartment):** U-Value= 2.08 W/m². K	Table 4-7, Wall-RHRA-O (54)
		M3- Intermediate thermal mass	Double hollow brick (110mm) with cavity	**Wall (house/ apartment):** U-Value= 1.54 W/m². K	Table 4-8, Wall-MTM-RHRA-M (56)

		M4- High thermal mass	Double hollow concrete block (190 mm) with cavity	**Wall (house/ apartment):** U-Value= 1.12 W/m². K	Table 4-9, Wall-MTM-RHRA-H (58)
Heat gain reduction	Blind control	**Base-Case** (Recommended)	$f_u = \frac{1}{1+e^{\lambda(I_f-100)}},$	Sigmoid function with Logit-scale factor(λ)= 0.2, cut-off irradiance= 100 W/m²	*
		M5- partially closed blinds		Logit-scale factor(λ)= 0.2, cut-off irradiance< 50 W/m²	*
Heat gain reduction	Glazing	**Base-Case:** Typical glazing	Single glazing	U= 5.8 W/m². K, SHGC= 0.84	*
		M6- Optimum level of glazing	Double glazing	U= 3.15 W/m². K, SHGC= 0.60	*
		M7- Highly insulated glazing	Calculated using "Glazing calculator NCC-2019" for houses (climate zone 6)	houses: U= 1.5 W/m²K, SHGC= 0.4	*
			Calculated using "Façade calculator NCC-2019" for apartment building (climate zone 5 and 6).	Apartments: U= 1.5 W/m². K, SHGC= 0.16 (for climate zone 5 and 6)	*
Heat gain reduction	Super cool roof-passive radiative cooling	**Base-Case:** Typical reflectivity, and emissivity	typical construction	Roof Albedo= 0.2, Roof emissivity= 0.9	*
		M8- Highly reflective, and emissive material	vinylidene fluoride-co-hexafluoropropene- passive radiative cooling	Roof Albedo= 0.96, Roof emissivity= 0.97	*
Heat gain reduction	Infiltration (infil)	**Base-Case:** Average-sealed	Typical building condition (national average for Sydney buildings)	1.0 ACH natural (20 ACH at 50 pascals)	0.1-2.0 ACH for residential buildings 0.5-2.0 ACH for commercial buildings, Source: ASHRAE-
		M9- Well-sealed	*	0.50 ACH natural (10 ACH at 50 pascals)	

		M10- Air-tight	Australian PH standards: infil <= 0.6ACH at 50 pascal	0.03 ACH natural (0.6 ACH at 50 Pascals)	Fundamentals chapter 16.15 and 16.29
Behavioral change	Cooling set points	**Base-Case**	In accordance with NatHERS cooling thermostat settings	24.5 $^{\circ}$C (Zone 6)/ 25.5C (Zone 5), Avg 25°C	*
		M11- 27°C cooling setpoint	Increased cooling setpoints (in accordance with WHO indoor thermal comfort limit)	27 $^{\circ}$C	
		M12- 28°C cooling setpoint		28 $^{\circ}$C	
Heat Dissipation	Nighttime cooling	**Base-Case:** 50% nighttime cooling	*	Window operable fraction= 0.5	*
		M13- 100% nighttime cooling	Operation time = 20:00-05:00	Window operable fraction>= 1.0	*
Landscape characteristics	Urban ground surface albedo	**Base-Case:** Typical condition	*	α = 0.2	*
		M14- Improved Albedo	*	α = 0.45	*
	Green surfaces evapotranspiration	**Base-case:** Drier Soil	Arid (0.1-0.2) Moist soil (0.6-0.8) Completely Wet: 1.0	K=0.4	*
		M15- Irrigated Soil		K= 0.7	*
Heat gain reduction and dissipation	Combination	**M16-** Intermediately Insulated envelope and nighttime cooling (M1+M13)		*	*
	Combination	**M17-** Highly Insulated envelope and nighttime cooling (M2+M13)		*	*
	Combination	**M18-** Intermediate thermal mass and nighttime cooling (M3+M13)		*	*
	Combination	**M19-** Highly thermal mass and nighttime cooling (M4+M13)		*	*

The adaptation strategies were arranged in four clusters, heat gain reduction (heat modulation/ protection), heat dissipation, behavioral modification, and modified landscape features. Heat gain reduction was examined with regard to insulation, thermal inertia, infiltration rates, glazing, shading, and passive daytime radiative cooling. The influence of different thermostat settings was studied in the context of behavioral modification. The impact of nighttime cooling was examined under heat dissipative measures. Improvements in urban surface albedo and green surface evapotranspiration rates were evaluated under landscape features. Additional information on the adaptation scheme is provided below and in Table 4-10.

4.7.3.1 Insulation:

Uninsulated scenarios: Brick Veneer is the most popular wall choice in NSW detached housing (45 percent), followed by the double brick wall (20 percent) [240]. For uninsulated cases, brick veneer was considered for both typologies, as shown in Table 4-7. Being the most popular choice for roof, the uninsulated flat concrete roof for apartments, whereas uninsulated cavity roof with timber planks for detached houses were considered (Table 4-7). Uninsulated concrete floors with ceramic tiles were considered for both typologies.

Insulated scenarios: In highly insulated scenarios, Rockwool was added to the roof, wall, and floor sections to satisfy the NCC DTS criteria, as shown in Table 4-9. The DTS criteria and U-values for all composites are also provided in Table 4-9. To address the overheating issue during extreme heat conditions, intermediately insulated scenarios were considered where an optimized level of insulation was provided in the roof, wall, and floor sections, as shown in Table 4-8.

4.7.3.2 Thermal Inertia:

There were three levels of thermal inertia considered: i) brick veneer– single leaf wall (110 mm thick brick), ii) double hollow brick wall (110 mm thick brick) with a cavity, and iii) double concrete hollow blocks (190 mm thick concrete blocks) with a cavity, as shown in Tables 4-7, 4-8, and 4-9 respectively.

4.7.3.3 Blind control/ shading:

CitySim uses the light-switch model for automated blinds control as proposed in [267]. The blind state (opened or closed) is a function of façade irradiance (W/m²), cut-off irradiance (W/m²), and logit scale factor (l) as discussed in [268], and calculated in [269] using a sigmoid function, shown in Table 4-10. The cut-off irradiance represents the irradiance value at which blinds get closed. Setting a higher cut-off irradiance, for instance, 1300 W/m², means keeping the blinds open as façade irradiance never reaches that value [267,268]. The base-case is simulated with the recommended blind control settings l=0.2, cut-off irradiance= 100 W/m², and as a sensitivity measure, cut-off irradiance is reduced to partially closed blinds.

4.7.3.4 Glazing:

Being the most commonly used window type for the buildings constructed before 1990 in NSW, single glazing was considered for the existing buildings (uninsulated scenario) for both typologies [270,271]. The highly insulated options were computed using "Glazing calculator NCC-2019" for houses and "Façade calculator NCC-2019" for apartments. For standardization, the output generated for zone-6 for both typologies was considered in all climatic zones of Sydney, as shown in Table 4-10. For intermediately-improved cases, the glazing conditions were considered as recommended in another study in Sydney [39].

4.7.3.5 Super cool roof- Passive daytime radiative cooling:

Recent development in passive daytime radiative cooling (PDRC) technologies – coatings with improved spectral properties having albedo greater than 0.96 and emissivity higher than 0.97 [219,272]- is a major breakthrough step toward counteracting extreme heat events and global climate change. Vinylidene fluoride-co-hexafluoropropene is one of the promising examples of such hierarchically porous poly coatings, that can be used as PDRC as applied in [273]. The same PDRC technology was considered in this dissertation and compared with typical construction materials (albedo= 0.2, and emissivity= 0.9), as shown in Table 4-10.

4.7.3.6 Airtightness:

According to several studies, the airtightness of the majority of Australian buildings is estimated between 15-60 ACH at 50 Pascals pressure [274–277], which is way higher than the infiltration standards set by the other countries, including the USA: 3-5 ACH, Canada: 3-5 ACH, France 5.5 ACH, Sweden: 2.9 ACH, UK: 10 ACH (+/- 50 pascals)[274]. The Passive House (PH) Australia recommends an airtightness level of 0.6 ACH (+/-50 Pascals) to reduce the heating and cooling needs [278]. In this dissertation, three scenarios of infiltration rates have been considered, i) according to the existing building condition –average infiltration rate of buildings in Sydney- 1.0 ACH natural (20 ACH at 50 Pascals) [274], ii) well-sealed envelope 0.5 ACH natural (10 ACH at 50 pascals), and iii) airtight envelope according to PH standards 0.03 ACH natural (0.6 ACH at 50 pascals), as shown in Table 4-10.

4.7.3.7 Setpoints- behavioral change:

The recommended cooling setpoints in NatHERS for Sydney climate zone 5 and zone 6 are 25.5 °C and 24.5 °C, respectively [243], which has been standardized to 25 °C in all climatic zones of Sydney. The impact of higher cooling setpoints 27°C and 28°C was also investigated on cooling energy consumption. According to WHO guidelines, these temperatures fall within the acceptable range [257].

4.7.3.8 Nighttime Cooling:

The nighttime cooling on CitySim-pro depends upon the windows' operable fraction, outdoor-indoor temperature gradient, and nighttime cooling schedule. The natural ventilation on CitySim is only activated when the outdoor-indoor thermal gradient is greater than 1°C. In the base-case, the window operable fraction was considered as 0.5 (50% opened windows), whereas as an adaptive measure, windows were considered fully opened from 0800PM-0500 AM when the temperature drops quickly at inland sites due to quick radiative cooling.

4.7.3.9 Higher ground surface albedo:

Previously, in the literature, the ground surface albedo was considered as 0.45 [217] and 0.7 [189]. However, 0.7 ground surface albedo may cause a glaring effect; therefore, in the dissertation, 0.45 albedo was considered and compared with the typical 0.2 ground surface albedo case, as shown in Table 4-10.

4.7.3.10 Green surface evapotranspiration/ irrigation impact:

The arid soil has an evapotranspiration factor (K-factor) of 0.1-0.2, moist soil has 0.6-0.8, and completely wet soil has 1.0. In this thesis, considering the local soil condition, K-factor was taken as 0.4 and then increased to 0.7, as shown in Table 4-10.

CHAPTER 5: THE ASSOCIATION BETWEEN URBAN OVERHEATING AND LARGE-SCALE WEATHER PATTERNS

SUMMARY:

Urban overheating (UO) and large-scale weather patterns may synergistically interact. The connection between meteorological factors and UO has been widely studied; nevertheless, the influence of large-scale weather patterns on UO, mainly during heatwaves, has never been explored. This chapter investigates the effect of large-scale weather patterns on Sydney's UO magnitude by employing a newly constructed GWTC. In three zones of Sydney, the UO's daily and seasonal fluctuations in relation to large-scale weather patterns were examined. Further, UO response to such global circulations during extreme heat events was studied. The daytime UO was reported exacerbating over the years, while nighttime UO magnitude was reduced. The humid-warm (HW) and warm (W) weather patterns were shown to be the primary cause of enhanced daytime UO during extreme heat events and in all other seasons, bringing the average UO (daily maximum) to 8 to 10.5 °C in western Sydney and 5 to 6.5 °C in inner Sydney. Further, the nocturnal UC was mainly attributed to dry-warm (DW) and warm (W) weather patterns, with the average UC (daily minimum) falling to -7.5 to -10°C in Western Sydney and -6 to -7.5 °C in inner Sydney. This study might be used to develop appropriate mitigation measures to help reduce the increased daytime temperatures in Sydney suburbs.

5.1 Background:

This section details the literature and methods explained in the previous chapters and are utilized here while associating the large-scale weather patterns with UO. The literature on synoptic climatology has been reviewed in section 2.3, where numerous large-scale weather classification systems are discussed, generally employed in urban/ bioclimatology. The literature regarding synergies between large-scale weather patterns and UO is discussed in section 3.2. The topographical and climatic features of the city are introduced in section 4.1. The locations studied in this dissertation are provided in section 4.2. The meteorological data utilized and the processing of data are explained in section 4.3. The primary methods employed to define the heatwaves are elaborated in section 4.4, while the heatwaves selected for this part are listed in section 4.4.2 and Table 4-4. The large-scale weather classification system utilized in this dissertation is described in section 4.5. The GWTC weather patterns and definitions are presented in Table 2-2. The methods employed to evaluate the interactions between UO and large-scale weather patterns are explained in section 4.7.2.

5.2 Chapter organization:

Section 5.3.1 displays the frequency distribution of large-scale weather patterns over Sydney from 1999 to 2017. In section 5.3.2, the frequency distribution of ΔT in three Sydney zones from 1999 to 2017 is explored, whereas, in section 5.3.3, the hourly/daily/seasonal fluctuations in ΔT over time are investigated. Section 5.3.4 relates large-scale weather trends to extreme UO/UC cases using the environment-to-circulation methodology. Section 5.3.5 links the diurnal variation in ΔT to large-scale weather patterns. In the following section, 5.3.6, seasonal fluctuations in ΔT are connected to large-scale weather patterns. The next section, 5.3.7, investigates the association between large-scale weather patterns and ΔT during heatwaves, followed by a discussion in section 5.4. The implications of the research and conclusion are presented in sections 5.5 and 5.6, respectively.

5.3 Results:

5.3.1 Large-scale weather patterns frequency distribution:

Sydney's frequency of large-scale weather patterns was studied from 1999 to 2017. The seasonal (S) weather pattern was the most frequent across all seasons (around 31 percent of the time), followed by warm (W: 18 percent), dry (D: 12 percent), humid (H: 10 percent), cool (C: 9 percent), dry-warm (DW: 7 percent), humid-warm (HW: 7 percent), humid-cool (HC: 3 percent), dry-cool (DC: 3 percent), and cold frontal passage (CFP: 1 percent) (Figure 5-1). The frequency of the warm frontal passage was practically negligible.

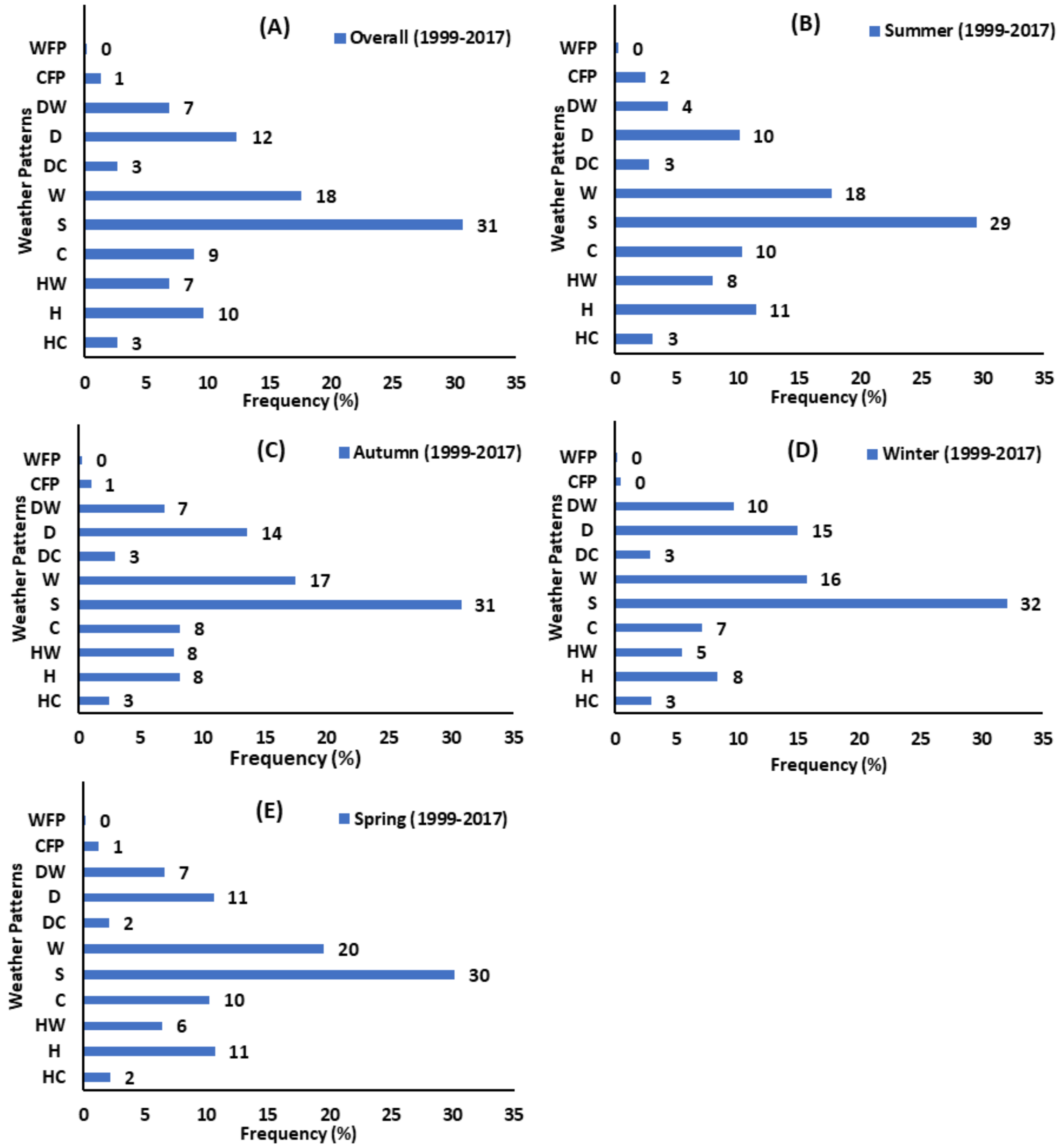

Figure 5-1 large-scale weather patterns frequency from 1999-2017, A) Overall, B) Summer, C) Autumn, D) Winter, E) Spring.

Summers had a greater frequency of warm (W), humid-warm (HW), humid (H), and cool (C) patterns, whereas these patterns occurred least frequently during winter. In contrast, dry (D) and dry-warm (DW) patterns rarely happened during the summer and more frequently throughout the winter. The frequency of seasonal (S) patterns was somewhat lower in summer (29 percent) compared to annual frequency (31 percent), while the frequency of warm (W) patterns was greater in summer (18 percent) and spring (20 percent). The humid-warm (HW) frequency increased by 8 percent over the summers but decreased during the winter (5 percent), compared to the annual frequency (7 percent). The humid (H) patterns rose from 8 percent in winter to 11 percent in summer and spring. The cool (C) patterns grew to 10 percent during the summer and spring, whereas it was 7 percent during the winter. The dry-cool (DC) and humid-cool (HC) patterns were nearly consistent during each season (3 percent). Compared to annual frequency (12 percent), the dry (D) patterns were least prevalent in summer (10 percent) and most frequent in winter (15 percent). Similarly, dry-warm (DW) frequency decreased to 4 percent in the summer but jumped to 10 percent in the winter, up from 7 percent annual frequency.

Over the years, the differences in large-scale weather patterns' frequency were also analyzed to comprehend which weather patterns had occurred more frequently (Figure 5-2). In recent years (2011-2017), the frequency of the warm weather patterns was found to have increased: dry-warm (6 to 11 percent), warm (14 to 19 percent), and humid-warm (7 to 11 percent). In contrast, the frequency of the following weather patterns has decreased in recent years: humid (12 to 8 percent), seasonal (32 to 28 percent), dry-cool (5 to 1 percent), and cool (10 to 4 percent).

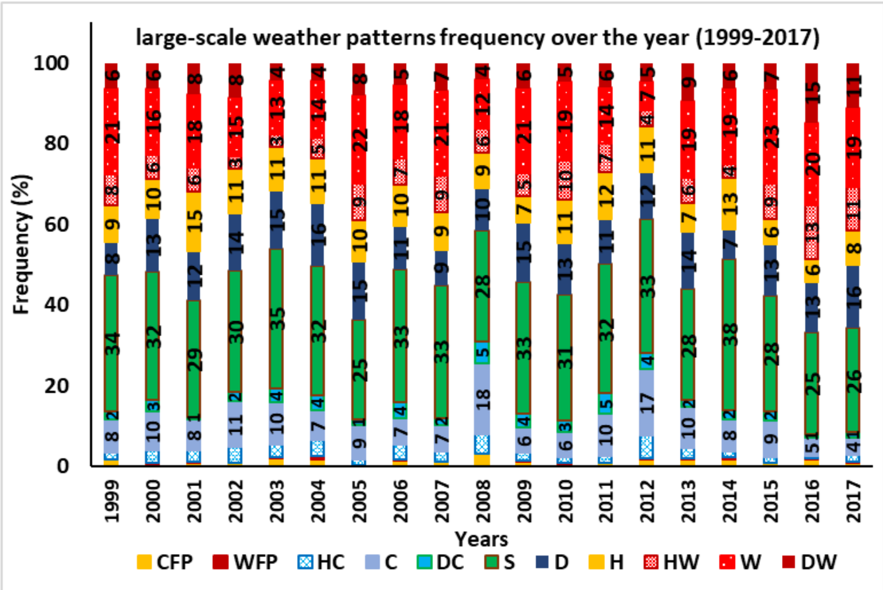

Figure 5-2 The large-scale weather patterns frequency over the year (1999-2017)

5.3.2 ΔT frequency distribution:

UO, UC, and ΔT are defined in section 4.7.1. The frequency distribution of ΔT during the day and night was analyzed at all locations from 1999 to 2017 (beginning in 2006 for CT and 2013 for LP) (Figure 5-3).

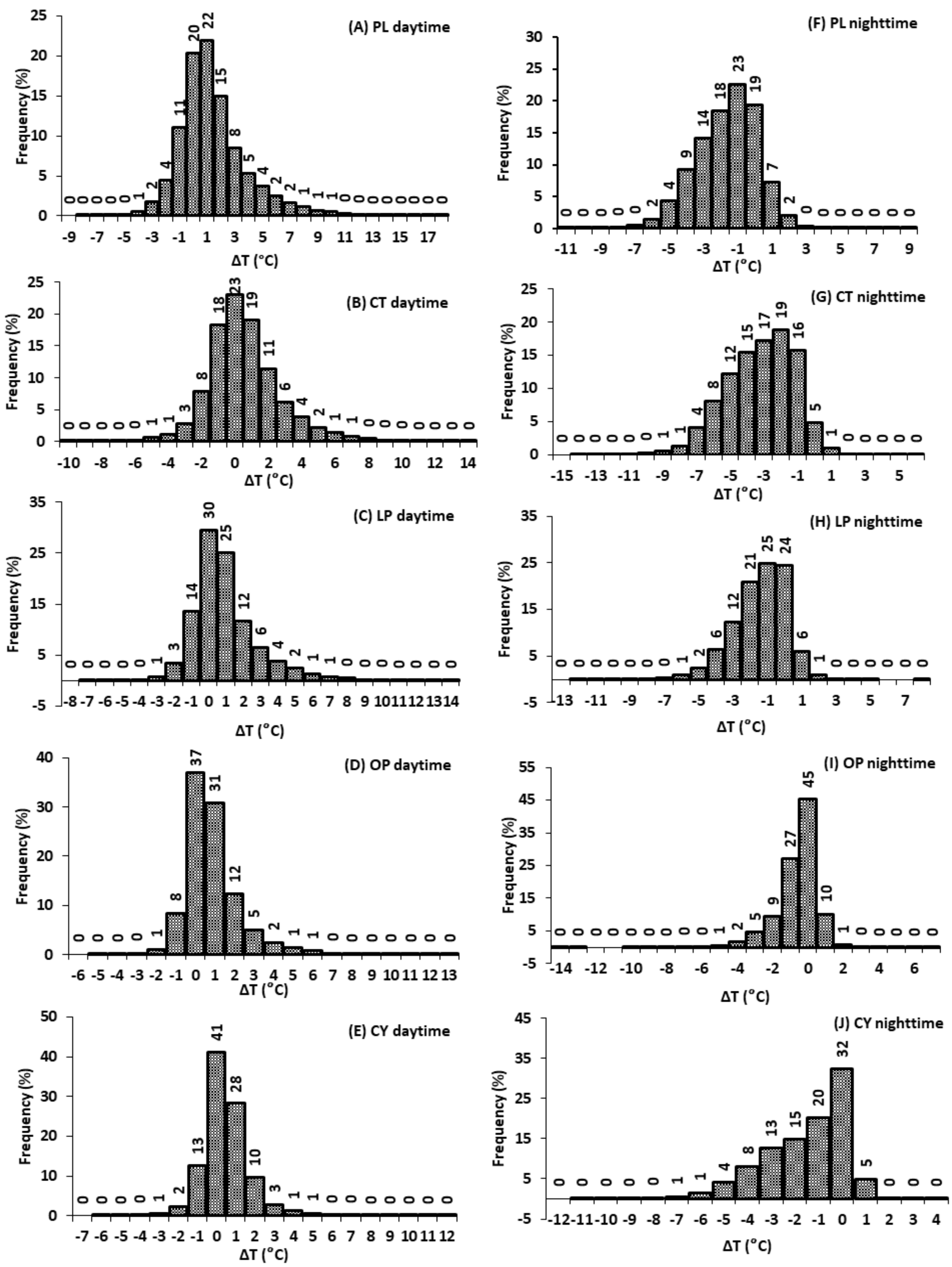

Figure 5-3 Diurnal and nocturnal ΔT frequency distribution at various locations in Sydney A) PL at daytime, B) CT at daytime, C) LP at daytime, D) OP at daytime, E) CY at daytime, F) PL at nighttime, G) CT at nighttime, H) LP at nighttime, I) OP at nighttime, J) CY at nighttime

UO (T_{suburb} - T_{CBD}) was deemed positive for more than 50 percent of the time during the day in all suburbs (PL: 62 percent, LP: 53 percent, OP: 53 percent) except CT (46 percent) and CY (43 percent). Further, as the distance from the coastline increased, the daytime UO exacerbated. The somewhat lower frequency of UO during the daytime in CY was attributable to its proximity to the coastline (7.5

km), whereas, at CT, the largest tree canopy cover (34.2 percent) and higher non-urban surfaces (38.5 percent) were the primary causes (Table 4-1). In contrast, more than 90 percent of the time, the ΔT was reported to be negative at night. The negative ΔT was more frequent at night due to a quicker radiative cooling process driven by the availability of more nonurban surfaces in the suburbs than in the city center.

5.3.3 ΔT intensity variations with time:

In order to appreciate the changes in UO/ UC magnitude over time, the fluctuations in ΔT magnitude from 1999 to 2017 were also examined. The investigation utilized hourly ΔT (independently for diurnal and nocturnal), daily maximum and minimum ΔT (for the whole duration), and daily maximum ΔT for summer and winter. Particularly after 2009, a rise in hourly daytime UO (Figure 5-4 A-E) and daily maximum UO (Figure 5-5 A-E) was observed. For example, the average hourly ΔT (daytime) after 2008 in western Sydney (PL) increased from 0.97°C (1999-2008) to 0.99°C (2009-2017) and from 0.31 °C to 0.51 °C in inner Sydney (OP). For the same period, the average daily maximum ΔT in western Sydney (PL) increased from 2.83 °C to 2.89 °C, and in Inner Sydney (OP) from 1.45 °C to 1.72 °C.

On the other hand, there was a decline in hourly nighttime ΔT (Figures 5-4 F-J) and daily minimum ΔT (Figure 5-5 F-J), dropping especially after 2008. For example, the average nightly hourly ΔT dropped from -2.11 to -2.13 °C in western Sydney (PL) and from -0.76 to -1.41 °C in inner Sydney (OP) after 2008. Similarly, the average daily minimum ΔT in western and inner Sydney fell from -2.90 °C to -2.93 °C and -1.30 °C to -2.09 °C, respectively. While examining the temporal fluctuations in daily maximum ΔT during summer and winter, generally, a rise in summer ΔT (Figures 5-6 A-E) and a decline in winter ΔT (Figures 5-6 F-J), especially after 2008, were observed. For example, after 2008, the average daily maximum ΔT in summer increased from 4.39 °C to 4.65 °C and from 1.93 °C to 2.26 °C in western and inner Sydney, respectively. Contrarily, the average maximum daily ΔT during winter declined in both western (1.47^{o}C to 1.3^{o}C) and inner Sydney (1.2^{o}C to 0.96^{o}C) after 2008.

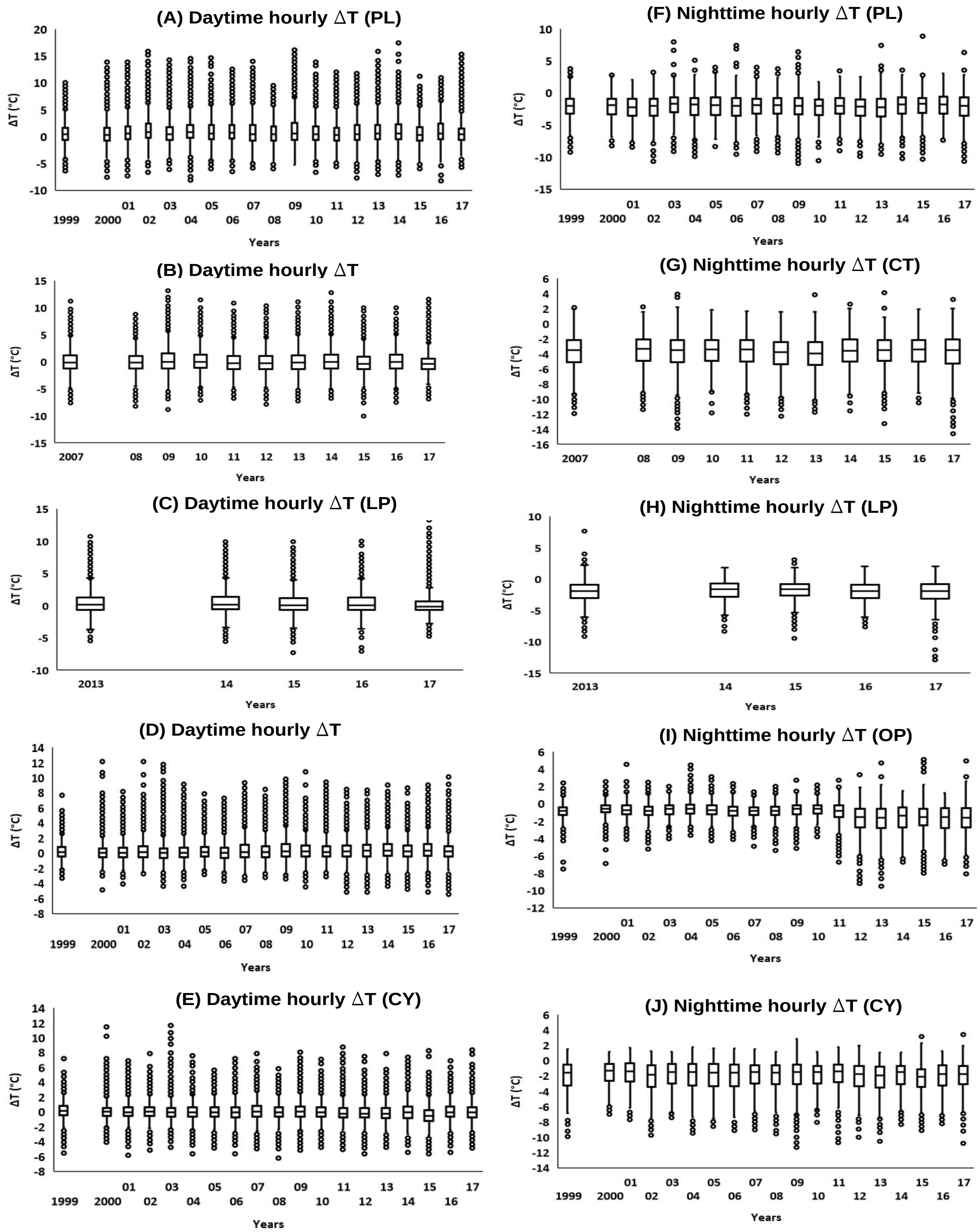

Figure 5-4: Variations in the daytime and nighttime hourly ΔT over time (1999-2017) at various Sydney locations, A) PL at daytime, B) CT (2006-2017) at daytime, C) LP (2013-2017) at daytime, D) OP at daytime, E) CY at daytime, F) PL at nighttime, G) CT (2006-2017) at nighttime, H) LP (2013-2017) at nighttime, I) OP at nighttime, J) CY at nighttime. The boxplots are plotted in accordance with standard convention (Q1-1.5*IQR and Q3+1.5*IQR), whereas the remaining dataset reflects the outliers.

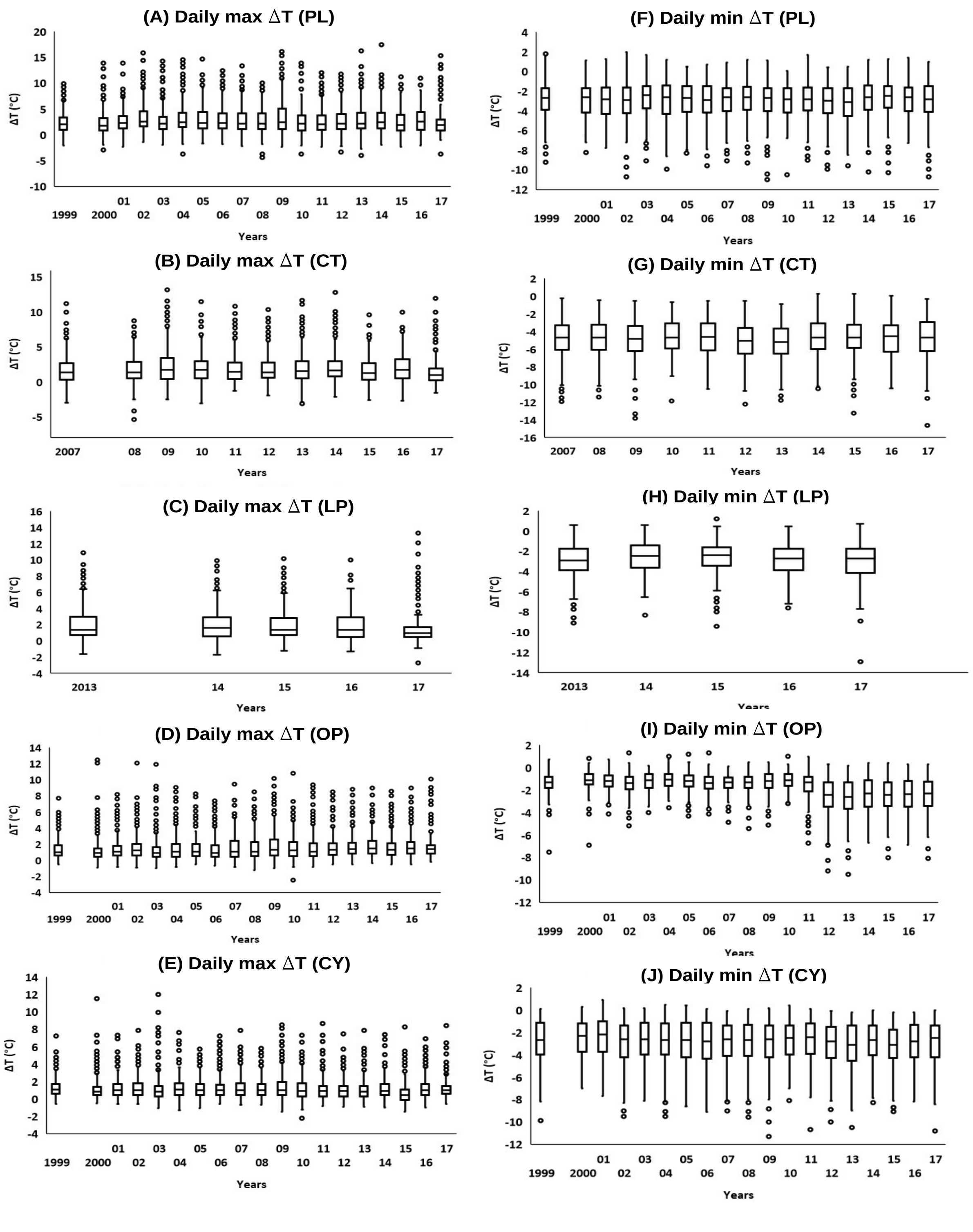

Figure 5-5: Variations in daily max ΔT and daily min ΔT over time (1999-2017) at various locations in Sydney, A) PL daily max, B) CT (2006-2017) daily max, C) LP (2013-2017) daily max, D) OP daily max, E) CY daily max, F) PL daily min, G) CT (2006-2017) daily min, H) LP (2013-2017) daily min, I) OP daily min, J) CY daily min. The boxplots are plotted in accordance with standard convention (Q1-1.5*IQR and Q3+1.5*IQR), whereas the remaining dataset reflects the outliers.

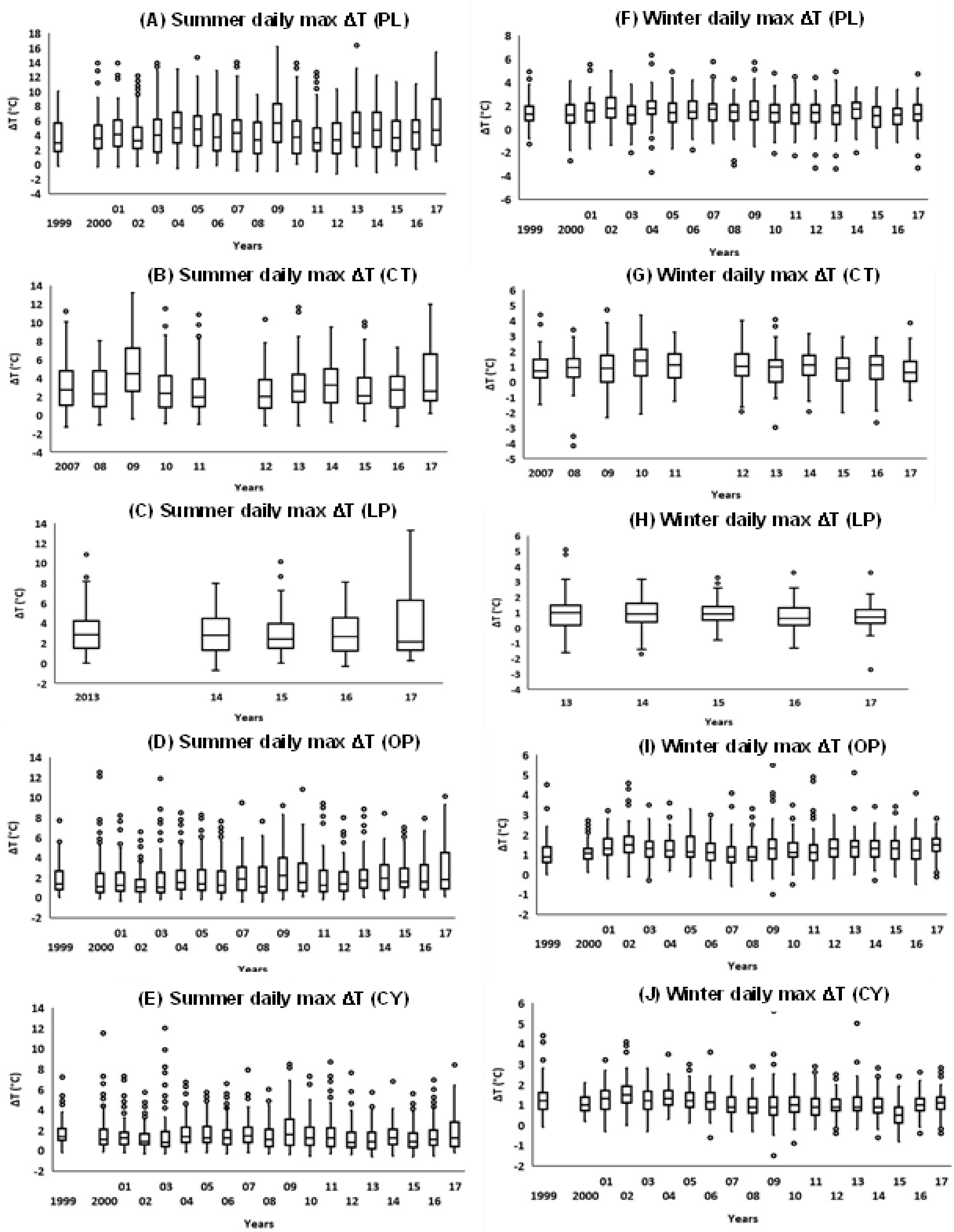

Figure 5-6: Variations in Summer daily max ΔT and winter daily max ΔT over time (1999-2017) at various locations in Sydney, A) PL- Summer, B) CT (2006-2017)- Summer, C) LP (2013-2017)- Summer, D) OP- Summer, E) CY- Summer, F) PL- winter, G) CT (2006-2017)- winter, H) LP (2013-2017)- winter, I) OP- winter, J) CY- winter. The boxplots are plotted in accordance with standard convention (Q1-1.5*IQR and Q3+1.5*IQR), whereas the remaining dataset reflects the outliers.

5.3.4 large-scale weather patterns and extreme UO/ UC cases:

In order to associate the large-scale weather patterns with UO/ UC, the top 5 percent of daily maximum ΔT (UO) and the bottom 5 percent of daily minimum ΔT (UC) were calculated in all zones of Sydney. Table 5-1 demonstrates the temperature thresholds for UO/ UC at various locations in Sydney. In western Sydney, the UO threshold temperatures were greater than in inner Sydney; however, depending on the peculiarities of each Sydney location, the UC threshold temperatures varied around the city.

Table 5-1: Temperature thresholds for the top 5 percent ΔT and bottom 5 percent ΔT at various locations in Sydney.

	ΔT (PL) [°C]	**ΔT(CT) [°C]**	**ΔT(LP) [°C]**	**ΔT (OP) [°C]**	**ΔT(CY) [°C]**
95th percentile of daily maximum ΔT	8.2	6.4	6.2	4.9	3.8
5th percentile of daily minimum ΔT	-6.5	-8.45	-6.1	-4.7	-6.6

Humid-warm (HW), warm (W), and humid (H) were the predominant weather patterns that aggravated the UO intensity in inner and western Sydney (Figures 5-7 A-E). In western Sydney, humid-warm (HW), whereas warm (W) weather patterns in inner Sydney were more aggressive. Further, while evaluating the frequency of these weather patterns during these top 5 percent of extreme UO occurrences (Figures 5-7 A-E), warm (W) weather patterns occurred more frequently, followed by humid-warm (HW), seasonal (S), and humid (H) patterns (80-90 percent of the time). In western Sydney, warm (W) patterns appeared roughly 38 percent, whereas humid-warm (HW) and humid (H) patterns happened approximately 17 percent and 15.5 percent of the time, respectively. Under these governing weather patterns (H, HW, and W), the average UO intensity in western Sydney varied between 8 to 10.5 °C (max: 13 to 17 °C), marginally more elevated under humid-warm and humid patterns. Similarly, warm (W) patterns were noticed around 48.5 percent of the time in inner Sydney, followed by humid-warm (HW: 20 percent) and humid (H: 11 percent). Under these prevailing conditions, the average UO intensity in inner Sydney was between 5 to 6.5°C (maximum: 10 to 12°C) and was somewhat greater under warm (W) patterns.

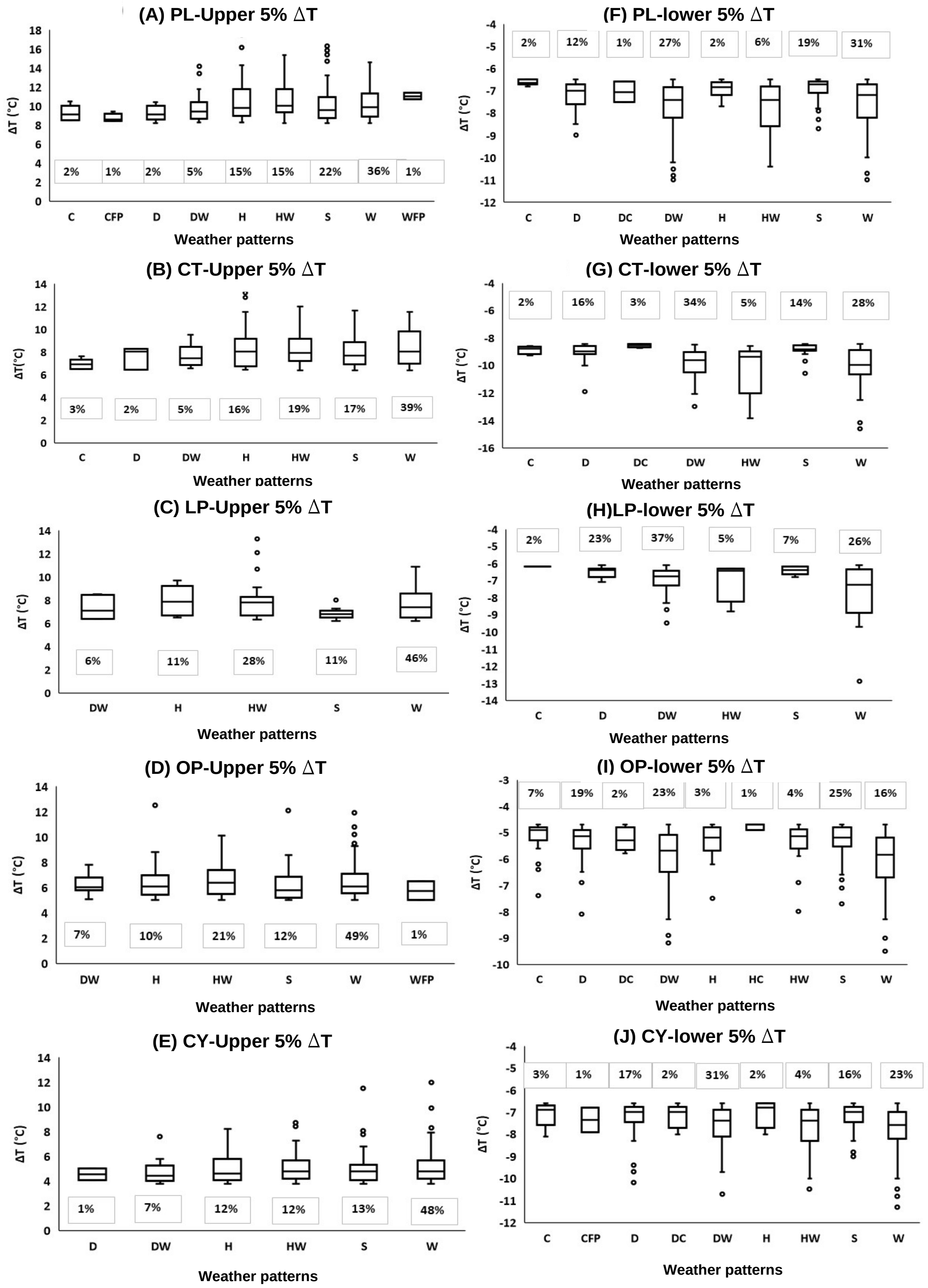

Figure 5-7: Top 5 percent (UO) and bottom 5 percent (UC) ΔT at various locations in Sydney under large-scale weather patterns. A) UO at PL, B) UO at CT, C) UO at LP, D) UO at OP, E) UO at CY, F) UC at PL, G) UC at CT, H) UC at LP, I) UC at OP, J) UC at CY. The boxplots are plotted in accordance with the standard convention **(**upper and lower extremes: Q1-1.5*IQR and Q3+1.5*IQR).

Despite the increased proportion of non-urban surfaces and tree canopy cover in western Sydney, increased absolute humidity under the humid-warm (HW) and humid (H) conditions might affect the evaporation/ evapotranspiration potential and ambient temperatures in the suburbs. Sydney's humid-warm (HW) conditions might be ascribed to tropical maritime Tasman weather systems originating from the northern Tasman Sea and are warm, moist, and unstable. Similarly, the temperate maritime airmasses are responsible for the region's humid (H) condition. These airmasses bring moist air from the ocean, whilst the blue mountains in the west may cause westerly Fohn-like winds on the leeward side to enhance temperatures by adiabatic warming, particularly in inland suburbs of Sydney. In contrast, warm (W) patterns had a greater impact on the UO magnitude in inner Sydney. The region's warm (W) and dry-warm (DW) conditions might be attributable to the extremely hot, dry, and unstable Tropical continental weather system originating from central Australia. Further, in inner Sydney, greater coastal wind mixing reduces the influence of humid (H) patterns (owing to the lower distance from the coast than Western Sydney). UO more severely impacts the suburbs as their distance from the coast increases.

While associating the UC with large-scale weather patterns (Figures 5-7 F-J), the dry (D) and dry-warm (DW) patterns were observed, replacing the humid (H) and humid-warm (HW) patterns (UO cases) in terms of frequency. From UO to UC, the frequency of humid (H) and humid-warm (HW) patterns declined from 12 to 2 percent and 20 to 5 percent, respectively, whereas the frequency of dry-warm (DW) and dry (D) patterns rose from 6 to 31 percent and from a negligible value to 16 percent, respectively. Further, seventy to eighty percent of the time, UC was accompanied by the dry (D), dry-warm (DW), and warm (W) weather patterns. However, warm (W), dry-warm (DW), and humid-warm (HW) were the most prevalent patterns in terms of UC magnitude, resulting in a reduction in suburban temperatures. In Western Sydney, the average UC intensity under the prevailing weather patterns (warm, dry-warm, and humid-warm) ranged from -7.5 to -10 °C (min: -11°C to -14.5 °C), whereas in inner Sydney, it ranged from -6.0 to -7.5 °C (min: -9.5 °C to -11.0 °C). The humid-warm (HW) and warm (W) weather patterns were comparatively more prevalent in western Sydney, whilst warm (W) and dry-warm (DW) were more visible in inner Sydney. Based on the findings - UO/UC linkage with large-scale weather patterns (Figures 5-7) and diurnal/nocturnal ΔT frequency distribution (Figure 5-3)- it is reasonable to assume that the exceptional UC incidents happened at night. The notion is founded on the fact that the Identical warmer weather patterns (HW, W, and DW) were causative for extreme UO and UC, and UC occurred 80 to 90 percent of the time at night. Therefore, the large-scale weather patterns associated with diurnal ΔT fluctuation were further investigated.

5.3.5 large-scale weather patterns and ΔT diurnal fluctuations:

The large-scale weather patterns in relation to daily daytime maximum ΔT (Figures 5-8 A-E) and daily nighttime minimum ΔT (Figures 5-8 F-J) were examined. The humid (H), humid-warm (HW), and warm (W) weather patterns in western Sydney, whereas humid-warm (HW) and warm (W) patterns in inner Sydney exacerbated the daytime UO. As depicted in Figure 5-1 A, the humid (H), humid-warm (HW), and warm (W) weather patterns occurred in around 35 percent of all instances: humid (H:10 percent), humid-warm (HW:7 percent), and warm (W:18 percent). In Western Sydney suburbs, the average maximum daytime ΔT under humid-warm (HW) and warm (W) weather patterns was between 2.8 to 3.8 °C (nearly identical under both weather patterns). The average maximum daytime ΔT was somewhat lower under the humid (H) weather pattern. The average daytime maximum ΔT in inner Sydney suburbs under prevailing weather patterns (humid-warm and warm) varied between 2.0 and 2.4 °C. Further, ΔT was proportional to the distance from the coast.

At night, the dry (D) and dry-warm (DW) weather patterns, coupled with warm (W) patterns, were in charge of minimum ΔT, Instead of humid (H) and humid-warm (HW) patterns. The warm (W), dry-warm (DW), and dry (D) weather patterns happened for 37 percent of the overall duration: warm (W:18 percent), dry-warm (DW: 7 percent), and dry (D: 12 percent) (Figure 5-1 A). The dry-warm (DW) weather patterns were primarily responsible for the lowest nighttime ΔT among the three weather patterns. Under the dry-warm (DW) patterns, the average nighttime minimum ΔT ranged between -4 to -6.5 °C in Western Sydney suburbs and between -2.5 to -4.5 °C in inner Sydney. Under other dominating weather patterns (dry and warm), the average nighttime minimum ΔT was relatively lesser: -3 °C to -5 °C in Western Sydney and -2.0°C to -3.3°C in inner Sydney.

The amplified daytime ΔT under humid-warm (HW) and humid (H) weather patterns were attributed to reduced latent heat flux in the suburbs since a considerable fraction of available energy was segmented into sensible heat flux, which elevated temperatures in the suburbs (particularly in Western Sydney). On the other hand, the Sydney CBD experienced lower daytime temperatures than inner and western Sydney due to the coastal breeze impression. In addition, urban shading may also contribute to Sydney CBD's lower daytime temperatures. Under warm (W) weather patterns, the amplified daytime ΔT was attributed to high-velocity continental winds, where advection from hot sources may elevate the inland temperatures and affect the ambient moisture.

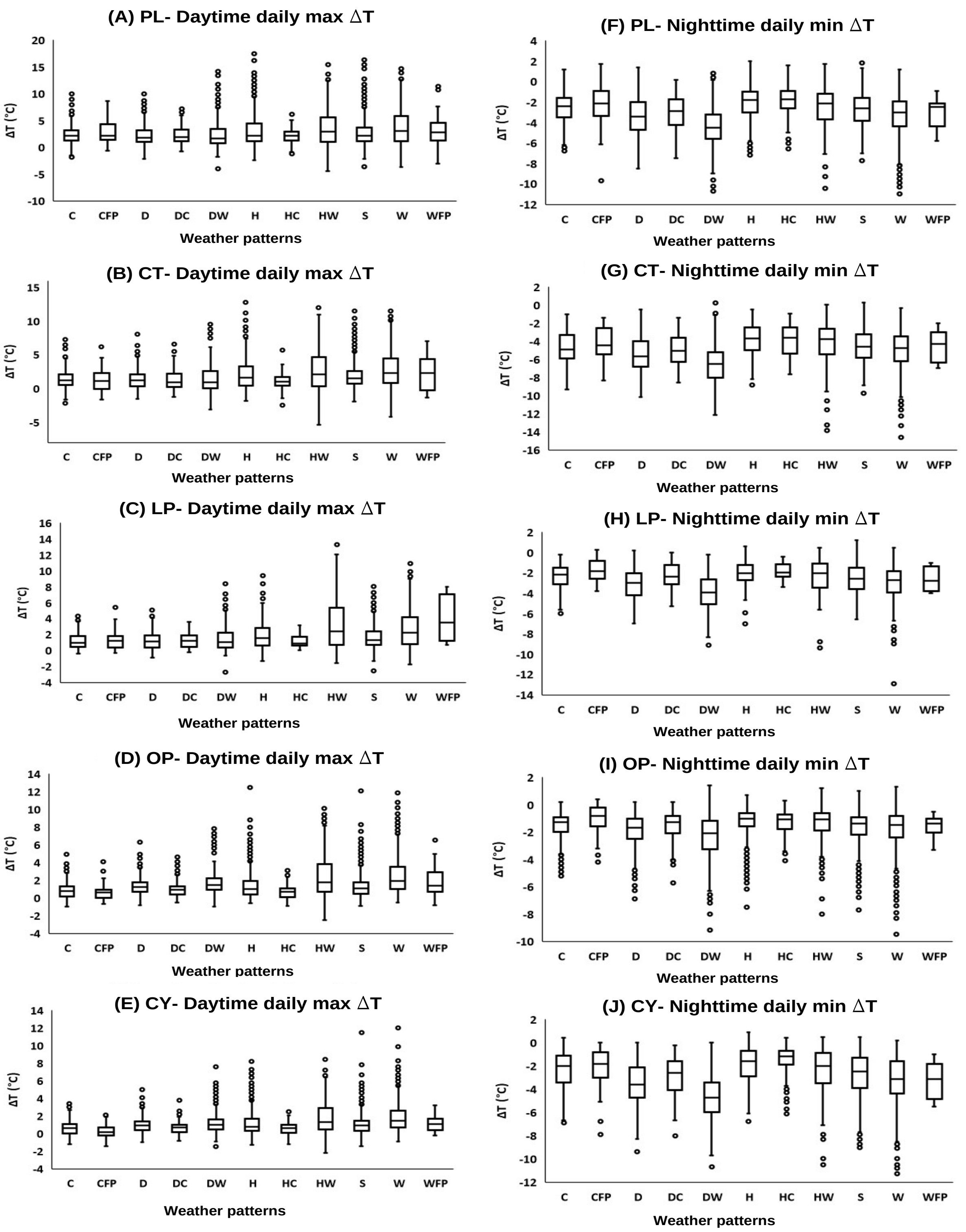

Figure 5-8: Daily max ΔT (daytime) and daily min ΔT (nighttime) at various locations in Sydney under large-scale weather patterns. A) Daily max ΔT at PL, B) Daily max ΔT at CT, C) Daily max ΔT at LP, D) Daily max ΔT at OP., E) Daily max ΔT at CY, F) Daily min ΔT at PL, G) Daily min ΔT at CT, H) Daily min ΔT at LP, I) Daily min ΔT at OP., J) Daily min ΔT at CY. The boxplots are plotted in accordance with standard convention (upper and lower extremes: Q1-1.5*IQR and Q3+1.5*IQR).

The dry-warm (DW), warm (W), and dry (D) patterns were more prevalent at night, emerging from the city's continental side. Advection from the continental winds has a lower impact at night because of low wind speed. Further, such dry weather patterns are typically associated with clear and calm meteorological conditions. The radiative cooling in the suburbs may be boosted by such dry, clear, and calm conditions at night, whilst longwave emissions in the urban fabric may increase the Sydney CBD temperature, resulting in daily minimum ΔT.

5.3.6 large-scale weather patterns and daily maximum ΔT seasonal variations:

The seasonal fluctuations in daily max ΔT were also associated with large-scale weather patterns. Summer (Figures 5-9 A-E) and autumn (Figures 5-9 F-J) were dominated by humid-warm (HW) and warm (W) weather patterns at all locations in Sydney, which amplified the daily maximum ΔT. The humid-warm (HW) and warm(W) weather patterns allude to the large-scale dualistic systems accessible on opposing ends of the city, one emerging from the coastline and the other from the continental end. In summer and autumn, the humid-warm (HW) and warm (W) weather patterns happened 25 percent of the total instances (humid-warm: 7.9 percent, warm: 17.7 percent) (Figures 5-1 B and C). During summer in western Sydney, the average daily maximum ΔT ranged from 4.5 to 6.0°C under humid-warm (HW) and warm (W) weather patterns, and 2.8 to 3.5°C in inner Sydney, marginally greater under humid-warm (HW) patterns. In autumn, the average daily maximum ΔT ranged from 2.0 to 2.6 °C in Western Sydney and 1.4 and 2.0 °C in inner Sydney, under dominating weather patterns (humid-warm, warm), with humid-warm marginally more aggressive.

During the spring, the humid-warm (HW), warm (W), and humid (H) weather patterns prevailed in Western Sydney, whilst humid-warm (HW) and warm (W) dominated in inner Sydney. Compared to humid (H) conditions, the average daily maximum ΔT in Western Sydney was comparatively greater under humid-warm (HW) and warm (W) patterns. The humid-warm (HW) and warm (W) weather patterns accounted for 27 percent (humid-warm: 6.4 percent, warm: 20 percent) of the springtime total (Figures 5-1 E). In Western Sydney, the average daily maximum ΔT ranged from 3.6 to 4.8 °C, while in inner Sydney, it ranged from 2.4 to 3.2 °C (nearly identical under humid-warm and warm patterns) (Figures 5-10 A-E). During winter, although the highest daily maximum ΔT was identified under humid-warm (HW) and warm (W) patterns in all suburbs, however, ΔT was also raised under humid-cool (HC) and cool (C) patterns in Western Sydney. Ten percent of the wintertime was characterized by humid-cool (HC) and cool (C) patterns (HC: 2.9 percent, C: 7.1 percent), whereas 21 percent of the wintertime was influenced by warm (W) and humid-warm (HW) patterns (W: 15.7 percent, HW: 5.5 percent) (Figure 5-1 D).

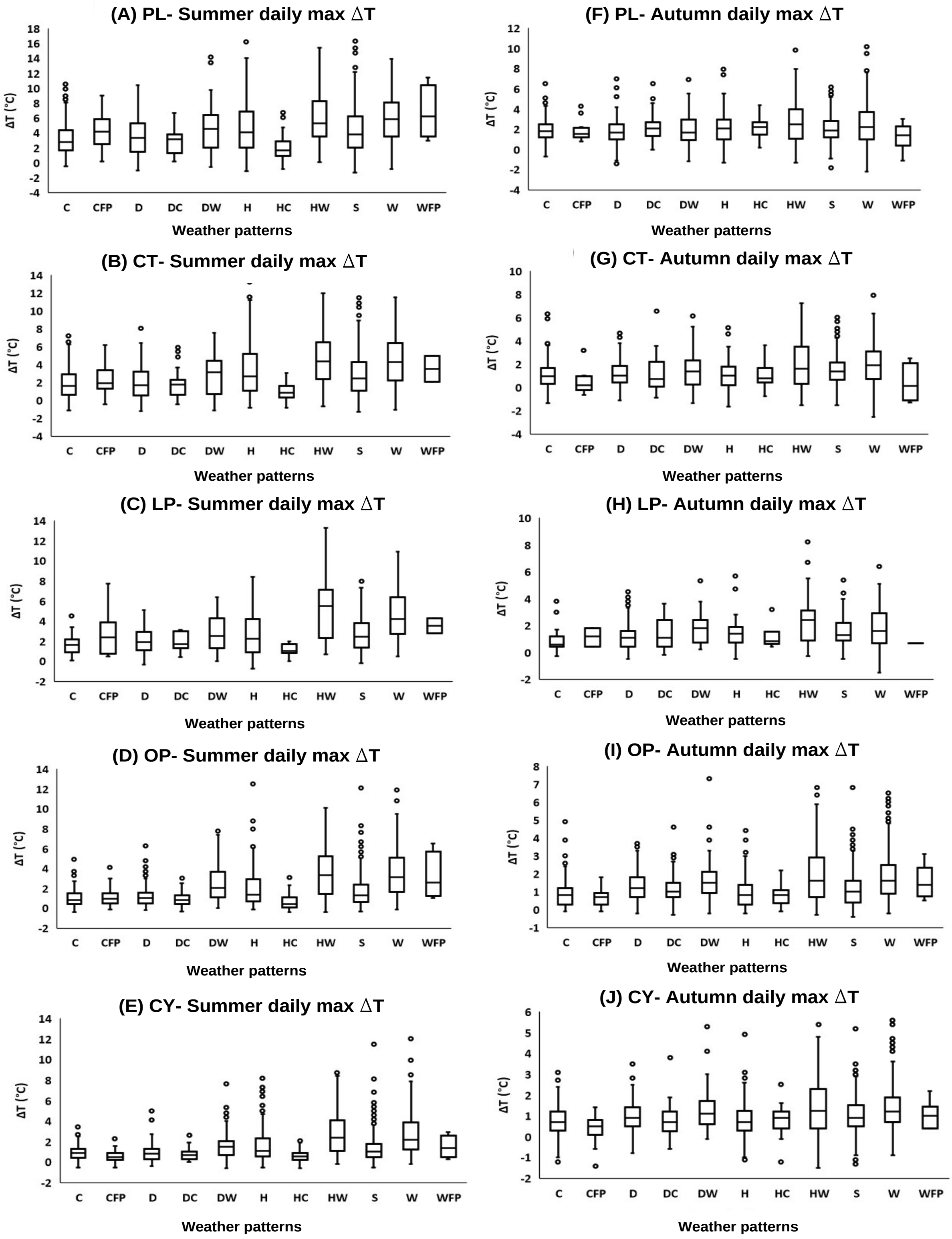

Figure 5-9: Large-scale weather patterns comparison with summer/autumn daily max ΔT (1999-2017). A) PL during summer, B) CT during summer, C) LP during summer, D) OP during summer, E) CY during summer, F) PL during autumn, G) CT during autumn, H) LP during autumn, I) OP during autumn, J) CY during autumn. The boxplots are plotted in accordance with standard convention (upper and lower extremes: Q1-1.5*IQR and Q3+1.5*IQR).

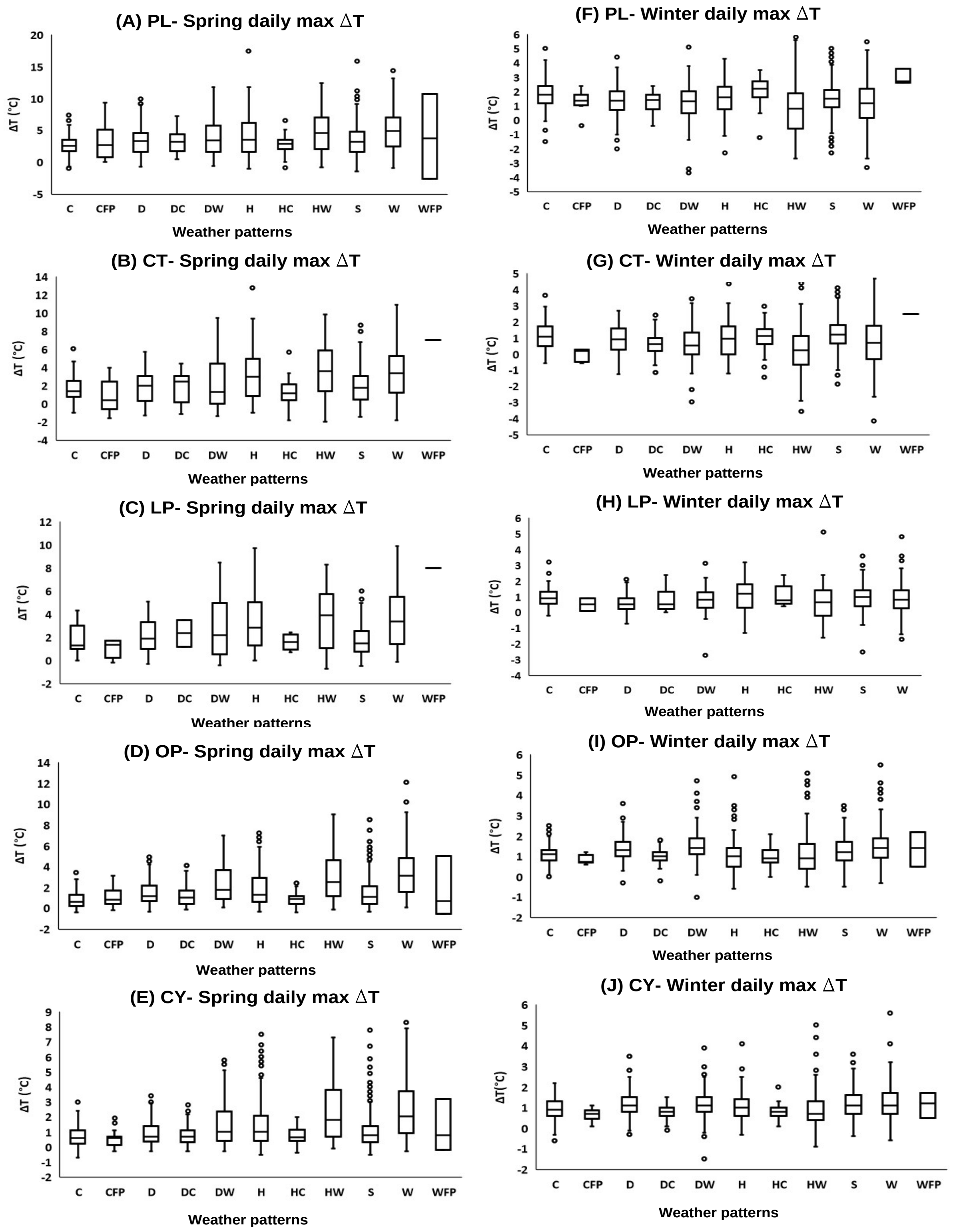

Figure 5-10: Large-scale weather patterns comparison with spring/winter daily max ΔT (1999-2017). A) PL during spring, B) CT during spring, C) LP during spring, D) OP during spring, E) CY during spring, F) PL during winter, G) CT during winter, H) LP during winter, I) OP during winter, J) CY during winter. The boxplots are plotted in accordance with standard convention (upper and lower extremes: Q1-1.5*IQR and Q3+1.5*IQR).

During winter, the average daily maximum ∆T variations in Western Sydney suburbs were between 0.6 to 2.0 °C under prevalent conditions, with humid-cool (HC) being the most aggressive, followed by cool (C), warm (W), and humid-warm (HW) patterns (Figure 5-10 F-J). Further, the humid (H) and seasonal (S) patterns were also accountable for amplified ∆T in Western Sydney. On the other hand, warm (W), dry-warm (DW), and humid-warm (HW) patterns were primarily responsible for amplified daily max ∆T in inner Sydney. In addition, dry (D) and seasonal (S) patterns also impacted inner Sydney during the winter. In inner Sydney, the average daily maximum ∆T varied from 1.0 to 1.3 °C under humid-warm (HW), warm (W), and dry-warm (DW) patterns (identical under all presiding weather patterns). Southern maritime air masses may be accountable for the humid-cool (HC) patterns in the Sydney region that brings cloudy weather with light precipitation during the winter.

5.3.7 large-scale weather patterns and daily maximum ∆T during heatwaves:

UO was also associated with large-scale weather patterns during heatwaves and backgrounds. The background conditions are defined in section 4.4.1. Initially, the large-scale weather pattern frequency during heatwaves and backgrounds was examined. During heatwaves, humid-warm (HW) and warm (W) patterns happened in around 76 percent of the instances (humid-warm: 52 percent, warm: 24 percent), followed by dry-warm (12 percent), humid (6 percent), and seasonal (6 percent) patterns (Figure 5-11 A).

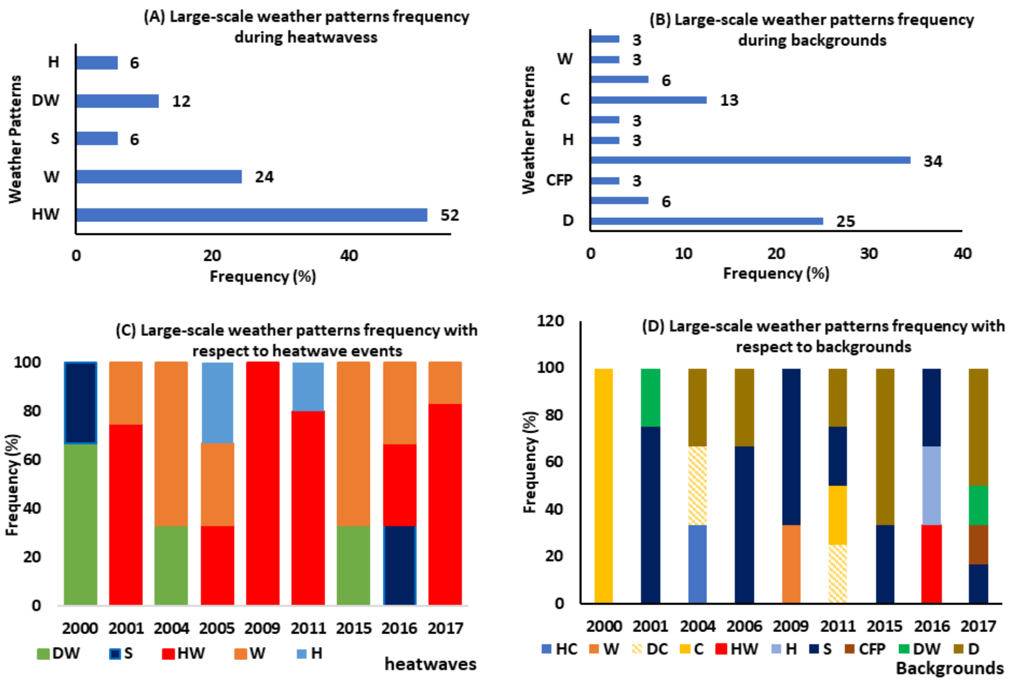

Figure 5-11: Large-scale weather patterns frequency during heatwaves and backgrounds. A) overall during heatwaves, B) Overall during backgrounds, C) Event-wise during heatwaves, D) Event-wise during backgrounds.

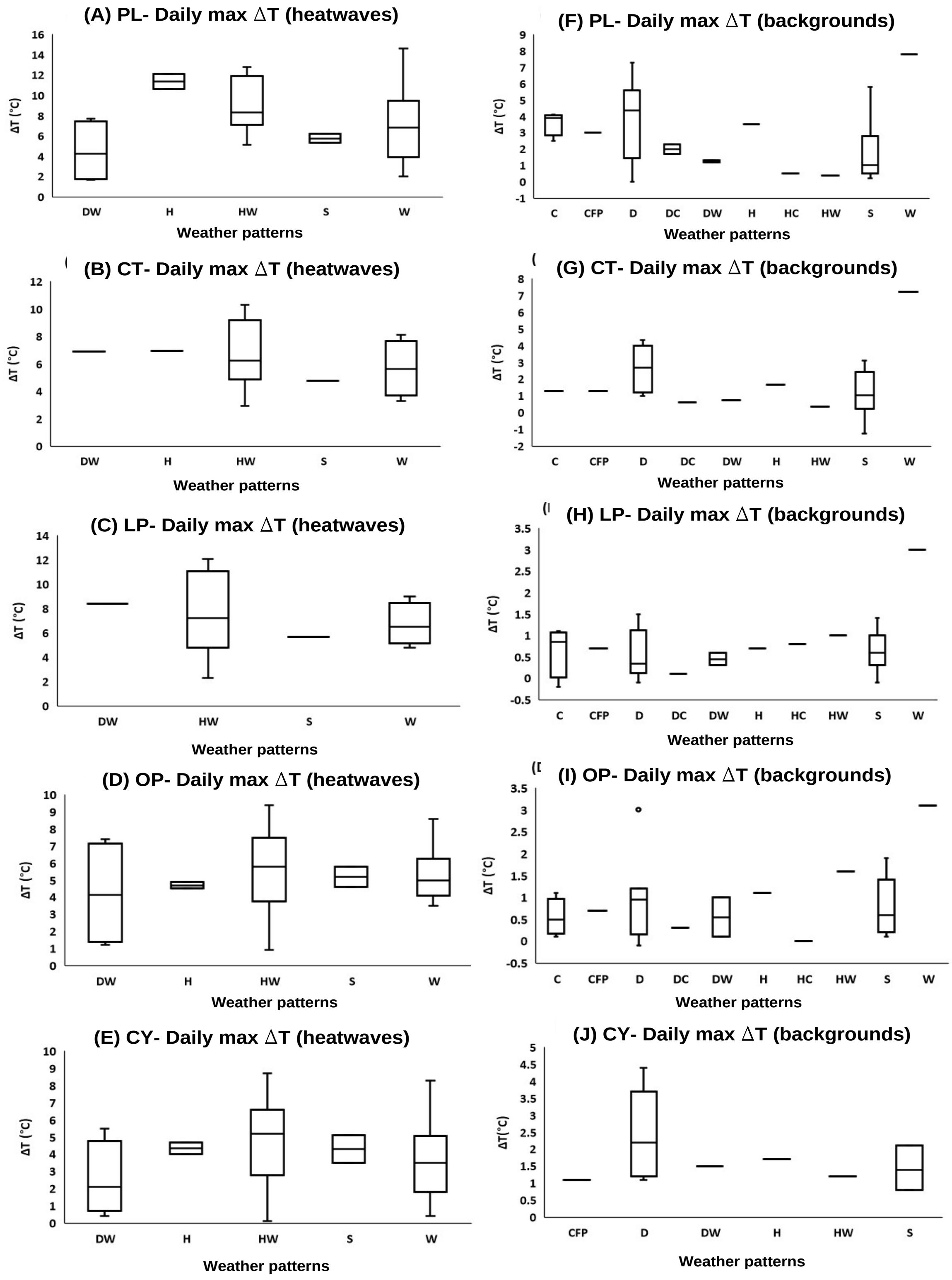

Figure 5-12: Large-scale weather patterns and daily max ΔT during heatwaves and background conditions A) PL during heatwaves, B) CT during heatwaves, C) LP during heatwaves, D) OP during heatwaves. E) CY during heatwaves, F) PL during backgrounds, G) CT during back grounds, H) LP during backgrounds, I) OP during backgrounds. J) CY during backgrounds. The boxplots are plotted in accordance with standard convention (upper and lower extremes: Q1-1.5*IQR and Q3+1.5*IQR).

During backgrounds, the most prevalent patterns were seasonal (S: 34 percent), dry (D: 25 percent), and cool (C: 13 percent). (Figure 5-11 B). The large-scale weather patterns frequency with respect to heatwave events was also investigated. The frequency of humid-warm (HW) patterns was elevated during recent heatwave events from 2009 to 2017 (Figure 5-11 C), whereas dry (D) patterns were observed more frequently during backgrounds (Figure 5-11 D). The humid-warm (HW) and warm (W) patterns exacerbated the UO intensity in all suburbs in Sydney during heatwaves. Under prevailing conditions (humid-warm and warm), the average UO intensity differed from 6 to 9 °C in Western Sydney suburbs and from 3.8 to 5.4 °C in inner Sydney suburbs, comparatively higher under humid-warm patterns (Figures 5-12 A-E). During backgrounds, UO intensity was more prevalent under dry (D) patterns in Western Sydney and under dry (D) and seasonal (S) patterns in inner Sydney (Figures 5-12 F-J). During the background, the average UO under dry (D) patterns was 2.4 to 4.0°C in Western Sydney, whereas, in inner Sydney, it ranged between 0.6 to 1.0°C under dry (D) and seasonal (S) patterns (identical under both patterns).

5.4 Discussion:

Urbanization significantly impacts the land-atmospheric interaction (energy and moisture transfer). Sydney is expanding west-southwestward, and the swift urban growth affects atmospheric circulation. The interactions between large-scale weather patterns and UO intensity were studied in Sydney. It was reported that warm weather patterns (dry-warm, warm, and humid-warm) had occurred more frequently, especially in later years. Explicitly, the frequency of humid-warm (HW) and warm (W) patterns increased significantly, particularly during the summer and during intense heat occurrences. These findings are comparable with those of a study conducted in North America, in which an increase in the frequency of generally warm (HW, DW, W) weather patterns and a decrease in the frequency of cool weather patterns (C, HC, DC) were noted [158]. Similar results were also reported in North Carolina, where moist tropical (humid-warm) weather patterns governed the summer [239].

Sydney's UO intensity grew as its distance from the coast increased, despite a larger fraction of tree canopy cover and potentially plantable surfaces in inner and Western Sydney. Identical findings were concluded in Los Angeles, where an exceptional thermal imbalance was detected at inland locations [72]. In the present study, the augmented UO was observed during the day under humid (H), humid-warm (HW), and warm (W) patterns (almost the whole year and during heatwaves). The increased moisture in the air under moist weather patterns (humid-warm- ascribed to tropical maritime Tasman weather system/ humid- related to temperate maritime weather system) kept the suburbs (inland locations) hotter during the day by lowering the region's latent heat flux potential. These findings are congruent with research conducted in New York, where greater daytime temperatures were recorded in rural locations than in urban areas under moist weather patterns (UC during the day) [87]. In contrast to suburbs, the coastal effect (stable temperatures owing to a consistent sea breeze under moist conditions) and urban shade were credited for the lower diurnal temperatures in Sydney CBD (nearby the coastline). Early in the day in Salamanca, the lesser urban temperatures were also attributed to urban shading [263]. In addition to humid-warm (HW) and humid (H) patterns, the high-velocity continental winds under warm (W) weather patterns (attributable to the tropical continental weather system) also increased the diurnal temperatures at Sydney's inland locations.

In the present study, the amplitude of the UC was greatest at night under dry-warm (DW), warm (W), and dry (D) weather patterns. The Sydney suburbs (inland locations) cooled quicker than the Sydney CBD under dry conditions (clear skies and calm breezes) owing to radiative cooling, whereas longwave emission from daytime heat storage enhanced overnight temperatures in CBD. In addition, urban shading might also hinder the cooling process in the Sydney CBD, as concluded in another study [167]. These findings are comparable with studies conducted in Atlanta [81] and the northeastern United States (New York, Philadelphia, and Baltimore) [82,87], in which a larger urban-rural thermal differential (UHI) was concluded at night during dry and warm weather. Different methods of $\triangle T$ computation resulted in exacerbated nighttime UO (UHI = T_{urb}-T_{rural}) in Atlanta and other US cities and higher overnight UC ($T_{suburbs}$ – T_{Urb}) in Sydney.

Previously, amplified UO was observed at night in several global studies under favorable large-scale weather patterns [74,79,82,87]. In the present study, contrary to previous investigations, daytime UO was positive between 50 and 62 percent of the time (across all seasons) in all three Sydney zones, whereas nocturnal UO was negative around 90 percent of the time at all locations. The varied results might be attributed to the city's proximity to the coast (reference station), urban shading, and the prevailing large-scale weather patterns. Some other coastal cities, like Athens [50] and Los Angeles [72], also observed a positive daytime UO, with the exception of Melbourne and Adelaide [58], where inland site choices resulted in a larger nighttime UO magnitude.

Under favorable weather patterns (humid-warm, warm, humid), the average daily maximum UO in Western Sydney ranged from 8 to 10.5 °C (max: 13 to 17 °C), while in inner Sydney, it was 5 to 6.5 °C (max: 10 to 12 °C). Sydney's UO intensity was exceptionally high when compared to earlier studies, where the maximum daily average UO was documented at 3.84 °C in Atlanta [81] and 3.5 °C in New York [87] under hot and dry weather patterns, whereas it was 2.8 °C in Buenos Aires [79], 3.6 °C in Melbourne [75], and 1.2 °C in Poznan [74] under anticyclonic conditions. Birmingham's average daily maximum UO (2.5°C) was likewise correlated with anticyclonic circulations [80]. As previously described, these anticyclonic circumstances were primarily associated with calm breezes and clear skies (dry conditions) and exacerbated the UO at night. The UO impact was more pronounced in Sydney due to a dualistic large-scale weather pattern (humid-warm and warm) available on opposing ends of the city. Further, the most intense UO occurrences were associated with warm (W) and humid-warm (HW) patterns, which also happened prevalently during extreme heat conditions.

5.5 Implication

The increased frequency of warm weather patterns (humid-warm-HW and warm-W) (particularly during summer and heatwaves) and rising urbanization in Western Sydney are concerning, especially for human health. The thermal risk would be higher for the underprivileged community, the elderly, and those with pre-existing health concerns, which might raise mortality and morbidity rates and place a greater strain on the health care system. The dry-warm (DW) and humid-warm (HW) were related to elevated mortality and morbidity during summer in New York [171] and Rome [133], while only humid-warm (HW) was triggering health issues in Shanghai. The increased frequency of humid-warm (HW)/warm (W) weather patterns in Sydney during summer and heatwaves will also enhance the anthropogenic heat owing to the increased usage of air conditioning [51,73], degrade the environment (owing to a rise in ozone formation) [43], and amplify the UO intensity. A projected rise in intense heat occurrences [222] and a projected spike in the number of Australians living in capital cities [231] would enhance the vulnerability of Sydneysiders. The intensity and frequency of such weather patterns can be reduced by adding moisture-retaining materials/systems, such as green roofs [69], vegetation, and cool materials in urban fabric [279].

5.6 Conclusion

This research investigated the association between UO and large-scale weather patterns during intense heat occurrences for the first time. UO was primarily noticed during the day (over 50 percent), whereas UC was predominantly recorded at night (above 90 percent) in Sydney. Warmer weather patterns (dry-warm, humid-warm, warm) were recorded more commonly in recent years. The warm (W) and humid-warm (HW) patterns were reported to occur more often during summer and heatwaves. During heatwaves, the humid-warm (HW), warm (W), and humid (H) patterns dominated and were also accountable for extreme daytime UO occurrences. Under humid-warm (HW) and warm (W) patterns, the daytime UO intensity (average daily maximum- sever UO cases) in Western Sydney was 8 to 10.5 °C (max: 13 to 17 °C), while in inner Sydney, it was 5 to 6.5 °C (max: 10 to 12 °C). The humid-warm/ humid patterns attributable to tropical maritime Tasman/ temperate maritime weather systems halted the evaporation/ evapotranspiration in the suburbs and exacerbated daytime UO in western Sydney. The warm (W) pattern was more governing in inner Sydney due to tropical continental airmasses' advection. The dry-warm (DW), dry (D), and warm (W) weather patterns were mainly responsible for UC at night. Under dry-warm (DW) and warm (W) patterns, the larger UC intensity (average daily minimum- sever UC cases) was recorded at -7.5 to -10°C (min: -11 to -14.5 °C) in Western Sydney and -6 °C to -7.5 °C (min: -9.5°C to -11.0 °C) in inner Sydney. Under the dry/ dry-warm patterns (associated with clear and calm meteorological conditions), the radiative cooling was enhanced in the suburbs, whereas the urban fabric's ability to trap long waves led to UC. Large-scale weather patterns influenced the local-scale UO in Sydney through dualistic weather systems (tropical maritime Tasman and tropical continental weather systems- available on opposing ends of the city), which negatively affected diurnal temperatures at inland locations whereas kept the Sydney CBD comparatively cooler. Appropriate mitigating devices should be designed to increase coastal wind penetration in the suburbs while reducing continental wind circulation.

CHAPTER 6: INTERACTIONS BETWEEN URBAN OVERHEATING AND HEATWAVES DURING AN EXTREME HEAT SPELL AT THE MOST AFFECTED LOCATION

SUMMARY:

Despite the growing frequency and severity of heatwaves, no agreement exists on the extent of urban overheating (UO) during heatwaves, and the potential association between the two occurrences remains unclear. This research investigates the relationships between UO and heatwaves in Sydney, a city influenced by opposing large-scale weather patterns. A comprehensive study was carried out, taking into account one of the most affected suburbs in western Sydney (PL) in comparison to Sydney CBD (OH). One of the most intense heatwave spells in recent decades, during the summer of 2017, was chosen to investigate the relationships between both phenomena. The peak average heatwave-background UO difference (△UO) was roughly 8 °C, indicating a robust relationship between UO and heatwave. Furthermore, the daytime UO impact was more evident during the heatwave than at night. The advective flux was determined to be the most critical interaction between UO and heatwaves, along with sensible and latent heat fluxes.

6.1 Background:

This section summarizes the data and methods employed in this chapter. The synergies between UO and heatwaves were investigated for one of Sydney's most affected suburbs (PL) compared to the city center (OH- in the coast's proximity). The literature on UO computational techniques and heatwave identification methods is detailed in sections 2.1.2 and 2.2.1. The literature on synergies between UO and heatwaves is reviewed in section 3.1. The geographical/ climatic characteristics of PL and OH are presented in sections 4.2.1 and 4.2.6. The meteorological data collection and processing are covered in section 4.3. In this chapter, the analyses were performed for the most intense heat occurrence in recent years (heatwave: 9-11th Feb 2017) in comparison to the background event (13-15th Feb 2017). During the heatwave in the summer of 2017, 93 percent of the NSW state was 10°C warmer than normal. The heatwave and background definition and further details about the selected heatwave/ background event are provided in section 4.4.1. The methods employed in this chapter are described in section 4.7.1. Further, details on UO (T_{PL}- T_{CBD}), $\triangle$AH (AH_{PL}- AH_{CBD}), and $\triangle$UO (hourly average UO $_{heatwave}$ - UO $_{background}$) can also be found in the same section. As indicated in section 4.7.1, the qualitatively hourly analyses were conducted to holistically examine the meteorological parameters (temperature, AH, wind speed, and wind direction) during the most intense heat occurrence. The synergies were identified initially for one selected heatwave/ background day. The selected heatwave day (11th Feb 2017) had the highest average daytime temperature at PL, whereas the selected background day (14th Feb 2017) had the lowest. On 9th, 10th, and 11th Feb, the average daytime temperature at PL were 31.1°C, 37.7°C, and 38.2°C, respectively. On the 13th, 14th, and 15th Feb, the average daytime temperature at PL were 26.4°C, 23.7°C, and 25.8°C, respectively. After the selected heatwave/ background day examination, the analyses were extended to the entire event.

6.2 Chapter organization:

Section 6.3 presents the qualitative hourly UO analysis of the entire heatwave/ background event. The daytime/ nighttime variations in sensible and latent heat fluxes on the selected heatwave/ background day are discussed in section 6.3.1.1. The variations in advective heat fluxes on the selected heatwave/ background day are elaborated in section 6.3.1.2. Section 6.3.2 holistically examined the entire heatwave/ background event. Discussion, limitations of the study, and conclusion are presented in sections 6.4, 6.5, and 6.6, respectively.

6.3 Results:

The hourly average UO intensity with standard deviations (SD) was computed for the entire heatwave and background spells to comprehend the variance in UO patterns during heatwaves. Similarly, AH variations in suburbs and Sydney CBD ($\triangle AH = AH_{suburb} - AH_{CBD}$) were also computed. A positive number in UO/ $\triangle$AH intensities indicates a greater sensible/ latent heat flux in the suburb, whereas a negative value indicates a greater sensible/latent heat flux at the Sydney CBD. The daytime UO intensity was significantly higher during the heatwaves (particularly in the afternoon) than during the background event (average peak approximately 10 °C during heatwave compared to 2°C during background at 05:00 pm) (Figure 6-1). The sensible, latent, and advective heat fluxes were investigated to comprehend UO variation during heatwaves.

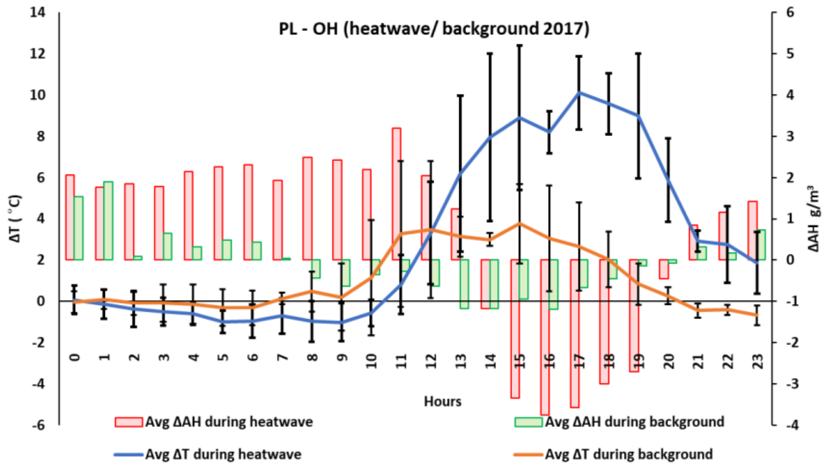

Figure 6-1: Average hourly UO and ΔAH (PL-OH) during heatwave (9-11th Feb 2017) & background (13-15th Feb 2017) events. The whiskers denote the standard deviation.

6.3.1 Analyses during the selected heatwave and background days:

6.3.1.1 Sensible and latent heat flux variations on the selected heatwave and background days:

Daytime variations: The daytime $\triangle$AH was negatively elevated throughout the heatwave day than on the background day (Figure 6-2). Typically, the evaporation rate rises due to increased surface temperatures during the heatwave, causing an increase in AH. The presence of greenery and the ground surface dampness increases the rate of evaporation/evapotranspiration. In rural/ suburban regions, evapotranspiration/ evaporation is generally more pronounced than in urban counterparts, resulting in lower rural/suburban ambient temperature. Figure 6-2 illustrates that the daytime UO intensity increased (positively) as the $\triangle$AH increased (negatively) during the heatwave day. Despite having higher potentially plantable surfaces and being surrounded by lakes, the daytime latent heat flux at PL during the heatwave day was lower than at the coastal location. Possible causes involve i) decreased evaporation at PL due to lower soil moisture, ii) advection from dry/hot air at PL (increased than usual during the heatwave), and iii) advection from moist coastal air (higher than usual during the heatwave) at Sydney CBD (owing to proximity to coast).

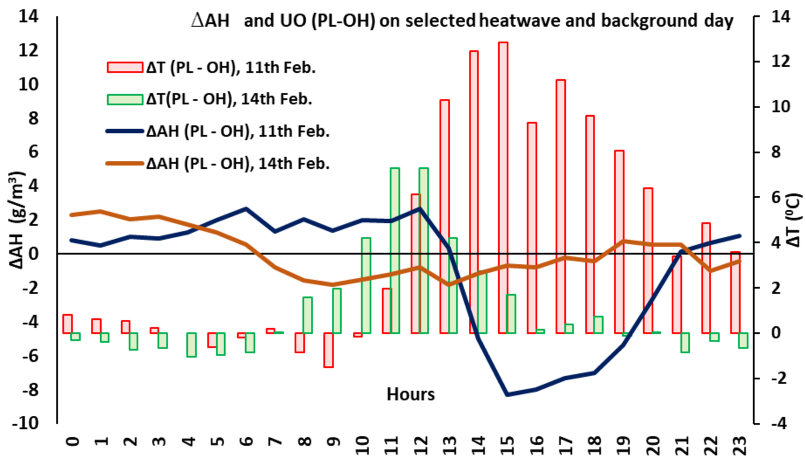

Figure 6-2: ΔAH and UO (PL-OH) during the selected heatwave (11th Feb 2017) and background (14th Feb 2017) days.

Nighttime variations: PL had higher AH at night on heatwave and background days than OH (Figure 6-3 B). The higher AH and lower temperature at night/ early morning in PL may be attributed to the higher proportion of non-urban surfaces (maintaining higher water content), lakes in the surrounding, and surface moisture evaporation produced due to condensation (early morning). Precipitation might potentially play a role in the increased soil moisture levels observed at PL on the 7th and 8th of February.

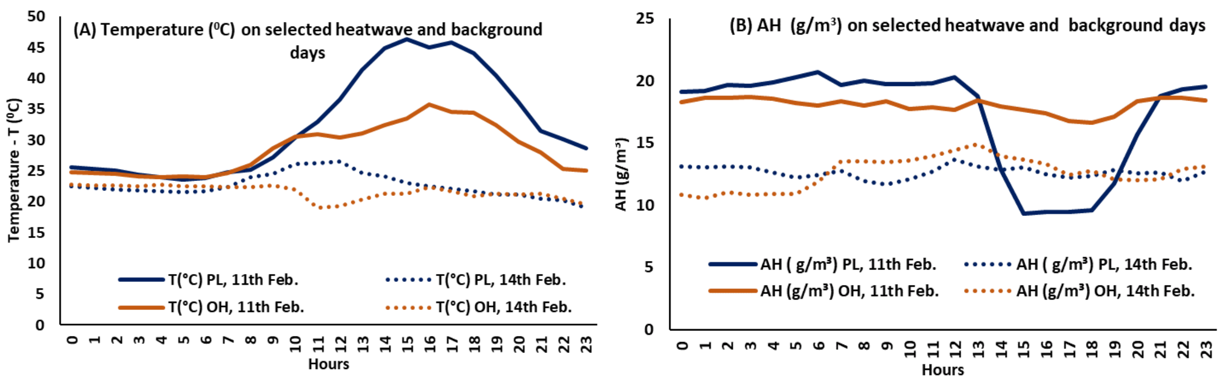

Figure 6-3: Temperature (°C) and AH (g/m³) profiles at PL & OH on selected heatwave (11th Feb 2017) & background (14th Feb 2017) days. (A) Temperature, (B) AH

The nighttime temperatures were nearly identical at both locations during the heatwave and background days (Figure 6-3 A). The air temperatures and AH at OH might be maintained by advection from the consistent sea breeze, whereas the quick radiative cooling at PL could lower nocturnal temperatures. Consequently, the extent of nighttime UO during both heatwave and background days was insignificant.

Another possible explanation for the elevated AH in the early morning is dew deposition, which occurs when heated soil evaporates extra surface moisture created by condensation. When the surface temperature falls below or equals the dew point temperature, the moisture from the air condenses, and dew forms. The ambient temperatures at PL and OH were contrasted with dewpoint temperatures during both heatwave and background events to determine the possibility of dew deposition. Figure 6-4 demonstrates that, in PL, dew formation was possible during heatwaves. Therefore, a rapid rise in AH in PL around 6 a.m. might result from surface moisture evaporation.

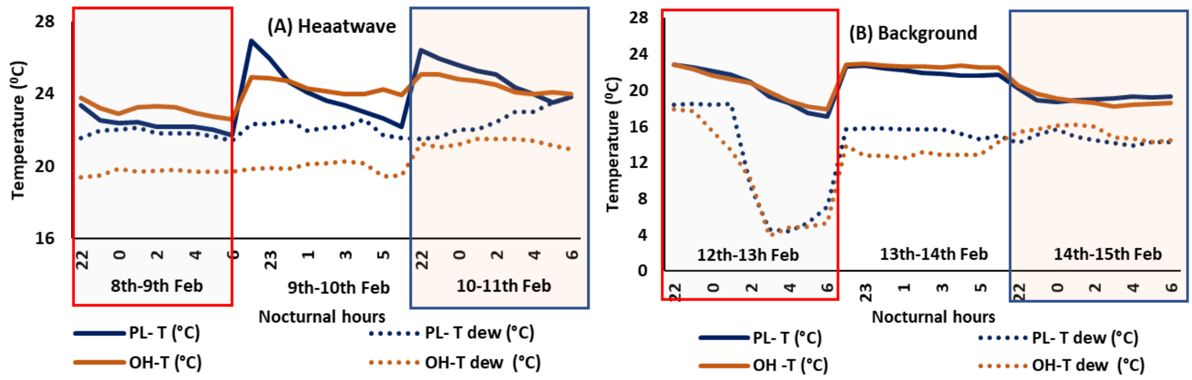

Figure 6-4: Nighttime ambient temperature (T) and dew point temperature (Tdew) at PL and OH during the heatwave (9-11th Feb 2017) and background events. (A) during the heatwave and (B) during the background event.

6.3.1.2 Advective heat flux variations on the selected heatwave and background days:

The variation in wind patterns during heatwave and background days was observed at PL and OH. The coastal and desert (continental) winds are represented by the letters C and D, respectively, as demonstrated in Figures 6-5. IE at PL and IW at OH reflect inland winds. Sections 4.2.1 and 4.2.6 show further information on the wind patterns convention at PL and OH. During the heatwave day, the daytime wind speed at PL climbed from 2 to 5 m/s, and the wind blew from the continental side of the city to PL (Figure 6-5 A). Simultaneously, the wind was blowing from the coastal end at Sydney CBD, as illustrated in Figure 6-5 C, and the UO intensity was considerably high. The wind speed at PL on the background day was comparatively higher than on the heatwave day; however, the wind penetrated from Inner Sydney to PL (Figure 6-5 B). Under the inland wind at PL, the UO intensity was fairly modest during the background day compared to the heatwave day.

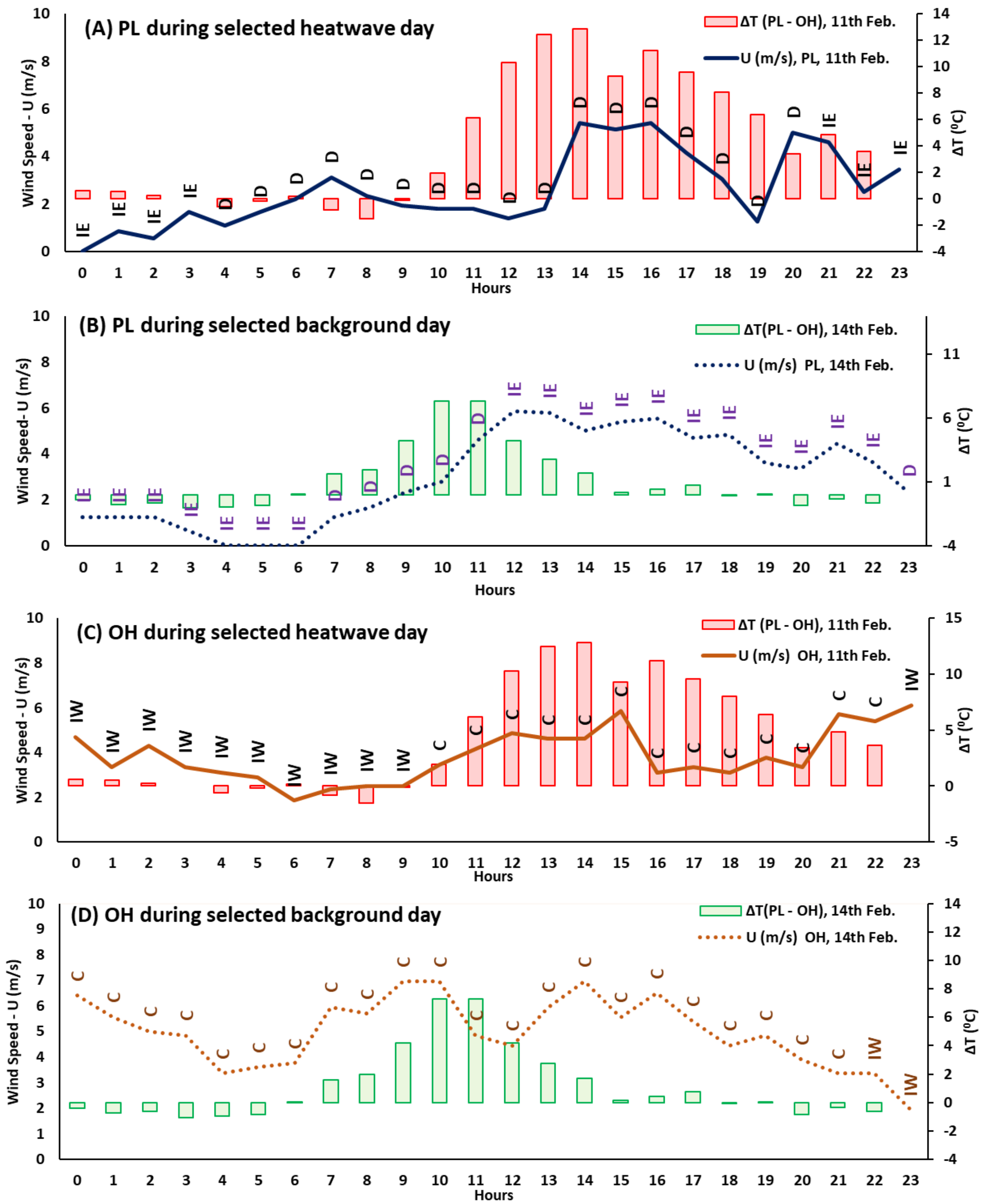

Figure 6-5: The association between wind pattern (speed and direction) and UO at PL and OH during selected heatwave (11th Feb 2017) and background (14th Feb 2017) days. (A) PL during selected heatwave day, (B) PL during selected background day, (C) OH during selected heatwave day, and (D) OH during selected background day.

When compared to the daytime, the nighttime wind direction at PL on the heatwave day (continental side to PL) and the background day (Inner Sydney to PL) did not alter substantially. However, wind speed and the extent of UO decreased at night. Contrarily, the nighttime wind direction at Sydney CBD was from the inland to the site during the heatwave day, whereas during the background day, it blew from the coast (Figure 6-5 D). The wind speed at OH was significantly greater during the background day than on the heatwave day.

6.3.2 Holistic assessment of the entire event:

PL: Heatwave daytime temperatures in PL were much higher than at OH on the selected heatwave day (Figure 6-3 A). The AH at PL declined sharply during this time and then began to rise again in the evening (Figure 6-3 B). Before noon, the AH was relatively high and steady at PL, but a sudden drop and then rise in AH indicated a shift in wind pattern. The wind at PL blew from the continental side for the whole heatwave day; nevertheless, the wind speed was rather moderate until 1 p.m. (Figure 6-5 A). Continental wind advection with an increased wind speed after 1 p.m. rendered the evaporation/ evapotranspiration inefficient at PL, resulting in a significant spike in temperature. At 4 p.m., the wind speed began to decrease, causing the ambient temperature to fall and the evaporation to resume, resulting in a rise in AH.

The examination of daytime temperatures at PL for the entire heatwave (9-11th Feb) and background (13-15th Feb) events revealed a continuous ascent from the first to the last heatwave day (Figure 6-6 A). In contrast, Figure 6-6 B demonstrates that PL's daytime latent heat flux decreased equally during three heatwave days. During the six heatwave and background days, the temperatures were lower at PL under IE wind patterns (Figures 6-7 A and B) with uncompromised AH. Contrarily, the temperature rose, and AH declined at PL under high-speed continental winds during three days of heatwaves (Figure 6-7 A). The advection from dry and warm continental wind swept the ambient moisture, halted the evaporation process, and increased the ambient temperature at PL.

OH: Contrary to PL, the daytime AH at OH was high and stable over both selected heatwave and background days (Figure 6-3 B), and low temperature also prevailed likewise (Figure 6-3 A). The maintained AH was attributed to advection from moist coastal winds since the wind blew from the coast to the city center on the heatwave and background days (Figures 6-5 C and D). Nevertheless, the wind speed was significantly greater on the background day, and consequently, the temperature in the city center was mild (Figure 6-3 A). On examining the entire heatwaves (9-11th Feb) and background (13-15th Feb) events at OH, it was established that throughout the heatwave and background events, the wind blew mostly from the coast towards the CBD during the day (Figure 6-7 C and D). However, when wind speed decreased, AH decreased owing to less advection from the ocean, and temperatures rose (Figures 6-6 C-D). Similarly, when the wind blew from the inland to the CBD, AH decreased, and temperatures rose.

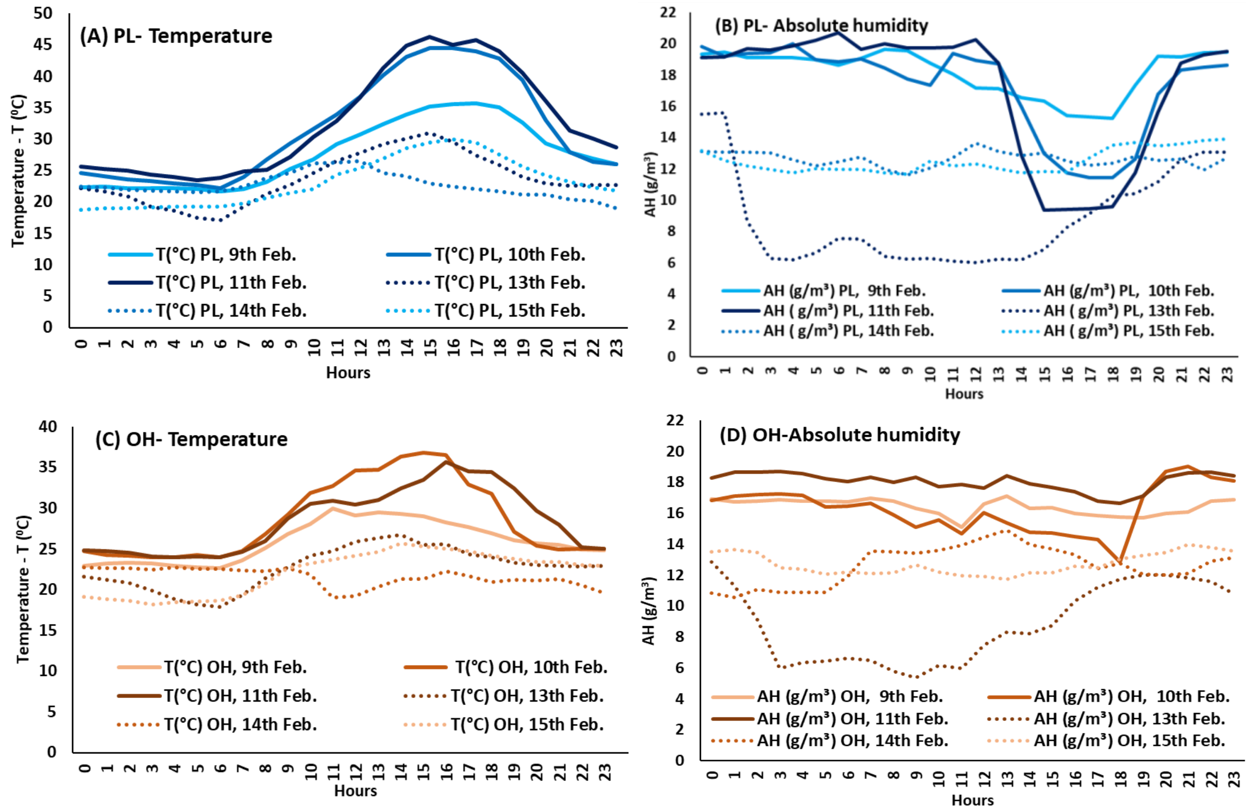

Figure 6-6: Temperature (°C) and AH (g/m3) at PL and OH during heatwave (9-11th Feb 2017) & background (13-15th Feb 2017) events. (A) Temperature at PL during the heatwave and background events, (B) AH at PL during the heatwave and background events, (C) Temperature at OH during the heatwave and background events, (D) AH at OH during heatwave and background events.

6.4 Discussion:

Rapid urbanization and intense heat occurrences provide a greater thermal threat to the urban population. An in-depth understanding is imperative to determine the causes exacerbating UO and altering the energy balance between various parts of the city during heatwaves. For the first time, the impact of heatwaves on UO was investigated in a coastal city (Sydney), influenced by the opposing large-scale weather system. The findings indicated that the UO increased during the heatwave, in contrast to earlier research that found no change or decline in the UO intensity during heatwaves [47,59].

The degree of UO was more evident during the day, particularly in the afternoon. These findings align with research conducted in coastal cities, where UO impact was more pronounced during the daytime [50,51]. In the prior research that contrasted rural and noncoastal (urban) locations, the nighttime UO effect was more pronounced during the heatwaves due to higher longwave emission from daytime heat storage and radiative cooling in rural areas [41,46,48,61,108]. In the present investigation, the nighttime UO intensity during heatwave was imperceptible. It resulted from quick radiative cooling in the suburb (PL) caused by non-urban surfaces and the sea breeze that maintained temperatures in the city center.

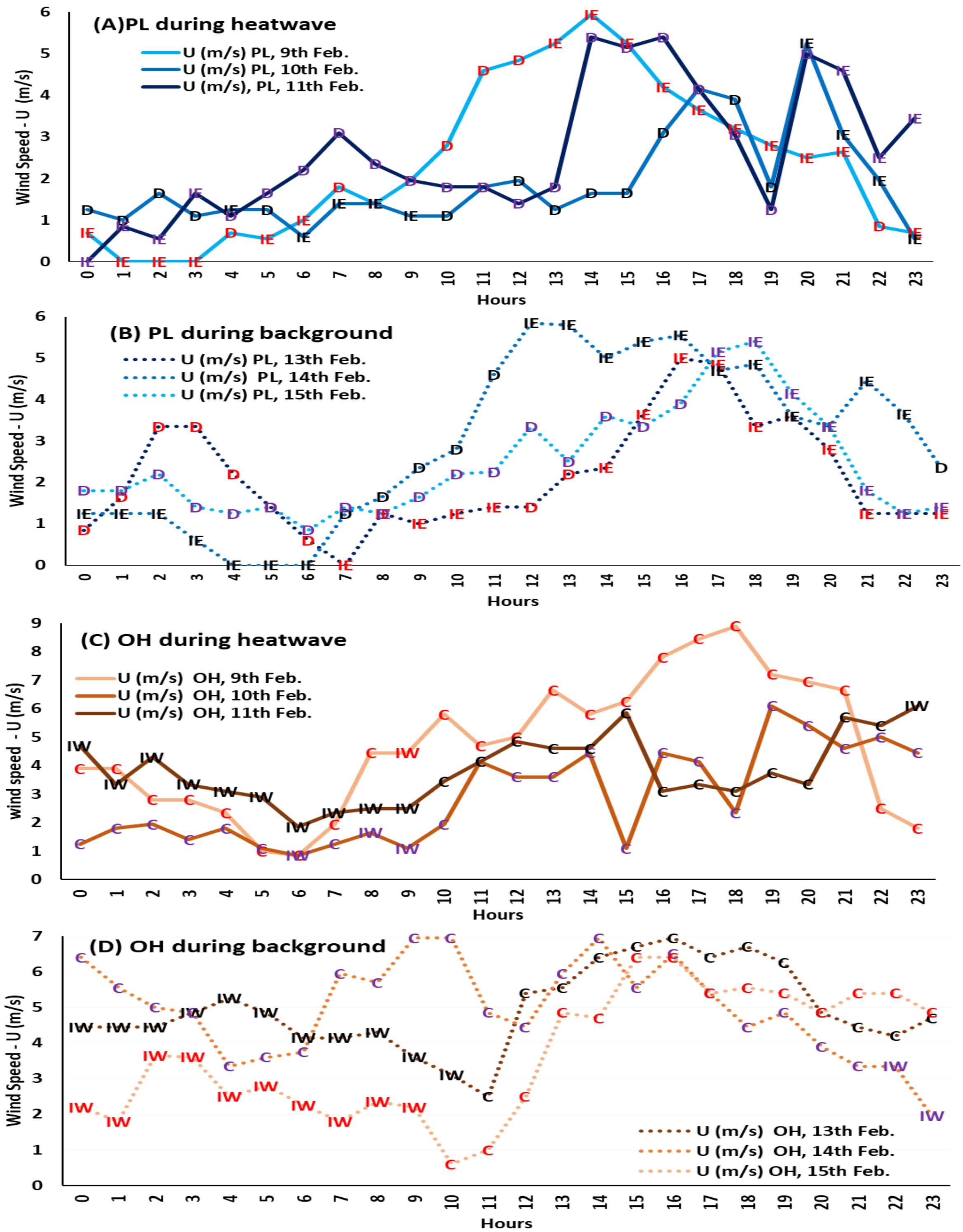

Figure 6-7: Wind Speed (m/s) & direction at PL and OH during the heatwave (9-11th Feb 2017) and background (13-15th Feb 2017) events. (A) PL during the heatwave event, (B) PL during the background event, (C) OH during the heatwave event, and (D) OH during the background event.

Approximately 8 °C separated the maximal average magnitude of UO during heatwaves and background events. In earlier research in coastal/ non-coastal cities, the highest variation between heatwave and background UO ranged between 1 and 2.5 °C [46,48,50,51]. Western Sydney was more susceptible to UO during heatwaves due to opposing large-scale weather systems on opposite ends of the city (heating source — continental winds and cooling source — coastal winds). The current research identified advective heat flux as the primary interaction between UO and heatwaves other than sensible and latent heat fluxes. For noncoastal cities, the advective heat flux was deemed insignificant; nevertheless, in coastal cities, it was one of the leading causes of UO exacerbation during heatwaves [50,51]. Urban-rural moisture differential was the key interaction between UO and heatwaves in noncoastal cities, where pronounced daytime UO impact was reported [41,48,50].

If the latent heat contrast in urban and surrounding areas is inadequate, the synergy between UO and heatwave may decline [48]. Extreme temperatures were recorded in France in 2003 as a result of decreased evaporation/ evapotranspiration, which was related to soil dampness [71]. In Beijing, China, higher disparities in latent heat flow between urban and rural regions were likewise regarded as the critical interaction between UO and heatwave [48]. However, in the current research, the winds impacted both sensible and latent heat fluxes at PL. Westerly continental winds rapidly depleted the ambient moisture at PL, lowering evaporation/evapotranspiration and the latent heat potential and raising ambient temperature. Contrarily, a consistent coastal wind in the city center during the heatwave kept temperatures and humidity stable. In general, a stronger regional wind lowers the scale of UO [4,263,280]; nevertheless, in the current research, stronger continental winds amplified the temperatures in the suburbs and consequently the UO intensity. The influence of coastal and continental winds on UO demonstrates the significance of advective heat flux and identifies it as the most significant interaction between UO and heatwaves in Sydney.

During intense heat occurrences, Sydney's population on the continental side is exposed to significant thermal risk owing to elevated outdoor temperatures. Consequently, the probability of heat-related mortality, morbidity, environmental quality deterioration, and a hike in power demand rises [29]. Suitable adaptation and mitigation strategies are required to demote the prevalence of continental winds in Sydney suburbs. These findings of the study may also be extended to other cities with comparable boundary conditions, including Casablanca (Morocco), Dubai (United Arab Emirates), Muscat (Oman), Dammam (Saudi Arabia), and Jeddah (Saudi Arabia), etc. [4,281,282].

6.5 Limitation:

Analyzing one heatwave/ background event to investigate the association between UO and heatwave was the limitation of this work. The findings can be corroborated by analyzing more heatwave episodes from recent years. In addition, this analysis may be improved by including more locations in inner and western Sydney.

6.6 Conclusion:

Heatwaves severity has increased in the recent decades, and deteriorating outdoor thermal comfort in metropolitan settings. This dissertation investigated the interactions between UO and heatwaves in the desert-affected coastal metropolis of Sydney, Australia. Consistent with the existing literature on coastal cities, the findings demonstrate a positive relationship between UO and heatwaves, exacerbated during the day rather than at night. The peak $\triangle$UO was roughly 8 °C, much higher than generally published estimates. The higher $\triangle$UO resulted from the presence of a dualistic large-scale weather system that became more prevalent during the heatwave. The increased harshness of urban climate during heatwaves has the potential to adversely impact human health, environmental quality, economy, and energy. In literature, urban-rural moisture difference was one of the primary causes of amplifying daytime UO during heatwaves. However, in the present research, the advective heat flux in the form of a dualistic weather system constituted the major interaction between UO and heatwave. Additionally, the advective heat flux also influenced the sensible and latent heat fluxes at both locations and exacerbated UO. Results will aid in formulating strategies to reduce excessive heat occurrences and develop remedies for UO.

CHAPTER 7: INTERACTIONS BETWEEN URBAN OVERHEATING AND HEATWAVES- A COMPARATIVE INVESTIGATION

SUMMARY:

UO overlaps with heatwaves, and urban thermal stress may intensify. The surface energy budget response to heatwaves is essential for predicting interactions between UO and heatwaves. Heatwave is a regional-scale phenomenon, and climatic variables can impact local conditions to modify the energy budget differential between urban and rural counterparts. In contrast to the previous chapter, the UO-heatwaves synergies were investigated in Sydney, taking into account the i) multiple heatwave/ background spells, ii) multiple locations in various zones of Sydney, and iii) geographical features (surface characteristics, land-coast distance, and population density). Reportedly, a correlation exists between UO and heatwaves in all zones of Sydney. As reported previously, advective heat flux as a dualistic circulation system was accountable for aggravating the UO intensity in all suburbs during heatwaves and modifying the available energy balance. The land-coastal distance was identified as a key contributor influencing the suburban-urban thermal gradient. In order to limit the occurrence of severe heatwaves in Sydney, surfaces with the capacity to hold a higher moisture content were prescribed, which will aid in activating the ventilation corridor for coastal wind penetration in western Sydney.

7.1 Background:

This section summarizes the data and methods utilized in this chapter. In contrast to chapter 6, where UO-heatwaves interactions were investigated for the most intense heatwave spell and at one of the most affected locations in Sydney, this chapter extends the analyses to multiple locations and numerous heatwave/ background spells. The purpose of the study was to validate the findings of the preceding chapter, as investigating the UO-heatwave interaction during a single heatwave/ background spell and at a single location in the city might yield contradictory results. Further, the impact of land-coast distance, population density, and geographical characteristics was also examined while assessing the UO-heatwaves interactions. The literature on UO computation, heatwave identification, and synergies between UO-heatwaves has been reviewed in sections 2.1.2, 2.2.1, and 3.1. The site characteristics of six locations (PL, CT, LP, OP, CY, OH) in three Sydney zones were outlined in section 4.2. The meteorological data collection and processing were presented in section 4.3. The heatwave/ background definitions and the spells (during three consecutive years) utilized in this chapter were elucidated in section 4.4.1 and listed in Table 4-3. The UO/ $\triangle$AH/ $\triangle$UO computational techniques and other methods employed in this chapter were summarized in section 4.7.1. In contrast to the preceding chapter, qualitatively hourly meteorological evaluations (temperature, AH, and wind pattern) were undertaken independently for the entire heatwave/ background event over three consecutive years, followed by the cumulative impact of all heatwave/ background spells. Further statistical models, including linear regression, were employed to validate the results.

7.2 Chapter organization:

The average UO and $\triangle$AH were examined initially during all heatwave/ background spells in 2015, 2016, and 2017 in three zones of Sydney (section 7.3). In order to explore the UO-heatwaves interactions, hourly variations in temperature (section 7.3.1), UO intensity (section 7.3.2), absolute humidity (section 7.3.3), and wind patterns (section 7.3.4) were investigated separately for each heatwave/ background spells during three consecutive years, at all locations. Later, the association between UO and influential wind patterns was established during all heatwave/ background spells (section 7.3.5). Following that, statistical models, including regression, were employed during all heatwaves/ backgrounds to validate the findings (sections 7.3.6). Lastly, the impact of geographical characteristics on UO intensity during heatwaves was assessed in the light of statistical results (section 7.3.7).

7.3 Results:

The average UO and average ΔAH were computed for selected heatwave/ background spells in 2015, 2016, and 2017 for all studied locations (Figure 7-1). The daytime UO was greater in all suburbs during heatwaves, particularly in the afternoon. The nocturnal UO intensity was nearly insignificant during heatwaves and backgrounds in all zones. During 2015, 2016, and 2017, the average heatwave-background UO difference (△UO) was approximately 4.5°C in the western Sydney suburbs and 3.8 °C in the inner Sydney suburbs. In 2015, the △UO in western Sydney was approximately 4 °C, rising to 5.5 °C in 2016 and 8 °C in 2017. In contrast, the △UO in inner Sydney remained at 4 to 4.5 °C across the three years. In conclusion, the △UO in inner Sydney and western Sydney in 2015 was nearly the same but grew successively in western Sydney.

Furthermore, it was revealed that as -ΔAH increased (due to decreasing daytime ambient moisture in the suburbs), the UO increased. The greater the -ΔAH, the greater the UO intensity was during heatwaves. During heatwaves, the -△AH was elevated in western Sydney, especially in the afternoon, compared to inner Sydney. Further, the △AH predominantly declined around noon and improved in the evening. During heatwaves, the average ΔAH dropped in western Sydney suburbs (from morning to afternoon) by roughly 4.2 g/m^3, while the reduction for the inner Sydney suburbs was between 2.5 and 3.0 g/m^3. The decline in the average △AH rose consecutively from 2015 to 2017, implying that in 2017, all suburbs, particularly in western Sydney, had lower daytime moisture during heatwaves than Sydney CBD. Initially, hourly assessments of each heatwave/ background spell were conducted to examine the day-to-day variation in meteorological variables. The summer 2017 hourly analyses are presented first, and the aggregate effect of the three years is then analyzed.

7.3.1 Variation in hourly temperature in all suburbs during the 2017 heatwaves:

During heatwaves, all suburbs' daytime temperatures rose steadily from the 9th to the 11th of February (Figure 7-2). However, in the western Sydney suburbs, the highest daytime temperature was recorded on the 11th of February, whereas in inner and eastern Sydney, the maximum daytime temperatures were recorded on the 10th of February. Sydney's inner and eastern regions experienced a considerable dip in daytime temperatures on February 11. PL reported the highest daytime temperature during the heatwave, followed by CT, LP, OP, CY, and OH. In contrast, the nighttime temperature in the Sydney CBD was higher than in all suburbs during heatwaves.

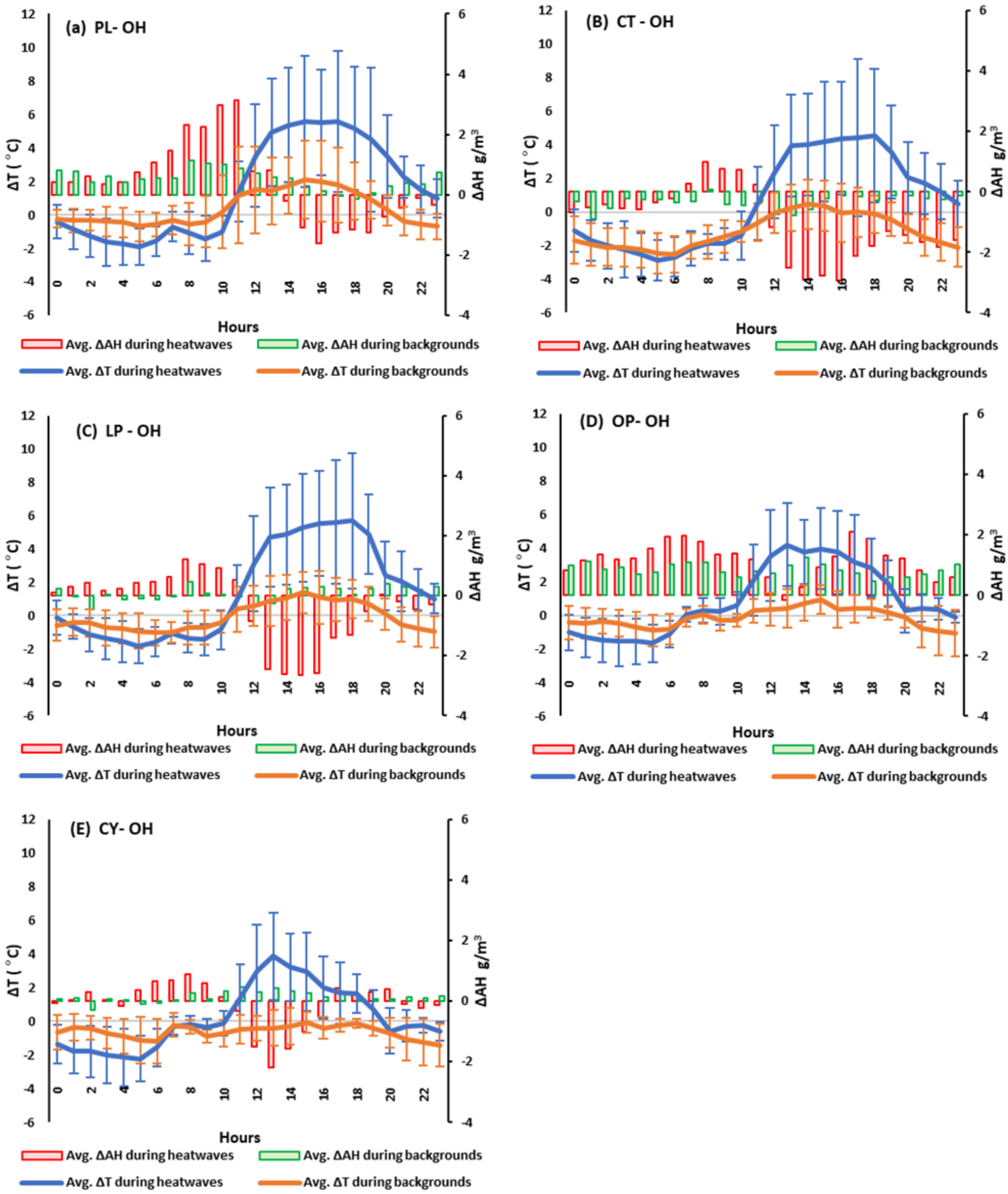

Figure 7-1: Average UO (arithmetic) with SD (whiskers) and average ΔAH (arithmetic) during heatwaves and backgrounds in 2015, 2016, and 2017 A) PL, B) CT, C) LP, D) OP, E) CY. The line graph demonstrates the average UO during heatwaves and backgrounds with the SD, while the bar plot illustrates the average ΔAH.

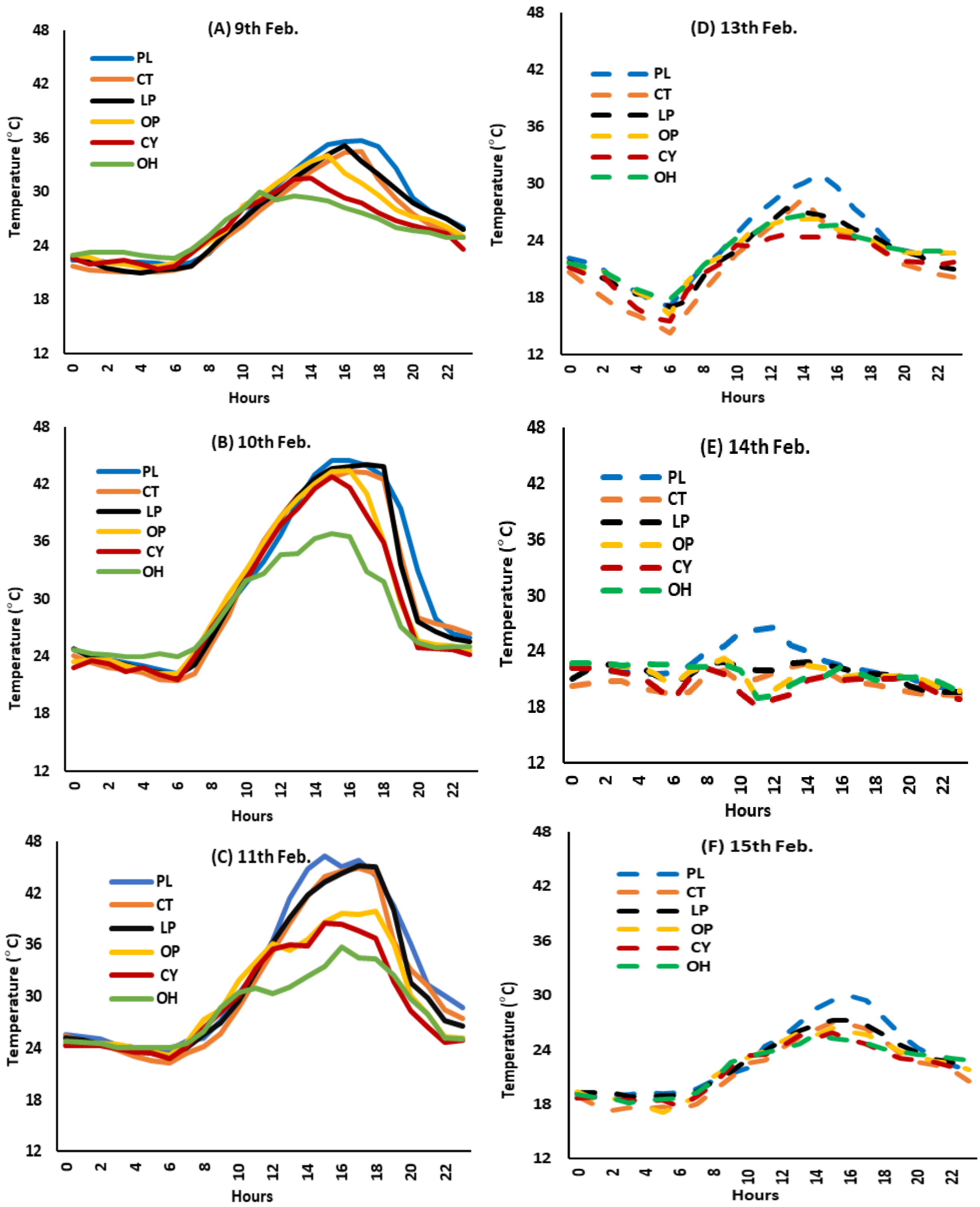

Figure 7-2: Temperature (°C) at various Sydney locations: During heatwaves, A) 9th Feb., B) 10th Feb., C) 11th Feb., During backgrounds, D) 13th Feb., E) 14th Feb., F) 15th Feb.

During the background, the daytime temperatures in all suburbs were recorded to drop continuously, including western Sydney. However, PL still recorded temperature hikes (Figure 7-2). On the first background day, the average daytime temperature in western Sydney suburbs declined by approximately 12 °C than the last heatwave day. Comparably, the average daytime temperature decline in the inner Sydney suburbs since the last heatwave day was approximately 10 °C. Identical temperature values and trends were recorded in the Sydney CBD as in Inner Sydney during the background.

7.3.2 Variation in hourly UO in all suburbs during the 2017 heatwaves:

In western Sydney suburbs, the average peak UO intensity was 7.5°C (the PL was the warmest), 5°C in OP, and 2.5°C in CY on the 9th of February (Figure 7-3). As of the 10th of February, the average peak UO in all western Sydney suburbs was over 12°C (except CT-10 °C), whereas at OP it rose to 8°C and at CY to 5°C. On February 11th, peak UO in western Sydney was nearly the same as on February 10th; however, it decreased to 5 °C in inner Sydney. During the background, the maximum peak daytime UO was approximately 2°C in the western Sydney suburbs, with the exception of PL, where it ranged from 4 to 6 °C. The highest daytime peak UO was either 1°C or less than 0°C during the background in inner Sydney.

7.3.3 Variation in hourly AH in all suburbs during the 2017 heatwaves:

During the heatwave, the ambient moisture was maintained in the morning according to the location's characteristics in all suburbs (Figure 7-4). However, AH unexpectedly declined in all suburbs around noon before regaining in the afternoon. The Sydney CBD was the least affected during the heatwave due to its proximity to the coast. Compared to the inner Sydney suburbs, the decline in ambient moisture was more evident in the western Sydney suburbs. On the 9th of February, the decrease in ambient moisture was less pronounced across all sites, with subsequent days exhibiting a sequential decline. On the 11th of February, however, the daytime ambient moisture in inner Sydney did not decrease and was actually greater than in Sydney's CBD.

The average AH at all locations during heatwaves was higher (because of high evaporation rates) than during the background (Table 7-1). The average AH in inner Sydney suburbs during heatwave/ background was greater than Sydney CBD. It was attributed to the higher proportion of non-urban surfaces in inner Sydney, closeness to other water bodies (river), and proximity to the coast (around 10km). PL in western Sydney and OP in inner Sydney have greater average ambient moisture than other suburbs due to the availability of water bodies in the surrounding.

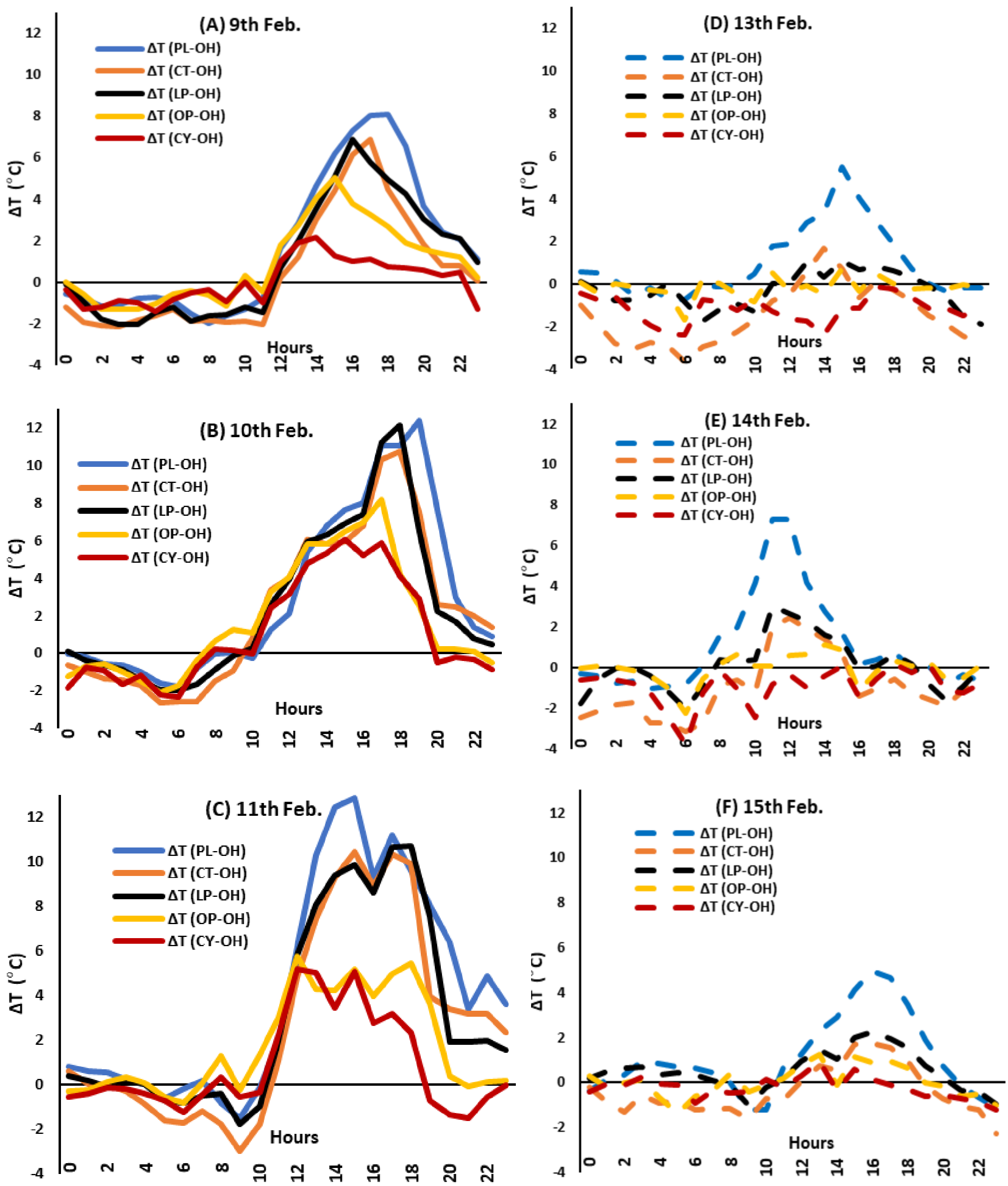

Figure 7-3: UO (°C) at various Sydney locations: During heatwaves, A) 9th Feb., B) 10th Feb., C) 11th Feb., During backgrounds, D) 13th Feb., E) 14th Feb., F) 15th Feb.

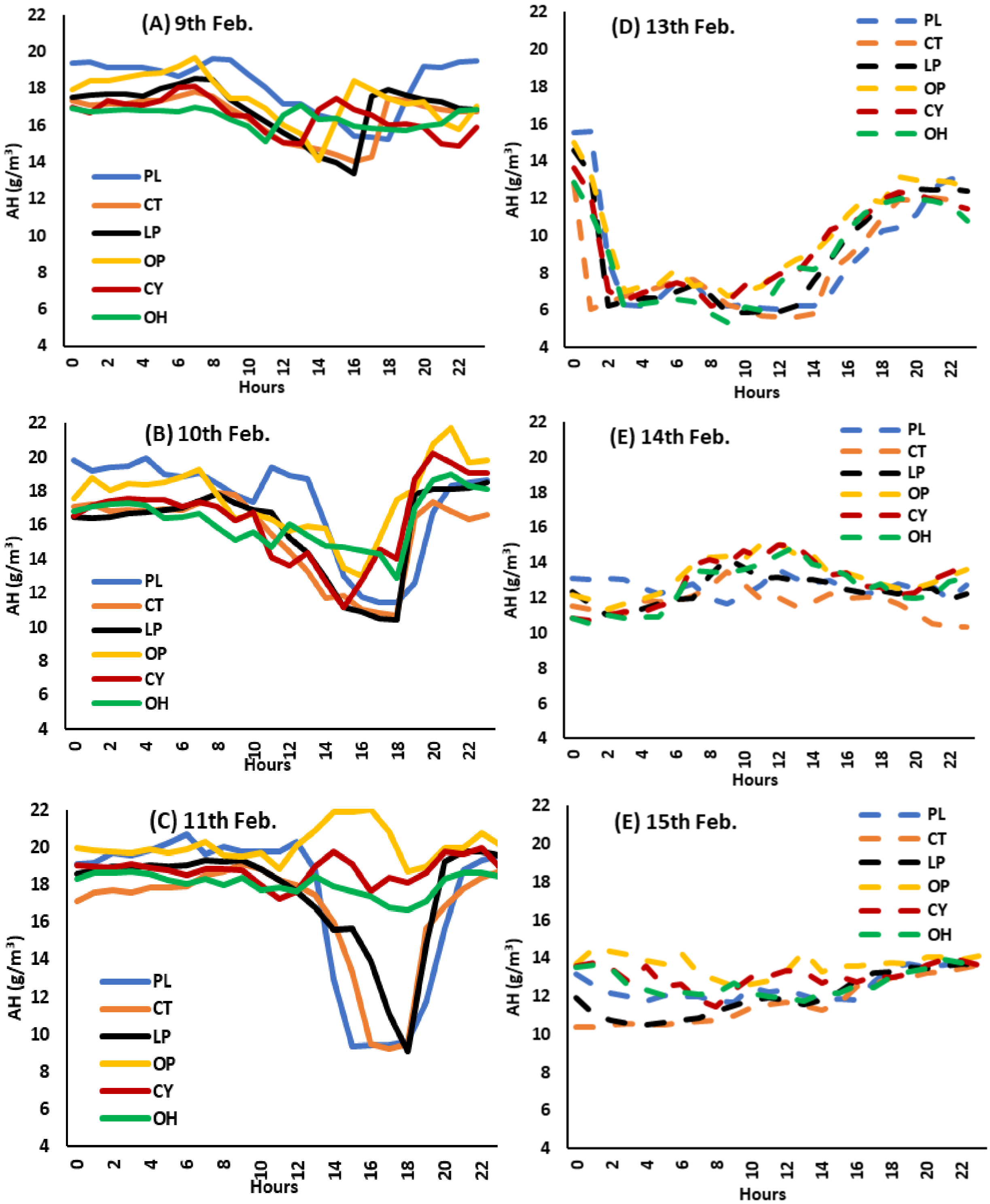

Figure 7-4: AH (g/m^3) at various Sydney locations: During heatwaves, A) 9th Feb., B) 10th Feb., C) 11th Feb., During backgrounds, D) 13th Feb., E) 14th Feb., F) 15th Feb.

Table 7-1: Meteorological parameters comparison during heatwaves and backgrounds (average values).

Parameters	PL	CT	LP	OP	CY	OH
Mean Temp (°C) heatwaves	30.59	29.47	29.84	29.10	28.30	27.65
Mean Temp(°C) backgrounds	23.15	21.15	22.21	22.02	21.31	22.11
Mean AH (g/m³) heatwaves	17.54	16.15	16.73	18.38	17.20	16.91
Mean AH (g/m³) backgrounds	11.33	10.58	11.14	12.29	11.77	11.39
Mean wind speed (m/s) heatwaves	2.29	1.99	2.01	2.61	3.40	3.81
Mean wind speed (m/s) backgrounds	2.52	2.32	2.28	2.99	3.61	4.54
Prevailing winds heatwaves	Desert-D (NW/SW)	Desert-D (NW/ SW)	Desert-D (NW/ SW)	Morning-noon: Inland wind- IW (NW/SW) Afternoon: Coastal winds-C (NE/ SE)	Morning-noon: Inland wind- IW (NW/SW) Afternoon: Coastal winds- C (NE/ SE)	Coastal- C (NE/SE)
Prevailing winds backgrounds	Inland- IE (NE/SE)	Inland- IE (NE/SE)	Inland- IE (NE/SE)	Coastal winds- C (NE/ SE)	Coastal winds- C (NE/ SE)	Coastal- C (NE/SE)

On 9th February, the maximum decline (morning to afternoon) in daytime ambient moisture in all western Sydney suburbs was approximately 23 percent (higher in LP), whereas, at OP, CY, and Sydney CBD, it was 28 percent, 18 percent, and 10 percent, respectively (Figure 7-4). The decline in ambient moisture in the western Sydney suburbs rose to 42 percent on 10th February, whereas inner Sydney suburbs recorded a drop of 33 percent, and Sydney CBD recorded a decline of 25 percent. On 11th February, the decline in ambient moisture in western Sydney suburbs climbed to 54 percent, whilst a rise of 15 percent in ambient moisture was seen in inner Sydney suburbs. The ambient moisture in the

Sydney CBD was lowered by 10 percent on February 11th. During the nighttime (heatwaves), the ambient moisture was relatively consistent in all suburbs, and AH values reflected the site's features. Similarly, throughout the background, daytime and nighttime ambient moisture were generally steady in all suburbs, with the exception of 13th February, when a significant reduction was seen at all locations at nighttime, followed by recovery during the day.

7.3.4 Variation in hourly wind pattern in all suburbs during the 2017 heatwaves:

Wind patterns were examined to understand all suburbs' decline in ambient moisture. Figures 7-5 and 7-6 present the analysis of wind patterns at all locations during heatwaves and backgrounds. As previously stated, Letter C and Letter D symbolize coastal and continental winds, respectively. Inland winds are represented as IE in western Sydney and IW in inner Sydney and the Sydney CBD. In section 4.2, specifics concerning these norms were described.

During daytime heatwaves, western Sydney was observed to be influenced by the continental winds, which led to a rise in ambient temperatures and a drop in ambient moisture, as illustrated in Figures 7-5 and 7-6. The higher the continental wind speed, the higher the temperatures and the lower the ambient moisture in the suburbs. This occurred due to continental air advection (dry and warm), which reduced evaporation/evapotranspiration efficacy by sweeping the ambient moisture, resulting in a dramatic increase in reported temperatures. During heatwaves and backgrounds, coastal winds influenced Sydney CBD; hence the city center was least affected during the day and at night. Further, it was observed that during daytime heatwaves, the opposing circulation system was more active since continental winds in western Sydney and coastal winds at Sydney CBD were prevailing simultaneously; hence the suburban-urban thermal contrast increased drastically (Figures 7-2 and 7-5). During heatwaves, inner Sydney was affected by coastal winds (C-in the afternoon) and inland winds (IW- in the morning). At OP (located in inner Sydney), inland winds (IW) were more prevailing and lasted longer during the day, therefore recording higher temperatures than CY. This is due to the greater distance of OP from the coast compared with CY.

During daytime in backgrounds, western Sydney was primarily influenced by inland winds (IE). However, occasionally, these winds were not penetrating the PL and causing an increase in UO. Coastal winds influenced inner Sydney during the daytime in backgrounds. At night, because of the reduced wind speed, the advection was less effective, and western, and inner Sydney suburbs cooled relatively faster owing to radiative cooling, whereas the Sydney CBD was kept cold by a continuous sea breeze simultaneously. Conclusively, nocturnal UO was almost insignificant.

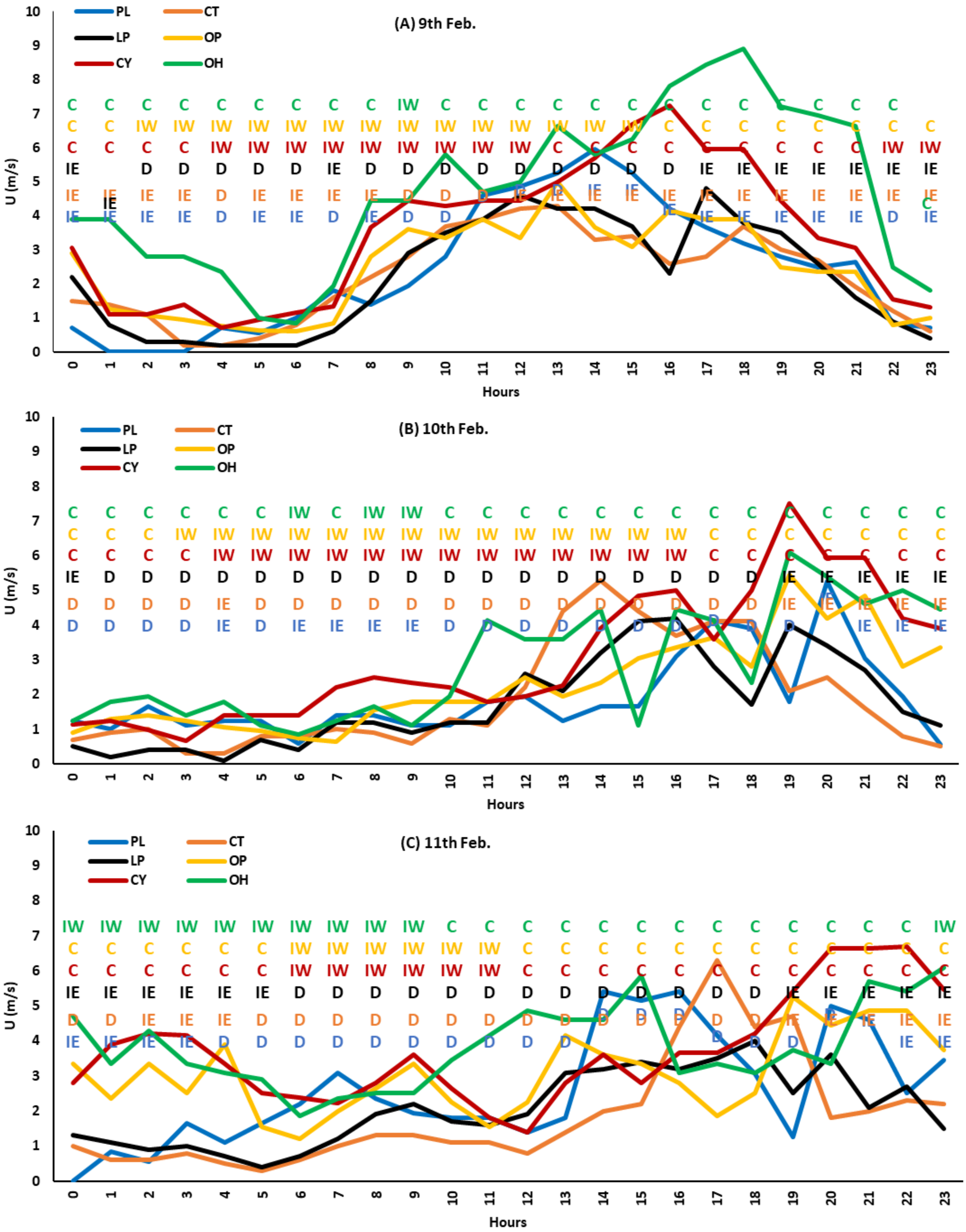

Figure 7-5: Wind speed U (m/s) and wind direction at various Sydney locations during heatwaves, A) 9th Feb., B) 10th Feb., C) 11th Feb.

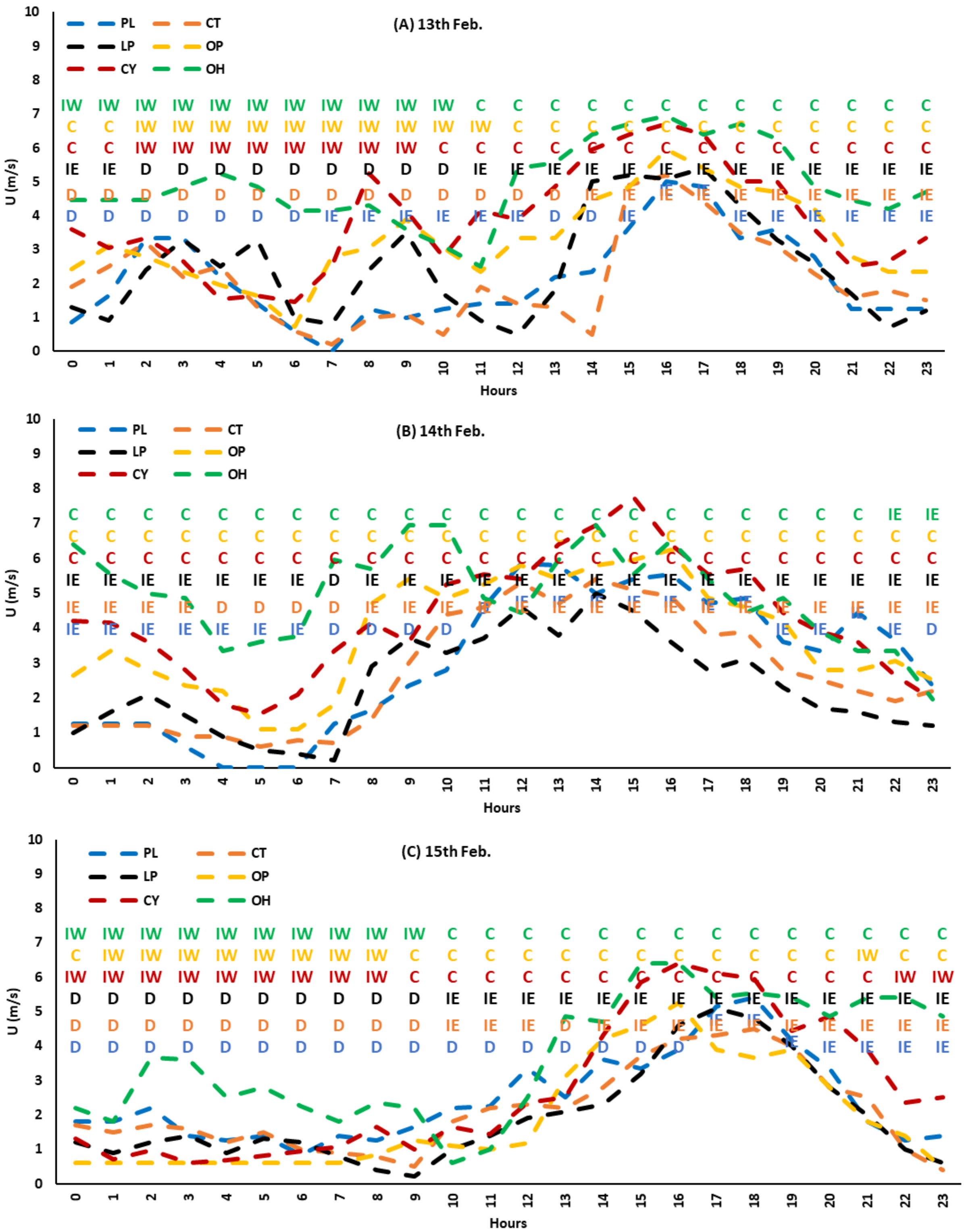

Figure 7-6: Wind speed U (m/s) and wind direction at various Sydney locations during backgrounds, D) 13th Feb., E) 14th Feb., F) 15th Feb.

7.3.5 The association between wind pattern and UO during all heatwave/ background spells (2015,2016,2017):

After studying each event individually, the daytime wind pattern's impact on UO for all selected heatwave/ background spells in 2015, 2016, and 2017 was assessed. The findings in all suburbs were comparable to the summer of 2017 (Figure 7-7). The greater daytime UO amplitude in western Sydney (maximum: 10 to 12 °C) and inner Sydney (maximum: 6 to 8 °C) during heatwaves was connected with high-speed continental winds (D) and inland winds (IW), respectively. Contrarily, the coastal winds also affected the UO intensity in inner Sydney and the inland winds (IE) in western Sydney during heatwaves when blowing with low wind speed. Western Sydney was influenced by continental winds around 70 to 80 percent of the daytime during heatwaves, compared to 20 to 35 percent during backgrounds. In contrast, the IW influenced inner Sydney during heatwaves around 54 percent of the daytime and only 10 to 15 percent of the time during background.

During the daytime in the background, western Sydney was predominantly influenced by IE (65 to 80 percent of the time), and inner Sydney was influenced by coastal winds (80 to 90 percent of the time). Thus, the peak UO was approximately 2 to 3°C in western Sydney suburbs, with the exception of PL, where the continental winds continued to amplify the UO intensity to almost 7°C when blowing at a greater wind speed. UO was minimal in inner Sydney suburbs during background spells (in association with both IW and coastal winds).

7.3.6 Statistical analyses during all heatwave/ background spells:

Statistical models, including regression, were also applied to examine the association between UO and the meteorological variables during heatwaves/ backgrounds. Table 7-2 displays the sample size (n), Pearson correlation coefficient (r), variance explained (r^2), and p-values during heatwaves/ backgrounds across multiple Sydney locations. A p-value lower than 0.05 is considered statistically significant (degree of confidence > 95 percent to reject the null hypothesis). During heatwaves, a moderately negative linear correlation was noticed between UO and $\triangle$AH in all suburbs (r = 0.37 to 0.72), with p-values less than 0.05 and explained variance (r^2) between 14 to 46 percent, indicating that $\triangle$AH is a substantial contributor to amplified UO intensity. The linear correlation between UO and $\triangle$AH during backgrounds was insignificant at most locations (r <0.1 and p-value > 0.05). Despite the higher non-urban surface proportion in the suburbs, the UO-$\triangle$AH inverse relation indicated the relevance of advective heat flux. Consequently, the correlation between i) UO and wind speed (continental winds in the suburbs) and ii) UO and wind speed (coastal winds at Sydney CBD) were also studied.

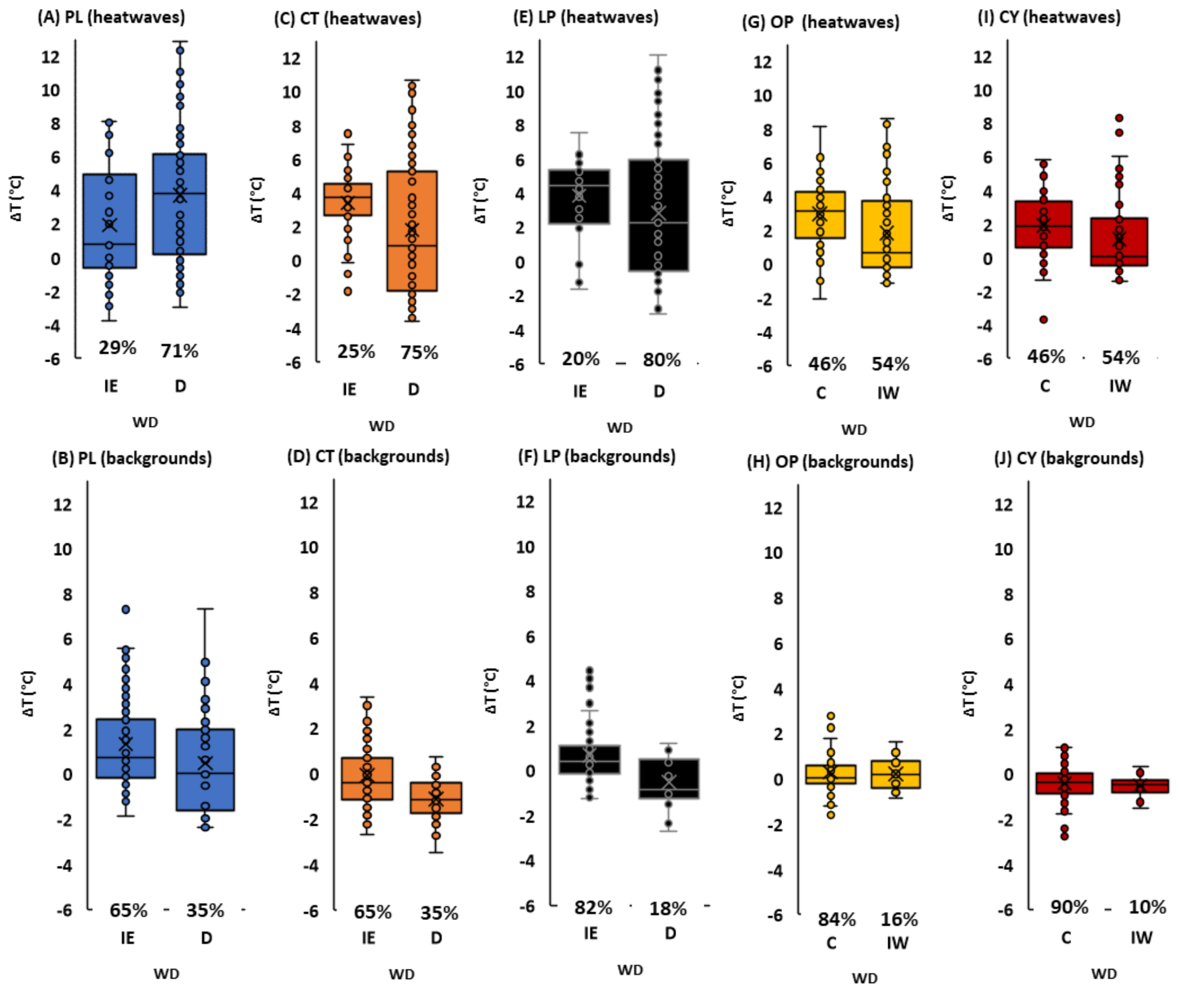

Figure 7-7: Daytime UO and wind direction (WD) comparison during heatwaves and backgrounds in summer 2015, 2016, and 2017. A) PL (heatwaves), B) PL (backgrounds), C) CT (heatwaves), D) CT (backgrounds), E) LP (heatwaves), F) LP (backgrounds), G) OP (heatwaves), H) Op (backgrounds), I) CY (heatwaves), J) CY (backgrounds).

During heatwaves, a weak linear correlation between continental winds and UO was observed In all suburbs (r = 0.2 to 0.36, p-values < 0.05, and r^2 = 4 to 13 percent), whereas during background, the correlation was invalid (r= 0.01 to 0.4 and p-values > 0.05 at the majority of locations). Conclusively, continental winds play a not-so-significant but visible impression on UO intensity during heatwaves. A moderate to strong linear correlation (r = 0.46 to 0.57, p-value < 0.05, and r^2 = 29 to 32 percent) was also observed between coastal winds and UO. The influence of coastal winds on UO was likewise significant during the backgrounds (r = 0.45 to 0.51, p-values < 0.05, and r^2 = 18 to 33 percent). Consequently, based on the statistical findings, coastal winds can be identified as the primary cause of UO exacerbation during heatwaves, as they increase the moisture content/ keep the temperature stable at Sydney CBD (by advection from the sea breeze) and not infiltrating at the inland locations. In addition, the influence of continental winds during heatwaves was also noteworthy.

Table 7-2: Pearson coefficient (r), variance (r^2), and p-value during heatwaves and backgrounds at Sydney's various locations.

		Heatwaves				Backgrounds			
Parameters	Station	**n**	**r**	**r^2**	**p**	**n**	**r**	**r^2**	**p**
ΔAH and UO	PL	216	-0.47	0.22	1.76E-13	216	-0.35	0.13	7.69E-08
	CT	216	-0.68	0.46	8.91E-31	216	-0.08	0.01	0.23
	LP	216	-0.72	0.44	8.85E-36	216	-0.06	0.003	0.40
	OP	216	-0.37	0.14	2.55E-08	216	-0.23	0.05	0.0005
	CY	216	-0.52	0.27	4.83E-16	216	0.09	0.01	0.19
Desert winds at suburb and UO	PL	125	0.25	0.06	0.004	95	0.40	0.16	6.34E-05
	CT	158	0.34	0.12	9.47E-06	114	0.17	0.03	0.071145
	LP	145	0.36	0.13	6.78E-06	81	0.01	0.00	0.947189
	OP	87	0.20	0.04	0.066194	55	0.31	0.10	0.019821
	CY	87	0.29	0.09	0.006049	53	0.07	0.01	0.599604
Coastal winds at OH and UO	PL	141	0.57	0.32	1.10E-13	129	0.57	0.33	7.68E-13
	CT	141	0.54	0.29	6.97E-12	129	0.46	0.21	3.19E-08
	LP	141	0.53	0.28	9.77E-12	129	0.45	0.20	1.07E-07
	OP	141	0.54	0.29	4.37E-12	129	0.43	0.18	4.08E-07
	CY	141	0.46	0.30	1.13E-08	129	0.45	0.18	0.011788

7.3.7 UO and geographical characteristics:

Typically, UO is affected by the higher proportion of urban surfaces, fewer water bodies in the surroundings, lower tree canopy cover, and coastal proximity. After analyzing the geographical characteristics in all suburbs (Table 4-1), it was observed that all western Sydney suburbs have a higher tree canopy cover (average of 28 percent) and potentially more plantable surfaces (average of 48 percent) than inner Sydney suburbs, which have a tree canopy cover (average 16.5 percent) and potentially plantable surfaces (average 27 percent). The tree canopy coverage in the Sydney CBD has further decreased to 15 percent, whereas only 13 percent of areas are potentially plantable. In summary, non-urban surfaces are reduced by 20 percent in inner Sydney and 30 percent in the Sydney CBD than the western Sydney. Even while western Sydney had a greater tree canopy cover and presumably more plantable areas, it was more influenced by UO. Conclusively, the UO increased from eastern to western Sydney as the distance from the nearest coast increased: PL (49 km), CT (28 km), LP (23 km), OP (13.5 km), CY (7.5 km), and OH (0.6 km). In addition, UO increased from eastern to western Sydney despite a decline in population density: PL (484 persons/km^2), CT (509.4 persons/km^2), LP (668.8 persons/km^2), OP (2527.88 persons/km^2), CY (4303 persons/km^2), and OH (6160 persons/km^2). Hence, the opposing circulations are more prevalent during heatwaves and impact UO intensity, regardless of population density and non-urban surface area.

7.4 Discussion

Urbanization significantly impacts land to atmospheric interactions (energy and moisture transfer). The ground surface characteristics have a significant impact on land-atmosphere interactions. Sydney is spreading to the city's western and southwestern sides. Despite having a greater proportion of non-urban surfaces, higher tree canopy cover, and lower population density (PD), the UO impact in western and inner Sydney was drastic. The UO intensity increased in parallel with the land-coast distance; therefore, distance from the coast was one of the primary contributors to creating thermal unbalance between inland-coastal locations. In Los Angeles, higher daytime temperatures were recorded for inland locations (away from the coast) and in highly urbanized areas, indicating a strong positive association between UO (with both land and ambient temperatures) and distance from the coast [72].

The land-coastal distance is crucial because of advection by the coastal breeze, which cools the Sydney CBD while not penetrating inland locations during heatwaves and exacerbating UO. These findings are consistent with research conducted in Athens and Shanghai, where advection from the coastal winds amplified UO [50,51]. Contrarily, despite being coastal cities, the coastal winds' impact was insignificant in Nicosia [60] and Melbourne, Adelaide, and Perth [58]. The choice of location may have impacted the findings in Australian cities, as locations farther from the coast were chosen to limit the influence of coastal winds [58]. Similarly, neglecting the geographical extent while detecting heatwaves might be a limitation of the Nicosia study [60]. In conclusion, location choice and geographical extension during heatwaves identification may influence the outcomes.

Coastal UO impact is typically greater than inland UO due to coastal wind influence [51]. In the current research, high-velocity continental winds also contributed to the UO intensification in addition to the high sea breeze impact. In fact, the average peak ΔUO reached 8 °C in western Sydney and 4 to 4.5 °C in inner Sydney, which was quite high when compared to previous studies, where the recorded difference was 5 °C in Baltimore [41], 4 °C in New York [109], 3.5 °C in Athens [50], 3 °C in Karachi [46], and 1 °C in Berlin [62]. The higher ΔUO in Sydney was attributed to the dualistic circulation system available on the opposing ends of the city.

In this study, the daytime UO intensity during heatwaves was magnified, while the nocturnal UO impact was insignificant in all three city zones. Los Angeles also observed the exacerbated daytime and unnoticed nocturnal UO impacts during heatwaves [72]. The varying boundary conditions substantially affect the results. Our findings are in tandem with most coastal cities, which demonstrated higher daytime UO influence during heatwaves [50,72], as opposed to non-coastal cities, where nocturnal UO impact was more pronounced [61,62]. A pronounced nocturnal UO impact in coastal cities was documented only in Melbourne and Adelaide, owing to the inland site selection [58]. These findings were also supported by a study in Shanghai, which found the exacerbated daytime UO intensity during heatwaves when compared to the coastal location, and amplified nocturnal UO when compared to the inland location [51]. Previously, amplified daytime UO was reported when computed with surface temperatures, whereas exacerbated nocturnal UO was reported when calculated with ambient temperature [159,262]. In the current study, however, a positive correlation between daytime UO and ambient temperatures was detected, and the influence of the coast/ distance from the coastline was more compelling.

The significant synergistic interaction between UO-heatwaves was the urban-rural moisture contrast in cities where the daytime UO impact was more evident [31,60]. The advective heat flux was the key synergy between UO and heatwave in the present study, interfering with the sensible and latent heat fluxes by reducing the efficacy of evaporation and evapotranspiration. The highest decline in ambient moisture was above 50 percent in western Sydney and about 30 percent in inner Sydney, owing to advection by continental winds. In Baltimore and Washington, DC, the urban-rural moisture differential also increased twofold during heatwaves compared to backgrounds [59]. The nocturnal UO impact in this study was negligible due to the suburb's quick radiative cooling and consistent temperatures in the Sydney CBD (owing to the steady sea breeze). Contrarily, the nocturnal UO impact during heatwaves was aggravated in previous studies due to increased urban heat storage capacity (increased heat storage during the day and emissions at night) and a rise in anthropogenic heat [58,63].

A prior study found a positive correlation between UO and population density (PD) [53]. However, due to the impact of opposing weather systems, the influence of population density was insignificant in the current investigation. Nevertheless, increased urban surfaces and PD in western Sydney will further reduce ambient moisture, resulting in more extreme heat events. Soil moisture deficit promotes the occurrence of heatwaves [71], and similar findings were reached in research conducted in NSW, Australia [283–285]. The 2017 heatwaves in Sydney were also attributable to lower upper soil moisture and less precipitation in the region [238]. Hence, further urban growth in western Sydney will diminish available soil moisture and intensify the synergies between UO and heatwaves by encouraging the occurrence of more heatwaves. Materials with a higher moisture-retention capacity, including green roofs, might be viable if they have access to an adequate water supply. Otherwise, as determined by [54], dry soil surfaces with limited evapotranspiration capability during long-lasting heatwaves can exacerbate UO. Coastal breezes do not always penetrate western Sydney (far-inland locations), even during backgrounds; hence, a ventilation corridor that permits the entry of coastal winds can be a solution for reducing the UO intensity in western Sydney.

7.5 Conclusion:

This study demonstrated a positive linkage between UO and heatwaves in Sydney, where a magnified daytime and insignificant nocturnal response was reported in various city zones. Aggravated daytime UO was linked to the region's boundary condition, with land-coast distance emerging as a primary driver. The peak average $\triangle$UO (heatwave-background UO difference) was approximately 8°C in western Sydney and 4 to 4.5 °C in inner Sydney. The land-coastal distance was critical due to the advection from two opposing sources (heating and cooling), which also regulated the region's sensible and latent heat fluxes. The decline in ambient moisture during the heatwave days was over 50 percent in western Sydney and around 30 percent in inner Sydney. The advection from the heating and cooling source during heatwaves illustrates the importance of dualistic large-scale weather circulations available on the opposing ends of the city. A correlation between UO and large-scale weather systems was already established in chapter 5.

The impact of population density and a higher proportion of potentially plantable surfaces on the UO intensity during heatwaves was insignificant. However, the heatwaves occurrences in Sydney will increase as urbanization continues in western Sydney. As a result, it will increase the load on the electric grids, leading to more blackouts like those in the summer of 2020. These blackouts will be more detrimental to the underprivileged communities, the aged and minors, and those with chronic health issues, who will also be at a greater risk of heat-related mortality and morbidity. In western Sydney, the UO intensity will be further exacerbated by anthropogenic heat emitted from air-conditioning devices during heatwaves as a result of higher external ambient temperatures. The extreme temperatures and sunny conditions during heatwaves will also accelerate ozone formation in the Sydney region, and the prevailing sea breeze in the post-heatwaves will allow pollutants to penetrate western Sydney, thereby degrading the air quality in this region.

CHAPTER 8: IMPACT OF LOCAL, REGIONAL, AND GLOBAL CLIMATIC CHANGES ON BUILT ENVIRONMENT:

SUMMARY:

The world's rapidly growing urban population, rising urban power demands, and greenhouse gas (GHG) emissions severely threaten the global climate. Multilevel climatic conditions (local, regional, and global) synergize and influence urban energy performance and indoor environmental quality (IEQ). The cumulative influence of such local, regional, and global climate changes on urban energy performance has never been evaluated. The synergic influence of UO and heatwaves on urban energy performance/ IEQ was examined in this study using the urban building energy model (UBEM). Furthermore, sensitivity studies were carried out utilizing adaptation strategies to assess the impact on cooling energy and IEQ. The cooling penalties were up to 650 percent, the rise in average indoor temperature was up to 5.8°C, and the degradation in passive survivability was up to 31 percent under the UO-heatwaves cumulative effect. The collective impact of multiple adaptation strategies resulted in cooling savings of up to 97 percent, a fall in the average indoor temperature of up to 2.34°C, and an improvement in passive survivability of up to 20 percent during extreme heat occurrences. The current study could aid revise building codes to mitigate global climate changes and enhance building resilience during heatwaves.

8.1 Background:

This section entails the data and method utilized in this chapter. The literature on microclimatic context/UO/ heatwave's impact on the building's thermal performance and possible adaptation measures to mitigate the multilevel climatic changes was reviewed in sections 3.3 and 3.4. Geographical characteristics of the studied locations (PL, OP, OH) in three zones of Sydney were presented in sections 4.2.1, 4.2.4, and 4.2.6. The meteorological data collection and processing were covered in section 4.3. The heatwaves utilized in this chapter during the summer (2015-16 and 2016-17) were summarized in section 4.4.3. Further, instead of using the 95th percentile (RTT metric), the 90th percentile of the daily maximum temperature was utilized to define the heatwave, and the building's thermal performance during heatwaves was compared to that of the remaining summer days (RSD). Further details on varying heatwave/ RSD definitions can be found in section 4.4.3. Instead of using building energy models (BEMs), the urban building energy model (UBEM) was utilized to evaluate the urban thermal performance. Further details on UBEM and the simulation tool can be found in section 4.6.2. The tools and methods employed to create the climate and horizon files for energy simulation were outlined in section 4.6.2.1. The residential settlements (HD/ LD) and climatic zones (NCC/ NatHERS) utilized for building thermal performance evaluation were detailed in section 4.6. The passive survivability standards employed in this research were encompassed in section 4.6.3. The methods used to evaluate the impact of multilevel climatic changes on the built environment were summarized in section 4.7.3. The building's thermal performance was evaluated in terms of urban cooling energy, indoor temperature, and passive survivability. The research was conducted in three phases. Initially, UO, heatwaves, and cumulative impact of UO-heatwaves were assessed on the building's thermal performance. In the second phase, sensitivity analyses were performed using numerous adaptation measures during extreme heat conditions. The combined impact of selected adaptation measures was examined during heatwaves and RSD in the third phase. The building envelope details (uninsulated, intermediately-insulated, and hyper-insulated envelope) have been provided in Tables 4.7, 4.8, and 4.9. The adaptation scenarios were listed in Table 4-10 and explained from sections 4.7.3.1 to 4.7.3.10.

8.2 Chapter organization:

Section 8.3 evaluates the spatiotemporal impact of UO, heatwaves, and the combined effect of UO-heatwaves on urban energy performance and IEQ of two residential settlements. Initially, the multi-level climatic impacts were examined on the urban energy performance (section 8.3.1.1), followed by the impact on indoor temperature (section 8.3.1.2) and passive survivability (section 8.3.1.3). In section 8.3.2, sensitivity analyses were performed using the nineteen adaptation measures (M1 to

M19). In section 8.3.2.1, the individual impact of adaptation strategies on cooling energy, while in section 8.3.2.2, the impact on IEQ (indoor temperature and passive survivability) was examined. Section 8.3.3 presents the cumulative impact of suitable adaptation strategies. The combined effect of adaptation strategies on cooling energy was examined in section 8.3.3.1, the impact on the indoor temperature in section 8.3.3.2, and the impact on passive survivability in section 8.3.3.3. Sections 8.4, 8.5, and 8.6 provide discussion, limitation, and conclusion, respectively.

8.3 Results:

As previously explained, the findings were organized into three categories: **i)** The current scheme (base-case): to evaluate the UO-heatwave cumulative effect on urban energy performance/ IEQ in both settlements and across both years; **ii)** Sensitivity analyses: to evaluate the impact of various adaptation strategies on cooling energy and IEQ, and **iii)** the aggregated impact of the best-suited adaptation strategies on cooling energy and IEQ. Figures 8-1 and 8-2 exhibit the graphical simulation findings for the base-case (LD/ HD settlements).

8.3.1 The current scheme:

8.3.1.1 The impact on cooling energy:

<u>Variation in cooling energy during heatwaves and RSD:</u> The cooling energy during heatwaves was 215 to 350 percent greater than during RSD for both settlements and years and in all three zones of the city (Figure 8-3). The cooling energy during heatwaves and RSD was greater in western Sydney and declined from the continental to the coastal end of the city. The higher cooling energy needs in western Sydney are ascribed to i) a lack of penetration of coastal winds during RSD and ii) strong continental winds during heatwaves, as established in chapters 5 and 7. The heatwave-RSD cooling energy differential was greater in the city's coastal districts since high-velocity coastal winds kept the coastal region cooler during RSD, whereas these winds were less influential (low speed) during heatwaves.

<u>Temporal variations in cooling energy:</u> Summer 2016-17 was recorded as "one of the warmest summers in Southeast Australia's history" [238]. In 2016-17, the cooling energy in western Sydney hiked by roughly 33 percent, and in inner and eastern Sydney increased by 15 to 16 percent during heatwaves, compared to the previous year for both settlements (Figure 8-3). The rise is attributable to intensifying dualistic large-scale weather systems, which are strengthening with growing urbanization in western Sydney. Similarly, cooling energy during RSD was greater in 2016-17 than the previous year in all zones (western Sydney: 45 percent, inner Sydney: 32 percent, and eastern Sydney: 22 percent).

Variation in cooling energy across various housing typologies (high density- HD and low density- LD settlements): LD (houses) settlements were required 100-140 percent more cooling energy than HD (apartment) settlements across both years during heatwaves and RSD, and in all zones (Figure 8-3).

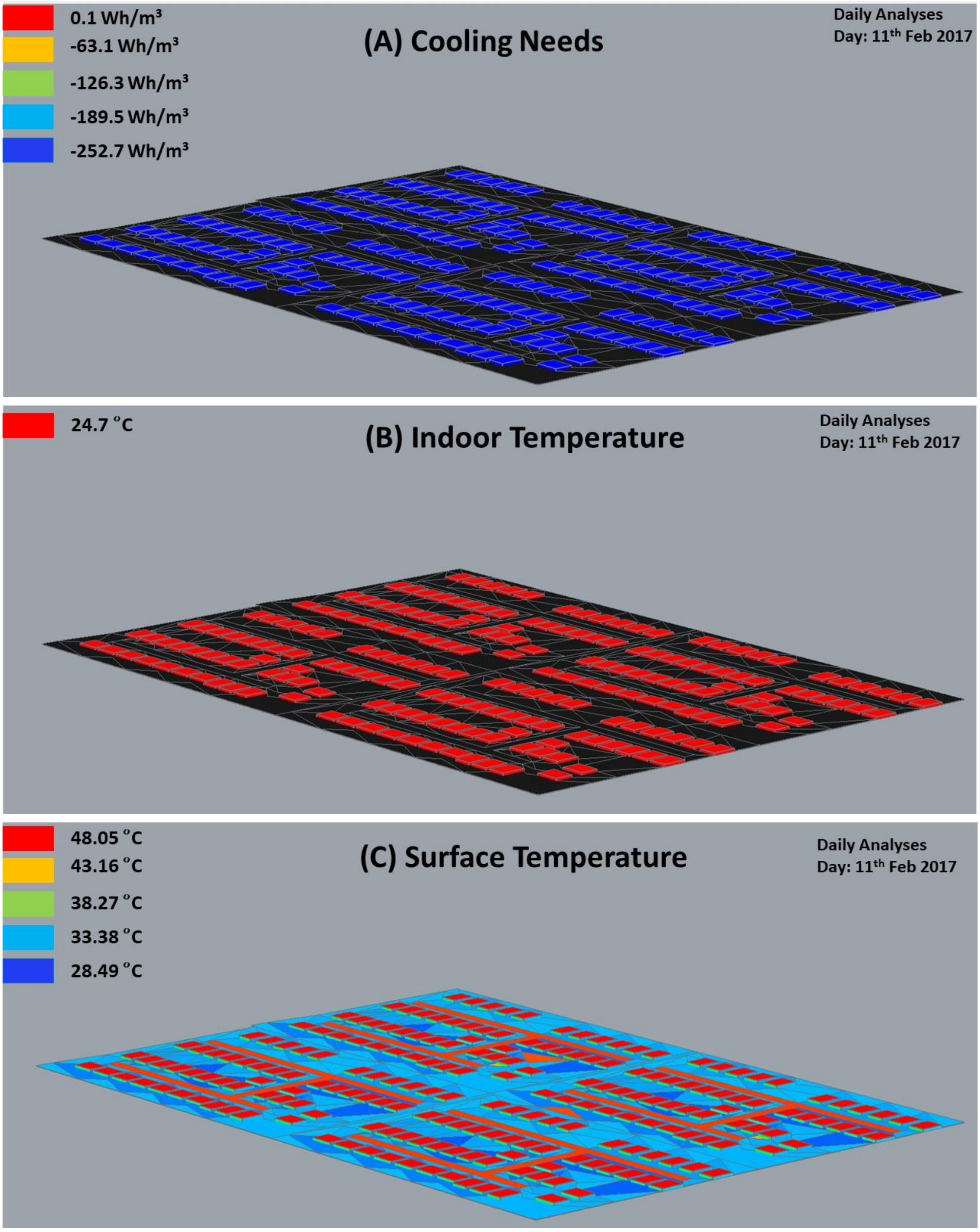

Figure 8-1: Daily cooling needs, indoor temperature, and surface temperature distribution for LD settlement (base-case) on 10th Feb 2017 at PL. A) cooling needs, B) Indoor temperature, and C) Surface temperature.

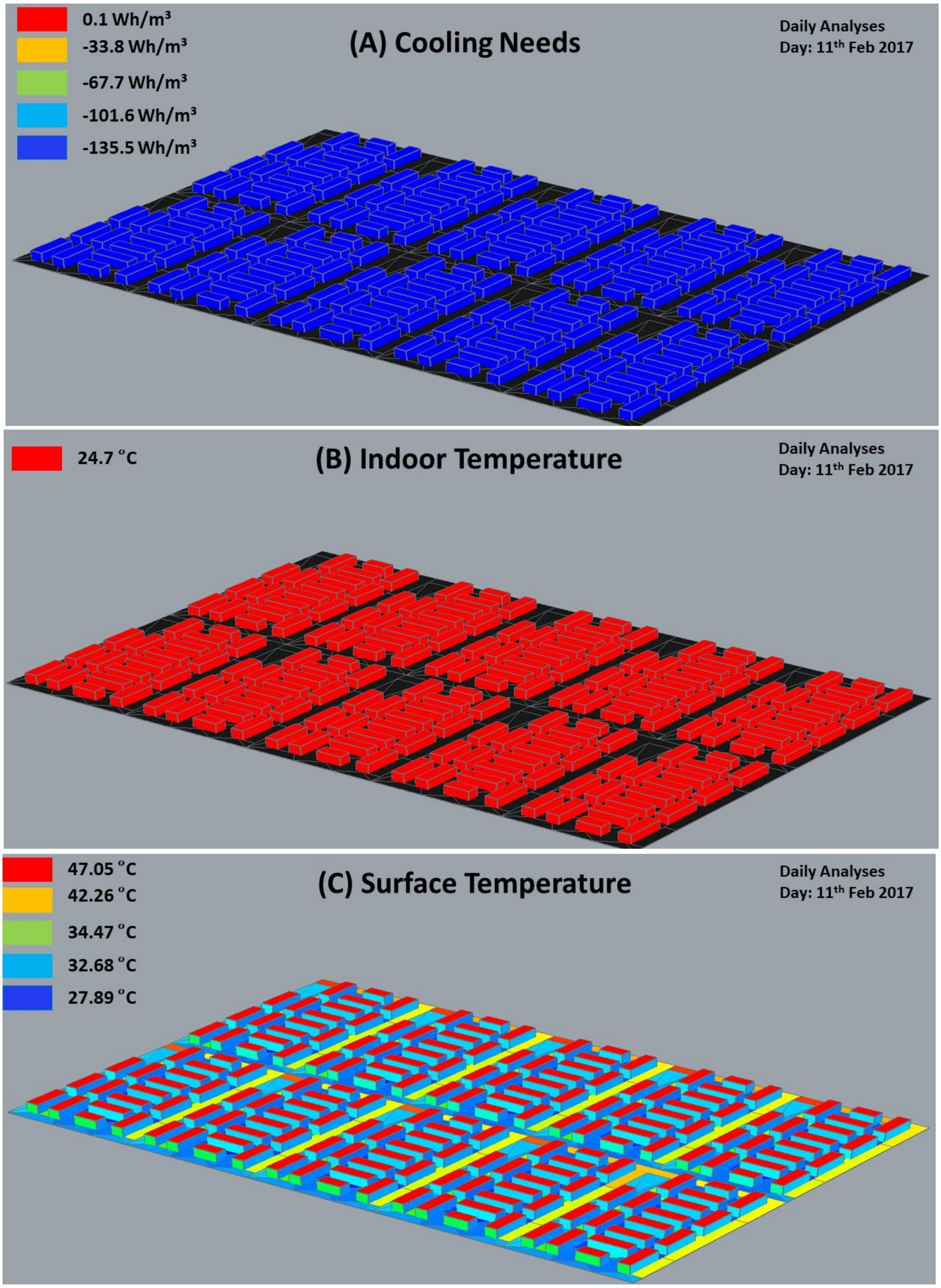

Figure 8-2: Daily cooling needs, indoor temperature, and surface temperature distribution for HD settlement (base-case) on 10th Feb 2017 at PL. A) cooling needs, B) Indoor temperature, and C) Surface temperature.

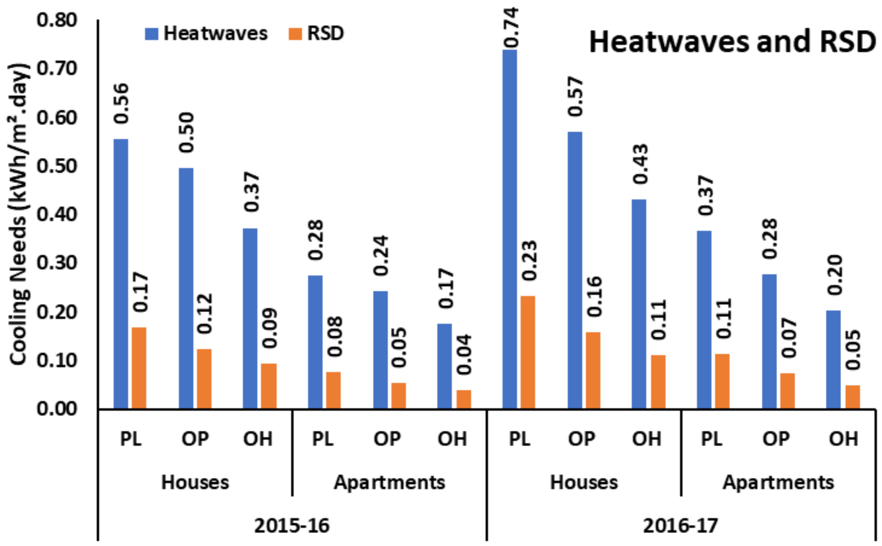

Figure 8-3: Cooling energy (kWh/m². day) comparison during heatwaves and RSD in three zones of Sydney (western Sydney: PL, inner Sydney: OP, and Sydney CBD: OH) for two settlements in two successive years.

The inter-building shading effect may account for lower cooling needs in HD settlements. Further, the LD-HD cooling needs variances were more pronounced during RSD than heatwaves, particularly in the suburbs closer to the coast: eastern Sydney 112 percent (heatwaves) to 134 percent (RSD), inner Sydney 104 percent (heatwaves) to 123 percent (RSD), against western Sydney 102 percent (heatwaves) to 115 percent (RSD). It might be ascribed to the influence of coastal breezes during RSD, which keeps high-rise apartments cooler than single-story dwellings. Though the LD-HD cooling energy difference in western Sydney was still large, a decreasing tendency in cooling needs contrast (LD-HD settlements) was noticed when evaluating the outcomes of temporal variation and heatwave-RSD cooling demand fluctuations. This might be ascribed to hot/ dry air advection from the continental side, which may reduce the shading benefits of tall structures.

<u>The UO impact on cooling energy:</u> The UO-induced cooling penalties in 2016-17 (relatively greater than the previous year) was roughly 72 to 130 percent in western Sydney and 32 to 50 percent in inner Sydney during heatwaves/ RSD and for both settlements (Figure 8-4A). Further, the penalties were comparatively greater (approximately 10 to 20 percent) in HD settlements (apartments) than in LD settlements (houses) during heatwaves/ RSD, owing to the greater influence of dualistic large-scale weather systems. The difference was more pronounced during RSD than during heatwaves (approximately 40 to 50 percent in western Sydney and 10 to 15 percent in inner Sydney) due to the impact of coastal breezes at Sydney CBD.

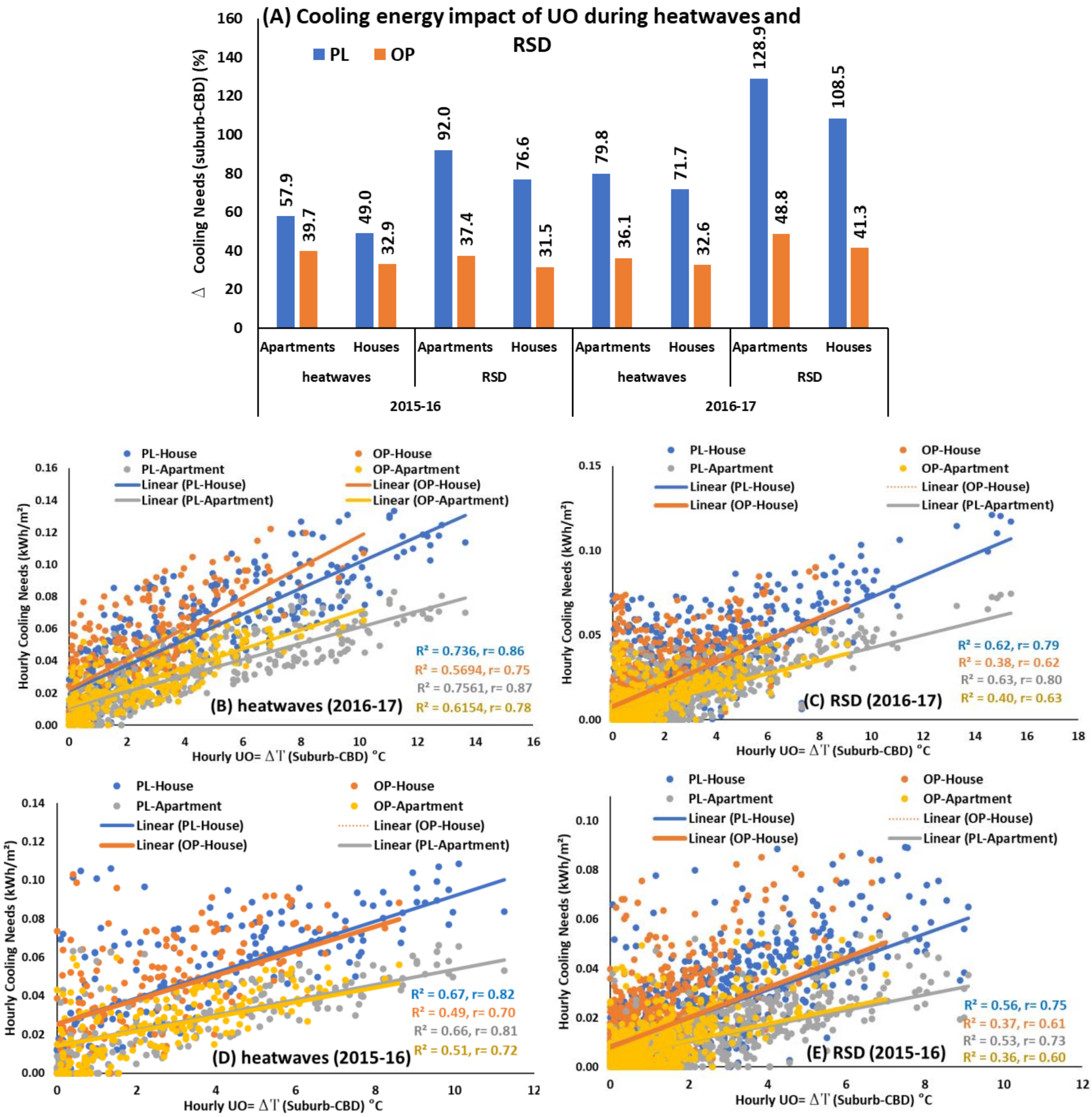

Figure 8-4: Cooling energy impact of UO during heatwaves and RSD in western Sydney (PL) and inner Sydney (OP) in comparison to Sydney CBD (OH) in 2015-16 and 2016-17 A) Δ cooling needs (suburb-CBD) (%) in both settlements during heatwaves and RSD, (B-E) linear correlation between hourly cooling needs (kWh/m²) and hourly UO (^{o}C) during heatwaves and RSD, B) during heatwaves (2016-17), C) during RSD (2016-17), D) during heatwaves (2015-16), E) during RSD (2015-16).

Furthermore, when correlating the UO-cooling energy in western Sydney using the regression model, a strong positive linear correlation was detected during both heatwaves (r>0.8) and RSD (r>0.73) (r^2 = 50 to 75 percent and p> 95 percent) for both settlements/ years (Figure 8-4 B-E). The r represents the Pearson coefficient, r^2 reflects the explained variance, whereas p denotes the confidence interval.

Similarly, a strong positive linear correlation (r= 0.7 to 0.8) during heatwaves and a moderate positive linear correlation (r>0.6) during RSD were observed in inner Sydney (r^2 = 36 to 61 percent and p>95 percent) for both settlements/ years. To summarize, during both heatwaves and RSD, the differences in cooling needs are more evident in the opposite parts of the city, which can be linked to the opposing large-scale weather system.

The UO-heatwaves cumulative impact on cooling energy: The UO-heatwave (combined) induced cooling penalties (suburbs during heatwaves compared to Sydney CBD during RSD) was approximately 500 to 650 percent in western Sydney and 400 to 500 percent in inner Sydney, comparatively higher for HD settlements, and higher in 2016-17 than the preceding year (Figure 8-3).

8.3.1.2 The impact on Indoor temperature:

The heatwaves-RSD variations in indoor temperature: The heatwave-RSD average hourly indoor temperature contrast was between 3.5°C and 5.0°C in 2016-17 in all suburbs (western Sydney: 5C°, inner Sydney: 4.5°C, and Sydney CBD: 3.5°C), slightly greater in LD settlements than HD settlements (Figure 8-5 A-D). Further, the difference was comparatively higher in 2016-17, and the contrast from the preceding year was between 0.5 and 1.5°C (Western Sydney: 1.5°C, Inner Sydney: 1.0°C, and Sydney CBD: 0.5°C) in both settlements.

The outdoor (O) – indoor (I) temperature variations: Surprisingly, during both heatwaves and RSD, the average hourly indoor temperature was comparatively greater in all zones of the city than the average hourly outdoor temperature during both years (Figure 8-5 A-D). The indoor to outdoor thermal contrast varied between 0.5 to 0.8°C in LD settlements and 0.2 to 0.6°C in HD settlements, comparatively higher during RSD than heatwaves. It demonstrates that these residential settlements function as hot boxes during the summer and extreme weather, and the inhabitants are rendered more vulnerable without mechanical cooling.

The LD-HD settlement's indoor temperature variations: In all three zones of Sydney, the LD-HD hourly indoor temperature contrast was around 0.2°C to 0.3°C during heatwaves and 0.1°C to 0.2°C during RSD, comparatively greater in 2015-16 than the following year (Figure 8-5 A-D). The lower thermal contrast between both settlements in the succeeding year demonstrates that further intensified opposing large-scale weather systems will lower the inter-building shading advantage of the tall buildings. Further, the dweller of such high-rise buildings on the continental end of the city might be negatively affected during extreme heat occurrences.

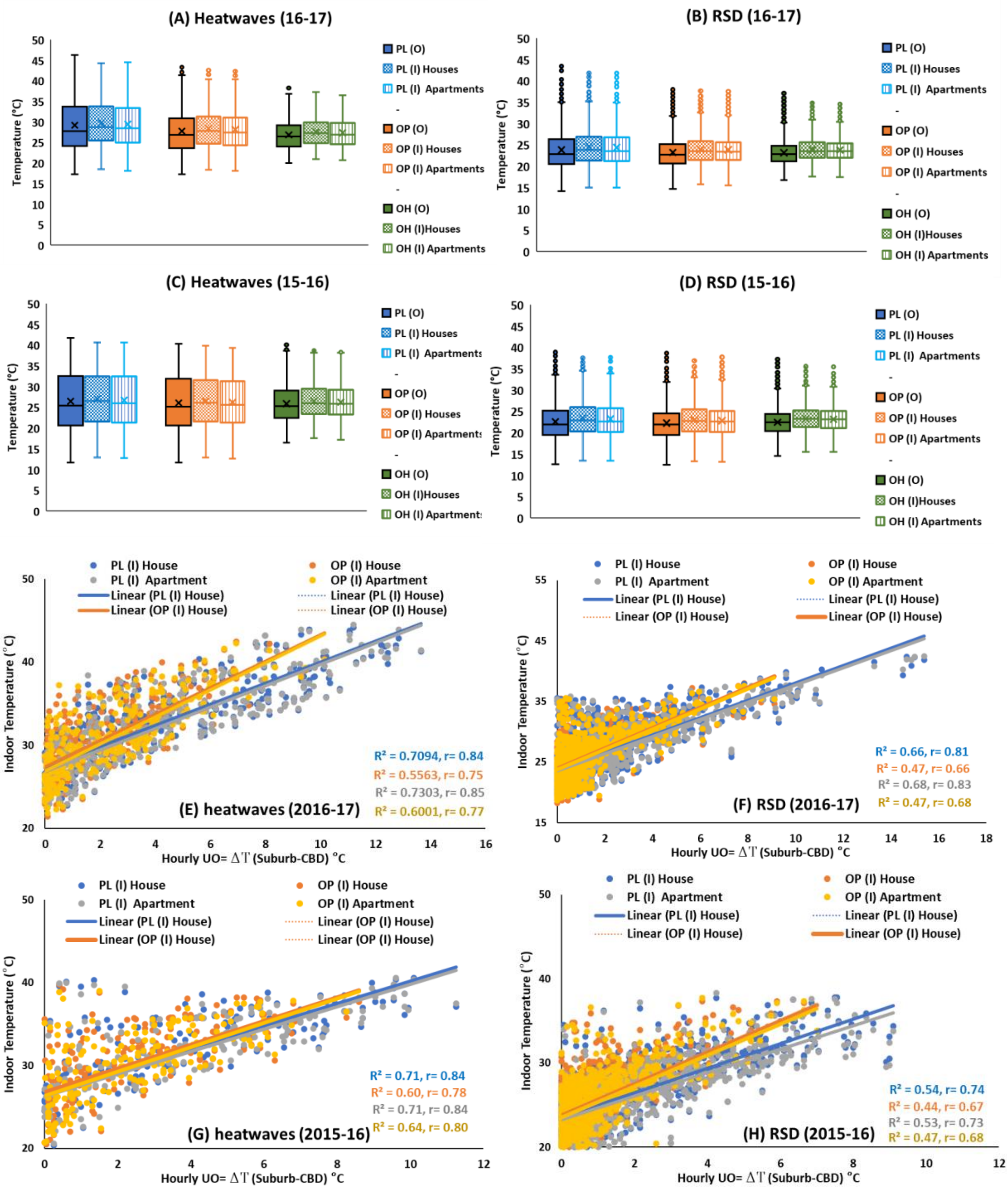

Figure 8-5: (A-D) Hourly indoor (I) and outdoor (O) temperature (^{o}C) in three zones of Sydney (western Sydney: PL, inner Sydney: OP, and Sydney CBD: OH) for both settlements during 2015-16 and 2016-17, A) during heatwaves (2016-17), B) during RSD (2016-17), C) during heatwaves (2015-16), D) during RSD (2015-16), **(E-H)** linear correlation between hourly indoor temperature (^{o}C) and hourly UO (^{o}C) during heatwaves and RSD, E) during heatwaves (2016-17), F) during RSD (2016-17), G) during heatwaves (2015-16), H) during RSD (2015-16)

The UO impact on Indoor temperature: UO significantly influenced indoor temperature during heatwaves, especially in western Sydney in 2016-17. Moreover, during heatwaves, the average hourly indoor thermal contrast in western and inner suburbs compared to Sydney CBD was roughly 2.2°C and 0.8°C in 2016-17, and 0.5°C and 0.1°C in 2015-16 for both settlements, respectively (Figure 8-5). The average hourly indoor thermal contrast for both settlements in western suburbs during RSD (2016-17) was 0.6°C, whereas it was negligible in the former year in western Sydney and both years in inner Sydney. Furthermore, while correlating the hourly UO with hourly indoor temperature (Figures 8-5 E-H), a strong linear positive correlation was documented in western Sydney during heatwaves and RSD (r>0.80) for both years/ settlements. For both years/ settlements in inner Sydney, there was a strong linear positive correlation (r= 0.75 to 0.80) during heatwaves and a moderate linear positive association (r= 0.65 to 0.68) during RSD. Under the UO-heatwaves combined effect, the average indoor temperature differential was similar to that reported during heatwaves (marginally elevated under the combined influence).

8.3.1.3 The impact on passive survivability:

The Outdoor (O) to indoor (I) passive survivability variations: Comparing outdoor to indoor passive survivability (above 32°C), the indoor hours during heatwaves were roughly 1 percent greater than outdoor hours in 2016-17 (relatively lower in the previous year), in both settlements (comparatively higher in the LD settlement) (Figure 8-6).

During RSD, the indoor-outdoor hours above 32°C were nearly identical in both settlements and in all zones. It signifies the increased susceptibility within both residential settlements, particularly during heatwaves. In addition, the indoor-outdoor passive survivability difference rose for lower temperatures brackets (with 26 °C being the highest). It reflects the indoor temperatures being higher than the outdoor temperatures for lower temperature thresholds and the differences between outdoor and indoor temperatures being smaller when exceeding the WHO recommendation. Therefore, the buildings provide almost no/minimal protection for the inhabitants during extreme temperatures.

The heatwaves-RSD passive survivability variations: The passive survivability (above 32°C) worsened by 23 to 25 percent in western Sydney, 16 to 20 percent in inner Sydney, and 8 to 11 percent in Sydney CBD during heatwaves compared to RSD, in both years and for both settlements (Figure 8-6).

The UO Impact on passive survivability: In 2016-17, under the impact of UO, the passive survivability (above 32°C) deteriorated by 18 to 21 percent in western Sydney and 7 to 8 percent in inner Sydney, relative to Sydney CBD, during heatwaves (Figure 8-6). During RSD, the passive survivability (above 32°C) deteriorated by 6 percent in western Sydney and 2 percent in inner Sydney compared to the

Sydney CBD in 2016-17. In 2015-16, comparable patterns were recorded with a somewhat lower proportion.

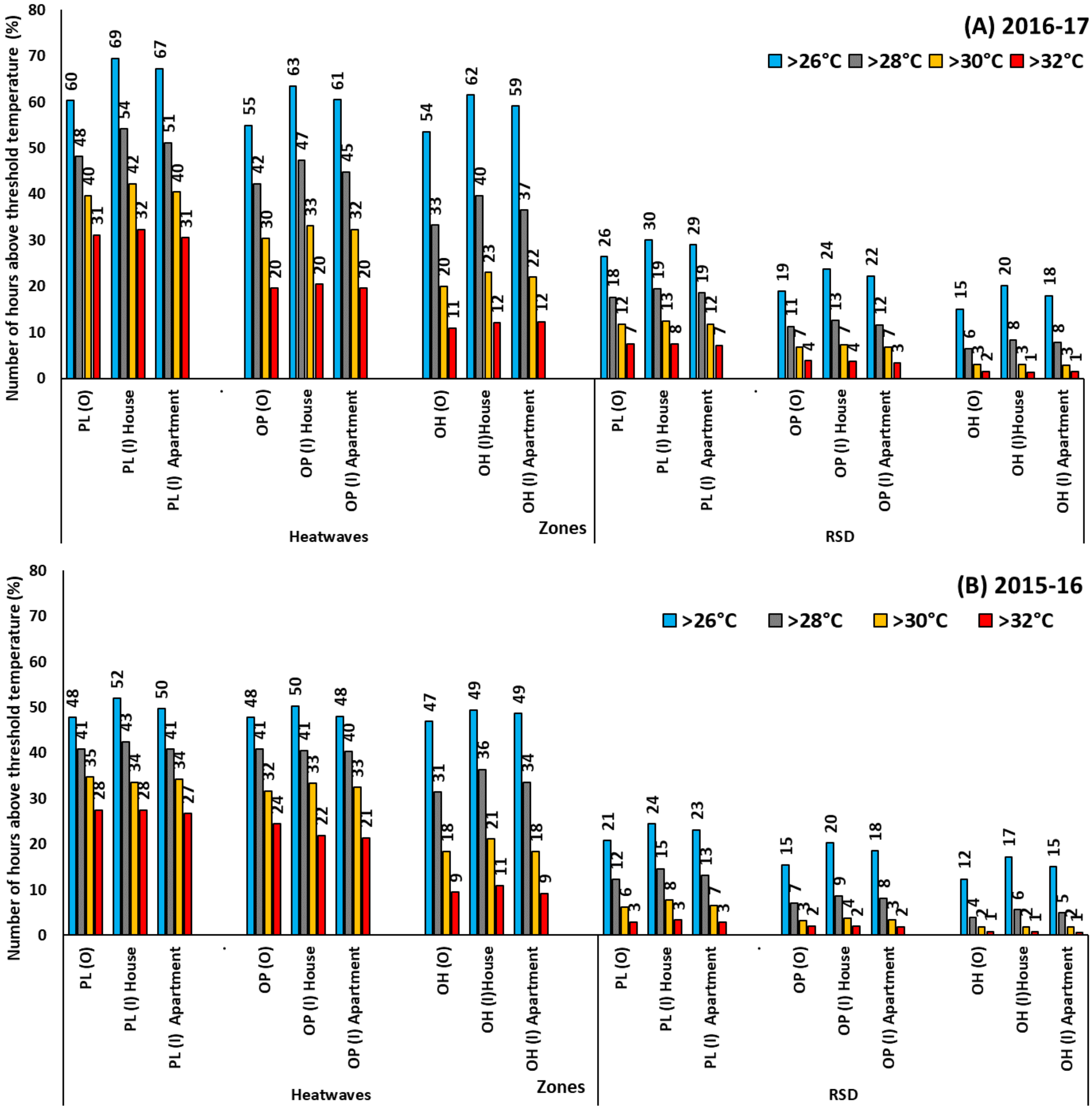

Figure 8-6: Hours above the threshold temperature (outdoor and indoor) (%) in three zones of Sydney (western Sydney: PL, inner Sydney: OP, and Sydney CBD: OH) during heatwaves and RSD for two settlements during 2015-16, and 2016-17, A) during 2016-17, B) during 2015-16.

<u>The HD-LD settlement's passive survivability comparison</u>: During heatwaves, the passive survivability (above 32°C) worsened by approximately 1 to 2 percent in LD settlements than HD in all city zones and during both years (Figure 8-6). During RSD, there was no significant difference.

The combined impact of UO-heatwaves on passive survivability: The passive survivability (above 32°C) deteriorated by 26 to 31 percent in western Sydney and 18 to 21 percent in inner Sydney compared to Sydney CBD (during RSD) under the cumulative effect of UO-heatwaves (Figure 8-6).

8.3.2 Sensitivity analyses:

8.3.2.1 The adaptation (strategies) impact on cooling energy:

Low-density (LD) settlement: During heatwave and RSD, the most effective adaptation strategies for cooling energy savings were changing the cooling setpoints from 25°C to 27°C (M11) and 28°C (M12). M12 lowered the cooling energy needs by 37 percent during heatwaves and 53 percent during RSD, while M11 lowered by 26 percent during heatwaves and 38 percent during RSD (Figure 8-7 A-B and Table 8-1). The second most productive adaptation strategy for houses was an insulated envelope. The greater the thermal insulation (M1 and M2), the greater the cooling savings.

Furthermore, compared to RSD, the insulation was more effective during heatwaves. Additionally, the energy performance was enhanced even more when the insulated envelope was combined with night cooling (M16 and M17). The cooling savings from intermediately insulated to highly insulated envelopes were approximately 28 to 35 percent during heatwaves and around 24 to 26 percent during RSD. The subsequent effective adaptation strategies were envelope airtightness (M9 and M10) and improved glazing (M6 and M7). During heatwaves and RSD, the higher the envelope airtightness, the better the energy performance. Similarly, highly improved glazing (which complied with NCC standards) outperformed intermediately insulated glazing during both heatwaves and RSD. During heatwaves and RSD, the envelope airtightness was responsible for 10 to 20 percent cooling savings (well-sealed to airtight envelope), while improved glazing was accountable for 10 to 17 percent cooling savings (intermediately improved to highly improved glazing).

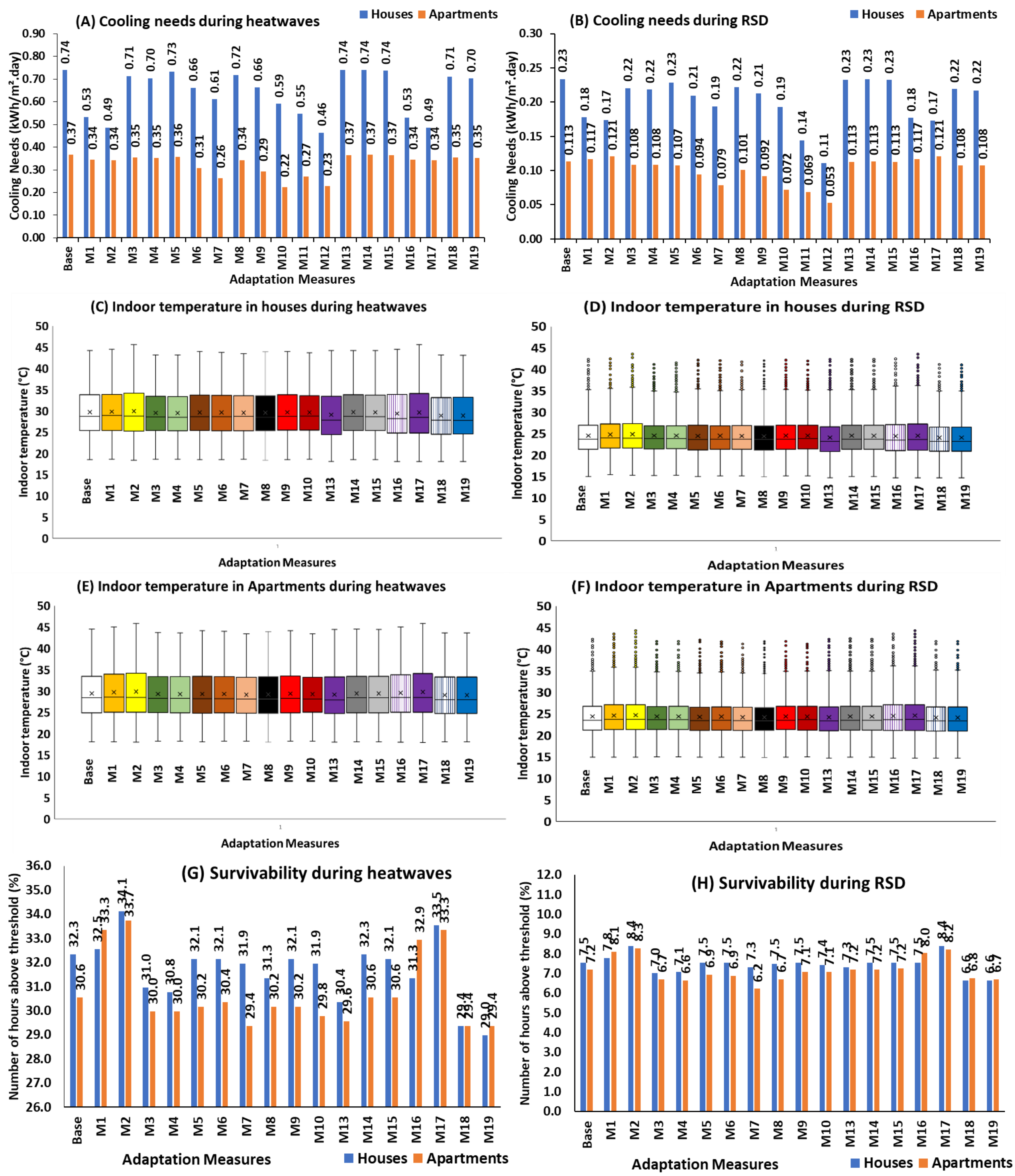

Figure 8-7: Sensitivity analyses- the impact of adaptation strategies on cooling energy, indoor temperature, and passive survivability during heatwaves and RSD for LD (houses) and HD (Apartments) settlements. A) cooling energy during heatwaves, B) cooling energy during RSD, C) Indoor temperature in LD settlement during heatwaves, D) Indoor temperature in LD settlement during RSD, E) Indoor temperature in HD settlement during heatwaves, F) Indoor temperature in HD settlement during RSD, G) Passive survivability during heatwaves, H) Passive survivability during RSD.

Table 8-1: The impact of adaptive measures on energy needs, mean indoor temperature, and passive survivability in LD and HD settlements during heatwaves and RSD.

	Heatwaves						RSD					
	Cooling energy ($kWh/m^2 . d$)		Average Indoor temperature (°C)		Passive survivability (%)		Cooling energy ($kWh/m^2 . d$)		Average Indoor temperature (°C)		Passive survivability (%)	
	LD	HD	LD	HD	LD	HD	LD	HD	LD	HD	LD	HD
Base	0.74	0.37	29.69	29.42	32.34	30.56	0.23	0.113	24.48	24.36	7.55	7.19
M1	0.53	0.34	29.81	29.71	32.54	33.33	0.18	0.117	24.77	24.58	7.79	8.09
M2	0.49	0.34	29.94	29.85	34.13	33.73	0.17	0.121	24.84	24.65	8.39	8.27
M3	0.71	0.35	29.51	29.29	30.95	29.96	0.22	0.108	24.49	24.34	7.00	6.70
M4	0.70	0.35	29.47	29.28	30.75	29.96	0.22	0.108	24.49	24.34	7.07	6.64
M5	0.73	0.36	29.63	29.31	32.14	30.16	0.23	0.107	24.42	24.26	7.55	6.94
M6	0.66	0.31	29.62	29.31	32.14	30.36	0.21	0.094	24.45	24.30	7.55	6.88
M7	0.61	0.26	29.56	29.12	31.94	29.37	0.19	0.079	24.42	24.18	7.31	6.22
M8	0.72	0.34	29.55	29.19	31.35	30.16	0.22	0.101	24.35	24.16	7.49	6.70
M9	0.66	0.29	29.67	29.36	32.14	30.16	0.21	0.092	24.50	24.36	7.55	7.07
M10	0.59	0.22	29.65	29.24	31.94	29.76	0.19	0.072	24.51	24.33	7.43	7.07
M11	0.55	0.27	*	*	*	*	0.14	0.069	*	*	*	*
M12	0.46	0.23	*	*	*	*	0.11	0.053	*	*	*	*
M13	0.74	0.37	29.07	29.14	30.36	29.56	0.23	0.113	24.06	24.15	7.31	7.19
M14	0.74	0.37	29.69	29.42	32.34	30.56	0.23	0.113	24.48	24.36	7.55	7.19
M15	0.74	0.37	29.67	29.41	32.14	30.56	0.23	0.113	24.47	24.36	7.55	7.25
M16	0.53	0.34	29.38	29.57	31.35	32.94	0.18	0.117	24.38	24.45	7.55	8.03
M17	0.49	0.34	29.62	29.76	33.53	33.33	0.17	0.121	24.51	24.56	8.39	8.21
M18	0.71	0.35	28.91	29.04	29.37	29.37	0.22	0.108	24.04	24.10	6.64	6.76
M19	0.70	0.35	28.90	29.04	28.97	29.37	0.22	0.108	24.05	24.11	6.64	6.70

During heatwaves and RSD, increased thermal inertia (M3 and M4) was the next most effective adaptation strategy for cooling savings. The greater the thermal inertia, the superior the thermal performance during heatwaves and RSD. The cooling savings were further boosted during heatwaves and RSD when thermal inertia was combined with night cooling (M18 and M19). Increased thermal inertia resulted in cooling savings of approximately 3.5 to 5 percent during heatwaves and 5.9 to 7 percent during RSD (intermediate thermal inertia to higher thermal inertia). The super cool roof (M8) produced approximately 3 to 5 percent (heatwaves-RSD) cooling savings, while improved blind control (M5) produced 1 to 2 percent (heatwaves-RSD). During heatwaves and RSD, nighttime cooling (M13) had a minor influence on cooling savings (approximately 0.13 percent and 0.30 percent, respectively). When the impact of the microclimatic context on cooling energy was measured, irrigated soil in urban green areas (M15) produced 0.35 to 0.58 percent cooling savings, while the impact of enhanced ground (roads/streets) albedo (M14) was negligible. It's possible that the lesser influence on cooling savings by the irrigated soil and ground albedo was related to simulation at a comparatively smaller scale (neighborhood scale). The cooling savings from M14 and M15 could be improved by examining the model at a district/city scale.

High-density (HD) settlement: Rising the cooling setpoints to 27°C and 28°C resulted in cooling savings of 27 percent and 38 percent during heatwaves, respectively, which further climbed to 39 percent and 53 percent during RSD, similar to LD settlement (Figures 8-7 A-B and Table 8-1). However, the cooling saving potential of the insulated envelope (with or without night cooling) during heatwaves was relatively less in apartments (intermediately insulated envelope= 5.6 percent and highly insulated envelope= 6.5 percent), which converted into a cooling penalty during RSD (intermediately insulated envelope= -3.4 percent, and highly insulated envelope= -7 percent). It's possible that the lower cooling savings of insulated envelopes in apartments are attributable to higher internal loads than in single-story houses. Additionally, lesser cooling benefits during heatwaves and cooling penalties during RSD in HD settlements could be due to lower base-case cooling requirements for HD settlements (almost half of the LD settlements). The second and third most efficient adaptation strategies in HD settlements for cooling savings were envelope airtightness and improved glazing. During heatwaves/ RSD, the cooling energy benefits in apartments were about 20 percent and 38 percent, respectively, from the well-sealed and airtight envelope. Compared to houses, the cooling benefits in apartments nearly doubled from envelope airtightness. Similarly, during heatwaves/RSD, cooling energy benefits from intermediately-improved and highly-improved glazing was approximately 16 percent and 28 percent, respectively, over 1.5 times greater than the LD settlements.

In HD settlements, cooling energy benefits from supercool roofs were approximately 6.5 percent during heatwaves and about 10.5 percent during RSD, almost double what they were in LD settlements. The indirect mitigation benefits of supercool roofs in high-rise buildings -enhanced natural ventilation in addition to lower surface temperature- could account for twofold cooling savings. Another factor contributing to the double cooling savings is that apartments have almost half the cooling needs of homes (base-case). In apartments with or without overnight cooling, the cooling energy benefits from increased thermal inertia were nearly comparable to those in houses. The cooling savings by blind control were approximately 2.7 to 5.2 percent (heatwaves-RSD), nearly twice that of houses. The cooling benefits in apartments were nearly the same as in houses from i) night ventilation, ii) irrigated soil in green areas, and iii) increased ground surface albedo.

8.3.2.2 The adaptation (strategies) impact on indoor thermal comfort and survivability:

Low-density (LD) settlement: During heatwaves and RSD, the most effective adaptation approach for improved IEQ in houses was higher thermal inertia paired with nocturnal cooling (Figures 8-7 C-H and Table 8-1). Due to intermediate (M18) and higher thermal mass (M19) coupled with nocturnal cooling, the average indoor temperature drops of 0.79°C and 0.45°C were documented during heatwaves and RSD, respectively. Furthermore, the passive survivability (above 32°C henceforth) was bettered by approximately 3 percent (32.5 to 29.37 percent) and 3.4 percent (32.5 to 28.97 percent) during heatwaves from M18 and M19, respectively, and by approximately 1 percent (7.6 percent to 6.6 percent) during RSD. The drop in average indoor temperature from increased thermal mass without nocturnal cooling (M3 and M4) was approximately 0.17 to 0.2°C during heatwaves, with no significant changes observed during RSD. When compared to M18 and M19, the impact of M3 and M4 on passive survivability was approximately half. The third most effective adaptation strategy in improving the IEQ was night cooling (M13), with an average drop in the indoor temperature of 0.61°C during heatwaves and 0.42°C during RSD. Additionally, M13 enhanced passive survivability by approximately 2 percent (32.5 to 30.4 percent) during heatwaves and about 0.24 percent (7.5 to 7.26 percent) during RSD.

IEQ was also improved with an intermediately insulated envelope paired with nocturnal cooling (M16), with average indoor temperature reductions of approximately 0.3°C during heatwaves and 0.10°C during RSD. Furthermore, M16-led passive survivability was enhanced by about 1 percent during heatwaves and a minor improvement during RSD. The intermediately insulated envelope (M1) and the highly insulated envelope (M2) performed inadequately without nocturnal cooling, with a 0.12°C and 0.25°C rise in average indoor temperature during heatwaves attributable to both measures, compared to a 0.30°C gain during RSD. Furthermore, passive survivability declined by 0.25 percent due to M1 during heatwaves and RSD, respectively, and 0.8 to 1.8 percent (RSD-heatwaves) due to M2. Even when paired with nocturnal cooling (M17), the highly insulated envelope failed to provide adequate indoor comfort, increasing the average indoor temperature during RSD, whereas the effect was negligible during heatwaves. Furthermore, a 1 to 1.2 percent decline in passive survivability was observed during heatwaves and RSD with M17.

During heatwaves and RSD, the supercool roof (M8) lowered the average indoor temperature by approximately 0.15°C and enhanced passive survivability by 1 percent. Indoor comfort was slightly improved during heatwaves from improved glazing (M6 and M7) and envelope airtightness (M9 and M10); however, the impact was insignificant during RSD. The highly improved glazing (M7) functioned better during both heatwaves and RSD than intermediately improved glazing (M6). Similarly, during heatwaves and RSD, the airtight envelope (M10) outperformed the well-sealed envelope (M9). The thermal comfort was also slightly enhanced by the blind control (M5) and irrigated soil in green areas (M15) (Table 8-1).

<u>High-density (HD) settlement</u>: During both heatwaves and RSD, the improved thermal mass paired with nocturnal cooling (M18 and M19) proved to be the most effective adaptation strategy in improving IEQ in the apartments, similar to LD settlement (Figure 8-7 C-H and Table 8-1). M18 and M19 yielded a 0.38°C decline in average indoor temperature during heatwaves and a 0.25°C drop during RSD. In addition, there was a 1 percent enhancement in passive survivability during heatwaves and half of it during RSD. Even though thermal inertia was three times less effective without nocturnal cooling, it still performed better than the base-case. The third most effective strategy was highly improved glazing (M7), lowering the average indoor temperature by 0.30°C during heatwaves and more than half of it during RSD. The passive survivability was enhanced by more than 1 percent during heatwaves and RSD.

Intermediately improved glazing (M6) was three times less beneficial during heatwaves and RSD than highly insulated glazing (M7). The next most effective strategy was nocturnal cooling (M13), which lowered the average indoor temperature by 0.25 to 0.30°C (RSD-heatwaves) and enhanced the passive survivability by 1 percent. The supercool roof (M8) declined the average indoor temperature from 0.20 to 0.23°C (RSD-heatwaves) and enhanced the passive survivability by 0.5 percent.

The airtight envelope (M10) lowered the average indoor temperature by 0.17°C during heatwaves and enhanced passive survivability by 0.80 percent. During heatwaves, the airtight envelope (M10) was more than twice as effective as the well-sealed (M9) envelope. During RSD, the envelope airtightness impact on IEQ was negligible. The blind control (M5) lowered the average indoor temperature by 0.1 to 0.15°C and enhanced passive survivability by 0.3 to 0.4 percent during both heatwaves and RSD. The insulated envelope was the least productive strategy, with or without nocturnal cooling. The intermediately insulated envelop (M1) and highly insulated envelop (M2) in the absence of nocturnal cooling raised the average indoor temperature by 0.29°C and 0.45°C during heatwaves, respectively, and by 0.2°C and 0.3°C during RSD. An average of 3 percent deterioration of the passive survivability during heatwaves and approximately 1 percent during RSD (more worsened from the highly insulated envelope) were recorded. The insulation paired with nocturnal cooling somewhat enhanced IEQ, but it was still less efficient than the base-case. The average indoor temperature of the intermediately insulated envelope coupled with nocturnal cooling (M16) was nearly similar to the base-case; nevertheless, the passive survivability deteriorated by more than 2 percent during heatwaves and approximately 0.8 percent during RSD. The average indoor temperature due to the highly insulated envelope coupled with nocturnal cooling (M17) was 0.2 to 0.34°C (RSD-heatwaves) greater, while passive survivability was over 1 to 2.5 percent (RSD-heatwaves) deteriorated than base-case.

Considering the sensitivity assessment and cooling energy and indoor comfort trade-off, the intermediately insulated envelope with nighttime cooling (M16), airtight envelope (M10), highly improved glazing (M7), 28°C cooling setpoints (M12), supercool roof (M8), improved blind control (M5), and irrigated soil in green areas (M15) were chosen for further simulation in three Sydney zones.

8.3.3 The cumulative impact of selected adaptive strategies:

8.3.3.1 The cooling energy response to combined strategies:

The cumulative effect of selected adaptation solutions yielded substantial cooling savings during heatwaves and RSD in both settlements and all zones (Figure 8-8A). During RSD, cooling savings were relatively greater (daily cooling requirements approaching zero) than during heatwaves. The effect was more pronounced in coastal districts and HD settlements than in inland locations and LD settlements. The neighborhood-scale interventions, such as supercool roofs, irrigated soil in green areas, and increased ground surface albedo, can promote the region's natural ventilation, allowing coastal winds to infiltrate inland locations. Improved natural ventilation may explain the greater cooling savings in high-rise buildings during heatwaves and RSD than in houses. The cooling energy savings ranged from 87 to 91 percent (western to eastern Sydney) in LD settlements and 94 to 97 percent in HD settlements during heatwaves, rising to 92 to 96 percent in LD settlements and 97 to 99.5 percent in HD settlements during RSD.

8.3.3.2 The indoor temperature response to combined strategies:

The cumulative effect of selected adaptation strategies during heatwaves and RSD also resulted in a significant drop in average indoor temperature for both settlements in all zones (Figures 8-8 B and C). The decline in average indoor temperature was more noticeable in inland locations and during heatwaves than in coastal districts or during RSD. It might be linked to higher average indoor temperatures for base-cases at inland locations/ during heatwaves, which were greatly decreased as a result of the adaptive measures and had a larger impact. Furthermore, compared to LD settlements, the drop in average indoor temperature was more noticeable in HD settlements during both heatwaves and RSD. During heatwaves, the average fall in indoor temperature was 0.74 to 1.6°C (eastern to western Sydney) in LD settlements and 1.35 to 2.34°C in HD settlements, whereas it was roughly 0.41 to 0.71°C in LD settlements and 0.71 to 1.26°C in HD settlements during RSD.

8.3.3.3 The passive survivability response to combined strategies:

The improvement in passive survivability was more pronounced at inland locations and during heatwaves, similar to indoor temperature (Figure 8-8D). During heatwaves, the passive survivability was enhanced by 7 to 10 percent (eastern to Western Sydney) in LD settlements and 12 to 20 percent in HD settlements, under the combined impact of adaptive strategies. During RSD, the passive survivability improved by 1 to 4 percent in LD settlements and 1.5 to 6 percent in HD settlements. During heatwaves, the number of hours that remained over threshold temperature (32°C) following the implementation of adaptation strategies in the HD settlements was 0 to 10 percent of total hours (eastern to western Sydney) and lower than 1 percent during RSD. The number of hours over the threshold temperature in LD settlements following adaptation strategies was 5 to 22 percent (eastern to western Sydney) of total hours during heatwaves and fewer than 3 percent during RSD. Mitigation strategies such as irrigated soil in green areas, supercool roofs, and increased ground albedo on a broader scale could help to improve thermal comfort even further.

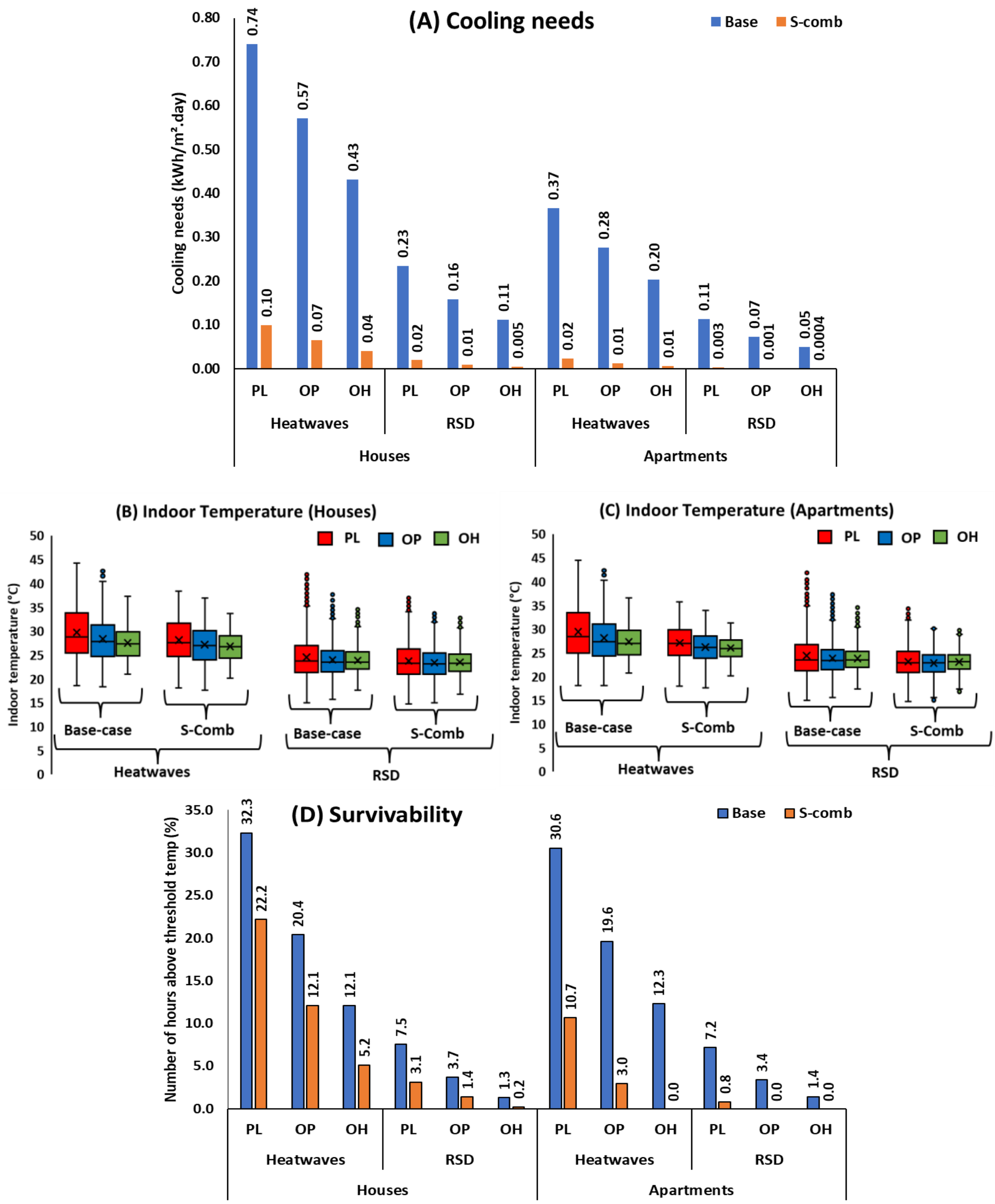

Figure 8-8: The cumulative impact of selected adaptation strategies during heatwaves and RSD, A) On cooling needs in houses and apartments, B) On indoor temperature in houses, C) On indoor temperature in apartments, D) On passive survivability in houses and apartments.

8.4 Discussion:

The cumulative impact of multilevel climatic conditions (local, regional, and global) on the built environment and human health is a global problem. The cooling penalties generated by the combined effect of UO-heatwaves, heatwaves, and UO were observed at up to 650 percent, 350 percent, and 130 percent, respectively, while exploring the impact of such local and regional climatic conditions on urban energy performance in the temperate climate of Sydney. Under the combined effect of UO-heatwaves, heatwaves, and UO, the average indoor temperature rose to 5.8°C, 5.0°C, and 2.2°C, respectively, while passive survivability worsened by up to 31 percent, 25 percent, and 20 percent. These findings are comparable with prior research [91,208,286], which revealed a rise in cooling demand and a decline in IEQ due to the combined effect of UO-HWs, albeit on a much smaller scale than the present study. The cooling penalties generated under the combined effect of UO-heatwaves, for example, were up to 196 percent in Rome, Italy, and the operative temperature rose up to 5°C [91]. The opposing large-scale weather systems – available on opposite ends of the city, which strengthen during intense heat spells– can be accountable for the unusually high cooling needs and worsening IEQ in the current study. Furthermore, earlier research were performed on a building scale, with the microclimatic context being ignored as a limitation. In San Francisco, when the building thermal performance was simulated with microclimatic settings, a considerable rise in cooling needs and indoor temperature was seen [6].

Due to the inter-building shading effect, the HD settlement (Apartment) fared better than the LD settlement (houses) in terms of cooling demand and IEQ during both heatwaves and RSD. These findings are consistent with a study conducted in Qianjiang Newtown, China, which concluded that an enclosed/ semi-enclosed building layout was more advantageous for energy and IEQ than large open block settings [187]. Nevertheless, the tall structures in coastal districts will not only prevent coastal breezes from reaching inland locations but will also put residents of tall buildings (at inlands) at greater risk of heat stress due to increased exposure to continental winds during excessive heat. Therefore, to make the city thermally resilient, the impact of a large-scale dualistic system on urban energy performance should also be considered in urban planning. The current study identified an upward trend in cooling needs and a decline in IEQ during heatwaves and RSD while examining the temporal fluctuations in urban energy performance. These patterns are similar to prior research that indicated that climate change would increase cooling demand, reduce heating needs, and degrade IEQ [20,176,210,212].

Buildings are generally thought to shelter residents from extreme weather; nevertheless, Sydney's existing housing stock failed, and indoor temperatures during heatwaves were greater than outdoor temperatures, especially in western suburbs. Furthermore, most Sydney residential buildings lack air conditioning units, and affordability is also a major concern in the western suburbs, which are more vulnerable to overheating and excessive heat. Heat-responsive/ resilient buildings may withstand prolonged periods of hot weather without mechanical ventilation; therefore, this study explored several adaptation strategies during heatwave and RSD.

Contrary to previous studies in which the insulated envelope was predominantly connected with the possibility of overheating [93,201,202], the intermediately insulated envelope paired with nocturnal cooling outperformed the uninsulated envelope in terms of both cooling energy and IEQ during both heatwaves and RSD in both settlements. In several studies, the insulated envelope was also linked to higher cooling needs in residential units during heatwaves in addition to overheating risk [92]. For instance, the insulated envelope was accountable for both a rise in cooling energy and a decline in IEQ in office buildings owing to their higher internal loads [20,39]. Nevertheless, in the current study, the intermediately insulated envelope performed better even in HD settlements when paired with nocturnal cooling, despite having higher internal loads. In addition to different climatic conditions, those studies were limited by omitting natural ventilation when evaluating the thermal performance of insulated envelopes. Furthermore, rather than evaluating the optimal insulation level during heatwaves, the hyper-insulated envelope was primarily compared against the uninsulated envelope, yielding contrasting results. For example, existing buildings (uninsulated) performed better in terms of IEQ during heatwaves than highly insulated star-rated buildings in Adeliade [202] and Melbourne [93]. Contrarily, in another study in Melbourne, a 5.4 star-rated intermediately insulated building performed better than the existing buildings during heatwaves [94]. In the current study, although the highly insulated envelope's energy performance was better than the intermediately insulated envelope (especially in LD settlement) during heatwaves, the passive survivability was declined. These findings are in line with literature in which the highly insulated envelope was reported to promote overheating during summer and heatwaves, as previously discussed. Moreover, in the current study, the highly insulated envelope was designed according to NCC DTS guidelines, implying that NCC-DTS standards do not mitigate the buildings' overheating issues. To summarize, an optimal level of insulation in a building envelope acts as a thermal barrier and offers more protection during heatwaves as compared to an uninsulated envelope, as well as being a trade-off between cooling needs and IEQ.

Higher thermal inertia combined with nocturnal cooling was found to be the most suitable choice in terms of IEQ during both heatwaves and RSD in the current study. These findings are in line with those of other studies conducted in Australia [207], Poland [213], and Spain [205], all of which found that higher thermal inertia enhanced building thermal performance during heatwaves. However, increasing thermal inertia was counterproductive at night during heatwaves in another study in Sydney [202], which could be ascribed to disregarding natural ventilation. Several buildings in Sydney are just metal clad, putting residents at greater risk of heat stress during heatwaves owing to lower thermal inertia. The literature has observed overheating, usually due to highly glazed windows and an airtight envelope, especially during heatwaves [93,287,288]. Unlike prior research, the airtight envelope (PH standard) and highly improved glazing (double-glazed according to NCC requirements) outperformed the leaky/well-sealed envelope and single-glazed/intermediately improved glazing. The highly Improved glazing and airtight envelope limit the daytime solar gain during extreme heat conditions, while nocturnal ventilation can alleviate overnight overheating problems. Nocturnal cooling was aided by rapid radiative cooling in Sydney suburbs (owing to a higher proportion of non-urban surfaces) and changes in the wind pattern at night during heatwaves, as documented in chapter 7. Otherwise, the airtight envelope would produce nocturnal overheating, as it did in Houston/ Phoenix-USA [204]. Furthermore, as several studies [274,276,277] have demonstrated, Sydney's housing stock is particularly leaky, making residents more exposed during heatwaves.

The supercool roofs may alter the urban heat fluxes and, subsequently, the building's energy balance and IEQ. In the current research, the supercool roof led to a considerable reduction in cooling energy and an improvement in IEQ during both heatwaves and RSD and in both settlements. These findings are consistent with the research conducted in several US cities [273]; nonetheless, the maintenance, aging, and glaring issues may require further consideration. During both heatwaves and RSD, maintaining the cooling setpoint at 28°C was the most successful adaptation approach for cooling energy benefits (38 to 55 percent) in the current dissertation. These findings align with a study conducted in Paris, France, which found that changing the cooling setpoint to 28°C resulted in a 43 percent cooling savings during heatwaves [206]. Furthermore, keeping the cooling setpoints at a higher degree during excessive heat will lower anthropogenic heat and outside temperature, resulting in improved IEQ. In the current study, enhancing green surface evaporation/evapotranspiration and ground albedo had a small but positive impact on urban energy needs and IEQ. Changing the model scale from neighborhood to district/city could boost the cooling advantages of these strategies while also increasing passive survivability.

8.5 Limitations:

The deployment of PDRC may counteract the building's peak cooling demand during excessive heat events by keeping the roof surface temperature under the ambient temperature. However, PDRC may incur heating costs throughout the winter due to the loss of the standard roof's passive advantages.

Since the study's primary focus was on the urban energy performance during intense heat occurrences, PDRC-induced heating penalties should also be explored.

8.6 Conclusion and recommendation:

Maintaining IEQ during heatwaves (without mechanical cooling) and reducing energy demand from buildings to mitigate the effects of climate change are urgent concerns. The synergistic impact of multilevel climatic conditions (local, regional, and global) on urban energy performance and IEQ were examined using the UBEM for two residential settlements in Sydney. Depending on location (coastal distance) and settlement type, the cooling penalty generated by the combined effect of UO-heatwaves varied between 400 and 650 percent. Similarly, under the synergistic influence of UO-heatwaves, the average indoor temperature rose between 3.2°C and 5.8°C, and passive survivability declined between 18 and 31 percent. The dualistic large-scale weather system, which becomes more intense during heatwaves, was the most critical driver in increasing cooling penalty and deteriorating IEQ. The adaptive strategies, namely, i) an optimally insulated envelope paired with nocturnal ventilation, ii) an airtight envelope (PH standards), iii) highly insulated windows (NCC standards), iv) enhanced natural ventilation using an optimum design concept-open floor plan, adequate cross ventilation, v) supercool roofs that alleviate urban heat, minimize building thermal gain, and improve regional ventilation, vi) optimal blinds operation during heatwaves, vii) behavioral modification and keeping the cooling setpoint at 28°C, especially during heatwaves, viii) increased green surfaces evaporation/evapotranspiration, and ix) enhanced ground surface albedo were the most appropriate strategies.

The sensitivity analyses determined that higher cooling setpoints were the most appropriate solutions for cooling savings during heatwaves and RSD. The cooling savings were up to 53 percent from changing the cooling setpoint from 25 to 28°C, comparatively higher during RSD than during heatwaves. The intermediately insulated envelope coupled with nocturnal cooling, an airtight envelope (PH standards), and highly insulated glazing (NCC standard) were documented as an optimal solution for both cooling energy savings and IEQ, especially in single-story houses. The supercool roof resulted in 3 to 10.5 percent cooling energy savings and also adequately improved the IEQ. In terms of IEQ, higher thermal inertia combined with nocturnal cooling was determined to be the most efficient strategy during heatwaves and RSD. The cumulative impact of selected adaptation strategies resulted in cooling savings of 87 to 97 percent during heatwaves and 91 to 99 percent during RSD. Similarly, the average indoor temperature declined from 0.74 to 2.34°C, and passive survivability was enhanced by 10 to 20 percent during heatwaves under the cumulative effect of adaptation strategies. The following recommendations were made based on the literature and findings of this study.

- Extreme weather and heatwaves are becoming the norm, and cities should be planned accordingly. Further, while assessing the building's environmental performance, the seasonal thermal performance should be determined instead of the annual performance to evaluate the influence of intense heat occurrences accurately. The adaptive solutions should be chosen to maintain a balance between energy savings and IEQ.
- The evaluation of building performance should avoid using TMY data, which does not reflect the local urban features. In cities such as Sydney, where the local, regional, and global climatic impacts are influential, the microclimatic context and thermal resilient planning should be made part of construction codes. It will limit the vulnerability and aid in correctly designing systems (grid capacity, HVAC system, etc.) based on peak loads.
- Current national construction standards may increase dependency on air conditioning to provide an ideal thermal comfort during summer and heatwaves, aggravating the UO intensity and heatwaves severity. Instead, a suitable combination of adaptation and mitigation strategies should be proposed and incorporated into the NCC's elemental provision to i) lower the outdoor temperature, ii) reduce the air conditioning reliance, iii) lower energy needs and GHG emissions, and iv) improve IEQ. The suitability of star-rated NatHERS buildings [243] or Australian passive house (PH) standards [289], which recommends the use of highly insulated envelopes with perfect airtightness, should be reconsidered in light of overheating concerns and the possibility of power outages in the coming years during intense heat occurrences.
- Instead of focusing on the thermal performance of individual buildings, it's critical to consider the entire microclimatic context when calculating energy needs and assessing IEQ. As a result, the effects of appropriate mitigation and adaptation measures should be evaluated and included in construction standards.

CHAPTER 9: CONCLUSION

9.1 Contribution to knowledge and main research work:

The global temperature is rising rapidly. The frequency and intensity of heatwaves have grown in the twenty-first century and are likely to increase further. UO is one of the well-documented climate change phenomena, affecting more than 400 cities. Rapid urbanization may alter the surface's sensible, latent, radiative, and dynamic response and influence local, regional, and global climate conditions. UO, heatwaves, and large-scale weather patterns may synergize and devastatingly impact the populations. Such multidimensional climate interactions have never been investigated. This dissertation examined the synergy between local, regional, and global climate conditions and their effects on the built environment. The research involved three major phases. Initially, the synergies between UO and large-scale weather patterns, particularly during heatwaves, were investigated. The second phase explored how UO interacts with regional-scale heatwaves and what are the primary contributors exacerbating UO. Lastly, the cumulative effect of local, regional, and global climatic changes on the built environment was evaluated. Table 9-1 presents the problem statements and research objective outlined in chapter 1 (section 1.3), with the related chapter and section numbers, where those research questions have been addressed.

This chapter has been arranged into four main sections. Section 9.2 provides the summary of interactions between UO and large-scale weather patterns. In section 9.3, the main findings of synergies between UO and heatwaves have been discussed. Section 9.4 summarizes the findings of the combined impact of climate changes on the built environment. The last section (9.5) entails the limitations and potential direction for the future.

Table 9-1: The problem statements and research objectives outlined in chapter 1:

Problem statements/ Research objectives	Related chapter	Related section
Problem statement-1: How does the local-scale UO interact with large-scale weather patterns and affect the communities? The main objectives while addressing the problem were:		
9.1 To investigate the variations in large-scale weather patterns over the year and comprehend which weather patterns have occurred more frequently.	Chapter 5	5.3.1
9.2 To evaluate the spatiotemporal variations in UO magnitude (variations in UO magnitude over the year, seasonal variations, and variations at multiple locations within the city).	Chapter 5	5.3.2 and 5.3.3
9.3 To comprehend the impact of various air masses according to their geographical characteristics.	Chapter 5	5.3.4
9.4 To investigate the association between UO and large-scale weather patterns:	-	-
9.4.1. To investigate the weather patterns causing the maximum 5 percent of UO magnitude over the years (for more than 15 years).	Chapter 5	5.3.4
9.4.2. To investigate the weather patterns causing the minimum 5 percent of UO magnitude over the years.	Chapter 5	5.3.4
9.4.3. To investigate the association between seasonal variations in UO magnitude and large-scale weather patterns.	Chapter 5	5.3.6
9.4.4. To investigate the association between diurnal variations in UO magnitude and large-scale weather patterns.	Chapter 5	5.3.5
9.4.5. To investigate the association between UO magnitude during heatwaves and large-scale weather patterns.	Chapter 5	5.3.7

Problem statement-2: How does local-scale UO interact with regional-scale heatwaves and affect the communities? The main objectives while addressing the problem were:		
9.5 To investigate the variation in UO magnitude during heatwaves, compared to the background conditions, and examine if synergies exist between both phenomena (positive, negative, or no change).	Chapters 6 and 7.	6.3, 7.3, 7.3.2
9.6 To investigate the key contributor affecting UO magnitude during heatwaves by utilizing the surface energy budget.	-	-
9.6.1. To analyze the impact of convective phenomena (sensible, latent heat fluxes) on UO during heatwaves compared to background conditions.	Chapters 6 and 7.	6.3.1.1, 6.3.2, 7.3.1, 7.3.3, 7.3.6
9.6.2. To analyze the impact of advection on UO during heatwaves compared to background conditions.	Chapters 6 and 7.	6.3.1.2, 6.3.2, 7.3.4, 7.3.5, 7.3.6
9.6.3. To analyze the impact of land-coastal distance on UO during heatwaves, compared to background conditions.	Chapters 6 and 7.	7.3.5, 7.3.6
9.6.4. To analyze the impact of site characteristics (potentially plantable surfaces, tree canopy cover, etc) on UO during heatwaves, compared to background conditions.	Chapters 6 and 7.	7.3.7
9.6.5. To analyze the impact of Population density on UO during heatwaves, compared to background conditions.	Chapters 6 and 7.	7.3.7
Problem statement-3: How does the built environment respond to the combined impact of local, regional, and global climatic changes? The main objectives while addressing the problem were:		
9.7 To investigate the impact of local-scale UO on urban cooling energy, indoor temperatures, and passive survivability.	Chapter 8	8.3.1.1 (energy), 8.3.1.2 (indoor temperature), 8.3.1.3 (survivability)

9.8 To investigate the impact of regional-scale heatwaves on urban cooling energy, indoor temperatures, and passive survivability.	Chapter 8	8.3.1.1 (energy), 8.3.1.2 (indoor temperature), 8.3.1.3 (survivability)
9.9 To investigate the synergistic impact of UO, heatwaves, and large-scale weather patterns on urban cooling energy, indoor temperatures, and passive survivability.	Chapter 8	8.3.1.1 (energy), 8.3.1.2 (indoor temperature), 8.3.1.3 (survivability)
9.10 To investigate the impact of urban density on urban cooling energy, indoor temperatures, and passive survivability under the influence of climate changes.	Chapter 8	8.3.1.1 (energy), 8.3.1.2 (indoor temperature), 8.3.1.3 (survivability)
9.11 To investigate the spatiotemporal variations in urban cooling energy needs, indoor temperatures, and passive survivability under the influence of climate changes.	Chapter 8	8.3.1.1 (energy), 8.3.1.2 (indoor temperature), 8.3.1.3 (survivability)
9.12 To investigate the impact of various adaptation measures under the influence of climate change.	Chapter 8	8.3.2, 8.3.3
9.13 To investigate the appropriateness of national construction codes (NCC) and examine how NCC thermally regulated buildings perform under the combined impact of climate change.	Chapter 8	8.3.2, 8.3.3

9.2 Interaction between UO and large-scale weather patterns in Sydney:

The synergies between UO and large-scale weather patterns have never been investigated, particularly during heatwaves. Using the GWTC to examine the frequency of weather patterns in Sydney over the past few years (1999 to 2017), it was determined that the frequency of warmer weather patterns has increased (dry-warm: 7 to 11 percent, warm: 14 to 19 percent, and humid-warm: 7 to 11 percent), while the frequency of humid (12 to 8 percent), seasonal (32 to 28 percent), dry-cool (5 to 1 percent), and cool (10 to 4 percent) has declined. After 2009, an increase in daytime UO intensity (average daily max and hourly) and a decline in nighttime UO intensity (average daily min and hourly) were documented. Similarly, an increase in summer daily maximum UO and a decline in winter daily maximum UO were recorded over time. Further, the daytime UO was positive in all three zones of Sydney more than half of the time from 1999 to 2017, whereas nighttime UO was negative 90 percent of the time. During heatwaves and extreme UO occurrences, humid-warm (HW), warm (W), and humid (H) weather patterns had a greater influence and were reported to occur more frequently. During heatwaves, humid-warm (HW) and warm (W) weather patterns happened for over 76 percent of the instances, followed by dry-warm (12 percent) and humid (6 percent) patterns. In western Sydney, humid-warm (HW) and humid (H) patterns, while the warm (W) patterns in inner Sydney were comparatively more aggressive. Nocturnal negative UO (UC) was predominantly detected under dry-warm (DW), warm (W), and dry (D) patterns.

The humid-warm (HW) patterns in the region were linked to tropical maritime Tasman airmasses (warm, moist, and unstable), whilst dry-warm (DW) and warm (W) patterns were related to tropical continental airmasses (hot, dry, and unstable), emerge from central Australia. A temperate marine weather system was associated with the region's humid (H) weather conditions. The humid-warm (HW)/ humid (H) and warm (W) weather patterns depict the dualistic large-scale weather system available on the opposing ends of the city. Daytime humid-warm (HW) and humid (H) patterns were more aggressive in western Sydney because they lowered evaporation/ evapotranspiration potential, partitioned more available energy into sensible heat, and raised air temperatures. The humid (H) patterns also amplified the daytime temperature in the suburbs through adiabatic warming while descending leeward from blue mountains in the west. Coastal winds under humid-warm (HW) and humid (H) patterns, on the other hand, kept the temperature in Sydney CBD stable while magnifying the UO. Due to the lower proportion of non-urban surfaces, warm (W) patterns were somewhat more dominating (than humid-warm/ humid) in inner Sydney. Therefore, the advection of tropical continental winds rendered inner Sydney more susceptible. The average daily max UO during extreme UO cases was 8 to 10.5°C (max: 13 to 17°C) in western Sydney and 5 to 6.5°C (max: 10 to 12 °C) in inner Sydney under aggressive weather patterns (humid-warm, and warm). The amplified daytime UO during summer, autumn, spring, and winter was also linked with humid-warm (HW) and warm (W) weather patterns.

Nocturnal dry-warm (DW) patterns were more impactful and accountable for UC. The dry-warm (DW) and dry (D) patterns are linked with calm wind and clear sky conditions. The radiative cooling became more pronounced in the suburbs, notably in western Sydney, under clear and calm climatic conditions at night. In contrast, comparatively raised nighttime temperatures in Sydney's city center were linked to nightly longwave emissions from daytime heat storage, resulting in UC. The average daily minimum

UC during extreme UC cases was -7.5 to -10 °C (min: -11 to -14.5°C) in western Sydney and -6 to -7.5°C (min: -9.5 to -11 °C) in inner Sydney under prevailing patterns (dry-warm and warm).

9.3 Interaction between UO and heatwaves in Sydney:

Daytime UO intensification [66], nighttime UO amplification [62], UO aggravation during both daytime and nighttime [154], no variation in UO intensity [122], and a declined UO [56] were concluded in the literature as inconsistent responses of UO to heatwaves. Similarly, urban-rural moisture contrast in daytime and heat storage at night was the major interactions between UO and heatwaves in addition to anthropogenic heat.

While examining the interactions between UO and heatwaves in Sydney, higher threshold temperatures (for heatwaves) were detected for western Sydney suburbs. The threshold temperature reduced from the inland to the coastal side of the city. In recent years, the heatwave frequency and severity have increased in Sydney, particularly after 2015. During 2015, 2016, and 2017, the peak average heatwave-background UO difference (ΔUO) was approximately 4.5°C in western Sydney and 3.8 °C in inner Sydney. Further, it was noticed that the ΔUO had increased successively (annually) after 2015, notably in western Sydney. In 2017, the ΔUO in western Sydney was around 8 °C, whereas it was 4 to 4.5 °C in inner Sydney. However, nighttime temperatures decreased in the suburbs during heatwaves, and the nocturnal UO intensity was either negative/ insignificant. On absolute humidity (AH) evaluation during heatwaves, western Sydney was noticed region's most impacted zone. AH declined during the heatwave day and rose in the afternoon. As heatwave days progressed, daytime AH fell by 20 to 55 percent in western Sydney, 15 to 35 percent in inner Sydney, and 10 to 25 percent in eastern Sydney. In contrast, nocturnal AH was sustained and consistent with site features. It was also determined that the moisture contrast (suburban-Sydney CBD) was inversely related to UO during heatwaves and backgrounds.

After examining the wind pattern, it was underscored that opposing advective fluxes influenced Sydney during daytime heatwaves (Figure 9-1). Western Sydney was mainly affected by continental winds originating from the continental side of the city, which increased temperatures in western Sydney and infrequently affected the inner Sydney during heatwaves. In contrast, the Sydney CBD was influenced by coastal breezes during heatwaves. Desert winds aggravated the temperatures in western Sydney due to warm-air advection, and when they blew at a faster speed, they swept away the ambient moisture. As a result, daytime AH declined in the suburbs during heatwaves, notably in western Sydney. In contrast, daytime coastal winds in Sydney's CBD sustained the temperature/ AH owing to the steady sea breeze. Western Sydney was influenced by continental winds 70 to 80 percent of the time during heatwaves, whereas inner Sydney was influenced by 54 percent. During backgrounds, the continental winds influenced western Sydney 20-35 percent of the time, while inner Sydney was affected around 10 to 15 percent of the time. In conclusion, during heatwaves, amplified daytime UO in Sydney was caused by two opposing heating and cooling advective processes, which also regulated the sensible and latent heat fluxes.

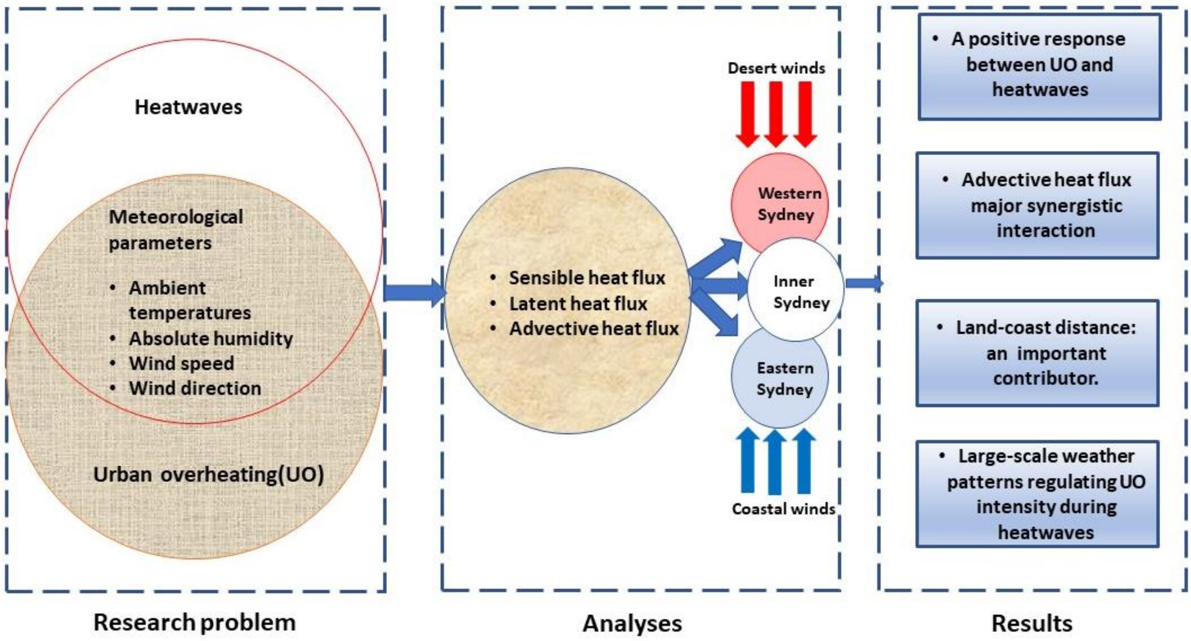

Figure 9-1: Synergies between UO and heatwaves in Sydney.

Contrarily, advection was ineffective at night due to the low wind speed. Instead, due to their larger fraction of non-urban surfaces, western Sydney and inner Sydney rapidly cooled at night, attributed to radiative cooling. In Sydney CBD, the nighttime temperatures were either slightly higher due to surface heat storage or almost the same as in the suburbs due to advection from coastal breezes. A holistic evaluation of all meteorological variables determined that the land-coast distance was the key contributor to enhanced daytime UO intensity in Sydney during heatwaves. It was concluded because continental winds became more dominant as the distance from the coast increased, despite the lower population density and a higher proportion of non-urban surfaces and tree canopy cover at inland locations.

Furthermore, more urbanized surfaces in western Sydney were determined to make the region more susceptible. The altered land-atmospheric moisture exchange would increase the frequency/ severity of heatwaves. It would further restrict coastal wind penetration in inland suburbs as continental winds become more prevalent.

9.4 The cumulative impact of climate changes on the built environment:

Buildings' thermal performance under the combined impact of local, regional, and global climatic changes has never been studied. Further, the microclimatic impact was largely disregarded while investigating the building thermal performance under the impact of climatic changes. This dissertation evaluated the urban energy performance and IEQ under the combined effect of UO, heatwaves, and large-scale weather patterns using the UBEM (Figure 9-2). Overall, a rise in cooling energy needs and a decline in IEQ were documented over time, especially during intense heat occurrences. The cooling energy hiked up to 130 percent, 350 percent, and 650 percent under UO, heatwaves, and the UO-heatwaves cumulative effect. The average indoor temperature rose by 2.2^{o}C, 5.0^{o}C, and 5.8^{o}C under UO, heatwaves, and UO-heatwaves cumulative effect. The passive survivability declined by 20 percent, 25 percent, and 31 percent under the impact of UO, heatwaves, and UO-heatwaves cumulative effect. The opposing large-scale weather systems (tropical maritime Tasman airmasses and tropical continental airmasses), available on the opposite ends of the city, were determined to be the major drivers, drastically increasing the cooling energy needs and deteriorating IEQ during extreme weather conditions.

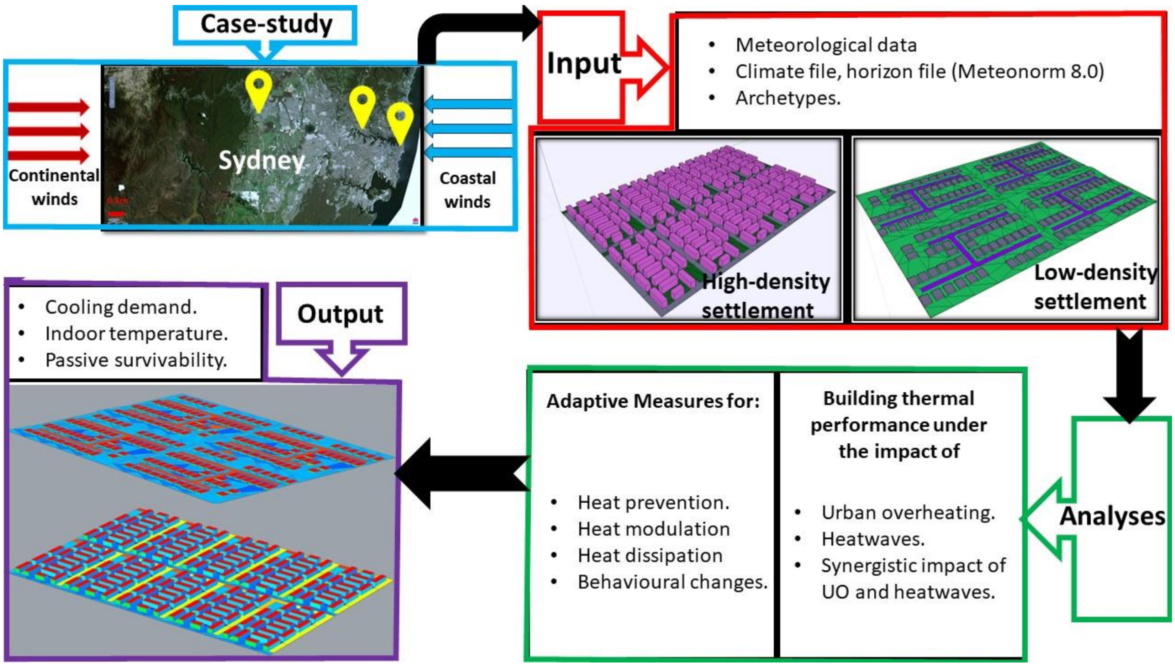

Figure 9-2: Urban energy performance and IEQ under the cumulative impact of multilevel climatic conditions

The high-rise apartment settlements (HD) outperformed the single-story housing settlements (LD) in terms of cooling energy and IEQ during heatwaves and RSD due to the inter-building shading effect. Nevertheless, the high-rise buildings in the city will block the coastal wind infiltration into the inland suburbs. Additionally, further urbanization will increase the severity of heatwaves and fortify the continental winds, making the residents of far-inland suburbs more vulnerable, especially those living in high-rise buildings. During both heatwaves and RSD, the average indoor temperatures were greater than the average outdoor temperatures, suggesting that existing buildings function as hot boxes, putting occupants at increased thermal risk rather than sheltering them.

Increasing the cooling setpoints (25 to 28°C) was the most energy-efficient measure in HD/LD settlements during both heatwaves and RSD, resulting in 37 (heatwaves) to 53 (RSD) percent cooling energy savings. The intermediately insulated envelope coupled with nocturnal cooling resulted in an optimal choice for both cooling savings and IEQ compared to the uninsulated or highly-insulated envelope, especially during heatwaves. The intermediately-insulated envelope paired with nocturnal cooling produced up to 28 percent cooling energy savings in single-story housing settlements, whereas in high-rise apartment settlements, the savings were comparatively lower owing to higher internal loads. The highly insulated envelope, with or without nocturnal cooling, enhanced the overheating issues in both settlements and deteriorated the IEQ. The highly insulated envelope was designed according to NCC DTS guidelines, implying that NCC-DTS standards do not mitigate the buildings' overheating issues.

In contrast to the literature, the airtight envelope (PH standards) and highly improved glazing (according to NCC standards) were also considered optimal choices compared to well-sealed/ leaky buildings or intermediately-insulated/ single glazing in terms of both cooling savings and IEQ. The overnight heating risk in the airtight envelope or the envelope with a highly-improved glazing system was regulated by nocturnal cooling. The cooling savings were up to 38 percent with an airtight envelope and up to 28 percent with highly glazed windows. Regarding IEQ, the higher thermal inertia paired with nocturnal cooling proved to be the ideal adaptive solution during both heatwaves and RSD. Mostly, the existing residential stock in the city has lower thermal inertia (uninsulated metal-clad, single-leaf construction system), putting the inhabitants at higher thermal risk during heatwaves. The supercool roofs reduced the cooling energy by up to 10.5 percent and adequately improved the IEQ. The blind control also resulted in 5.2 percent cooling savings during heatwaves and RSD. The impact of urban-scale strategies, including irrigated greenery/ enhanced ground albedo, was insignificant due to simulating at the neighborhood scale. Both measures' direct/ indirect benefits can be enhanced by modeling them at the district/ city scale.

The cooling savings under the cumulative effect of suitable adaptation strategies were between 87 and 99.5 percent during heatwaves and RSD in both settlements. The average indoor temperature dropped between 0.74 to 2.34°C during heatwaves and 0.71 to 1.6 °C during RSD (for both settlements) under the cumulative effect of suitable adaptive strategies. The suitable adaptive strategies improved passive survivability by 7 to 20 percent during heatwaves and 1 to 6 percent during RSD. The IEQ can be further improved by employing suitable mitigation measures.

9.5 Limitations and potential directions for future research:

1. The synergistic impact of UO, heatwaves and large-scale weather patterns was examined on energy consumption and IEQ. The combined impact of multilevel climatic conditions should also be evaluated on human health (mortality, morbidity), the economy, and environmental quality (ozone formation, etc.).
2. Primarily, the adaptation strategies were assessed under the combined impact of multilevel climatic conditions. The impact of various mitigation strategies should also be tested in association with large-scale weather patterns during heatwaves.
3. The simulation scale of urban-scale adaptation strategies, including super cool roofs, ground albedo, and green surface irrigation, should be extended from neighborhood to district/ city scale to comprehend the improvement in IEQ under the multilevel climatic conditions.
4. The multilevel climatic change impact was mainly examined for residential settlements. The impact on mixed-use or other settlements, including commercial hubs, should also be investigated. Accordingly, changes in local commercial building codes (e.g., the National Australian Built Environment Rating System- NABERS) should be proposed to counteract the global climate change impact.
5. The UBEMs are in the development phase, and various adaptive measures couldn’t be investigated due to the limitations of CitySim. For instance, nocturnal cooling was effective in Sydney suburbs, even during heatwaves, owing to the rapid radiative cooling. The natural nocturnal cooling was only investigated since the varying ventilation rates can't be simulated on the software. The improved nocturnal cooling with higher ventilation rates will significantly improve the daytime buildings' performance during extreme heat events. It will also aid in incorporating the other adaptive measures, including ground-coupled cooling, evaporative cooling, cooling with windcatchers/ solar chimney, etc.

REFERENCES:

1. Santamouris, M.; Haddad, S.; Fiorito, F.; Osmond, P.; Ding, L.; Prasad, D.; Zhai, X.; Wang, R. Urban heat island and overheating characteristics in Sydney, Australia. An analysis of multiyear measurements. *Sustain.* **2017**, *9*, 712.
2. Cui, L.; Shi, J. Urbanization and its environmental effects in Shanghai, China. *Urban Clim.* **2012**, *2*, 1–15.
3. Oke, T.R.; Mills, G.; Christen, A.; Voogt, J.A. *Urban Climates*; Cambridge University Press: Cambridge, 2017; ISBN 9781139016476.
4. Santamouris, M. Analyzing the heat island magnitude and characteristics in one hundred Asian and Australian cities and regions. *Sci. Total Environ.* **2015**, *512–513*, 582–598.
5. Wu, J. Making the Case for Landscape Ecology: An Effective Approach to Urban Sustainability. *Landsc. J.* **2008**, *27*, 41–50.
6. Perkins, S.E. A review on the scientific understanding of heatwaves-Their measurement, driving mechanisms, and changes at the global scale. *Atmos. Res.* 2015, *164–165*, 242–267.
7. Meehl, G.A.; Tebaldi, C. More intense, more frequent, and longer lasting heat waves in the 21st century. *Science* **2004**, *305*, 994–7.
8. Liu, X.; Tian, G.; Feng, J.; Ma, B.; Wang, J.; Kong, L. Modeling the Warming Impact of Urban Land Expansion on Hot Weather Using the Weather Research and Forecasting Model: A Case Study of Beijing, China. *Adv. Atmos. Sci.* **2018**, *35*, 723–736.
9. Sheridan, S.C.; Lee, C.C. Temporal Trends in Absolute and Relative Extreme Temperature Events Across North America. *J. Geophys. Res. Atmos.* **2018**.
10. Seneviratne, S.I.; Donat, M.G.; Mueller, B.; Alexander, L. V. No pause in the increase of hot temperature extremes. *Nat. Clim. Chang.* **2014**, *4*, 161–163.
11. Horton, R.M.; Mankin, J.S.; Lesk, C.; Coffel, E.; Raymond, C. A Review of Recent Advances in Research on Extreme Heat Events. *Curr. Clim. Chang. Reports* **2016**, *2*, 242–259.
12. MetLink Royal Meteorological Society UK Climate – Metlink Weather & Climate Teaching Resources Available online: https://www.metlink.org/secondary/key-stage-4/air/ (accessed on Dec 30, 2020).
13. IPCC *Climate Change 2014: Synthesis Report. Contribution of Working Groups I, II and III to the Fifth Assessment Report of the Intergovernmental Panel on Climate Change*; 2014; ISBN 9789291691432.
14. Roderick, M.L.; Hobbins, M.T.; Farquhar, G.D. Pan Evaporation Trends and the Terrestrial Water Balance. II. Energy Balance and Interpretation. *Geogr. Compass* **2009**, *3*, 761–780.
15. Santer, B.D.; Mears, C.; Wentz, F.J.; Taylor, K.E.; Gleckler, P.J.; Wigley, T.M.L.; Barnett, T.P.; Boyle, J.S.; Bruggemann, W.; Gillett, N.P.; et al. Identification of human-induced changes in atmospheric moisture content. *Proc. Natl. Acad. Sci.* **2007**, *104*, 15248–15253.
16. Basu, R. Relation between Elevated Ambient Temperature and Mortality: A Review of the Epidemiologic Evidence. *Epidemiol. Rev.* **2002**, *24*, 190–202.
17. Coates, L.; Haynes, K.; O’Brien, J.; McAneney, J.; de Oliveira, F.D. Exploring 167 years of vulnerability: An examination of extreme heat events in Australia 1844–2010. *Environ. Sci. Policy* **2014**, *42*, 33–44.

18. Patz, J.A.; Campbell-Lendrum, D.; Holloway, T.; Foley, J.A. Impact of regional climate change on human health. *Nature* **2005**, *438*, 310–317.

19. Santamouris, M.; Kolokotsa, D. On the impact of urban overheating and extreme climatic conditions on housing, energy, comfort and environmental quality of vulnerable population in Europe. *Energy Build.* **2015**, *98*, 125–133.

20. Zinzi, M.; Carnielo, E.; Mattoni, B. On the relation between urban climate and energy performance of buildings. A three-years experience in Rome, Italy. *Appl. Energy* **2018**, *221*, 148–160.

21. Santamouris, M. Cooling the buildings – past, present and future. *Energy Build.* **2016**, *128*, 617–638.

22. Stathopoulou, E.; Mihalakakou, G.; Santamouris, M.; Bagiorgas, H.S. On the impact of temperature on tropospheric Ozone concentration levels in urban environments. In Proceedings of the Journal of Earth System Science; 2008.

23. Zhang, J.; Rao, S.T.; Daggupaty, S.M. Meteorological processes and ozone exceedances in the northeastern United States during the 12-16 July 1995 episode. *J. Appl. Meteorol.* **1998**.

24. Diem, J.E.; Stauber, C.E.; Rothenberg, R. Heat in the southeastern United States: Characteristics, trends, and potential health impact. *PLoS One* **2017**.

25. Ulpiani, G. On the linkage between urban heat island and urban pollution island: Three-decade literature review towards a conceptual framework. *Sci. Total Environ.* **2021**, *751*, 141727.

26. Heck, P.; Zanetti, A.; Enz, R.; Green, J.; Suter, S. *Natural catastrophes and man-made disasters in 2003. Sigma Rep. 1/2004, Swiss Re Tech. Rep., Zurich, Switzerland, 10 pp*; 2004;

27. Filkov, A.I.; Ngo, T.; Matthews, S.; Telfer, S.; Penman, T.D. Impact of Australia's catastrophic 2019/20 bushfire season on communities and environment. Retrospective analysis and current trends. *J. Saf. Sci. Resil.* **2020**, *1*, 44–56.

28. Salimi, M.; Al-Ghamdi, S.G. Climate change impacts on critical urban infrastructure and urban resiliency strategies for the Middle East. *Sustain. Cities Soc.* **2020**, *54*, 101948.

29. Santamouris, M. Recent progress on urban overheating and heat island research. Integrated assessment of the energy, environmental, vulnerability and health impact. Synergies with the global climate change. *Energy Build.* **2020**, *207*, 109482.

30. Santamouris, M. Regulating the damaged thermostat of the cities - Status, impacts and mitigation challenges. *Energy Build.* **2015**, *91*, 43–56.

31. Zhao, L.; Oppenheimer, M.; Zhu, Q.; Baldwin, J.W.; Ebi, K.L.; Bou-Zeid, E.; Guan, K.; Liu, X. Interactions between urban heat islands and heat waves. *Environ. Res. Lett.* **2018**, *13*, 9326.

32. Brooke Anderson, G.; Bell, M.L. Heat waves in the United States: Mortality risk during heat waves and effect modification by heat wave characteristics in 43 U.S. communities. *Environ. Health Perspect.* **2011**, *119*, 210–218.

33. Robine, J.M.; Cheung, S.L.K.; Le Roy, S.; Van Oyen, H.; Griffiths, C.; Michel, J.P.; Herrmann, F.R. Death toll exceeded 70,000 in Europe during the summer of 2003. *Comptes Rendus - Biol.* **2008**, *331*, 171–178.

34. Tong, S.; Wang, X.Y.; Yu, W.; Chen, D.; Wang, X.Y. The impact of heatwaves on mortality in Australia: a multicity study. *BMJ Open* **2014**, *4*, e003579.

35. Vaneckova, P.; Beggs, P.J.; Jacobson, C.R. Spatial analysis of heat-related mortality among the elderly between 1993 and 2004 in Sydney, Australia. *Soc. Sci. Med.* **2010**, *70*, 293–304.

36. Schaffer, A.; Muscatello, D.; Broome, R.; Corbett, S.; Smith, W. Emergency department visits, ambulance calls, and mortality associated with an exceptional heat wave in Sydney, Australia, 2011: a time-series analysis. *Environ. Heal.* **2012**, *11*, 3.

37. Peters, A.; Schneider, A. Cardiovascular risks of climate change. *Nat. Rev. Cardiol.* **2020**.

38. Yin, Q.; Wang, J. The association between consecutive days' heat wave and cardiovascular disease mortality in Beijing, China. *BMC Public Health* **2017**, *17*, 223.

39. Garshasbi, S.; Haddad, S.; Paolini, R.; Santamouris, M.; Papangelis, G.; Dandou, A.; Methymaki, G.; Portalakis, P.; Tombrou, M. Urban mitigation and building adaptation to minimize the future cooling energy needs. *Sol. Energy* **2020**, *204*, 708–719.

40. Linnerud, K.; Mideksa, T.K.; Eskeland, G.S. The Impact of Climate Change on Nuclear Power Supply. *Energy J.* **2011**, *32*.

41. Li, D.; Bou-Zeid, E. Synergistic Interactions between Urban Heat Islands and Heat Waves: The Impact in Cities Is Larger than the Sum of Its Parts. *J. Appl. Meteorol. Climatol.* **2013**, *52*, 2051–2064.

42. Pyrgou, A.; Hadjinicolaou, P.; Santamouris, M. Enhanced near-surface ozone under heatwave conditions in a Mediterranean island. *Sci. Rep.* **2018**, *8*.

43. NSW Government. *Summer ozone episode from 11 to 12 February 2017, https://www.environment.nsw.gov.au/research-and-publications/publications-search/summer-ozone-episode-from-11-to-12-february-2017*; 2019;

44. Physick, W.; Cope, M.; Lee, S. The impact of climate change on ozone-related mortality in Sydney. *Int. J. Environ. Res. Public Health* **2014**.

45. Broome, R.A.; Fann, N.; Cristina, T.J.N.; Fulcher, C.; Duc, H.; Morgan, G.G. The health benefits of reducing air pollution in Sydney, Australia. *Environ. Res.* **2015**, *143*, 19–25.

46. Rizvi, S.H.; Alam, K.; Iqbal, M.J. Spatio -temporal variations in urban heat island and its interaction with heat wave. *J. Atmos. Solar-Terrestrial Phys.* **2019**, *185*, 50–57.

47. Brázdil, R.; Budíková, M. An urban bias in air temperature fluctuations at the Klementinum, Prague, The Czech Republic. In Proceedings of the Atmospheric Environment; Elsevier Science Ltd, 1999; Vol. 33, pp. 4211–4217.

48. Li, D.; Sun, T.; Liu, M.; Yang, L.; Wang, L.; Gao, Z. Contrasting responses of urban and rural surface energy budgets to heat waves explain synergies between urban heat islands and heat waves. *Environ. Res. Lett.* **2015**, *10*, 054009.

49. Cheval, S.; Dumitrescu, A.; Bell, A. The urban heat island of Bucharest during the extreme high temperatures of July 2007. *Theor. Appl. Climatol.* **2009**, *97*, 391–401.

50. Founda, D.; Santamouris, M. Synergies between Urban Heat Island and Heat Waves in Athens (Greece), during an extremely hot summer (2012). *Sci. Rep.* **2017**, *7*, 10973.

51. Ao, X.; Wang, L.; Zhi, X.; Gu, W.; Yang, H.; Li, D. Observed Synergies between Urban Heat Islands and Heat Waves and Their Controlling Factors in Shanghai, China. *J. Appl. Meteorol. Climatol.* **2019**, *58*, 1955–1972.

52. Zhao, L.; Lee, X.; Smith, R.B.; Oleson, K. Strong contributions of local background climate to

urban heat islands. *Nature* **2014**, *511*, 216–219.

53. Schatz, J.; Kucharik, C.J. Urban climate effects on extreme temperatures in Madison, Wisconsin, USA. *Environ. Res. Lett.* **2015**, *10*, 094024.

54. Ward, K.; Lauf, S.; Kleinschmit, B.; Endlicher, W. Heat waves and urban heat islands in Europe: A review of relevant drivers. *Sci. Total Environ.* **2016**, *569–570*, 527–539.

55. Diffenbaugh, N.S.; Pal, J.S.; Giorgi, F.; Gao, X. Heat stress intensification in the Mediterranean climate change hotspot. *Geophys. Res. Lett.* **2007**, *34*, L11706.

56. Scott, A.A.; Waugh, D.W.; Zaitchik, B.F. Reduced Urban Heat Island intensity under warmer conditions. *Environ. Res. Lett.* **2018**, *13*, 064003.

57. Kumar, R.; Mishra, V. Decline in surface urban heat island intensity in India during heatwaves. *Environ. Res. Commun.* **2019**, *1*, 031001.

58. Rogers, C.D.W.; Gallant, A.J.E.; Tapper, N.J. Is the urban heat island exacerbated during heatwaves in southern Australian cities? *Theor. Appl. Climatol.* **2019**, *137*, 441–457.

59. Ramamurthy, P.; Bou-Zeid, E. Heatwaves and urban heat islands: A comparative analysis of multiple cities. *J. Geophys. Res.* **2017**, *122*, 168–178.

60. Pyrgou, A.; Hadjinicolaou, P.; Santamouris, M. Urban-rural moisture contrast: Regulator of the urban heat island and heatwaves' synergy over a mediterranean city. *Environ. Res.* **2020**, *182*, 109102.

61. Basara, J.B.; Basara, H.G.; Illston, B.G.; Crawford, K.C. The Impact of the Urban Heat Island during an Intense Heat Wave in Oklahoma City. *Adv. Meteorol.* **2010**, *2010*, 1–10.

62. Fenner, D.; Holtmann, A.; Meier, F.; Langer, I.; Scherer, D. Contrasting changes of urban heat island intensity during hot weather episodes. *Environ. Res. Lett.* **2019**, *14*, 124013.

63. Imran, H.M.; Kala, J.; Ng, A.W.M.; Muthukumaran, S. Impacts of future urban expansion on urban heat island effects during heatwave events in the city of Melbourne in southeast Australia. *Q. J. R. Meteorol. Soc.* **2019**, *145*, 2586–2602.

64. Katavoutas, G.; Founda, D. Response of Urban Heat Stress to Heat Waves in Athens (1960–2017). *Atmosphere (Basel).* **2019**, *10*, 483.

65. Argüeso, D.; Evans, J.P.; Fita, L.; Bormann, K.J. Temperature response to future urbanization and climate change. *Clim. Dyn.* **2014**, *42*, 2183–2199.

66. Khan, H.S.; Santamouris, M.; Paolini, R.; Caccetta, P.; Kassomenos, P. Analyzing the local and climatic conditions affecting the urban overheating magnitude during the Heatwaves (HWs) in a coastal city: A case study of the greater Sydney region. *Sci. Total Environ.* **2021**, *755*, 142515.

67. Vahmani, P.; Ban-Weiss, G.A. Impact of remotely sensed albedo and vegetation fraction on simulation of urban climate in WRF-urban canopy model: A case study of the urban heat island in Los Angeles. *J. Geophys. Res. Atmos.* **2016**, *121*, 1511–1531.

68. Sailor, D.J. A green roof model for building energy simulation programs. *Energy Build.* **2008**, *40*, 1466–1478.

69. Khan, H.; Asif, M. Impact of Green Roof and Orientation on the Energy Performance of Buildings: A Case Study from Saudi Arabia. *Sustainability* **2017**, *9*, 640.

70. Sun, T.; Kotthaus, S.; Li, D.; Ward, H.C.; Gao, Z.; Ni, G.-H.; Grimmond, C.S.B. Attribution and

mitigation of heat wave-induced urban heat storage change. *Environ. Res. Lett.* **2017**, *12*, 114007.

71. Fischer, E.M.; Seneviratne, S.I.; Vidale, P.L.; Lüthi, D.; Schär, C. Soil moisture-atmosphere interactions during the 2003 European summer heat wave. *J. Clim.* **2007**, *20*, 5081–5099.

72. Vahmani, P.; Ban-Weiss, G.A. Impact of remotely sensed albedo and vegetation fraction on simulation of urban climate in WRF-urban canopy model: A case study of the urban heat island in Los Angeles. *J. Geophys. Res. Atmos.* **2016**, *121*, 1511–1531.

73. Khan, H.; Asif, M.; Mohammed, M. Case Study of a Nearly Zero Energy Building in Italian Climatic Conditions. *Infrastructures* **2017**, *2*, 19.

74. Półrolniczak, M.; Kolendowicz, L.; Majkowska, A.; Czernecki, B. The influence of atmospheric circulation on the intensity of urban heat island and urban cold island in Poznań, Poland. *Theor. Appl. Climatol.* **2017**, *127*, 611–625.

75. Morris, C.J.G.; Simmonds, I. Associations between varying magnitudes of the urban heat island and the synoptic climatology in Melbourne, Australia. *Int. J. Climatol.* **2000**, *20*, 1931–1954.

76. Morris, C.J.G.G.; Simmonds, I.; Plummer, N. Quantification of the Influences of Wind and Cloud on the Nocturnal Urban Heat Island of a Large City. *J. Appl. Meteorol.* **2001**, *40*, 169–182.

77. Tan, J.; Zheng, Y.; Tang, X.; Guo, C.; Li, L.; Song, G.; Zhen, X.; Yuan, D.; Kalkstein, A.J.; Li, F.; et al. The urban heat island and its impact on heat waves and human health in Shanghai. *Int. J. Biometeorol.* **2010**, *54*, 75–84.

78. Oke, T.R.; Runnalls, K.E. Dynamics and controls of the near-surface heat island of vancouver, british Columbia. *Phys. Geogr.* **2000**.

79. Bejar�n, R.A.; Camilloni, I.A. Objective method for classifying air masses: an application to the analysis of Buenos Aires' (Argentina) urban heat island intensity. *Theor. Appl. Climatol.* **2003**, *74*, 93–103.

80. Zhang, F.; Cai, X.; Thornes, J.E. Birmingham's air and surface urban heat islands associated with lamb weather types and cloudless anticyclonic conditions. *Prog. Phys. Geogr.* **2014**, *38*, 431–447.

81. Grady Dixon, P.; Mote, T.L. Patterns and causes of Atlanta's urban heat island-initiated precipitation. *J. Appl. Meteorol.* **2003**, *42*, 1273–1284.

82. Sheridan, S.C.; Kalkstein, L.S.; Scott, J.M. An evaluation of the variability of Air mass character between urban and rural areas. *Biometeorol. Urban Climatol. Turn Millenn.* **2000**, 487–490.

83. Brazel, A.; Gober, P.; Lee, S.; Grossman-Clarke, S.; Zehnder, J.; Hedquist, B.; Comparri, E. Determinants of changes in the regional urban heat island in metropolitan Phoenix (Arizona, USA) between 1990 and 2004. *Clim. Res.* **2007**, *33*, 171–182.

84. Unger, J. Heat island intensity with different meteorological conditions in a medium-sized town: Szeged, Hungary. *Theor. Appl. Climatol.* **1996**, *54*, 147–151.

85. Szegedi, S.; Kircsi, A. The effects of the synoptic conditions on development of the urban heat island in Debrecen, Hungary. *Acta Climatol. Chorol.* **2003**, *36–37*, 111–120.

86. Mihalakakou, G.; Flocas, H.A.; Santamouris, M.; Helmis, C.G. Application of neural networks to the simulation of the heat island over Athens, Greece, using synoptic types as a predictor.

J. Appl. Meteorol. **2002**, *41*, 519–527.

87. Hardin, A.W.; Liu, Y.; Cao, G.; Vanos, J.K. Urban heat island intensity and spatial variability by synoptic weather type in the northeast U.S. *Urban Clim.* **2018**, *24*, 747–762.

88. Li, C.; Zhou, J.; Cao, Y.; Zhong, J.; Liu, Y.; Kang, C.; Tan, Y. Interaction between urban microclimate and electric air-conditioning energy consumption during high temperature season. *Appl. Energy* **2014**, *117*, 149–156.

89. Litardo, J.; Palme, M.; Borbor-Cordova, M.; Caiza, R.; Macias, J.; Hidalgo-Leon, R.; Soriano, G. Urban Heat Island intensity and buildings' energy needs in Duran, Ecuador: Simulation studies and proposal of mitigation strategies. *Sustain. Cities Soc.* **2020**, *62*, 102387.

90. Hirano, Y.; Fujita, T. Evaluation of the impact of the urban heat island on residential and commercial energy consumption in Tokyo. *Energy* **2012**, *37*, 371–383.

91. Zinzi, M.; Agnoli, S.; Burattini, C.; Mattoni, B. On the thermal response of buildings under the synergic effect of heat waves and urban heat island. *Sol. Energy* **2020**, *211*, 1270–1282.

92. Pyrgou, A.; Castaldo, V.L.; Pisello, A.L.; Cotana, F.; Santamouris, M. On the effect of summer heatwaves and urban overheating on building thermal-energy performance in central Italy. *Sustain. Cities Soc.* **2017**, *28*, 187–200.

93. Willand, N.; Ridley, I.; Pears, A. Relationship of thermal performance rating, summer indoor temperatures and cooling energy use in 107 homes in Melbourne, Australia. *Energy Build.* **2016**, *113*, 159–168.

94. Alam, M.; Rajeev, P.; Sanjayan, J.; Zou, P.X.W.; Wilson, J. Mitigation of heat stress risks through building energy efficiency upgrade: a case study of Melbourne, Australia. *Aust. J. Civ. Eng.* **2018**, *16*, 64–78.

95. Climates, U.; Oke, T.R.; Columbia, B.; Climates, B.L.; Climate, U.; Service, M.; Medal, P.; Canadian, R.; Society, G.; Medal, M.; et al. *Urban Climates*; ISBN 9780521849500.

96. *World Urbanization Prospects: The 2018 Revision*; UN, 2019; ISBN 9789210043144.

97. Elsayed, I.S.M. Mitigation of the urban heat island of the city of Kuala Lumpur, Malaysia. *Middle East J. Sci. Res.* **2012**, *11*, 1602–1613.

98. Klok, L.; Zwart, S.; Verhagen, H.; Mauri, E. The surface heat island of Rotterdam and its relationship with urban surface characteristics. *Resour. Conserv. Recycl.* **2012**, *64*, 23–29.

99. Stone, B.; Norman, J.M. Land use planning and surface heat island formation: A parcel-based radiation flux approach. *Atmos. Environ.* **2006**.

100. A, B.; S, L.; S, B. Urban Heat Island Effect: It's Relevance in Urban Planning. *J. Biodivers. Endanger. Species* **2017**, *05*.

101. Akbari, H.; Bell, R.; Brazel, T.; Cole, D.; Estes, M.; Heisler, G.; Hitchcock, D.; Johnson, B.; Lewis, M.; McPherson, G.; et al. Urban heat island basics. In *Reducing Urban Heat Islands: Compendium of Strategies | Heat Island Effect | US EPA*; 2008.

102. Hu, Z.; Yu, B.; Chen, Z.; Li, T.; Liu, M. Numerical investigation on the urban heat island in an entire city with an urban porous media model. *Atmos. Environ.* **2012**.

103. Sailor, D.J. Energy Buildings and Urban Environment. In *Climate Vulnerability*; Elsevier, 2013; Vol. 3, pp. 167–182.

104. RIZWAN, A.M.; DENNIS, L.Y.C.; LIU, C. A review on the generation, determination and

mitigation of Urban Heat Island. *J. Environ. Sci.* **2008**, *20*, 120–128.

105. Li, Y.; Schubert, S.; Kropp, J.P.; Rybski, D. On the influence of density and morphology on the Urban Heat Island intensity. *Nat. Commun.* **2020**.

106. Barlow, J.F. Progress in observing and modelling the urban boundary layer. *Urban Clim.* **2014**, *10*, 216–240.

107. Memon, R.A.; Leung, D.Y.C. Impacts of environmental factors on urban heating. *J. Environ. Sci.* **2010**, *22*, 1903–1909.

108. Li, D.; Sun, T.; Liu, M.; Wang, L.; Gao, Z. Changes in wind speed under heat waves enhance urban heat islands in the Beijing metropolitan area. *J. Appl. Meteorol. Climatol.* **2016**, *55*, 2369–2375.

109. Tewari, M.; Yang, J.; Kusaka, H.; Salamanca, F.; Watson, C.; Treinish, L. Interaction of urban heat islands and heat waves under current and future climate conditions and their mitigation using green and cool roofs in New York City and Phoenix, Arizona. *Environ. Res. Lett.* **2019**, *14*, 034002.

110. Nichol, J.E.; Fung, W.Y.; Lam, K.; Wong, M.S. Urban heat island diagnosis using ASTER satellite images and 'in situ' air temperature. *Atmos. Res.* **2009**, *94*, 276–284.

111. Chew, L.W.; Liu, X.; Li, X.-X.; Norford, L.K. Interaction between heat wave and urban heat island: A case study in a tropical coastal city, Singapore. *Atmos. Res.* **2021**, *247*, 105134.

112. Bohnenstengel, S.I.; Evans, S.; Clark, P.A.; Belcher, S.E. Simulations of the London urban heat island. *Q. J. R. Meteorol. Soc.* **2011**, *137*, 1625–1640.

113. Perkins, S.E.; Alexander, L. V. On the Measurement of Heat Waves. *J. Clim.* **2013**, *26*, 4500–4517.

114. Mishra, V.; Ganguly, A.R.; Nijssen, B.; Lettenmaier, D.P. Changes in observed climate extremes in global urban areas. *Environ. Res. Lett.* **2015**, *10*, 024005.

115. Habeeb, D.; Vargo, J.; Stone, B. Rising heat wave trends in large US cities. *Nat. Hazards* **2015**, *76*, 1651–1665.

116. Australian Government Bureau of Meteorology Understanding heatwaves Available online: http://www.bom.gov.au/australia/heatwave/knowledge-centre/understanding.shtml (accessed on Apr 18, 2022).

117. Bureau of Meteorology (BOM), A. Australian daily climate extreme area maps Available online: http://www.bom.gov.au/cgi-bin/climate/extremes/extreme_maps.cgi?map=tmax&year=2017&mon=2&day=11&colour=colour (accessed on Jun 6, 2022).

118. Chen, K.; Bi, J.; Chen, J.; Chen, X.; Huang, L.; Zhou, L. Influence of heat wave definitions to the added effect of heat waves on daily mortality in Nanjing, China. *Sci. Total Environ.* **2015**, *506–507*, 18–25.

119. Tong, S.; FitzGerald, G.; Wang, X.-Y.; Aitken, P.; Tippett, V.; Chen, D.; Wang, X.; Guo, Y. Exploration of the health risk-based definition for heatwave: A multi-city study. *Environ. Res.* **2015**, *142*, 696–702.

120. Collins, D.A.; Della-Marta, P.M.; Plummer, N.; Trewin, B.C. Trends in annual frequencies of extreme temperature events in Australia. *Aust. Meteorol. Mag.* 2000, *49*, 277–292.

121. Alexander, L. V.; Zhang, X.; Peterson, T.C.; Caesar, J.; Gleason, B.; Klein Tank, A.M.G.; Haylock, M.; Collins, D.; Trewin, B.; Rahimzadeh, F.; et al. Global observed changes in daily climate extremes of temperature and precipitation. *J. Geophys. Res. Atmos.* **2006**, *111*, D05109.

122. Richard, Y.; Pohl, B.; Rega, M.; Pergaud, J.; Thevenin, T.; Emery, J.; Dudek, J.; Vairet, T.; Zito, S.; Chateau-Smith, C. Is Urban Heat Island intensity higher during hot spells and heat waves (Dijon, France, 2014–2019)? *Urban Clim.* **2021**, *35*, 100747.

123. Fischer, E.M.; Schär, C. Consistent geographical patterns of changes in high-impact European heatwaves. *Nat. Geosci.* **2010**, *3*.

124. Nairn, J.; Fawcett, R. *Defining heatwaves: heatwave defined as a heat-impact event servicing all communiy and business sectors in Australia*; 2013;

125. Russo, S.; Sillmann, J.; Sterl, A. Humid heat waves at different warming levels. *Sci. Rep.* **2017**, *7*, 1–7.

126. Koutsoyiannis, D.; Langousis, A. Precipitation. In *Treatise on Water Science*; Elsevier, 2011; Vol. 2, pp. 27–77 ISBN 9780444531933.

127. Colucci, S.J. ANTICYCLONES. In *Encyclopedia of Atmospheric Sciences*; Elsevier, 2003; pp. 142–146.

128. Yarnal, B. Synoptic climatology in environmental analysis. A primer. *Environ. Int.* **1993**, *19*, 529-.

129. Lee, C.C. Reanalysing the impacts of atmospheric teleconnections on cold-season weather using multivariate surface weather types and self-organizing maps. *Int. J. Climatol.* **2017**, *37*, 3714–3730.

130. Huth, R. Synoptic-climatological applicability of circulation classifications from the COST733 collection: First results. *Phys. Chem. Earth, Parts A/B/C* **2010**, *35*, 388–394.

131. Philipp, A.; Bartholy, J.; Beck, C.; Erpicum, M.; Esteban, P.; Fettweis, X.; Huth, R.; James, P.; Jourdain, S.; Kreienkamp, F.; et al. Cost733cat - A database of weather and circulation type classifications. *Phys. Chem. Earth* **2010**.

132. Kalkstein, L.S.; Nichols, M.C.; David Barthel, C.; Scott Greene, J. A new spatial synoptic classification: Application to air-mass analysis. *Int. J. Climatol.* **1996**, *16*, 983–1004.

133. Sheridan, S.C. The redevelopment of a weather-type classification scheme for North America. *Int. J. Climatol.* **2002**.

134. Lee, C.C. The development of a gridded weather typing classification scheme. *Int. J. Climatol.* **2015**.

135. Lee, C.C. The gridded weather typing classification version 2: A global-scale expansion. *Int. J. Climatol.* **2020**.

136. Sheridan, S. Spatial synoptic classification (SSC) Available online: http://sheridan.geog.kent.edu/ssc.html (accessed on Apr 9, 2021).

137. Lee, C.C. Gridded weather typing classification (GWTC) Available online: https://www.personal.kent.edu/~cclee/gwtc2global.html (accessed on Apr 9, 2021).

138. Lee, C.C. GWTC-2 Global Available online: https://www.personal.kent.edu/~cclee/gwtc2global.html (accessed on Jun 6, 2022).

139. Cleugh, H.; Grimmond, S. Urban Climates and Global Climate Change. In *The Future of the*

World's Climate; Elsevier, 2012; pp. 47–76.

140. Luvall, J.C.; Quattrochi, D.A.; Rickman, D.L.; Estes, M.G. BOUNDARY LAYER (ATMOSPHERIC) AND AIR POLLUTION | Urban Heat Islands. In *Encyclopedia of Atmospheric Sciences*; Elsevier, 2015; pp. 310–318.

141. Santamouris, M.; Cartalis, C.; Synnefa, A.; Kolokotsa, D. On the impact of urban heat island and global warming on the power demand and electricity consumption of buildings - A review. *Energy Build.* **2015**, *98*, 119–124.

142. Yang, J.; Tham, K.W.; Lee, S.E.; Santamouris, M.; Sekhar, C.; Cheong, D.K.W. Anthropogenic heat reduction through retrofitting strategies of campus buildings. *Energy Build.* **2017**, *152*, 813–822.

143. CRUTZEN, P. New Directions: The growing urban heat and pollution ?island? effect?impact on chemistry and climate*1. *Atmos. Environ.* **2004**, *38*, 3539–3540.

144. Boehme, P.; Berger, M.; Massier, T. Estimating the building based energy consumption as an anthropogenic contribution to urban heat islands. *Sustain. Cities Soc.* **2015**, *19*, 373–384.

145. Arnfield, A.J. Two decades of urban climate research: a review of turbulence, exchanges of energy and water, and the urban heat island. *Int. J. Climatol.* **2003**, *23*, 1–26.

146. Zhao, D.; Wu, J. Contribution of Urban Surface Expansion to Regional Warming in Beijing, China. *J. Appl. Meteorol. Climatol.* **2017**, *56*, 1551–1559.

147. Fischer, E.M.; Oleson, K.W.; Lawrence, D.M. Contrasting urban and rural heat stress responses to climate change. *Geophys. Res. Lett.* **2012**, *39*, 8.

148. Wang, J.; Yan, Z.; Quan, X.-W.; Feng, J. Urban warming in the 2013 summer heat wave in eastern China. *Clim. Dyn.* **2017**, *48*, 3015–3033.

149. Ngarambe, J.; Nganyiyimana, J.; Kim, I.; Santamouris, M.; Yun, G.Y. Synergies between urban heat island and heat waves in Seoul: The role of wind speed and land use characteristics. *PLoS One* **2020**, *15*, e0243571.

150. Ramamurthy, P.; Li, D.; Bou-Zeid, E. High-resolution simulation of heatwave events in New York City. *Theor. Appl. Climatol.* **2017**.

151. Taha, H. Urban climates and heat islands: albedo, evapotranspiration, and anthropogenic heat. *Energy Build.* **1997**, *25*, 99–103.

152. Ramamurthy, P.; Bou-Zeid, E.; Smith, J.A.; Wang, Z.; Baeck, M.L.; Saliendra, N.Z.; Hom, J.L.; Welty, C. Influence of Subfacet Heterogeneity and Material Properties on the Urban Surface Energy Budget. *J. Appl. Meteorol. Climatol.* **2014**, *53*, 2114–2129.

153. Unger, J.; Skarbit, N.; Kovács, A.; Gál, T. Comparison of regional and urban outdoor thermal stress conditions in heatwave and normal summer periods: A case study. *Urban Clim.* **2020**, *32*, 100619.

154. He, X.; Wang, J.; Feng, J.; Yan, Z.; Miao, S.; Zhang, Y.; Xia, J. Observational and modeling study of interactions between urban heat island and heatwave in Beijing. *J. Clean. Prod.* **2020**, *247*, 119169.

155. Gillett, N.P.; Stott, P.A. Attribution of anthropogenic influence on seasonal sea level pressure. *Geophys. Res. Lett.* **2009**, *36*, L23709.

156. Roderick, M.L.; Hobbins, M.T.; Farquhar, G.D. Pan evaporation trends and the terrestrial

water balance. I. Principles and observations. *Geogr. Compass* **2009**.

157. Willett, K.M.; Gillett, N.P.; Jones, P.D.; Thorne, P.W. Attribution of observed surface humidity changes to human influence. *Nature* **2007**, *449*, 710–712.

158. Lee, C.C.; Sheridan, S.C. Trends in weather type frequencies across North America. *npj Clim. Atmos. Sci.* **2018**.

159. Oke, T.R. The energetic basis of the urban heat island. *Q. J. R. Meteorol. Soc.* **1982**, *108*, 1–24.

160. Schatz, J.; Kucharik, C.J. Seasonality of the urban heat island effect in Madison, Wisconsin. *J. Appl. Meteorol. Climatol.* **2014**.

161. Dixon, P.G.; Mote L., T. Patterns and Causes of Atlanta's Urban Heat Island – Initiated Precipitation. *J. Appl. Meteorol.* **2003**.

162. Henry, J.A.; Dicks, S.E.; Marotz, G.A. Urban and rural humidity distributions: Relationships to surface materials and land use. *J. Climatol.* **1985**, *5*, 53–62.

163. Zhang, N.; Gao, Z.; Wang, X.; Chen, Y. Modeling the impact of urbanization on the local and regional climate in Yangtze River Delta, China. *Theor. Appl. Climatol.* **2010**.

164. Zhang, N.; Zhu, L.; Zhu, Y. Urban heat island and boundary layer structures under hot weather synoptic conditions: A case study of Suzhou City, China. *Adv. Atmos. Sci.* **2011**, *28*, 855–865.

165. Oke, T.R. *Boundary Layer Climates. 2d ed. Routledge, 435 pp.*; 1987;

166. Lee, D.O. Urban climates. *Prog. Phys. Geogr. Earth Environ.* **1984**, *8*, 1–31.

167. Chow, W.T.L.; Roth, M. Temporal dynamics of the urban heat island of Singapore. *Int. J. Climatol.* **2006**.

168. Shahmohamadi, P.; Che-Ani, A.I.; Maulud, K.N.A.; Tawil, N.M.; Abdullah, N.A.G. The Impact of Anthropogenic Heat on Formation of Urban Heat Island and Energy Consumption Balance. *Urban Stud. Res.* **2011**.

169. Alonso, M.S.; Labajo, J.L.; Fidalgo, M.R. Characteristics of the urban heat island in the city of Salamanca, Spain. *Atmosfera* **2003**, *16*.

170. Adams, R.E.; Lee, C.C.; Smith, E.T.; Sheridan, S.C. The relationship between atmospheric circulation patterns and extreme temperature events in North America. *Int. J. Climatol.* **2020**.

171. Sheridan, S.C.; Lin, S. Assessing Variability in the Impacts of Heat on Health Outcomes in New York City Over Time, Season, and Heat-Wave Duration. *Ecohealth* **2014**, *11*, 512–525.

172. Vanos, J.K.; Cakmak, S.; Bristow, C.; Brion, V.; Tremblay, N.; Martin, S.L.; Sheridan, S.S. Synoptic weather typing applied to air pollution mortality among the elderly in 10 Canadian cities. *Environ. Res.* **2013**, *126*, 66–75.

173. Lee, C.C. A systematic evaluation of the lagged effects of spatiotemporally relative surface weather types on wintertime cardiovascular-related mortality across 19 US cities. *Int. J. Biometeorol.* **2015**.

174. Attia, S.; Levinson, R.; Ndongo, E.; Holzer, P.; Berk Kazanci, O.; Homaei, S.; Zhang, C.; Olesen, B.W.; Qi, D.; Hamdy, M.; et al. Resilient cooling of buildings to protect against heat waves and power outages: Key concepts and definition. *Energy Build.* **2021**, *239*, 110869.

175. European Commission The European Green Deal Available online: https://ec.europa.eu/info/sites/default/files/european-green-deal-communication_en.pdf

(accessed on Dec 31, 2021).

176. Bilardo, M.; Ferrara, M.; Fabrizio, E. Resilient optimal design of multi-family buildings in future climate scenarios. *E3S Web Conf.* **2019**, *111*.

177. Jacob, A.; Tiwari, B.N.; Rankine, H.; Beerepoot, M.; Dacanay, M.L.; Jiwanji, M.; Kharrazi, A.; Kim, S.H.; Lee, A.; O'Connell, D.; et al. Transformation towards sustainable and resilient societies in Asia and the Pacific. **2018**.

178. International Energy Agency Buildings: A source of enormous untapped efficiency potential Available online: https://www.iea.org/topics/buildings (accessed on Jan 5, 2022).

179. Asif, M.; Dehwah, A.; Ashraf, F.; Khan, H.; Shaukat, M.; Hassan, M. Life Cycle Assessment of a Three-Bedroom House in Saudi Arabia. *Environments* **2017**, *4*, 52.

180. Mutschler, R.; Rüdisüli, M.; Heer, P.; Eggimann, S. Benchmarking cooling and heating energy demands considering climate change, population growth and cooling device uptake. *Appl. Energy* **2021**, *288*, 116636.

181. International Energy Agency Is Cooling the Future of Heating? Available online: https://www.iea.org/commentaries/is-cooling-the-future-of-heating (accessed on Jan 6, 2022).

182. International Energy Agency (IEA) Cooling Available online: https://www.iea.org/reports/cooling (accessed on Jan 5, 2022).

183. Maller, C.J.; Strengers, Y. Housing, heat stress and health in a changing climate: promoting the adaptive capacity of vulnerable households, a suggested way forward. *Health Promot. Int.* **2011**, *26*, 492–498.

184. Microclimate - Glossary of Meteorology Available online: https://glossary.ametsoc.org/wiki/Microclimate (accessed on Dec 17, 2021).

185. Mauree, D.; Coccolo, S.; Kaempf, J.; Scartezzini, J.-L. Multi-scale modelling to evaluate building energy consumption at the neighbourhood scale. *PLoS One* **2017**, *12*, e0183437.

186. Hong, T.; Xu, Y.; Sun, K.; Zhang, W.; Luo, X.; Hooper, B. Urban microclimate and its impact on building performance: A case study of San Francisco. *Urban Clim.* 2021, *38*.

187. Yang, F.; Jiang, Z. Urban building energy modelling and urban design for sustainable neighbourhood development-A China perspective. *IOP Conf. Ser. Earth Environ. Sci.* **2019**, *329*.

188. Jandaghian, Z.; Berardi, U. Analysis of the cooling effects of higher albedo surfaces during heat waves coupling the Weather Research and Forecasting model with building energy models. *Energy Build.* **2020**, *207*, 109627.

189. Santamouris, M.; Haddad, S.; Saliari, M.; Vasilakopoulou, K.; Synnefa, A.; Paolini, R.; Ulpiani, G.; Garshasbi, S.; Fiorito, F. On the energy impact of urban heat island in Sydney: Climate and energy potential of mitigation technologies. *Energy Build.* **2018**, *166*, 154–164.

190. Toparlar, Y.; Blocken, B.; Maiheu, B.; van Heijst, G.J.F. Impact of urban microclimate on summertime building cooling demand: A parametric analysis for Antwerp, Belgium. *Appl. Energy* **2018**, *228*, 852–872.

191. Li, X.; Zhou, Y.; Yu, S.; Jia, G.; Li, H.; Li, W. Urban heat island impacts on building energy consumption: A review of approaches and findings. *Energy* **2019**, *174*, 407–419.

192. Su, M.A.; Ngarambe, J.; Santamouris, M.; Yun, G.Y. Empirical evidence on the impact of urban overheating on building cooling and heating energy consumption. *iScience* **2021**, *24*, 102495.

193. Salvati, A.; Coch Roura, H.; Cecere, C. Assessing the urban heat island and its energy impact on residential buildings in Mediterranean climate: Barcelona case study. *Energy Build.* **2017**, *146*.

194. Palme, M.; Inostroza, L.; Villacreses, G.; Lobato-Cordero, A.; Carrasco, C. From urban climate to energy consumption. Enhancing building performance simulation by including the urban heat island effect. *Energy Build.* **2017**, *145*, 107–120.

195. Yang, X.; Peng, L.L.H.; Jiang, Z.; Chen, Y.; Yao, L.; He, Y.; Xu, T. Impact of urban heat island on energy demand in buildings: Local climate zones in Nanjing. *Appl. Energy* **2020**, *260*.

196. Sedaghat, A.; Sharif, M. Mitigation of the impacts of heat islands on energy consumption in buildings: A case study of the city of Tehran, Iran. *Sustain. Cities Soc.* **2022**, *76*, 103435.

197. Romano, P.; Prataviera, E.; Carnieletto, L.; Vivian, J.; Zinzi, M.; Zarrella, A. Assessment of the urban heat island impact on building energy performance at district level with the EUReCA platform. *Climate* **2021**, *9*.

198. Gupta, R.; Gregg, M. Assessing energy use and overheating risk in net zero energy dwellings in UK. *Energy Build.* **2020**, *158*, 897–905.

199. Porritt, S.M.; Cropper, P.C.; Shao, L.; Goodier, C.I. Ranking of interventions to reduce dwelling overheating during heat waves. *Energy Build.* **2012**, *55*, 16–27.

200. McLeod, R.S.; Hopfe, C.J.; Kwan, A. An investigation into future performance and overheating risks in Passivhaus dwellings. *Build. Environ.* **2013**, *70*, 189–209.

201. Figueiredo, A.; Figueira, J.; Vicente, R.; Maio, R. Thermal comfort and energy performance: Sensitivity analysis to apply the Passive House concept to the Portuguese climate. *Build. Environ.* **2016**, *103*, 276–288.

202. Hatvani-Kovacs, G.; Belusko, M.; Pockett, J.; Boland, J. Heat stress-resistant building design in the Australian context. *Energy Build.* **2018**, *158*, 290–299.

203. Sakka, A.; Santamouris, M.; Livada, I.; Nicol, F.; Wilson, M. On the thermal performance of low income housing during heat waves. *Energy Build.* **2012**, *49*, 69–77.

204. Baniassadi, A.; Sailor, D.J. Synergies and trade-offs between energy efficiency and resiliency to extreme heat – A case study. *Build. Environ.* **2018**, *132*, 263–272.

205. Gómez, G.; Frutos, B.; Alonso, C.; Martín-Consuegra, F.; Oteiza, I.; De Frutos, F.; Castellote, M.M.; Muñoz, J.; Torre, S.; Fermoso, J.; et al. Selection of nature-based solutions to improve comfort in schools during heat waves. *Int. J. Energy Prod. Manag.* **2021**, *6*, 157–169.

206. Viguié, V.; Lemonsu, A.; Hallegatte, S.; Beaulant, A.L.; Marchadier, C.; Masson, V.; Pigeon, G.; Salagnac, J.L. Early adaptation to heat waves and future reduction of air-conditioning energy use in Paris. *Environ. Res. Lett.* **2020**, *15*.

207. Han, J.; Chen, D.; Wang, X. Multi-criteria heatwave vulnerability assessment of residential wall systems. *Energy Build.* **2013**, *66*, 373–383.

208. Paolini, R.; Zani, A.; Meshkinkiya, M.; Lucia, V.; Laura, A.; Antretter, F.; Poli, T.; Cotana, F. The hygrothermal performance of residential buildings at urban and rural sites : Sensible and latent energy loads and indoor environmental conditions. *Energy Build.* **2017**, *152*, 792–803.

209. Zhang, C.; Kazanci, O.B.; Levinson, R.; Heiselberg, P.; Olesen, B.W.; Chiesa, G.; Sodagar, B.; Ai, Z.; Selkowitz, S.; Zinzi, M.; et al. Resilient cooling strategies – A critical review and qualitative assessment. *Energy Build.* **2021**, *251*, 111312.

210. Roshan, G.R.; Oji, R.; Attia, S. Projecting the impact of climate change on design recommendations for residential buildings in Iran. *Build. Environ.* **2019**, *155*, 283–297.

211. Kroll, D.; Breen Lovett, S.; Jimenez-Bescos, C.; Chisnall, P.; Aitchison, M. Passive house vs. passive design: sociotechnical issues in a practice-based design research project for a low-energy house. *Archit. Sci. Rev.* **2020**, *63*, 361–371.

212. Haddad, S.; Barker, A.; Yang, J.; Kumar, D.I.M.; Garshasbi, S.; Paolini, R.; Santamouris, M. On the potential of building adaptation measures to counterbalance the impact of climatic change in the tropics. *Energy Build.* **2020**, *229*, 110494.

213. Kuczyński, T.; Staszczuk, A. Experimental study of the influence of thermal mass on thermal comfort and cooling energy demand in residential buildings. *Energy* **2020**, *195*.

214. Pomianowski, M.; Heiselberg, P.; Zhang, Y. Review of thermal energy storage technologies based on PCM application in buildings. *Energy Build.* **2013**, *67*, 56–69.

215. Ahmed, T.; Kumar, P.; Mottet, L. Natural ventilation in warm climates: The challenges of thermal comfort, heatwave resilience and indoor air quality. *Renew. Sustain. Energy Rev.* **2021**, *138*.

216. Schünemann, C.; Schiela, D.; Ortlepp, R. How window ventilation behaviour affects the heat resilience in multi-residential buildings. *Build. Environ.* **2021**, *202*.

217. Jandaghian, Z.; Berardi, U. Analysis of the cooling effects of higher albedo surfaces during heat waves coupling the Weather Research and Forecasting model with building energy models. *Energy Build.* **2020**, *207*, 109627.

218. Karimpour, M.; Belusko, M.; Xing, K.; Boland, J.; Bruno, F. Impact of climate change on the design of energy efficient residential building envelopes. *Energy Build.* **2015**, *87*, 142–154.

219. Santamouris, M.; Feng, J. Recent Progress in Daytime Radiative Cooling: Is It the Air Conditioner of the Future? *Buildings* **2018**, *8*, 168.

220. Raeissi, S.; Taheri, M. Skytherm: an approach to year-round thermal energy sufficient houses. *Renew. Energy* **2000**, *19*, 527–543.

221. Alexander, L.; Perkins, S. Debate heating up over changes in climate variability. *Environ. Res. Lett.* **2013**, *8*, 041001.

222. Cowan, T.; Purich, A.; Perkins, S.; Pezza, A.; Boschat, G.; Sadler, K. More Frequent, Longer, and Hotter Heat Waves for Australia in the Twenty-First Century. *J. Clim.* **2014**, *27*, 5851–5871.

223. Khan, H.S.; Santamouris, M.; Kassomenos, P.; Paolini, R.; Caccetta, P.; Petrou, I. Spatiotemporal variation in urban overheating magnitude and its association with synoptic air-masses in a coastal city. *Sci. Rep.* **2021**, *11*, 6762.

224. Livada, I.; Synnefa, A.; Haddad, S.; Paolini, R.; Garshasbi, S.; Ulpiani, G.; Fiorito, F.; Vassilakopoulou, K.; Osmond, P.; Santamouris, M. Time series analysis of ambient air-temperature during the period 1970–2016 over Sydney, Australia. *Sci. Total Environ.* **2019**, *648*, 1627–1638.

225. Phillips, N. Climate change made Australia's devastating fire season 30% more likely. *Nature* **2020**.

226. Australian Bureau of Statistics 3218.0- Regional Population Growth, Australia, 2017-2018, Available online: https://www.abs.gov.au/AUSSTATS/abs@.nsf/Lookup/3218.0Main+Features12017-18?OpenDocument (accessed on Jan 15, 2020).

227. Australian Bureau of Statistics (ABS) Climate and the Sydney 2000 Olympic Games Available online: https://www.abs.gov.au/AUSSTATS/abs@.nsf/Previousproducts/1301.0Feature Article32000 (accessed on Feb 10, 2020).

228. Australian Bureau of Statistics Australian Statistical Geography Standard: Volume 4-Significant Urban Areas, Urban Centres and Localities, Section of State. **2011**, *4*, 29–31.

229. BYRNE, M.; YEATES, D.K.; JOSEPH, L.; KEARNEY, M.; BOWLER, J.; WILLIAMS, M.A.J.; COOPER, S.; DONNELLAN, S.C.; KEOGH, J.S.; LEYS, R.; et al. Birth of a biome: insights into the assembly and maintenance of the Australian arid zone biota. *Mol. Ecol.* **2008**, *17*, 4398–4417.

230. Yun, G.Y.; Ngarambe, J.; Duhirwe, P.N.; Ulpiani, G.; Paolini, R.; Haddad, S.; Vasilakopoulou, K.; Santamouris, M. Predicting the magnitude and the characteristics of the urban heat island in coastal cities in the proximity of desert landforms. The case of Sydney. *Sci. Total Environ.* **2020**, *709*, 136068.

231. Australian Bureau of Statistics (ABS) 3218.0 - Regional Population Growth, Australia, 2012-2013 Available online: https://www.abs.gov.au/AUSSTATS/abs@.nsf/featurearticlesbyCatalogue/3E7856B69D50B387CA258291001DFE59?OpenDocument (accessed on Feb 15, 2020).

232. Ivan Demography and destiny in Western Sydney Available online: https://blog.id.com.au/2018/population/population-trends/demography-and-destiny-in-western-sydney/ (accessed on Oct 30, 2020).

233. Khan, H.S.; Paolini, R.; Santamouris, M.; Caccetta, P. Exploring the Synergies between Urban Overheating and Heatwaves (HWs) in Western Sydney. *Energies 2020, Vol. 13, Page 470* **2020**, *13*, 470.

234. Jacbos, B.; Mikhailovich, N.; Delaney, C. *Benchmarking Australia's Urban Tree Canopy: An i-Tree Assessment, Final Report 2014, prepared for Horticulture Australia Limited by the Institute for Sustainable Futures, University of Technology Sydney.*; 2014;

235. Australian Government Bureau of Meteorology Climate Data Online Available online: http://www.bom.gov.au/climate/data/index.shtml?bookmark=201 (accessed on Feb 15, 2020).

236. NSW Government. Sydney air quality monitoring stations Available online: https://www.environment.nsw.gov.au/topics/air/monitoring-air-quality/sydney/monitoring-stations (accessed on Nov 21, 2020).

237. Estévez, J.; Gavilán, P.; Giráldez, J. V. Guidelines on validation procedures for meteorological data from automatic weather stations. *J. Hydrol.* **2011**, *402*, 144–154.

238. Australian Government Bureau of Meteorology *Special Climate Statement 61—exceptional heat in southeast Australia in early 2017*; 2017;

239. Zarzar, C.; Dyer, J. The influence of synoptic-scale air mass conditions on seasonal precipitation patterns over North Carolina. *Atmosphere (Basel).* **2019**, *10*, 624.

240. Daly, D.; Kokogiannakis, G.; Aghdaei, N.; Cooper, P. NSW Housing Typology Development Project: Final Report. *NSW Off. Environ. Herit.* **2016**.

241. Santamouris, M; Haddad, S; Garshasbi, S; Bartesaghi, C; Paolini, R. Sydney's Third City Final report. *CRC Low Carbon living* **2019**, 1–316.

242. Carnieletto, L.; Ferrando, M.; Teso, L.; Sun, K.; Zhang, W.; Causone, F.; Romagnoni, P.; Zarrella, A.; Hong, T. Italian prototype building models for urban scale building performance simulation. *Build. Environ.* 2021, *192*.

243. NatHERS *Nationwide House Energy Rating Scheme (NatHERS) - Software Accreditation Protocol*; 2019;

244. ASHRAE Nonresidential cooling and heating load calculations. In *ASHRAE Handbook-Fundamentals (SI)*; 2017.

245. Australian Building Codes Board (ABCB) Building Classifications, All NCC volumes: Part A6. **2020**.

246. Australian Building Codes Board (ABCB) Australia Climate zone map Available online: https://www.abcb.gov.au/resource/map/climate-zone-map-australia (accessed on Oct 28, 2021).

247. Australian Building Codes Board (ABCB) Climate zone map for New South Wales (NSW) and Australian Capital Territory (ACT) Available online: https://www.abcb.gov.au/resource/map/climate-zone-map-nsw (accessed on Oct 28, 2021).

248. Sola, A.; Corchero, C.; Salom, J.; Sanmarti, M. Multi-domain urban-scale energy modelling tools: A review. *Sustain. Cities Soc.* **2020**, *54*, 101872.

249. Sola, A.; Corchero, C.; Salom, J.; Sanmarti, M. Simulation tools to build urban-scale energy models: A review. *Energies* **2018**, *11*.

250. Hong, T.; Chen, Y.; Luo, X.; Luo, N.; Lee, S.H. Ten questions on urban building energy modeling. *Build. Environ.* **2020**.

251. Reinhart, C.F.; Dogan, T.; Jakubiec, J.A.; Rakha, T.; Sang, A. UMI - An urban simulation environment for building energy use, daylighting and walkability. *Proc. BS 2013 13th Conf. Int. Build. Perform. Simul. Assoc.* **2013**, 476–483.

252. Robinson, D.; Haldi, F.; Kämpf, J.; Leroux, P.; Perez, D.; Rasheed, A.; Wilke, U. Citysim: Comprehensive micro-simulation of resource flows for sustainable urban planning. *IBPSA 2009 - Int. Build. Perform. Simul. Assoc. 2009* 2009, 1083–1090.

253. Fonseca, J.A.; Nguyen, T.A.; Schlueter, A.; Marechal, F. City Energy Analyst (CEA): Integrated framework for analysis and optimization of building energy systems in neighborhoods and city districts. *Energy Build.* **2016**, *113*, 202–226.

254. Emmanuel, W.; Jérôme, K. A verification of CitySim results using the BESTEST and monitored consumption values. *Build. Simul. Appl.* 2015, *2015-Febru*, 215–222.

255. Judkoff, R.; Neymark, J. *International Energy Agency building energy simulation test (BESTEST) and diagnostic method*; Golden, CO (United States), 1995;

256. Meteonorm Handbook part I: Software - Global Meteorological Database Version 7 Software and Data for Engineers , Planers and Education. **2020**, 84.

257. World Health Organization *WHO Housing and health guidelines*; 2018; ISBN 9789241550376.

258. Chartered Institution of Building Services Engineers *CIBSE Guide A: Environmental Design*; 2006; ISBN 9781903287668.

259. Chartered Institution of Building Services Engineers *CIBSE Guide A:2016 - Environmental Design*; 2015; ISBN 9781903287668.

260. Purtill, J. Heatwaves may mean Sydney is too hot for people to live in "within decades" Available online: https://amp-abc-net-au.cdn.ampproject.org/c/s/amp.abc.net.au/article/12993580 (accessed on Jan 24, 2021).

261. Voogt, J..; Oke, T.. Thermal remote sensing of urban climates. *Remote Sens. Environ.* **2003**, *86*, 370–384.

262. Nichol, J.; Wong, M.S. Modeling urban environmental quality in a tropical city. *Landsc. Urban Plan.* **2005**, *73*, 49–58.

263. Alonso, M.; Fidalgo, M.; Labajo, J. The urban heat island in Salamanca (Spain) and its relationship to meteorological parameters. *Clim. Res.* **2007**, *34*, 39–46.

264. Australian Building Codes Board (ABCB) National Construction Code: Building Code of Australia 2019 - Volume One. **2019**, 750.

265. Australian Building Codes Board (ABCB) National Construction Code: Building Code of Australia 2019 - Volume Two. **2019**, 599.

266. Lesosai Lesosai ecological and energy optimization and certification software. Available online: https://lesosai.com/ (accessed on Nov 8, 2021).

267. Reinhart, C.F. Lightswitch-2002: a model for manual and automated control of electric lighting and blinds. *Sol. Energy* **2004**, *77*, 15–28.

268. KÄMPF, J.H. On the Modelling and Optimisation of Urban Energy Fluxes, 2009, Vol. 4548.

269. Function for shading calculation Available online: https://www.wolframalpha.com/input/?i2d=true&i=plot+Divide%5B1%2C%5C%2840%291%2Bexp%5C%2840%290.2*%5C%2840%29x-100%5C%2841%29%5C%2841%29%5D+from+0+to+500 (accessed on Nov 9, 2021).

270. Australian Building Codes Board (ABCB) Building Code of Australia (BCA)-1996-Amdt 13-Class 2 to Class 9 Buildings. **1996**, 245–259.

271. Australian Building Codes Board (ABCB) Building Code of Australia (BCA)-1996-Amdt 13-Class 1 and Class 10 Buildings - Housing Provisions. **1996**.

272. Mandal, J.; Fu, Y.; Overvig, A.C.; Jia, M.; Sun, K.; Shi, N.N.; Zhou, H.; Xiao, X.; Yu, N.; Yang, Y. Hierarchically porous polymer coatings for highly efficient passive daytime radiative cooling. *Science (80-.).* **2018**, *362*, 315–319.

273. Baniassadi, A.; Sailor, D.J.; Ban-Weiss, G.A. Potential energy and climate benefits of super-cool materials as a rooftop strategy. *Urban Clim.* **2019**, *29*.

274. Ambrose, M.; Syme, M. Air Tightness of New Australian Residential Buildings. *Procedia Eng.* **2017**, *180*, 33–40.

275. Marlow, A. Is Passivhaus suitable for warm climates? Available online: https://thefifthestate.com.au/columns/spinifex/is-passivhaus-suitable-for-warm-climates/ (accessed on Nov 9, 2021).

276. Jewell, C. Push for air tightness standards as CSIRO uncovers poor new build performance. Available online: https://thefifthestate.com.au/innovation/building-construction/push-for-air-tightness-standards-as-csiro-uncovers-poor-new-build-performance/ (accessed on Nov 9,

2021).

277. Australian Institute of Refrigration Air Conditioning and Heating (AIRAH) Air tightness metrics to improve Australian building envelope integrity. **2017**, *3000*.

278. Australian passive house Association (APHA) Passive House Criteria Available online: https://passivehouseaustralia.org/APHA/What_is_Passive_House/Criteria/APHA/What_is_Passive_House/Criteria.aspx?hkey=34f3fc0e-f4a0-4a0e-a8e2-12486461aa48 (accessed on Aug 30, 2021).

279. Santamouris, M.; Yun, G.Y. Recent development and research priorities on cool and super cool materials to mitigate urban heat island. *Renew. Energy* **2020**, *161*, 792–807.

280. Camilloni, I.; Barrucand, M. Temporal variability of the Buenos Aires , Argentina , urban heat island. *Theor. Appl. Climatol.* **2012**, *107*, 47–58.

281. Peng, S.; Piao, S.; Ciais, P.; Friedlingstein, P.; Ottle, C.; Bréon, F.-M.; Nan, H.; Zhou, L.; Myneni, R.B. Surface Urban Heat Island Across 419 Global Big Cities. *Environ. Sci. Technol.* **2012**, *46*, 696–703.

282. Bahi, H.; Rhinane, H.; Bensalmia, A.; Fehrenbach, U.; Scherer, D. Effects of Urbanization and Seasonal Cycle on the Surface Urban Heat Island Patterns in the Coastal Growing Cities: A Case Study of Casablanca, Morocco. *Remote Sens.* **2016**, *8*, 829.

283. Herold, N.; Kala, J.; Alexander, L. V. The influence of soil moisture deficits on Australian heatwaves. *Environ. Res. Lett.* **2016**, *11*, 064003.

284. Perkins, S.E.; Argüeso, D.; White, C.J. Relationships between climate variability, soil moisture, and Australian heatwaves. *J. Geophys. Res. Atmos.* **2015**, *120*, 8144–8164.

285. Parker, T.; Quinting, J.; Reeder, M. The synoptic-dynamics of summertime heatwaves in the Sydney area (Australia). *J. South. Hemisph. Earth Syst. Sci.* **2019**, *69*, 116.

286. Palme, M.; Inostroza, L.; Villacreses, G.; Lobato-Cordero, A.; Carrasco, C. From urban climate to energy consumption. Enhancing building performance simulation by including the urban heat island effect. *Energy Build.* **2017**, *145*, 107–120.

287. Mulville, M.; Stravoravdis, S. The impact of regulations on overheating risk in dwellings. *Build. Res. Inf.* **2016**, *44*, 520–534.

288. McLeod, R.S.; Hopfe, C.J.; Kwan, A. An investigation into future performance and overheating risks in Passivhaus dwellings. *Build. Environ.* **2013**, *70*, 189–209.

289. Australian passive house Association (APHA) Passive House Criteria Available online: https://passivehouseaustralia.org/APHA/What_is_Passive_House/Criteria/APHA/What_is_Passive_House/Criteria.aspx?hkey=34f3fc0e-f4a0-4a0e-a8e2-12486461aa48 (accessed on Nov 9, 2021).